

EXPERIMENTAL INVESTIGATION OF THE MECHANICAL BEHAVIOUR AND STRUCTURE OF THE BOVINE PERIODONTAL LIGAMENT

THÈSE N° 2902 (2003)

PRÉSENTÉE À LA FACULTÉ SCIENCES ET TECHNIQUES DE L'INGÉNIEUR

Institut d'ingénierie des systèmes

SECTION DE GÉNIE MÉCANIQUE

ÉCOLE POLYTECHNIQUE FÉDÉRALE DE LAUSANNE

POUR L'OBTENTION DU GRADE DE DOCTEUR ÈS SCIENCES

PAR

Colin SANCTUARY

Bachelor of Engineering - Metallurgical, McGill University, Canada
et de nationalité canadienne

acceptée sur proposition du jury:

Prof. I. Botsis, directeur de thèse

Dr U. Belser, rapporteur

Prof. M. Chiba, rapporteur

Prof. A. Curnier, rapporteur

Dr D. Pioletti, rapporteur

Lausanne, EPFL
2003

ህዳር ፳፯
ጥቅምት ፳፯ ዓ.ም. ጳጳስ ጳውሎስ
ጳጳስ ጳውሎስ ጳጳስ ጳውሎስ
ጳጳስ ጳውሎስ ጳጳስ ጳውሎስ
ጳጳስ ጳውሎስ ጳጳስ ጳውሎስ
ጳጳስ ጳውሎስ ጳጳስ ጳውሎስ
ጳጳስ ጳውሎስ ጳጳስ ጳውሎስ
ጳጳስ ጳውሎስ ጳጳስ ጳውሎስ



Acknowledgements

I wish to express my gratitude to my thesis director, Prof. John Botsis, for his guidance, weekly meetings and fruitful discussions during the work of this thesis. A study of this nature would not have been possible had it not been for his understanding, patience and kindness.

I would also like to thank Prof. Alain Curnier for his comments and contribution throughout the progression of this work. His advice influenced the way in which I approached numerous problems. Jörn Justiz also deserves particular thanks for his ongoing help and frequent advice that contributed to the development of the project; remember ‘myatt’, Ticino and the numerous nicknames we came up with to describe the PDL.

The members of the PDL group deserve my thanks for their contribution on the medical and biological aspects: Prof. Urs Belser, Dr. Anselm Wiskott, Dr. Susanne Scherrer, Dr. Dieter Bosshardt, and Dr. Tatsuya Shibata. I express my thanks also to the members of the jury for their comments. And to the Swiss National Science Foundation Grant no. 3152-055863.98, and R’Equip 2001 21-64562.01 for financing this study.

The design of the machines and experiments would not have been possible without the expertise of our workshop team, particularly to Gino Crivellari and Marc Jeanneret.

To my LMAF colleagues with whom I have had many, *many* coffee breaks: Aïssa, Anna, Anne, Brian, Christian, Eric, Fabiano, Federico, Gabriel, Jarek, Joel, Larissa, Laurent, Matteo, Michel, Mostafa, Paola, Philippe B., Philippe Z., Stefan, Thomas G., Thomas R.

To my friends who shared those many moments during my four years in Lausanne; moments in the Alps, moments on/in the lake, countless moments. All these moments have made up four very precious years of my life, and though they cannot be seen in this thesis, they very much fill the spaces between the lines of this work.

A special thanks to my loving family. Look to the runes.

Abstract

One of the key problems in dental biomechanics is the prediction of tooth mobility under functional loads. Understanding tooth displacement due to load is becoming more important as new solutions in dental restorations, prosthodontics and orthodontic treatments become increasingly more advanced. The mechanical characterization of the alveolar bone, the tooth and the periodontal ligament surrounding the root of the tooth, is necessary to predict tooth mobility. The common assumption is that the periodontal ligament acts as the major element in the stress distribution to the supporting tissues. Obtaining parameters that describe periodontal ligament mechanical behaviour is a challenging problem. Isolating the tissue for testing, the small size of the specimen, and the necessity to maintain, as much as possible, the ligament *in vitro* under normal physiological conditions, are all factors that contribute to the complexity of the problem. The aim of this thesis is twofold and can be subdivided into two primary objectives. The first objective is to describe its morphology, anatomy, histology and structure of the components in order to determine its geometric parameters at different length scales. The second objective is to determine its mechanical properties by identifying key parameters through shear and uniaxial tension-compression tests.

Four studies are performed to describe the morphology, anatomy and histology of the periodontal ligament. First, macroscopic and microscopic measurements of the tooth, bone, and the periodontal ligament are obtained. Second, a bovine first molar system is reconstructed in three dimensions from microcomputerized tomography scans. Third, the morphology of the ligament is observed during deformation using optical microscopy. Fourth, the histology of bovine periodontium tissue is investigated.

In order to characterise the mechanical behaviour of the bovine periodontal ligament, custom- designed machines and gripping devices are constructed to subject specially-prepared tissue specimens to shear and uniaxial tension-compression experiments. Shear experiments are performed on 2 millimetre thick transverse sections, and specimens of tooth-ligament-bone of approximately 8x5x2 millimetres for uniaxial experiments. All specimens are obtained from first molar sites of freshly slaughtered bovines. In both shear and uniaxial testing, the specimens are subjected non-destructively to preconditioning, stress-relaxation, constant strain rate, and sinusoidal loading profiles before testing to rupture.

The experiments reported in this thesis elucidate geometrical and mechanical characteristics of the periodontal ligament. Concerning its geometry, a variation in collagen fibre orientation is observed in transverse sections, moreover the symmetry of the shear tests in the apico-coronal direction suggests the periodontal ligament is vertically isotropic. Uniaxial specimens, however, may be considered to be transverse isotropic. Concerning its mechanical behaviour, the periodontal ligament is nonlinear viscoelastic in that it exhibits stiffening, nonlinear elasticity, and nonlinear pseudo-plastic viscosity. The interaction between various constituents of the periodontal ligament (collagen fibres, blood vessels, interstitial fluid etc...) during deformation contribute to the observed stress-strain response of this tissue. A nonlinear viscoelastic model presented in the literature, *the Power Law*, adequately simulates the nonlinear behaviour of the periodontal ligament using finite element analysis.

Version abrégée

La prédiction de la mobilité de la dent est une des majeures difficultés de la biomécanique dentaire. Une meilleure compréhension des mécanismes de déplacement d'une dent sous charge est importante dans l'avancement des technologies dans les domaines des restaurations dentaires, des implants dentaires, et de l'orthodontologie. Afin de prédire le mouvement d'une dent, il est nécessaire de caractériser les propriétés mécaniques de l'alvéole, de la dent et du ligament dentaire entourant la racine de la dent. Le ligament dentaire affecte considérablement la distribution de contraintes dans les tissus entourant la dent. Les paramètres qui décrivent les propriétés mécaniques du ligament dentaire sont à ce jour inconnus. La reproduction *in vitro* des conditions physiologiques, la préparation de l'échantillon, contribuent à la difficulté du problème. Le but de cette thèse est, d'une part de caractériser la morphologie, l'anatomie, l'histologie et la structure du ligament dentaire afin de déterminer sa configuration géométrique, et d'autre part, de déterminer ses propriétés mécaniques en soumettant le ligament dentaire aux expériences de cisaillement et de traction-compression.

Quatre études sont effectuées pour décrire la morphologie, l'anatomie et l'histologie du ligament dentaire du bovin. Dans un premier temps, des mesures macroscopiques et au microscope de la dent, de l'os et du ligament sont effectuées. Dans un deuxième temps, une première molaire est reconstruite en trois dimensions à partir de scans de la microtomographie computerisée. Dans un troisième temps, la morphologie du ligament dentaire est observée pendant sa déformation en utilisant la microscopie optique. Et dans un quatrième temps l'histologie du tissu du periodontium est examinée.

Afin de caractériser la mécanique du ligament dentaire bovin, un appareillage spécifique est conçu et construit pour tester des échantillons de l'os-ligament-dent en cisaillement, et en tension-compression. Les expériences de cisaillement sont effectuées sur des coupes transversales de 2 millimètres d'épaisseur, et de traction-compression sur échantillons ayant les dimensions d'approximativement 8x5x2 millimètres. Tous les échantillons sont sectionnés d'une première molaire obtenue d'un bovin immédiatement après abattage. Tant pour les tests de traction-compression que de cisaillement, les échantillons sont soumis à un chemin de déformation non-destructif consistant en préconditionnement, relaxation, taux de déformation constant, et sinusoidal, avant d'être déformés à la rupture.

Les résultats présentés dans cette thèse clarifient les caractéristiques de la géométrie et la mécanique du ligament dentaire. Concernant sa géométrie, une variation de l'orientation des fibres de collagène est observée dans une coupe transverse de la dent. De plus, la symétrie des courbes de contrainte-déformation obtenues lors des expériences de cisaillement suggère une isotropie verticale. Cependant, le ligament dentaire serait transverse isotrope en ce qui concerne les échantillons uniaxiaux. Concernant son comportement mécanique, le ligament dentaire est viscoélastique nonlinéaire; c'est-à-dire nonlinéaire élastique de durcissement, et une viscosité nonlinéaire pseudo-plastique. Ce comportement est dû à l'interaction des constituants du ligament dentaire (fibres de collagène, vaisseaux sanguins, fluide interstitiel etc...) pendant sa déformation. En utilisant un modèle nonlinéaire viscoélastique de la littérature, *la loi puissance*, ce comportement peut être simulé numériquement en vue d'analyses par éléments finis.



Table of Contents



Acknowledgements

<i>Abstract</i>	<i>i</i>
<i>Version abrégée</i>	<i>iii</i>
<i>Table of Contents</i>	<i>v</i>
<i>List of Figures</i>	<i>ix</i>
<i>List of Tables</i>	<i>xv</i>
<i>Notation and Abbreviations</i>	<i>xvii</i>

Chapter 1

Introduction

1.1 Soft Biological Tissues	3
1.2 Objectives	4
1.2.1 Structure of this Thesis	5

Chapter 2

Review of Literature & Background

2.1 The Periodontium is an Articulation	9
2.2 Ligaments and Morphology	10
2.3 The Periodontal Ligament and Morphology	11
2.3.1 Anatomy of the Tooth-PDL-Bone System	12
2.3.2 The Periodontium	13
2.3.3 Components of the PDL Responsible for Mechanical Function	14
2.4 Experimental Characterization of PDL Mechanical Behaviour	17
2.4.1 PDL Mechanical Testing Techniques	17

2.4.2	Reported Experimental Loading Profiles on PDL	19
2.4.3	Use of Material Properties in Finite Element Models	22
2.5	Theoretical Modeling of the PDL Mechanical Behaviour	22
2.5.1	Elasticity of the Periodontal Ligament	22
2.5.2	Viscosity of the Periodontal Ligament	24
2.6	Continuum Mechanics, Biomechanics and the Constitutive Equation	25
2.6.1	Continuum Mechanics Background	25
2.6.2	Non Linear Homogeneous Isotropic Elasticity	29
2.6.3	Linear Homogeneous Isotropic Elasticity: Kirchhoff-St. Venant Law	29
2.7	Viscoelasticity and Biological Tissue	30
2.7.1	Linear Elastic Solid	31
2.7.2	Linear Viscous Fluid	32
2.7.3	Response of a Viscoelastic Material	33
2.7.4	Characterizing Material Properties	34
2.7.5	Response of a Linear Viscoelastic Material	38
2.7.6	Preconditioning and Hysteresis of Soft Living Tissue	41

Chapter 3

Materials and Methods

3.1	Tissue Selection	45
3.1.1	Why not Human?	45
3.1.2	Why Bovine?	46
3.1.3	Why 1st Molar?	47
3.1.4	Selecting and Obtaining Bovine Mandibles	47
3.2	3D Reconstruction of First Molar from CT Scans	48
3.2.1	Methodology	48
3.2.2	Principles of X-Ray CT	48
3.3	Histology Studies	50
3.3.1	Research Methodology	50
3.3.2	Determination of Fibre Density	51
3.4	Uniaxial Specimens	51
3.4.1	Methodology and Specific Procedures	51
3.4.2	Initial Uniaxial Studies	57
3.4.3	Tests on Uniaxial Samples	58
3.4.4	Sequential Testing of Uniaxial Specimens	62
3.4.5	Treatment of Data	64
3.5	Shear Specimens	66
3.5.1	Design of the Periodontal Ligament Shear Testing Machine	67
3.5.2	Methodology and Specific Procedures	68
3.5.3	Tests to determine the mechanical behaviour of PDL Shear Specimens	69
3.5.4	Treatment of Shear Data	75

Chapter 4

Results: Geometry, Structure and Histology

4.1 Geometrical Measurements taken from Specimens	81
4.1.1 Uniaxial Specimen Dimensions	82
4.1.2 Shear Specimen Dimensions	83
4.2 Geometrical Measurements taken from μ CT scans	84
4.2.1 3D Reconstruction Method.	84
4.2.2 General Dimensions of the Bovine First Molar	88
4.2.3 Periodontal Ligament Width from 3D Reconstruction	88
4.3 Variation of PDL Width with Root Depth	89
4.4 Morphology of Uniaxial Specimen During Loading	91
4.4.1 Expulsion of Fluid from Periodontal Ligament in Compression	91
4.4.2 Apparition of Voids when PDL is Pulled in Tension.	92
4.4.3 Rupture Tests with Sequenced Image Acquisition.	93
4.4.4 Observation of a Single Collagen Fibre Bundle in Rupture.	94
4.5 Histology	97
4.5.1 Preliminary Histology Study	98
4.5.2 Fractal Measurements.	99
4.5.3 Advanced Histology Study.	100
4.6 Discussion of Geometry, Morphology and Histology Results.	109

Chapter 5

Results: Uniaxial Behaviour

5.1 Preconditioning.	113
5.2 Constant Strain Rate Deformation Tests	115
5.2.1 Verifying Linear Scaling Property	116
5.3 Constant Strain Rate Deformation and Recovery History	121
5.3.1 What does this say about the behaviour of periodontal ligament?.	123
5.4 Uniaxial Stress Relaxation of the Periodontal Ligament	124
5.4.1 Zero Definition and Stress Relaxation	124
5.4.2 Relaxation Tests of PDL at Different Strain Levels.	126
5.4.3 Verification of the Linear Scaling Property of Relaxation Response	128
5.4.4 Verification of the Hypothesis of Variables Separation.	129
5.4.5 Verification of Superposition Property of Relaxation Responses	130
5.5 Sinusoidal Response of the Periodontal Ligament.	131
5.5.1 Transient Stress Response to Sinusoidal Strain History	132
5.5.2 Effect of Frequency on the Sinusoidal Response of the PDL	137
5.6 Rupture	142
5.6.1 Rupture Tests at Different Strain Rates	143
5.7 Regional Effects on Mechanical Behaviour of PDL	144
5.8 Discussion of Uniaxial Results.	153

Chapter 6

Results: Shear Behaviour

6.1 Initial Studies	159
6.1.1 Amplitude	159
6.2 Mechanical Response of the Periodontal Ligament in Shear	160
6.2.1 Zeroing.	161
6.2.2 Shear Response of PDL Subjected to Triangular Cycles	161
6.2.3 Shear Stress Relaxation of Periodontal Ligament	161
6.2.4 Shear Behaviour of Periodontal Ligament subjected to Sinusoidal Oscillations	163
6.2.5 Shear Rupture of Periodontal Ligament	167
6.3 Discussion of Shear Results.	169

Chapter 7

Application to Numerical Models

7.1 Stress Analysis Applied to Reconstructed 3D Bovine Molar	175
7.1.1 Problem Definition	175
7.1.2 Mesh	177
7.1.3 Analysis of Stress Distributions: Linear Elastic PDL	179
7.1.4 Implementing Non-Linear Experimental Data of the PDL	185

Chapter 8

Summary, Conclusion and Perspectives

8.1 Summary	191
8.1.1 Structure, Morphology and Histology of PDL	191
8.1.2 Uniaxial Behaviour of PDL	192
8.1.3 Shear Behaviour of PDL	193
8.1.4 Summary of Numerical Modeling Results	194
8.2 Conclusions	195
8.3 Recommendations	196
<i>References</i>	197
<i>Appendix A: Machine Specifications</i>	205
<i>Appendix B: The Power Law: a nonlinear viscoelastic model for the PDL</i>	211

List of Figures

Figure 1.1: Structure of PDL studies and how they are inter-related	6
Figure 2.1: Microstructural hierarchy of ligaments, evidences are gathered from x-ray, electron microscopy (EM), scanning electron microscopy (SEM) and optical microscopy (OM) (based on a model by [Nigg and Herzog 1994]).	10
Figure 2.2: The tooth unit showing the major features of the system including the tooth, PDL and the alveolar bone.	12
Figure 2.3: Schematic of what is known about the hierarchy of the human PDL at the (a) alveolus junction and (b) the cementum junction.	16
Figure 2.4: Chart of finite-element papers and reference to published experimental results . . .	23
Figure 2.5: Reference and present configurations used in the Lagrangian description.	26
Figure 2.6: A typical stress-strain curve for the periodontal ligament in tension.	30
Figure 2.7: Schematic of a mechanical spring representing a linear elastic solid. (a) mechanical analog - linear spring, (b) force-elongation relation for the spring.	32
Figure 2.8: Schematic of a mechanical dash-pod, or viscous damper, representing a linear elastic solid. (a) mechanical analog - viscous damper, (b) force-elongation relation for the viscous damper.	33
Figure 2.9: Three-Parameter Standard Viscoelastic Model	33
Figure 2.10: Steps at (a) different strain levels E_1 , E_2 and E_3 and (b) corresponding stress relaxation functions G_1 , G_2 and G_3	35
Figure 2.11: Constant strain rate profile (a) with a rate defined by α and (b) a corresponding stress response. Note that the stress response is determined by the relaxation function G	36
Figure 2.12: Constant strain rate deformation and recovery history	37
Figure 2.13: Response of ligament tissue subjected to sinusoidal oscillations. The stress function, S , is dependent on $E(\omega)$ and $\delta(\omega)$	38
Figure 2.14: Linear scaling: step strains at different strain levels and corresponding normalised stress relaxation for when (a) linear scaling is observed and, (b) no linear scaling is observed.	40
Figure 2.15: Graphical representation of the use of superposition to construct a strain history response to two step-stress histories.	41
Figure 2.16: The effect of (a) preconditioning ligament tissue by subjecting it to cyclic loading, and (b) hysteresis: the difference in the loading and unloading stress-strain curves. The area between the loading and unloading curves quantifies the hysteresis of the material.	42
Figure 3.1: Experimental setup of the μ - computerised tomography scanner	49
Figure 3.2: Obtaining an intact first molar site from a bovine mandible	54
Figure 3.3: Schematic describing how transverse sections are cut from block containing first molar*.	55

Figure 3.4: Schematic describing the cutting of uniaxial specimens from transverse sections*	56
Figure 3.5: Schematic showing how uniaxial specimen was clamped into the grips of the machine*	57
Figure 3.6: Defining the zero of a ligament specimen	59
Figure 3.7: Triangular and harmonic preconditioning	60
Figure 3.8: Step-strain Experimental Relaxation Response : Experimental	61
Figure 3.9: Rupture curve of uniaxial specimen with parameters obtained from each curve	63
Figure 3.10: Schematic of (a) PDL uniaxial sample in tensile machine showing (b) bone and tooth and (c) how the data is interpreted from simple traction tests.	67
Figure 3.11: Technical drawing of the PDL Shear Testing Machine	70
Figure 3.12: Design of the custom-made grips for PDL shear test specimens *	71
Figure 3.13: Photograph of Shear Testing Machine after construction.	72
Figure 3.14: Rupture curve of shear specimen with parameters obtained from each curve.	73
Figure 3.15: Schematic of (a) PDL shear specimen in machine showing (b) bone and tooth and how (c) the data obtained from the shear test is used to interpret results.	77
Figure 4.1: Dimensions of the PDL specimens	82
Figure 4.2: Measured Dimensions of the Shear Specimens	83
Figure 4.3: Image acquisition of bovine first molar using μ CT scanner.	85
Figure 4.4: Tracing of the contours from (a) the original image, (b) the modified image to produce (c) the traced contour of the tooth.	86
Figure 4.5: The steps of method 1 (a) all the contours, (b) the successive joining of the surfaces, and (c) the joining of the different parts.	86
Figure 4.6: The steps of method 2 (a) import a reduced number of contours to (b) perform smoothing and then perform (c) blending to obtain (d) a reconstruction with a realistic form.	87
Figure 4.7: Method 3 involved creating the undulated surface (a) before using a smoothing function to produce (b).	87
Figure 4.8: Measurement of PDL width from μ CT scans: (a) tooth showing the transverse sections used for measuring the PDL width, with yellow indicating the transverse section shown in (b).	89
Figure 4.9: PDL width with depth	90
Figure 4.10: PDL, bone and tooth showing difficulty in defining interface for measurements (viewed by optical microscope at 4x magnification).	90
Figure 4.11: Uniaxial specimen in its initial state (a) pushed into (b) compression showing fluid expulsion from the PDL, with fluid resorption when pulled to initial state (c).	92

Figure 4.12: Apparition of voids when PDL is pulled in tension. The circular void appearing implies the presence of a blood vessel in the PDL at this location.	93
Figure 4.13: Magnified view of a single collagen fibre bundle.	94
Figure 4.14: Sequenced image acquisition during rupture of PDL (a - f) shown here at 5X magnification	95
Figure 4.15: Sequenced image acquisition during rupture of PDL (g - k) with optical microscope shown here at 5X magnification and rupture curve	96
Figure 4.16: Micrographs of undecalcified ground sections showing (a) transverse section of a bovine third molar, and (b) the transverse section magnified on a section of the periodontium at a magnification of 5x.	98
Figure 4.17: (a) Micrograph of an undecalcified ground section showing definition of xy-coordinate system to (b) measure an angle, α , to quantify the preferential fibre direction. Histogram (bottom) showing the distribution of fibre direction around the entire contour of the tooth.	99
Figure 4.18: Micrographs of undecalcified ground sections showing the method to determine fractal dimensions of the bone-ligament junction using (a) circles of small radius, and (b) larger radius.	100
Figure 4.19: Micrographs showing transverse section of an undecalcified ground section (a) of a distal first molar root apical from apex of bovine first molar with (b) detail of alveolar bone and (c) periodontium.	102
Figure 4.20: Micrograph of a decalcified thin section of periodontium showing insertion points at alveolus junction and cementum junction.	104
Figure 4.21: Image analysis of periodontium showing decalcified thin section of periodontium and insertion points at alveolus junction and cementum junction to quantify fibre density	105
Figure 4.22: Micrograph of a decalcified section showing the middle region of the PDL showing density and wavy structure of collagen fibres	106
Figure 4.23: Micrographs of macerated decalcified tissue showing intact collagen matrix and insertion points into bone and cementum.	107
Figure 4.24: Micrograph of undecalcified ground sections showing vasculature of the PDL.	108
Figure 5.1: Preconditioning	114
Figure 5.2: Histograms showing distribution of percent differences between first and second stress maxima in compression and tension	115
Figure 5.3: (a) 4 constant strain rate deformation curves at 4 different strain rates, and (b) showing the dependency of the maximum tangent modulus on strain rate.	117
Figure 5.4: Verification of linear scaling property: (a) the plot of equation 5.8 if the PDL displayed the linear scaling property, and (b) actual experimental results from testing linear scaling property.	120
Figure 5.5: Results of Constant Strain Rate Deformation and Recovery History	122

Figure 5.6: Third Order Exponential Decay Function	124
Figure 5.7: Relaxation at zero	127
Figure 5.8: Relaxation at different strain levels	129
Figure 5.9: (a) normalised stress relaxation curves at 2 strains (E=0.2 & E=0.4) for bovine PDL uniaxial specimens.	130
Figure 5.10: Superposition of Relaxation Responses	131
Figure 5.11: Sine Test : stress/strain vs. time 1 cycle and corresponding stress strain curve at 1 Hz of a typical specimen.	132
Figure 5.12: Transient state to stable state of PDL under sinusoidal oscillations	134
Figure 5.13: Frequency effect on Stress versus Strain Curves	138
Figure 5.14: Stress and strain as functions of time for a selection of frequencies	139
Figure 5.15: Stress as a function of strain for a selection of frequencies	140
Figure 5.16: Effect of frequency on phaselag expressed as $\tan \delta$ versus frequency	141
Figure 5.17: Rupture curve of Uniaxial Periodontal performed on Uniaxial Specimen	142
Figure 5.18: Rupture curve at different Strain Rates.	144
Figure 5.19: Effect of location of specimen on compression phaselag	147
Figure 5.20: Effect of location of specimen on tension phaselag	148
Figure 5.21: Regional Effects of PDL on Maximum Stress	149
Figure 5.22: Effect of specimen location on Maximiser strain	150
Figure 5.23: Effect of specimen location on strain energy density	151
Figure 5.24: Effect of specimen location on maximum tangent modulus	152
Figure 5.25: Summary of parameters obtained from rupture curves for animal A and animal B	153
Figure 6.1: Preliminary increasing triangular profile	160
Figure 6.2: Results of a typical sample showing (a) the response of a shear specimen subjected to a triangular deformation profile with (b) load deformation curves.. . . .	161
Figure 6.3: Normalised relaxation curves in coronal and apical directions	162
Figure 6.4: Phaselag with frequency	165
Figure 6.5: Sinusoidal curves of shear specimen	166
Figure 6.6: Shear Strain versus Shear Stress curves obtained from harmonic oscillations of PDL	167
Figure 6.7: Rupture curves	169
Figure 7.1: Actual experimental results shown by (a) used to define the non-linear elastic law, and (b) the linear law estimated based on curve (a).	176

Figure 7.2: Boundary conditions (a) zero displacement, (b) coronal-apical load, (c) lingual-buccal load, and (d) mesial-distal load.	178
Figure 7.3: Meshing of the tooth, ligament and bone showing how the elements in the bone increase in size as the distance increases from the ligament.	178
Figure 7.4: Mesh using linear tetrahedron elements of (a) the tooth, (b) the ligament and (c) the alveolar bone	179
Figure 7.5: Amplified movements of the tooth when subjected to an coronal-apical load of 10 N showing tooth (a) before loading, (b) during partial loading, and (c) fully loaded.	180
Figure 7.6: Sagittal section of the discretized first molar subjected to a coronal-apical load of 10 N showing the Von Mises stress distribution. Maximum value, in red, 0.43 MPa)	181
Figure 7.7: Von Mises Stress at the surface of the tooth when the tooth is subjected to a coronal-apical load of 10 N (maximum stress, in red, 0.43 MPa). Seen here is the tooth without the surrounding bone and ligament viewed (a) from lingual-buccal and (b) from apical-coronal.	182
Figure 7.8: Von Mises Stress of the PDL when the tooth is subjected to a coronal-apical load of 10 N (maximum strain, in red, $E=0.015$). Seen in (a) is a sagittal section of the system clearly showing the relatively large deformation of the ligament with respect to the bone and tooth, and (b) the ligament seen in the apical-coronal direction.	182
Figure 7.9: Amplified movements of the tooth when subjected to an lingual-buccal load of 10 N showing tooth (a) before loading, (b) during partial loading, and (c) fully loaded	183
Figure 7.10: The result of applying a 10N lingual-buccal load showing (a) the field of Von Mises stress on the tooth (maximum, in red, 1.2 MPa) and (b) the field of Von Mises strain on the ligament (maximum, in red, $E=0.012$).	184
Figure 7.11: Amplified movements of the tooth when subjected to a distal-mesial load of 10 N showing tooth (a) before loading, (b) during partial loading, and (c) fully loaded	184
Figure 7.12: The result of applying a 10N distal-mesial load showing (a) the field of Von Mises stress on the tooth (maximum, in red, 1.3 MPa) and (b) the field of Von Mises strain on the ligament (maximum, in red, $E=0.01$).	185
Figure 7.13: Comparing sagittal sections showing the Von Mises Stresses of the same tooth where PDL is (a) linear elastic, and (b) non-linear elastic ligament using experimental data. Maximum values, in red, 0.5 MPa.	186
Figure 7.14: Comparing the Von Mises Stresses at the surface of the same tooth when a coronal-apical load of 10 N is applied and considering the PDL to be (a) linear elastic, and (b) non-linear elastic ligament using experimental data. Maximum values, in red, 0.5 MPa.	187
Figure 7.15: Comparing the Von Mises Strain of the PDL when a coronal-apical load of 10 N is applied to the crown of the tooth, and considering the PDL to be (a) linear elastic, and (b) non-linear elastic ligament using experimental data. Maximum values, in red, $E=0.05$	187

List of Tables

Table 2.1 Comparison of PDL width of selected species.	14
Table 2.2 Summary of literature describing the collagen fibres of human PDL	15
Table 2.3 Summary of experimental techniques used to determine material parameters of PDL	18
Table 2.4 Comparison of Uniaxial, Shear and Whole Tooth Testing Methods of PDL	19
Table 3.1 CT Scanning characteristics	49
Table 3.2 Summary of sinusoidal sequential loading of uniaxial specimens.	64
Table 3.3 Summary of sinusoidal sequential loading of shear specimens..	75
Table 4.1 Average Dimensions of Uniaxial Specimens.	82
Table 4.2 Average Dimensions of Shear Specimens.	83
Table 4.3 General dimensions of the bovine first molar	88
Table 5.1 Summary of dependence of strain rate, , on the maximum tangent modulus, ϵ	116
Table 5.2 Parameters describing the relaxation curves in figure 5.7 fit to a third order exponential function	125
Table 5.3 Parameters describing and in figure 5.8 fit to a third order exponential function.	128
Table 5.4 Data of Effect of frequency on phaselags, δ_c & δ_t	141
Table 5.5 Summary of dependence of strain rate on the PDL rupture parameters..	143
Table 6.1 Parameters describing a normalised G_g in figure 6.3 fit to a third order exponential function	162
Table 6.2 Shear data of effect of frequency on phaselags in shear.	165
Table 7.1 Summary of components and their mechanical behaviour parameters.	177
Table 7.2 Mesh characteristics for each component	179
Table 7.3 Force application cases studied	179



Notation and Abbreviations



PDL	Periodontal ligament
STL	Standard template format
TTL	Transistor-Transistor Logic
EM	Electron microscopy
SEM	Scanning electron microscopy
OM	Optical microscopy
CT	Computerised tomography
CAD	Computer-Aided design
μ CT	Micro Computerised tomography
EDTA	Ethylenediaminetetra acetic acid
NaOH	Sodium hydroxide
NaCl	Sodium chloride
SLS	Selective laser sintering
bv	Blood vessel
fb	Fibroblast
ob	Osteoblast
cb	Cementoblast
Sh	Sharpey's fibres
CR	Crimp
H	Haversian systems
P	Pulp cavity
D	Dentin
C	Cementum
α	Arbitrary constant
μ	Viscosity
c	Viscosity
F	Load
w_{PDL}	Width of periodontal ligament
b	Breadth of uniaxial Specimen
th	Thickness of uniaxial Specimen

P	Perimeter of periodontal ligament around tooth/bone
Δ	Change in displacement
D	Displacement as measured by displacement sensor
L	Length
T	Time
t	Time
s	Time
E	Green-Lagrange strain
E_0	Strain at time = 0
σ	Cauchy stress
P	Piola-Kirchhoff stress I
S	Piola-Kirchhoff stress II
ε	Elastic modulus or Young's modulus (maximum tangent modulus for periodontal ligament)
q_{HH}	Measured load in HH direction
τ	Shear stress
γ	Shear strain
k	Spring constant [
f	Frequency
H	Hysteresis
ω	Angular velocity
δ	Phaselag
ζ	Maximum shear tangent modulus
$G(t)$	Relaxation function
Ψ	Strain energy density
F	Deformation gradient
H	Displacement gradient

-
-
-

•

•

•

“The beginning of knowledge is the discovery of something we do not understand.”

Frank Herbert

•

•

•



Introduction

1.1 Soft Biological Tissues

Only in the last half century has the mechanical behaviour of living tissues been studied widely and quantitatively. Research in this domain is now referred to as the field of *biomechanics*. Biomechanics seeks to understand the mechanics of living systems.

A better understanding of the biomechanics of an organism helps us to understand its normal function, predict changes when subjected to alterations, and propose methods of artificial intervention. In fact, biomechanics has contributed to virtually every modern advance of medical science and technology. Surgery, for example, seems unrelated to biomechanics, yet healing and rehabilitation are intimately related to the stress and strain in tissues.

Soft, extendible tissues, such as ligaments, are capable both of carrying the necessary loads and of growth and evolution, and are essential to the development of living things. Unlike rigid engineering materials, such as steel, many of the ordinary tissues of animals commonly operate at strains between 30 and 100 percent, and these strains are fully recoverable once the tissue rests. The strength and mechanical behaviour of soft tissues have generally been considered incidental to growth mechanisms and metabolic functions, which is probably why the biomechanics of soft living tissue has not been subject to much study in the past.

Dental Biomechanics

It is common knowledge that teeth are required to reduce the food into particles small enough to swallow, and also to increase the surface area of food particles we ingest to ensure a more efficient digestion. Nevertheless, chewing is part of everybody's daily life and it is no surprise that the jaw muscle is the strongest muscle of the human body. However, few realise the subtle care Nature has taken in the design of our teeth. Have you

ever wondered why crooked teeth can be straightened with an orthodontic apparatus, commonly known as *braces*? Did you know that teeth are not just rigidly connected to your jaw bone? In fact, if you try to gently wiggle one of your teeth you will feel that it moves slightly. This movement is due to the periodontal membrane, or periodontal ligament (PDL), that anchors the tooth to the bone of the jaw. The PDL thus acts as a sling for the tooth within its socket, permitting slight movements which cushion the impact of chewing. Moreover, the mechanism that permits tooth movement during orthodontic treatment is directly related to the PDL. Because the PDL is so soft compared to the bone and tooth, both highly mineralized tissue, it is the PDL that is responsible for tooth mobility. Seeking to understand the mechanisms of tooth mobility can be referred to as the field of *dental biomechanics*.

One of the key problems in dental biomechanics is the prediction of tooth mobility under functional loads. Understanding tooth displacement under load is becoming more important as new solutions in dental restorations, prosthodontics and orthodontic treatments become increasingly more advanced. The mechanical characterization of the PDL, the surrounding alveolar bone and tooth is necessary to predict tooth mobility. The common assumption is that the PDL acts as the major element in the stress distribution to the supporting tissues. Obtaining parameters that describe PDL mechanical behaviour is a challenging problem. Isolating the tissue for testing, the small size of the specimen, and the necessity to maintain, as much as possible, the ligament in normal physiological conditions, are all factors that contribute to the complexity of the problem.

The research presented in this thesis will have an impact on the development of new solutions in dental restorations, prosthodontic and orthodontic treatments. Moreover, the developed methodology will be applicable to other tissues such as articulation ligaments, tendons and membranes.

1.2 Objectives

The overall objective of this research is to experimentally characterize the displacement of a tooth under functional loading. However, the complexity of the PDL's structure is such that extensive investigations are required for a full characterization of this intricate connective tissue. The approach to the study of the problem of tooth mobility in this thesis, therefore, consists of two primary objectives:

- 1 Describe the morphology, anatomy, histology, and the structure of its components in order to determine the geometric configuration of the PDL.
- 2 Determine the mechanical properties of the PDL by identifying parameters to describe its behaviour.

1.2.1 Structure of this Thesis

This thesis is divided into eight chapters. After an introductory chapter containing the statement of objectives, Chapter 2 is dedicated to a review of literature and a presentation of basic theory to establish a framework for the design of the methodology. A description of the materials and the methodologies for histological, morphological, structural and mechanical studies are presented in Chapter 3.

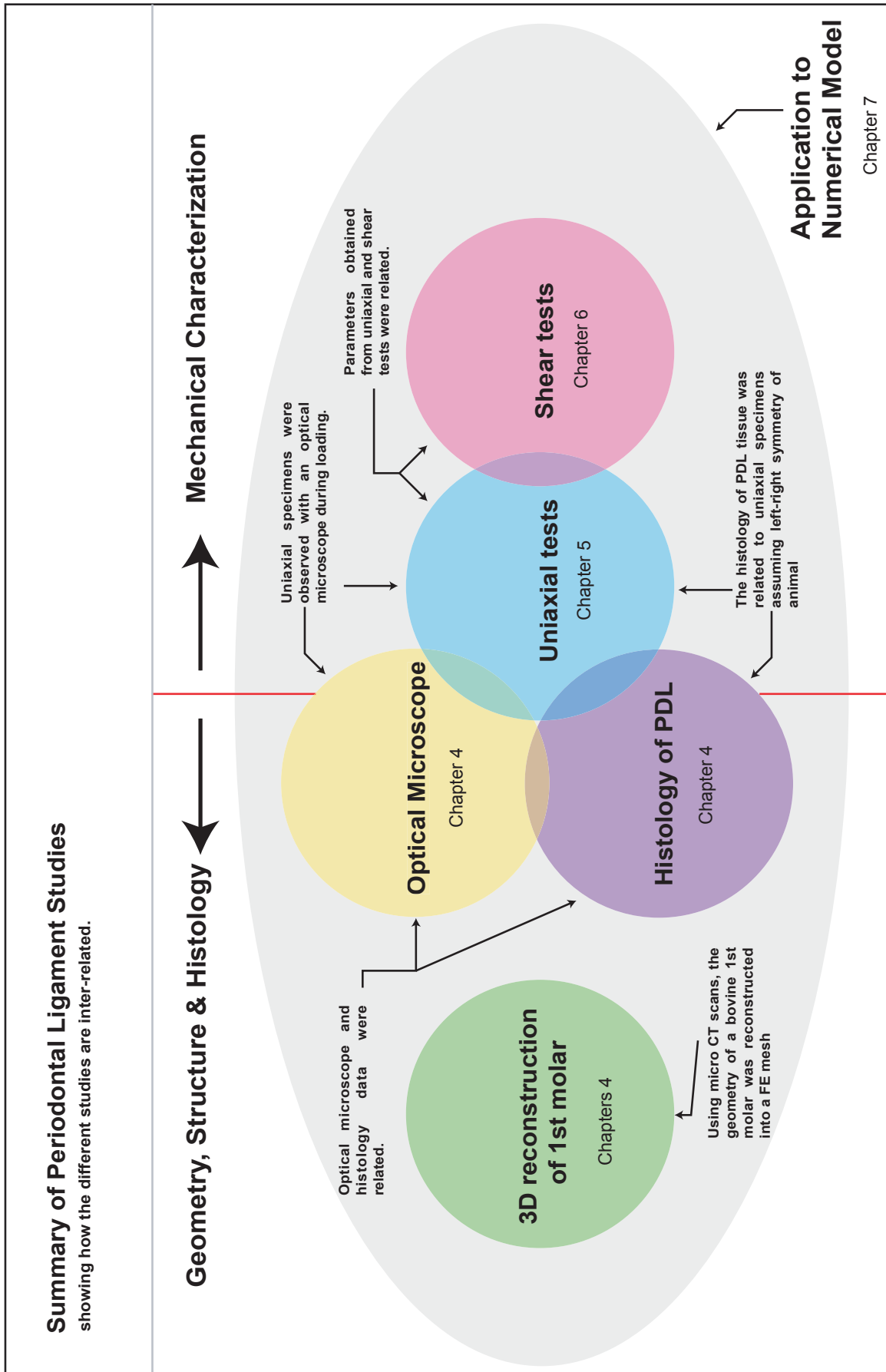
Chapter 4 presents results from studies that investigate the morphology, anatomy, histology, and the structure of the PDL. Chapter 5 is dedicated to describing the behaviour of uniaxial PDL specimens, and Chapter 6 discusses its behaviour in shear.

Based on the interpretation of the results from chapters 4, 5 & 6, a finite element analysis based on experimental results is performed on a 3D tooth reconstructed from μ CT scans in Chapter 7.

Finally, a summary of the thesis and suggestions for further work are given in Chapter 8.

The experimental studies are inter-related and are summarised in figure 1.1.

Figure 1.1 Structure of PDL studies and how they are inter-related



-
-
-

•

•

•

“I am not one who was born in the possession of knowledge;
I am one who is fond of antiquity, and earnest in seeking it there.”

Confucius

•

•

•

2

Review of Literature & Background

The periodontal ligament (PDL) is subject to study in a vast number of fields. Studies on its development, healing, pathology, biochemistry, molecular mechanisms, immunology and biology, to mention only a few, are extensive, most of which are beyond the scope of this thesis.

In this chapter, an overview of what is known about ligaments, in general terms, is given. This general information is then paralleled to what is and what is not known about the PDL as described in the literature. Concerning the PDL, two areas are reviewed. First, in order to know the geometric configuration of the PDL, literature concerning its morphology is examined. Second, the mechanical properties of the PDL identified in the literature is reviewed.

2.1 The Periodontium is an Articulation

The PDL is in fact a joint, or articulation. Articulations can be classified into three general types [Putz and Pabst 1994]:

- **synarthroses**, or immovable articulations, do not have an articular cavity and provide no mobility. Following ossification, these articulations are called synosteoses, and their function is principally to provide stability, and to absorb energy in cases of trauma. An example of a synarthrosis is the cranium.
- **diarthroses**, or synovial articulations, admit large ranges of movement, have bone covered in cartilage and are enveloped by a ligamentous capsule filled with synovial fluid. An example of a darthrosis is the knee joint.

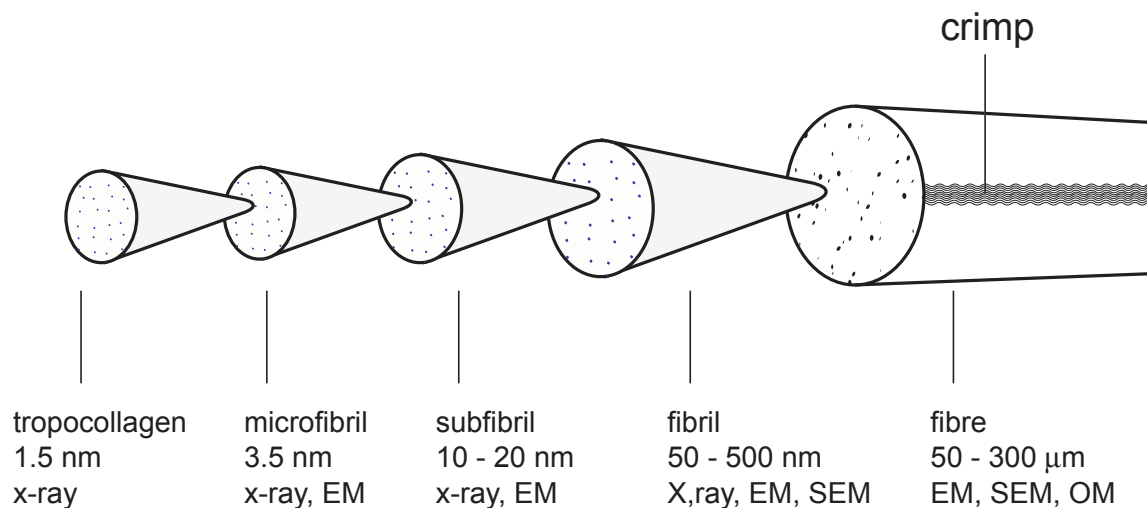
- **amphiarthroses**, do not have an articular cavity and connect bone to bone by ligamentous or cartilagenous tissue. The anchoring of teeth to the mandible by the PDL, called a **gomphosis**, is an example of this kind of articulation.

2.2 Ligaments and Morphology

The etymological origin of the word *ligament* can be traced to the latin verb *ligare* meaning *to attach*, and latin word *ligamen* meaning a string or a thread, most likely due to the filamentous, fibrous structure of ligament tissue. The primary function of ligaments is, true to its latin origin, to connect bone to bone to form an articulation, but they also ensure the passive stability of the movement of the bone-ligament-bone system. Not to be confused with tendons, a ligament has both ends inserted into bones, whereas a tendon has only one insertion. The primary function of tendons also differs in that their role is to transfer the muscular forces to the skeleton [Putz and Pabst 1994].

The morphology of the ligament as it inserts into the bone varies gradually; the fibrocytes (fibre cells) are transformed into groups of osteocytes (bone cells), first arranged in rows and then gradually dispersed into the pattern of the bone, by the way of an intermediate stage, in which the cells resemble chondrocytes (differentiated cells responsible for secretion of extracellular matrix). The collagen fibres are continuous and can be followed into the calcified tissue [Fung 1993].

Figure 2.1 Microstructural hierarchy of ligaments, evidences are gathered from x-ray, electron microscopy (EM), scanning electron microscopy (SEM) and optical microscopy (OM) (based on a model by [Nigg and Herzog 1994]).



On the macroscopic scale, a ligament resembles a collection of filamentous strings connected together to form a fibrous material. Examining the hierarchical structure of ligaments shows this tissue to be finely more complex, see figure 2.1. On the microscopic scale, ligaments are enveloped in a flexible membrane that are rich in cells, blood vessels and nerve-endings. The extracellular matrix is made up of a hierarchy of structures starting with the ligament itself of a given anatomical dimension, fibre bundles (diameter, $d=300-1000\ \mu\text{m}$), fibres (diameter, $d=50-300\ \mu\text{m}$), a fibril ($d=50-500\ \text{nm}$), a subfibril ($d=10-20\ \text{nm}$), microfibril ($d=3.5\ \text{nm}$) and ending with the tropocollagen molecule ($d=1.5\ \text{nm}$). Fibre bundles are not connected to one another, which allows a fibre bundle to slide with respect to the bundles around it. The ligament is made up of more than fibrous material. The extra-cellular matrix is comprised of two-thirds by weight of water and seems to exist in free-form linked by the weak Van der Waals polar bonds. Diffusion in water, a well-known phenomenon in biology, is the major transport mechanism of nutrients and waste of the fibroblasts. The interaction of the proteoglycans within the ligament hence determine the internal friction and thus define the viscous properties of the tissues.

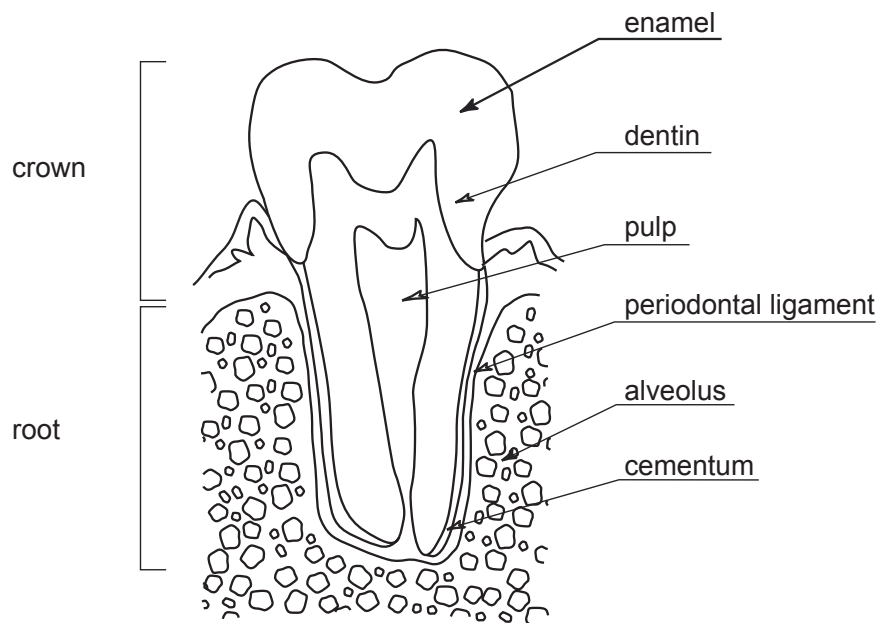
The collagen molecule secreted by the fibroblasts is the fundamental solid unit of the ligament as it makes up roughly three-quarters of the ligament by dry volume.

Elastin is a hydrophobic protein and an important constituent of the elastic fibres present in ligaments. These fibres can undergo large deformations, yet their rigidity remains inferior to that of collagen fibres. The inter connectivity of elastin forms a fibrous network, however, no periodicity is observed in electron microscopy. Elastin attaches itself to the architecture of the microfibrils as the elastic fibres are formed.

2.3 The Periodontal Ligament and Morphology

As the word *periodontal* implies, *perio* meaning *to surround* and *dontal* meaning *tooth*, the PDL is the soft connective tissue that connects the bone of the alveolus to the cementum, a bone-like tissue.

Figure 2.2 The tooth unit showing the major features of the system including the tooth, PDL and the alveolar bone.



2.3.1 Anatomy of the Tooth-PDL-Bone System

The PDL is part of the tooth-periodontium-bone system. Figure 2.2 is a schematic of tooth anatomy and situates the PDL with respect to the tooth unit system. As this figure shows, the tooth is composed of several layers [Young and Heath 2002].

- A layer of enamel, a hard, acellular and highly mineralized tissue, which makes up the **crown**, comes into direct contact with food during mastication.
- **Dentin** is a hard, avascular connective tissue making up the bulk of the tooth in both the crown and root regions.
- **Pulp**, a soft connective tissue containing the neurovascular components of the tooth.
- The **periodontium** is the term used to collectively describe the tissues involved in tooth support and attachment apparatus of the tooth. The periodontium consists of four supporting tissues:
 - 1 **cementum**, a bone-like protective covering of the tooth root.
 - 2 **periodontal ligament**, a complex connective tissue layer that immediately surrounds the root and connects it to the alveolus.
 - 3 **gingiva**, the soft tissue which overlies the bone and forms a protective collar around the tooth.
 - 4 **alveolus**, or alveolar bone, the hard tissue which surrounds the tooth root.

2.3.2 The Periodontium

The periodontium is primarily responsible for tooth mobility. The PDL shares the same general morphology of other ligaments, however, remains more complex in almost every aspect. The periodontium as an articulation is more complex, mechanics aside, to describe in shape, size and morphology than most other ligaments in the body. Ligaments generally have an easily identifiable preferred direction of filamentous tissue, for example, the colateral medial ligament of the knee. For the PDL, however, although it is believed to have a preferred fibre-direction, it remains unknown. If this direction were to be known, it would probably vary not only with the depth of the tooth, but also with the radial heterogeneity of the collagen fibres. The huge discrepancy of material parameters observed in the literature through extensive experimentation of the PDL can be attributed, to a large extent, to the difficulty in characterizing its structure.

A significant amount of research has been performed to identify the structure of the PDL, and a great deal is known about its biological composition in humans. Structurally, the PDL is composed of several elements, standard in ligament tissue [Putz and Pabst 1994]:

- collagen fibres
- elastic fibres
- vasculature and lymphatics
- cellular components
- ground substance, and
- nerve fibres.

The PDL space is often described in literature and textbooks as being thicker more gingivally, gradually becoming thinner as one moves towards the centre of rotation of the tooth, from where it becomes thicker in the apical direction [Coolidge 1937; Ralph and Thomas 1988]. The PDL width, the distance between the alveolar bone and the tooth at a given site, has been measured in humans with an average width as approximately 200-250 μm . For rats it is around 150 μm [Komatsu and Chiba 1993], for monkeys around 250 μm [Wills et al. 1976], for pigs around 250 μm , and for bovine around 500 μm [Pini et al. 2002].

Table 2.1 Comparison of PDL width of selected species

Specie	PDL width (μm)
Human	200-250
Rat	120-200
Monkey	200-250
Pig	250-300
Bovine	400-500

The physical function of the PDL is a considerable problem in dental biomechanics and is the focus of this thesis work. The PDL also has three other primary functions also subject to considerable research but are not covered in this thesis: (i) nutritional, (ii) sensory, and (iii) formative.

2.3.3 Components of the PDL Responsible for Mechanical Function

In Materials Science, a first step to understand the mechanics of any material involves studying the morphology of the material. Applying this to the PDL gives insight into its structural components and allows for one to deduce the mechanisms involved when it is subjected to stress or strain. The task of understanding the structure of biological tissues has become a science and art in itself. With the development of biological and histological investigation techniques, many articles and textbooks describe in detail the biology of the PDL, however, little has been done to relate PDL biology to its mechanical behaviour. The components of the periodontium are outlined in section 2.3.2. The following sections describe these components and, to some extent their role, in mechanical behaviour.

Collagen Fibres in the PDL

Collagen is a basic structural element for soft and hard tissues in animals. It gives mechanical integrity and strength to our bodies. Its importance to man may be compared to the importance of steel to our civilization: steel is what most of our vehicles, utensils, buildings, bridges, and instruments are made of. Collagen is the main load carrying element in blood vessels, skin, tendons, cornea, bonem fascia, etc.... [Fung 1993].

The mechanical properties of collagen are therefore important to biomechanics. But, again, in analogy with steel, studies must not only consider the properties of all kinds of steels, but also the properties of steel structures. Studies of collagen molecules, how the molecules wind themselves together into fibrils, how the fibrils are organized into fibres, and fibres into various tissues have been performed [Putz and Pabst 1994]. In each stage of structural organization, new features of mechanical properties are acquired. Since in

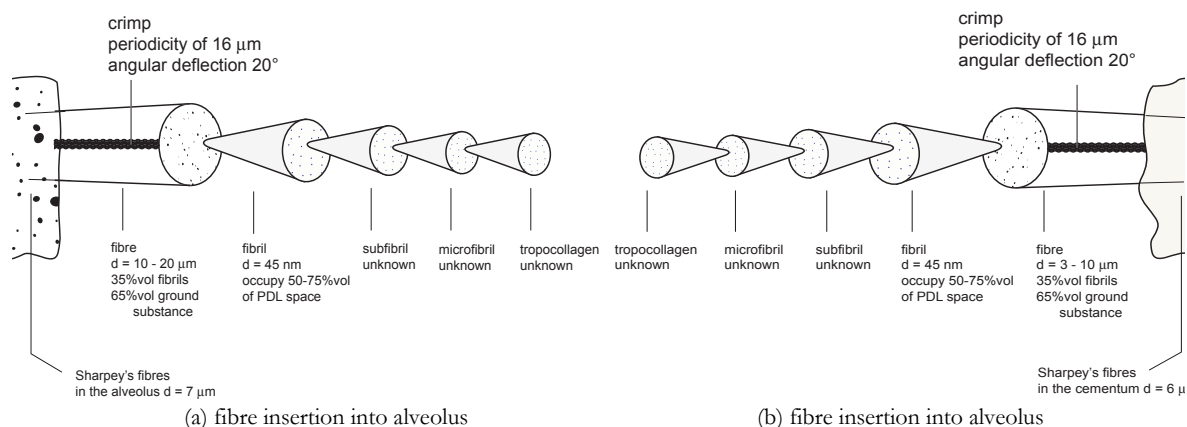
physiology and biomechanics, major attention is focused on the organ and tissue level, the relationship between function and morphology of collagen in different organs must be studied [Fung 1993].

With respect to human PDL, much work has been done to describe the biology of PDL collagen. Little information, however, is given in the literature that relates the collagen structure to the mechanical behaviour for PDL. Table 2.2 gives a summary of major works that describe collagen fibres in human PDL. Using the data outlined in Table 2.2, the schematics shown in figure 2.3 summarise what is currently known about the structural dimensions of the collagen fibres of the PDL.

Table 2.2 Summary of literature describing the collagen fibres of human PDL

Reference	Observation
[Mühlemann 1967]	Collagen fibrils occupy 53-74% volume of the PDL space.
[Jones and Boyde 1972; Jones and Boyde 1974]	Sharpey's fibres on alveolar bone have mean diameters of 7 μm . Sharpey's fibres on the cementum have mean diameters of 6 μm .
[Daly et al. 1974]	Collagen fibrils occupy 50-75% volume of the PDL space.
[Berkovitz et al. 1981]	Cross section of fibres viewed under transmission electron microscope showed that fibres are composed of 35% volume fibrils and 65% ground substance.
[Sloan 1982]	Fibers on cementum side are numerous and are around 3-10 μm in diameter. Fibers on alveolar side are less numerous and are around 10-20 μm in diameter.
[Gathercole 1987]	The crimp of fibrils in the fibre is regular with a periodicity of 16 μm and an angular deflection of 20°
[Berkovitz 1990]	Major type of collagen in the PDL is type I. 20% of collagen is of type III. Fibril diameters do not increase with age.
[Sloan and Carter 1995]	Fibril diameters in human PDL have mean diameters of roughly 45 nm.

Figure 2.3 Schematic of what is known about the hierarchy of the human PDL at the (a) alveolus junction and (b) the cementum junction.



Elastic Fibres in the PDL

Elastin fibres have been reported in several animal species, however, no study to date has been made which reports the presence of elastin in humans, rats, monkeys, mice [Sloan and Carter 1995]. In animals where elastin has been reported, these fibres are arranged perpendicularly to collagen fibre bundles. This information provides insight into the crosslinking between collagen fibre bundles, however, no definite study concludes this theory.

Vasculature in the PDL

It is generally reported and accepted in textbooks that the PDL is highly vascular. Vessel volume is considerable and it has been reported that changes in periodontal pulsation in relation to increasing loads and blood pressure occur [Imamura et al. 2002]. Vasculature makes up between 9 and 11 % volume of the PDL space [Sims 1987].

Ground Substance in the PDL

Ground substance consists of 30% by weight of glycolipids, glycoproteins, glycosaminoglycans and proteoglycans, and 70% by weight of bound water [Berkovitz et al. 1995]. It has been established that these macromolecules contribute to the viscous behaviour due to their resistance to flow under shear loading [Pini et al. 2002].

It has also been reported that water binding capacity of the PDL plays a role in mechanical function [Ferrier and Dillon 1983]. This study also implies that the water binding in the ligament could account for the viscoelastic properties at low stress, but not at higher stress.

2.4 Experimental Characterization of PDL Mechanical Behaviour

A thorough overview of the different research papers that have tested PDL tissue in humans, rodents, pigs and monkeys is part of a thesis work at the University of Medicine & Dentistry of New Jersey [Durkee 1996]. This work remarks that in the 1930s, first mechanical tests were performed on the PDL, in which several assumptions were made regarding its mechanical behaviour. These assumptions state that the PDL:

- 1 is incompressible,
- 2 is homogeneous,
- 3 is isotropic
- 4 is of uniform thickness, and
- 5 behaves in a linear-elastic manner.

Durkee also points out, and rightly so, that these initial assumptions have been reiterated in the literature up to the year 1996. Since 1996, further studies have been performed and still, no elaboration of the aforementioned assumptions has been made.

The summary of works reported in literature is presented in table 2.3. This table shows to what extent research relevant to the mechanics of the PDL tissue has been done, and how it has evolved in the past 30 years. The terms used in the heading of the table 2.3 are discussed in section 2.4.1.

2.4.1 PDL Mechanical Testing Techniques

In the literature, there are three general types of tests that have been used to study the PDL.

- The **whole tooth test**, involves the extraction or intrusion of a whole intact tooth.
- The **shear test**, involves extracting a thin transverse section of tooth, bone and PDL normal to the long axis of the tooth. Clamping the bone to a fixed table, and fixing the tooth part to a moveable device enables for the tooth-part to be extracted, or intruded, along the former long-axis of the tooth, thus testing the shear behaviour of the ligament. To present, shear tests have been performed in either the coronal (extrusive) direction or the apical (intrusive) direction, however, not both.
- The **uniaxial test**, involves extracting a small portion of bone, PDL and tooth which can then be placed into a tensile testing machine by clamping the bone and tooth portions of the sample.

Table 2.3 Summary of experimental techniques used to determine material parameters of PDL

Year and Author	uniaxial	shear	whole tooth	E (MPa)	Poisson ratio	rupture tests	constant strain rate	sinusoidal	relaxation	preconditioning	morphology	material
[Toms et al. 2002]		✓		3.62					✓	✓		human
[Toms et al. 2002]		✓							✓	✓		human
[Pini et al. 2002]	✓			7.0		✓				✓		
[Komatsu and Chiba 2001]	✓					✓	✓				✓	rat
[Durkee 1996]	✓				<0.45	✓	✓			✓		
[Komatsu and Chiba 1996]		✓				✓	✓				✓	rat
[Komatsu and Chiba 1993]		✓				✓						rat
[Chiba and Komatsu 1993]		✓		0.77-1.11		✓						rat
[Chiba et al. 1990]		✓		0.45-1.34		✓	✓				✓	rat
[Yamane et al. 1990]		✓		0.75-1.45		✓	✓					rat
[Chiba and Komatsu 1988]			✓			✓	✓				✓	rat
[Mandel et al. 1986]		✓		3.20-2.40		✓	✓					human
[Ferrier and Dillon 1983]*						✓	✓					pig
[Ralph 1980]	✓			3.10		✓	✓					human
[Atkinson and Ralph 1977]	✓			3.73		✓	✓				✓	human
[Daly et al. 1974]			✓			✓	✓			✓		human

The advantages and disadvantages of the uniaxial, shear and whole tooth tests are outlined in table 2.4.

Surprisingly, most studies on PDL have been designed to study the tissue as if it were a linear-elastic solid by subjecting it to constant strain rate deformation. Although PDL was reported as showing non-linear behaviour over 60 years ago, almost all experimental studies have considered the PDL in rupture tests with the exception of some recent relaxation studies most recently by [Toms et al. 2002]. The majority of literature reports an elastic modulus however nothing has been said about a Poisson's ratio. It is only until recently that attempts in describing non-linearity have been attempted.

2.4.2 Reported Experimental Loading Profiles on PDL

The experimental work summarised in table 2.3 shows how the majority of studies tested the PDL to rupture at a given constant strain rate. With the exception of recent works, little attention has been given to the rate effects. It was shown that the mechanical behaviour of rat PDL is time-dependant [Komatsu and Chiba 1993], but this time dependency has not yet been quantified. Relaxation tests on human PDL strongly supports the notion of time-dependency, however, a simple understanding of this time-dependency remains unclear, and not studied according to viscoelastic theory. Basic theory of time-dependency and viscoelasticity of soft tissues is presented in section 2.7.

Table 2.4 Comparison of Uniaxial, Shear and Whole Tooth Testing Methods of PDL

Test	Advantages	Disadvantages
Uniaxial	<ul style="list-style-type: none"> • it is possible to test the ligament in both compression and tension • the easily measurable specimen dimensions make for more accurate load-deformation to stress-strain conversions • the small size of the specimen simplifies, to some extent, experimental interpretation of data • more realistic when constitutive equations are of interest • possible to observe sample with optical microscope during testing to observe morphological changes 	<ul style="list-style-type: none"> • small size of sample making it difficult to prepare handle, delicate, and easy to damage • must determine minimum size of sample in order to ensure an acceptable amount of damage to PDL structure and fibres • <i>in vivo</i> tests not possible
Shear	<ul style="list-style-type: none"> • allows to test in the physiological direction of loading (e.g. simulate chewing on thin section of tooth in natural loading direction) • testing in one direction, either extrusive or intrusive, is simple 	<ul style="list-style-type: none"> • testing in both apical and coronal direction is more difficult • the stress calculations are less accurate since measured load values must be approximated over irregular form the tooth • <i>in vivo</i> tests not possible
Whole Tooth	<ul style="list-style-type: none"> • possible to perform this test <i>in vivo</i>. • useful to study tooth mobility under functional loading to validate a numerical model. 	<ul style="list-style-type: none"> • <i>in vivo</i> tests are limited to small strains to remain well below pain-threshold of subject • testing apparatus to be placed into mouth is difficult to design • measured behaviour must be averaged over the entire root • highly irreproducible results from tooth to tooth due to the complex 3D geometry of a root.

The time-dependent effects of the PDL are most probably responsible for the large discrepancy in material parameters, namely the elastic modulus, reported in literature. Comparing the constant strain rates used in rupture experiments gives values ranging

from $0.01 \mu\text{m} \cdot \text{s}^{-1}$ to $200 \mu\text{m} \cdot \text{s}^{-1}$, or 4 orders of magnitude. The variation of reported elastic moduli spans almost 2 orders of magnitude based on experimental results, and over 4 orders of magnitude based on numerical studies.

Taking into account the time-dependency of the PDL remains crucial to its characterization. It is for this reason that the PDL must be subjected to **preconditioning**, **relaxation** tests (and/or) **creep** tests, and **sinusoidal** oscillations to better understand its complex behaviour. These different types of loading profiles are discussed in section 2.7.4.

Overview of Whole Tooth Movement Studies

It was shown that maxillary incisors demonstrate characteristic soft tissue response, and that upon load removal, the teeth return to rest position in two phases, first an immediate recoil, and second a slow viscous return to the original position [Parfitt 1960].

Monkeys have been used in tooth movement studies [Picton and Wills 1978; Picton 1984] and it was postulated that polymerization of ground substance molecules occurred at low load levels resulting in a decrease in tooth mobility [Picton 1989]. Extrusive movements were always less than intrusive displacements when the teeth were subjected to cyclic tensile and compressive loads [Picton 1986]. It was suggested that the most apical fibres at the base of the tooth root were stretched to their fullest extent after only a small extrusive displacement.

In addition to the intrusive/extrusive type testing, mobility due to horizontal loading of incisors, i.e. distal/mesial and buccal/lingual directions, has also been studied in intact [Picton and Davies 1967] and traumatized [Picton and Slatter 1972] monkeys *in vivo*. As the tooth was loaded, it was observed that the root would move in the direction opposite to the applied load. As the load direction was reversed, however, the root was found to move in the same direction as the applied load. This finding could be explained by a shifting of the centre of rotation of the tooth. This phenomena was also observed by Nagerl [Nagerl H et al. 1991].

Studies on human teeth have also been performed *in vivo* [Daly et al. 1974]. A custom-made loading device was used to apply torsional loads to human incisors showing a non-linear response with hysteresis. The hystereses increased with the frequency of loading, however, no explanation was offered to describe this behaviour.

Whole tooth extraction has been performed by inserting a small diameter loading rod inserted into the pulp canal to pull out an entire tooth in order to determine the ultimate strength of the PDL of the whole tooth. It is worthwhile to note that pulling a tooth out of its socket is not a measure of the ultimate tensile strength, but of an averaged ultimate shear strength if the PDL is considered as a continuum.

Overview of Uniaxial Testing of PDL

Tests in 1D on small samples of PDL have been performed by obtaining intact bone-PDL-tooth segments and pulling apart the bone and the tooth. In one study, the bone fragment and the tooth were each attached to acrylic rods [Atkinson and Ralph 1977] before being pulled apart. In this study, it was found that the said elastic properties of the ligament were not affected by the rate of loading. Ralph [Ralph 1980] also studied the ultimate strength of the PDL in humans using freshly extracted teeth with remaining fragments of PDL and bone. This study showed that the PDL fibres rupture in a step-like manner. Extensive work in traction has been performed by Chiba and Komatsu on rat and rabbit tissue [Chiba and Komatsu 1980; Chiba and Komatsu 1988; Komatsu 1988; Chiba et al. 1990; Chiba and Komatsu 1993; Komatsu and Chiba 1993; Komatsu and Chiba 1996; Komatsu and Chiba 1996; Komatsu and Viidik 1996; Komatsu and Chiba 2001]. The primary focus of these works has been to identify the rupture mechanisms and rupture parameters of the PDL.

With respect to uniaxial testing, little work has been performed in the physiological range of the PDL, thus the functional loading parameters have yet to be identified.

Overview of Shear Testing of PDL in Transverse Sections

Few shear-type experiments have been performed on transverse sections of the periodontium. A study on human autopsy material involved pushing teeth out from clamped transverse sections of the mandible [Mandel et al. 1986]. All samples were loaded to failure and load curves demonstrated typical non-linear soft tissue behaviour. Chiba [Chiba et al. 1990; Chiba and Komatsu 1993] also measured the load and relative deformation required to push rat teeth directly out of their sockets. It was noted that when a tooth is extruded from its socket, the fibres ruptured unevenly due to the root curvature and to the different alignment of the fibres. Toms [Toms et al. 2002; Toms et al. 2002] has also performed shear tests on human cadaverous tissue following the same technique as Mandel [Mandel et al. 1986]. Before rupturing the specimen, relaxation tests were also performed giving rise to some characteristic relaxation times for human PDL in shear.

In all three studies [Mandel et al. 1986; Chiba et al. 1990; Toms et al. 2002; Toms et al. 2002], the loading of these specimens was performed in only the extrusive direction so information as to the shear behaviour of the PDL in the intrusive direction remains unknown. Comparing the behaviour in the intrusive and extrusive directions would give information as to the isotropy or anisotropy of the tissue.

2.4.3 Use of Material Properties in Finite Element Models

Modulus of elasticity and Poisson's Ratio

Referring to the thesis by Durkee [Durkee 1996] and confirmed by a more recent review of literature in the thesis work by Pini [Pini 1999], the elastic modulus of the PDL in finite element (FE) articles span almost four orders of magnitude (see section 2.4.2). This discrepancy is too great to be attributed to any intrinsic property of the ligament. With regards to the Poisson's ratio, for which values can theoretically range between 0.0 to 0.5, FE articles assume values between 0.0 and 0.499. One could attribute the variation of Poisson's ratio to the non-existence of any such value in the literature. In fact, most FE papers do not cite their sources of the elastic modulus, nor of the Poisson's ratio. Figure 2.4 summarises the finite-element studies on the tooth system, and indicates where papers cite the material parameters used in their specific model. On one hand, the literature shows a considerable amount of interest in this field that has evolved since the 1930s. On the other hand, it shows the lack of collaboration and exchange of data between the PDL experimental world and the PDL numerical world. With reference to section 2.4, finding experimental data suitable for a FE modelisation is difficult, which explains, to some extent, the approximations made in most numerical analyses of PDL.

In short, progress in numerical analyses and FE modelisation, whether in the scope of dental implantology, operative dentistry, fixed prostheses, removable prostheses, facial and cranial skeletal structures or dental materials, are significantly hindered in that no reliable experimental data exist to allow accurate prediction of tooth mobility.

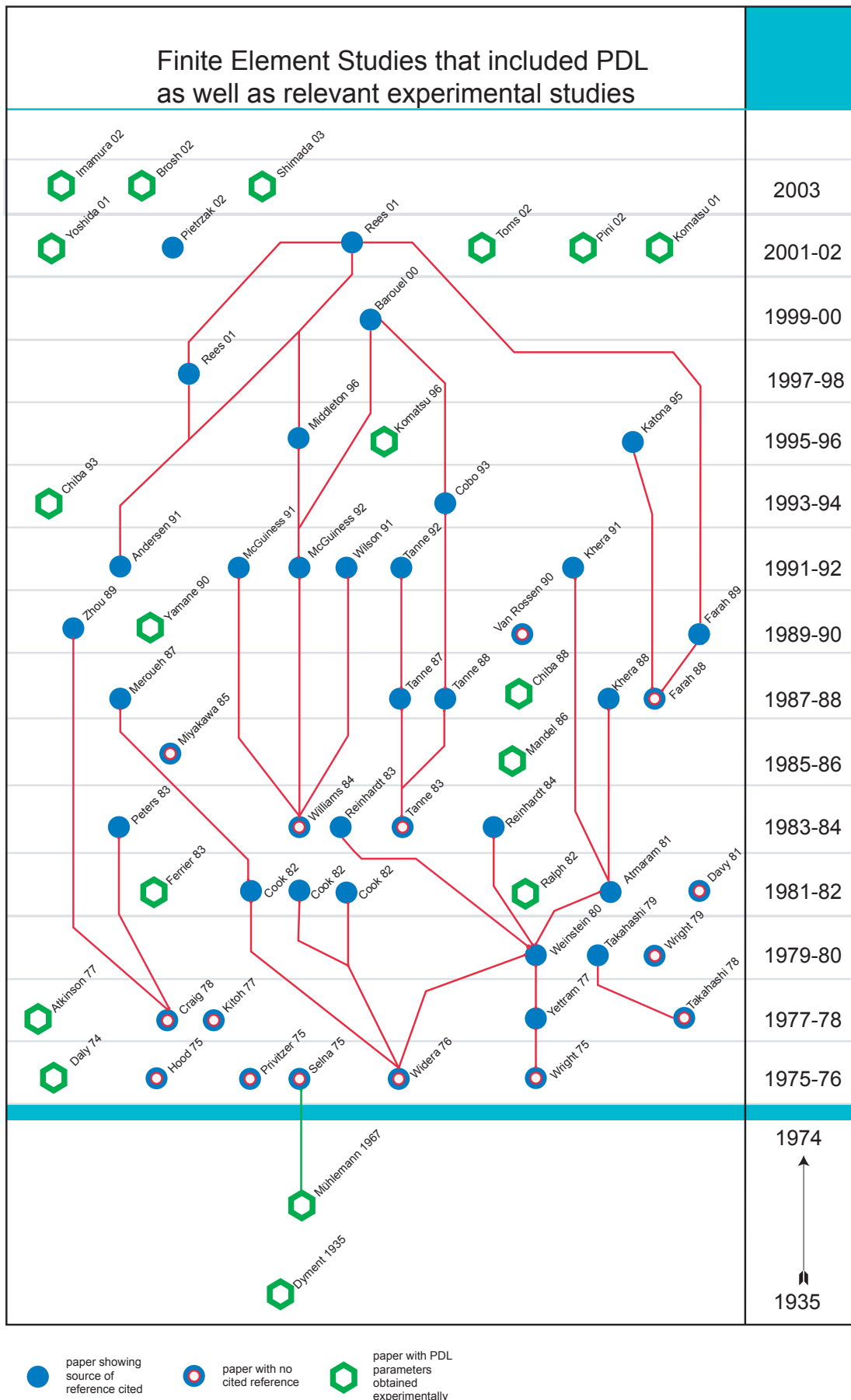
2.5 Theoretical Modeling of the PDL Mechanical Behaviour

Modeling the mechanical behaviour of the PDL is essential to predict tooth mobility. A tooth being virtually rigid and connected to an almost as rigid alveolar bone clearly leads one to assume that tooth displacement is governed primarily by the PDL. The major problem in dental biomechanics, is therefore the modeling of PDL mechanical behaviour.

2.5.1 Elasticity of the Periodontal Ligament

In general, attempts to describe PDL behaviour is simplistic. It is seen from experimental data that the PDL behaves in a nonlinear fashion, however, almost all constitutive laws which have been used are based on the assumption that the PDL is linear elastic, i.e. small strain, stress is proportional to strain and loading rate independence. More recently, nonlinear elastic laws, i.e. large strains and stiffening elasticity, have been presented to describe PDL behaviour. For both the linear and nonlinear cases, the PDL is considered to be homogeneous-isotropic and time-independent.

Figure 2.4 Chart of finite-element papers and reference to published experimental results



Linear Elastic Isotropic Models to Describe PDL Behaviour

The Hooke-Lamé law (see equation 2.21) describes a linear elastic, time-independent isotropic material. Only two parameters are required to describe such a material: (i) the elastic modulus, or Young's modulus, and (ii) Poisson's ratio. Rees [Rees and Jacobsen 1997] gives an overview of the elastic moduli and Poisson's ratio reported in literature. Most simulations of tooth mobility use Hooke-Lamé to describe PDL behaviour [Williams and Edmundson 1984; Tanne et al. 1988; Middleton et al. 1990; McGuinness et al. 1992; Wilson et al. 1994; Tanne et al. 1998] however using such a law to describe PDL behaviour assumes small strains, linear elasticity, homogeneity and isotropy, all of which are contradictory to the observed PDL behaviour determined through experiments.

Nonlinear Elastic Isotropic Models to Describe PDL Behaviour

Durkee [Durkee 1996] used a piece-wise linear law determined from experiments on uniaxial specimens (to see what is meant by uniaxial specimens, see section 3.4). The non-linearity defined in this analysis remains unclear, as it fails to consider the geometric and material hypotheses of the law, i.e. small vs. large strain etc..., are not specified.

In a study performed by Pietrzak [Pietrzak et al. 2002], the PDL behaviour is described by a nonlinear elastic *split* law. Based on the linear elastic law of St. Venant-Kirchhoff, the split law is developed for large strains and requires four material coefficients to describe PDL behaviour: (i) the elastic modulus, (ii) Poisson's ratio, (iii-iv) and two exponents defining the curvatures of the uniaxial compression and tension curves. This law is able to describe the nonlinear stiffening behaviour of the PDL much more accurately than in previous works and has been verified with experimental works presented by Pini [Pini 1999; Pini et al. 2002].

A new nonlinear stiffening power elastic law with application to the PDL is currently being developed and is the work of the thesis by Justiz [Justiz 2004].

2.5.2 Viscosity of the Periodontal Ligament

There are few works in literature that have considered viscosity in the modeling of the PDL. Models that do exist have only proposed linear viscous elements. A nonlinear viscous description of the PDL has, to our knowledge, not been done.

Linear Viscous Laws and the PDL

The behaviour of the PDL has been compared to the Kelvin-Voigt (parallel), Maxwell (series) and Zener-Poynting (standard) rheological models. Bien [Bien and Ayers 1965] used the Maxwell model to describe the relaxation of a rat tooth. Wills and Picton [Wills et al. 1972; Picton and Wills 1978] suggested that a Voigt model could be used to describe PDL creep. Provatidis [Provatidis 2000] has used more sophisticated models and

finite-element techniques to suggest viscoelastic behaviour, however, only Middleton [Middleton et al. 1990] has attempted to simulate the PDL using a linear viscoelastic law.

Nonlinear Viscous Laws and the PDL

Nonlinear viscoelastic models would include large strains and strain-rate, nonlinear elasticity and nonlinear viscosity. In other words, such a model would consider the geometric and kinematic nonlinearities and consider its mechanical behaviour to be non-Hookean elastic and non-Newtonian viscous. To our knowledge, no models of this complexity have been reported in the literature for the PDL.

2.6 Continuum Mechanics, Biomechanics and the Constitutive Equation

In the biological world, atoms and molecules are organised into cells, tissues organs, and individual organisms. The focus of biomechanics is in the movement of matter inside and around the organisms. Because the PDL is being studied at the cellular, tissue, organ and organism level, it is sufficient to take Newton's laws of motion as an axiom.

In mathematics, the real number system is a continuum. Between any two real numbers there is another real number. The classical definition of a material continuum is an isomorphism of the real number system in a three-dimensional Euclidean space: between any two material particles there is another material particle.

In this section, the framework of continuum mechanics is summarized and the major parameters used to interpret the experimental results of this thesis are presented.

2.6.1 Continuum Mechanics Background

Continuum mechanics aims at describing motion of continuous deformable bodies by means of the force, moment and energy balance principles as well as constitutive laws relating the kinematic to the dynamic aspects. The hypothesis of continuity presumes that the dimensions of the bodies are sufficiently large with respect to their microscopic structure.

Kinematics

In material or Lagrangian description chosen for our purposes, each particle of a body \mathbf{B} is labelled by its reference position \mathbf{x} at $t = 0$. The present deformed position \mathbf{y} at time t of each particle is defined by a map of the reference position \mathbf{x} (see figure 2.5):

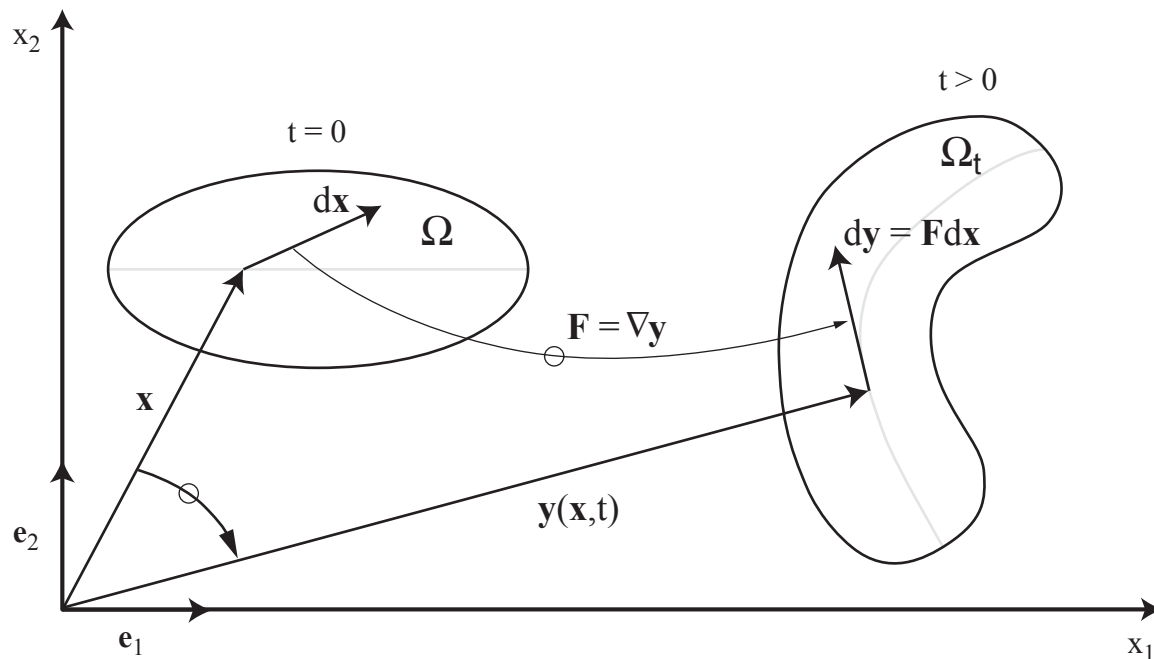
$$\mathbf{y} = \mathbf{y}(\mathbf{x}, t) \quad \text{with} \quad \mathbf{y}(\mathbf{x}, 0) = \mathbf{x} \quad (\text{EQ 2.1})$$

The map $\mathbf{y}(\mathbf{x},t)$ transforming the reference configuration Ω of the body \mathbf{B} into the present configuration Ω_t is called motion or deformation.

The associated displacement is defined as:

$$\mathbf{u} = \mathbf{u}(\mathbf{x}, t) \equiv \mathbf{y}(\mathbf{x}, t) - \mathbf{x} \tag{EQ 2.2}$$

Figure 2.5 Reference and present configurations used in the Lagrangian description.



The deformation of an infinitesimal linear element $d\mathbf{x}$ is given by:

$$d\mathbf{y} = \mathbf{F}d\mathbf{x} \tag{EQ 2.3}$$

where \mathbf{F} is the asymmetric deformation gradient:

$$\mathbf{F} = \mathbf{F}(\mathbf{x}, t) \equiv \nabla \mathbf{y} = \frac{d\mathbf{y}}{d\mathbf{x}}(\mathbf{x}, t) \tag{EQ 2.4}$$

The displacement gradient \mathbf{H} is defined as:

$$\mathbf{H} = \mathbf{H}(\mathbf{x}, t) \equiv \nabla \mathbf{u} = \mathbf{F} - \mathbf{I} \tag{EQ 2.5}$$

The rates of the deformation and displacement gradients are equal (note that the *dot* denotes a time-derivative):

$$\dot{\mathbf{F}} = \nabla \dot{\mathbf{y}} = \frac{\partial^2 \mathbf{y}}{\partial \mathbf{x} \partial t}(\mathbf{x}, t) = \dot{\mathbf{H}} \quad (\text{EQ 2.6})$$

An objective measure of deformation is given by the symmetric Green-Lagrange material strain tensor (\mathbf{T} denotes the transpose of \mathbf{H}):

$$\mathbf{E} = \mathbf{E}(\mathbf{x}, t) \equiv \frac{1}{2}(\mathbf{F}^T \mathbf{F} - \mathbf{I}) = \frac{1}{2}(\mathbf{H} + \mathbf{H}^T + \mathbf{H}^T \mathbf{H}) \quad (\text{EQ 2.7})$$

For small deformations ($\|\mathbf{E}\| \ll 1$):

$$\mathbf{E} \cong \frac{1}{2}(\mathbf{H} + \mathbf{H}^T) \quad (\text{EQ 2.8})$$

$$\dot{\mathbf{E}} \cong \frac{1}{2}(\dot{\mathbf{H}} + \dot{\mathbf{H}}^T) \quad (\text{EQ 2.9})$$

Dynamics

The external forces that act on the solid are divided into body and contact forces. They are assumed to be continuously distributed over Ω . The present body and inertial force densities are defined per unit volume of the reference configuration:

$$\mathbf{b} = \mathbf{b}(\mathbf{x}, t) \quad (\text{EQ 2.10})$$

$$\quad (\text{EQ 2.11})$$

$$\rho \ddot{\mathbf{y}} = \rho(\mathbf{x}, t) \ddot{\mathbf{y}}(\mathbf{x}, t)$$

where ρ is the material density defined in the reference configuration Ω . The present contact forces are characterized by a nominal stress vector defined per unit reference area:

$$\mathbf{p} = \mathbf{p}(\mathbf{x}, t) \quad (\text{EQ 2.12})$$

The external forces are then assumed to produce internal contact forces $\partial\mathbf{q}$ on the surface $\partial\omega_o$ of any part $\omega_o \subseteq \Omega_o$ again represented by a nominal stress vector \mathbf{p} defined per unit area of the reference configuration, which depends only on the surface orientation:

$$d\mathbf{q} = \mathbf{p}(\mathbf{x}, t, \mathbf{n}(\mathbf{x}))dA \quad (\text{EQ 2.13})$$

where $\mathbf{n}(\mathbf{x})$ refers to the outward unit normal to the surface $\partial\omega_o$ and dA to its area element. Applying the balance principle of force to an infinitesimal tetrahedron, Cauchy's theorem states that the nominal stress vector \mathbf{p} depends linearly on \mathbf{n} and thus demonstrates the existence of an asymmetric nominal (Piola-Kirchhoff-I) stress tensor \mathbf{P} such that:

$$\mathbf{p}(\mathbf{x}, t, \mathbf{n}(\mathbf{x})) = \mathbf{P}(\mathbf{x}, t)\mathbf{n}(\mathbf{x}) \quad (\text{EQ 2.14})$$

An objective measure of internal forces per unit area is given by the symmetric material (Piola-Kirchhoff-II) stress tensor:

$$\mathbf{S} = \mathbf{S}(\mathbf{x}, t) = \mathbf{F}^{-1}(\mathbf{x}, t)\mathbf{P}(\mathbf{x}, t) \quad (\text{EQ 2.15})$$

Under the assumption of small deformations ($\|\mathbf{E}\| \ll 1$):

$$\mathbf{S}(\mathbf{x}, t) \cong \mathbf{P}(\mathbf{x}, t) \quad (\text{EQ 2.16})$$

The Piola-Kirchhoff stress tensor is discussed in further detail in section 2.6.3.

2.6.2 Non Linear Homogeneous Isotropic Elasticity

A tensor function $\hat{\mathbf{S}} = \mathbf{E} \rightarrow \hat{\mathbf{S}}[\mathbf{E}]$ that satisfies $\hat{\mathbf{S}}[\mathbf{RER}^T] = \mathbf{R}\hat{\mathbf{S}}[\mathbf{E}]\mathbf{R}^T$ for all rotations \mathbf{R} is said to be isotropic. The most general form of a non linear elastic isotropic and homogeneous material can be expressed

$$\mathbf{S} = \mathbf{S}[\mathbf{E}] = \alpha\mathbf{I} + \beta\mathbf{E} + \gamma\mathbf{E}^2 \quad (\text{EQ 2.17})$$

where

$$\alpha = \alpha(E_1, E_2, E_3)$$

$$\beta = \beta(E_1, E_2, E_3)$$

$$\gamma = \gamma(E_1, E_2, E_3)$$

such that E_1 , E_2 and E_3 are the first, second and third invariants of tensor \mathbf{E} , respectively. For equation 2.17, α , β and γ are specific to any given material whereas \mathbf{I} , \mathbf{E} and \mathbf{E}^2 , are said to be generators common to all materials.

2.6.3 Linear Homogeneous Isotropic Elasticity: Kirchhoff-St. Venant Law

The material law for linear elastic homogeneous isotropic materials, also known as the Kirchhoff-St. Venant law, is deduced from equation 2.17. The invariants E_1 , E_2 and E_3 are 1st, 2nd and 3rd degree homogeneous functions of \mathbf{E} respectively and in this case only $E_1 = \text{tr}\mathbf{E}$ will remain. Its coefficients α , β and γ of \mathbf{I} , \mathbf{E} and \mathbf{E}^2 are a function, a constant and nul, respectively, giving

$$\mathbf{S}[\mathbf{E}] = (\alpha_0 + \alpha_1 \text{tr}\mathbf{E})\mathbf{I} + \beta_0\mathbf{E} \quad (\text{EQ 2.18})$$

The condition imposed by its initial reference state $\mathbf{S}[\mathbf{0}] = \alpha_0\mathbf{I} = \mathbf{0}$ implies that $\alpha_0 = 0$ which, with a change of notation, leads to the classic expression of the Kirchhoff-St. Venant Law:

$$\mathbf{S}[\mathbf{E}] = \lambda \text{tr}(\mathbf{E})\mathbf{I} + 2\mu\mathbf{E} \quad (\text{EQ 2.19})$$

where

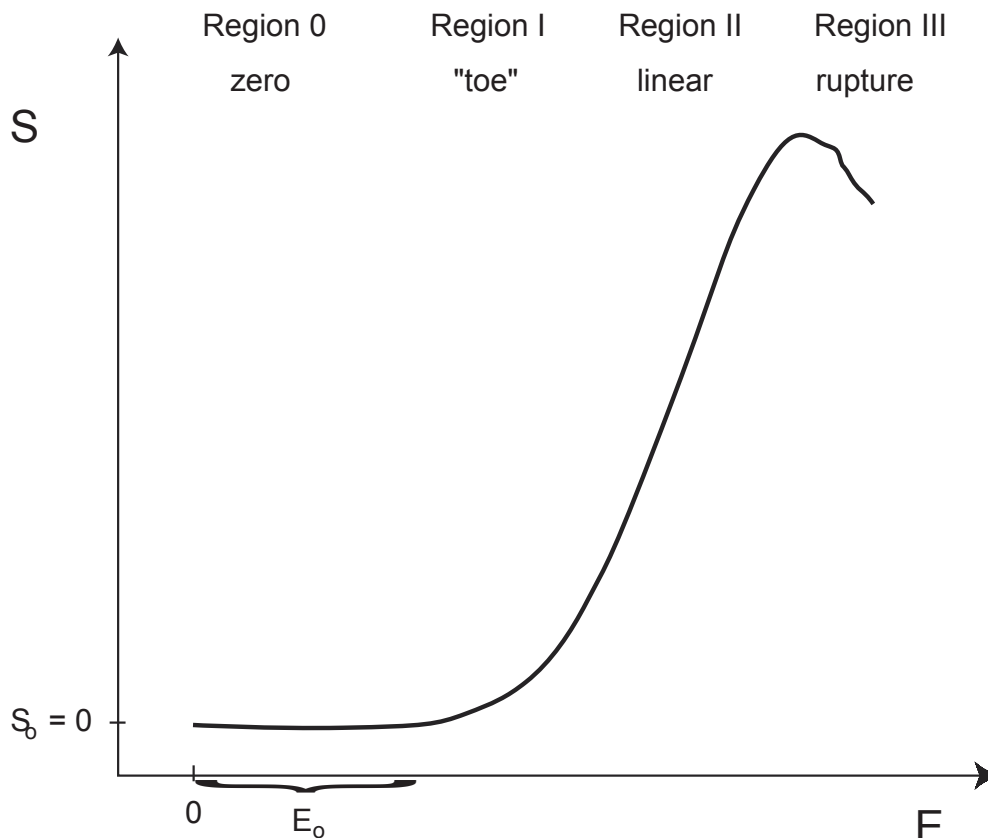
λ = Lamé partial tensile *elastic constant*

μ = Lamé shear *elastic constant*

2.7 Viscoelasticity and Biological Tissue

A typical stress-strain curve for a ligament tested in simple uniaxial elongation at a constant strain rate is shown in figure 2.6. This curve can be divided into four distinct regions. In region I, the load in the ligament increases exponentially with increasing deformation. In region II, the relationship is fairly linear. In region III, the relationship is nonlinear and ends with rupture. Region I is often referred to as the “toe” region and usually represents the physiological range of the tissue under normal function. The regions II and III correspond to the reserve strength of the ligament. Region 0 is not discussed in the literature. In fact, Fung’s biomechanics textbook [Fung 1993] and the majority of articles do not report data in this “zero” region and results are defined with a zero starting only in region I. Although not reported in the literature, results from this thesis show that region “zero” is fundamental in understanding the mechanical behaviour of the PDL.

Figure 2.6 A typical stress-strain curve for the periodontal ligament in tension.



It is accepted that ligament tissue is intrinsically viscoelastic. For the PDL, notions of viscoelastic behaviour have been reported in experimental papers [Wills et al. 1972; Wills et al. 1976; Komatsu and Chiba 1993; Durkee 1996; van Driel et al. 2000]. Examining these works, however, points out a lack in the interpretation of viscoelastic response. The fact that a stress vs. strain plot of a ligament deformed under a constant load is not a straight line cannot solely be taken as an indication that the material response is nonlinear. This characteristic is seen to be a natural consequence of time dependency (see section 2.7.3). The extent of deviation from a straight line encountered in an experiment depends on several factors, namely the strain rate and the maximum strain imposed on the specimen. To examine the influence of time, the scaling and superposition properties of linearity of response can be used as part of a broader testing program that take into account rate effects. Rate effects, i.e. linearity of response, strain rates and relaxation curves, are discussed later in this section.

2.7.1 Linear Elastic Solid

The one-dimensional response of an elastic solid is analogous to a linear spring (see figure 2.7a) where the force-deformation relation is given by:

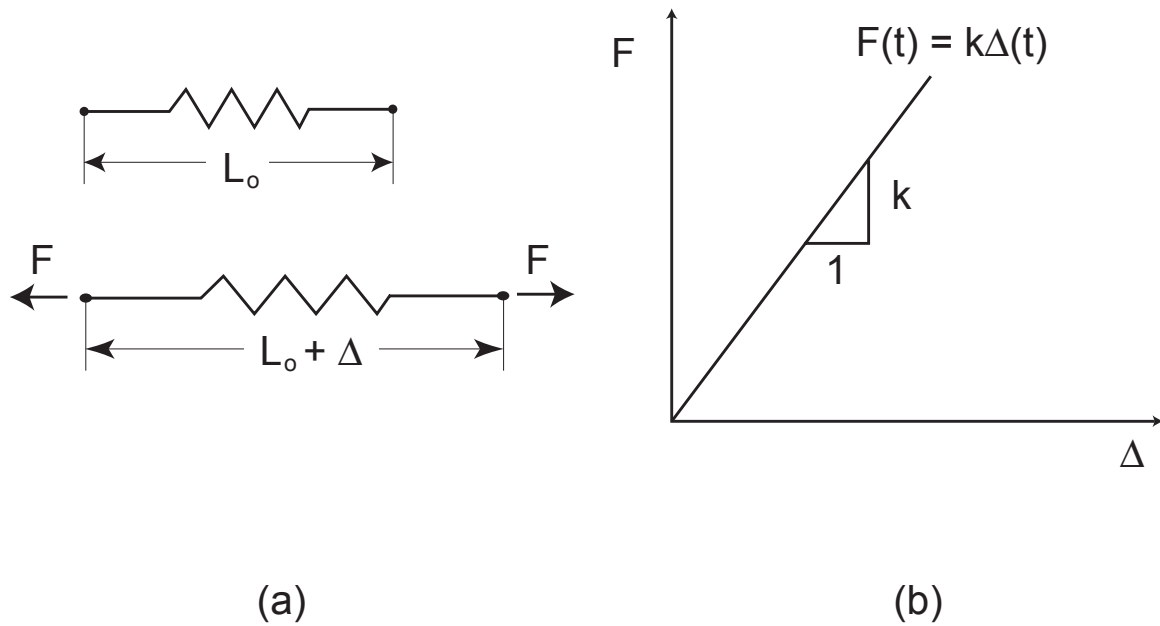
$$F = k \cdot \Delta \quad (\text{EQ 2.20})$$

where F is the force, Δ is the elongation, and k is the spring constant. By associating the force F with the stress S and elongation Δ with the strain E the stress-strain relation is obtained:

$$S(t) = \varepsilon \cdot E(t) \quad (\text{EQ 2.21})$$

where ε is the Young's modulus, or modulus of elasticity. Past research on the PDL has most often taken this approach to describe the mechanical response of the PDL. (see section 2.4.2).

Figure 2.7 Schematic of a mechanical spring representing a linear elastic solid. (a) mechanical analog - linear spring, (b) force-elongation relation for the spring.



2.7.2 Linear Viscous Fluid

The one-dimensional response of a linear viscous fluid can be represented by a viscous damper as shown in figure 2.8. A viscous damper, or dashpot, is represented as a piston in an oil bath in a cylinder. The damper response is characterized by the relation

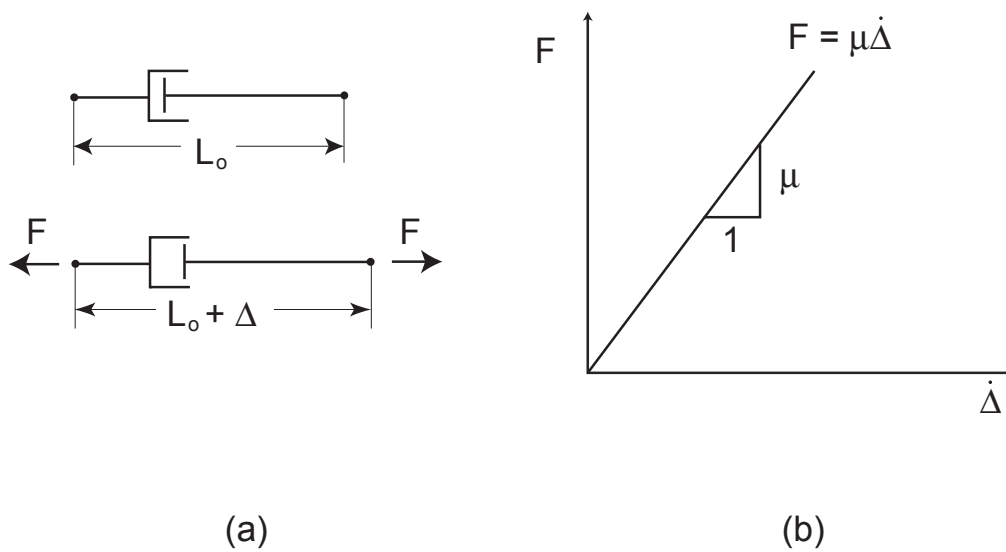
$$F = c \cdot \dot{\Delta} \tag{EQ 2.22}$$

where c is viscosity and $\dot{\Delta}$ is the elongation rate $d\Delta/dt = \dot{\Delta}$. This implies that the stress-strain relation of a linear viscous fluid is given by

$$S = \mu \cdot \dot{E}(t) \tag{EQ 2.23}$$

where μ represents the viscosity, the fluid's material property.

Figure 2.8 Schematic of a mechanical dash-pod, or viscous damper, representing a linear elastic solid. (a) mechanical analog - viscous damper, (b) force-elongation relation for the viscous damper.



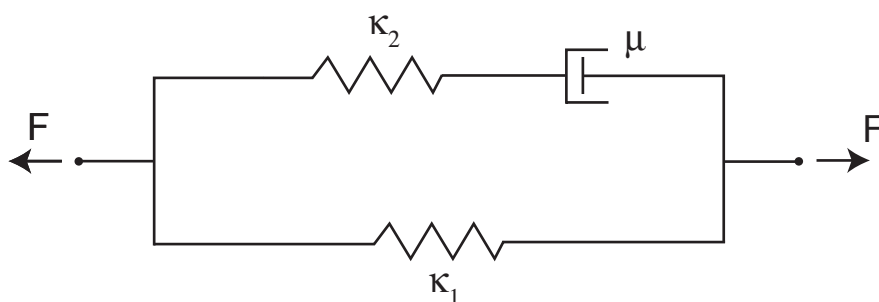
2.7.3 Response of a Viscoelastic Material

Viscoelastic response in one-dimension can be described as a combination of elastic solid and viscous fluid responses. There is no unique mechanical analog which describes a viscoelastic system, rather there are plenty. Mechanical analogs to viscoelastic behaviour are a combination of springs and dashpots into more complicated mechanical systems that capture the time dependent mechanical response. For a deeper look into the theory of viscoelasticity refer to the book by Wineman [Wineman and Rajagopal 2000].

Three-Parameter Standard Viscoelastic Model

The simplest model that provides a satisfactory simulation of observed viscoelastic response is the Zener-Poynting model, also known as the standard model. A schematic of the mechanical analog of the standard model is shown in figure 2.9.

Figure 2.9 Three-Parameter Standard Viscoelastic Model



2.7.4 Characterizing Material Properties

The mechanical response of a linear elastic solid can be characterized by (i) showing that S is proportional to E , and (ii) determining the slope of the S - E curve. The slope is all that is needed to describe the mechanical response of such a material and therefore the slope, or elastic modulus, is considered as a material property. In fact, the shape of the entire S - E curve is a material property, but since the S - E curve of the linear elastic solid is simply a straight line, it is more convenient to describe its material property with the elastic modulus. If one is given a material whose S - E plot is non-straight or curved, then it is no longer possible to describe the material with a single parameter and the problem of characterizing the material has become more difficult. Thus, the entire S - E curve, called the function $f(E)$ is the material property which describes this material with a non-linear response.

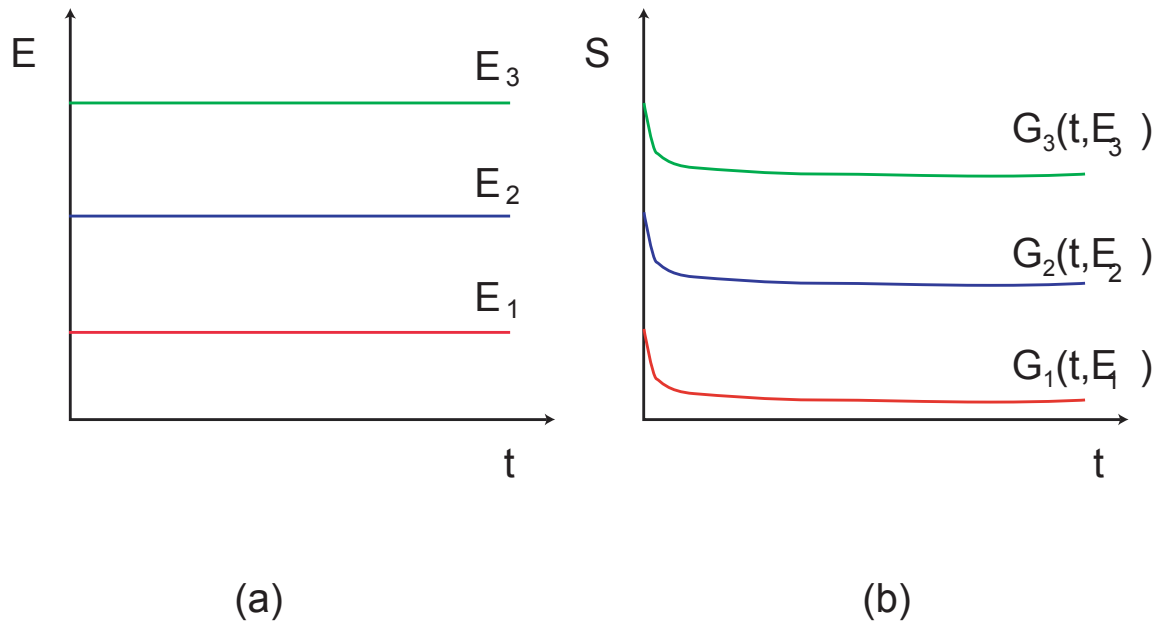
Characterizing a viscoelastic material involves a similar approach. Standard tests can be performed for determining its mechanical response, however, the entire response curve would characterize the material rather than just a single parameter. Within the scope of this thesis, three non-destructive tests have been chosen that can be performed to help characterize the material response of the PDL [Wineman and Rajagopal 2000]. They are:

- 1 stress relaxation tests,
- 2 constant strain rate deformation tests,
- 3 sinusoidal oscillations tests.

Stress Relaxation Test

A specimen subjected to step strain at different strain levels is shown in Figure 2.10. For each step strain value, there is a corresponding stress relaxation curve. Let $G(t, E_i)$ denote the relaxation function at time t at strain E_i ; since $E(t) = 0$ for $t < 0$, it is also required that $G(t, S_i) = 0$ for $t < 0$. The function $G(t, E_i)$ is a response function for the material.

Figure 2.10 Steps at (a) different strain levels E_1 , E_2 and E_3 and (b) corresponding stress relaxation functions G_1 , G_2 and G_3 .



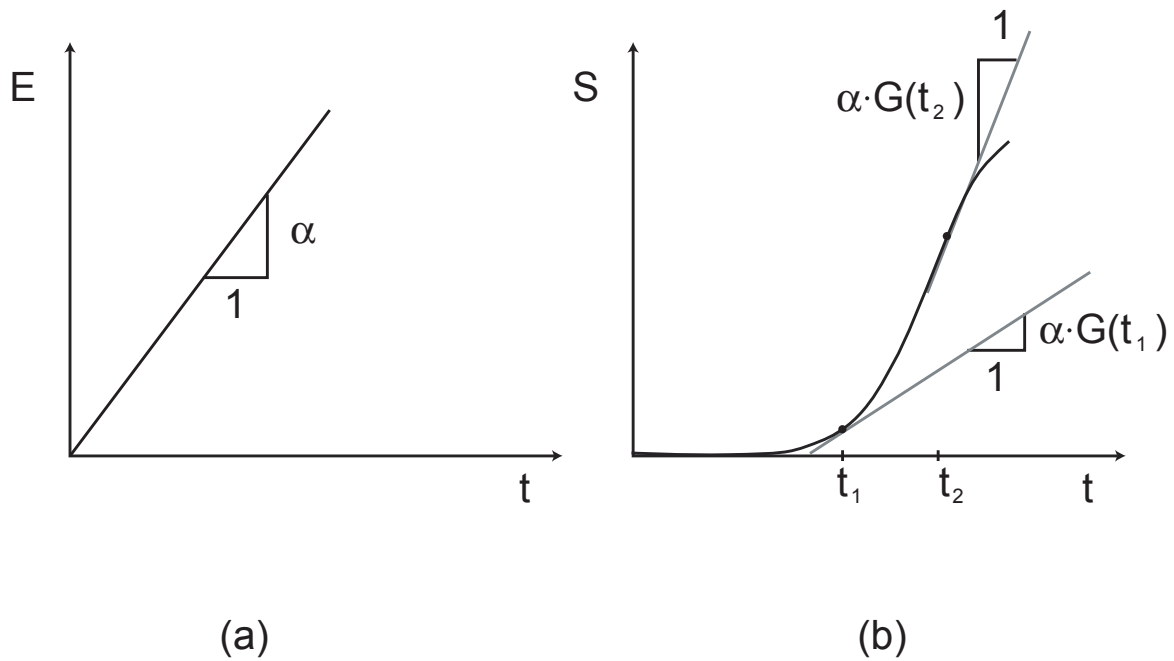
Constant Strain Rate Deformation

A common test used to study the mechanical response of materials and viscoelastic materials deforms a test piece at a constant deformation. Figure 2.11a shows the strain profile of such a test, and figure 2.11b shows a typical stress response. The strain history can be described by

$$E(s) = \alpha \cdot s \quad (\text{EQ 2.24})$$

where time, s , is such that $s \in [0, t]$ where α is the strain rate.

Figure 2.11 Constant strain rate profile (a) with a rate defined by α and (b) a corresponding stress response. Note that the stress response is determined by the relaxation function G .



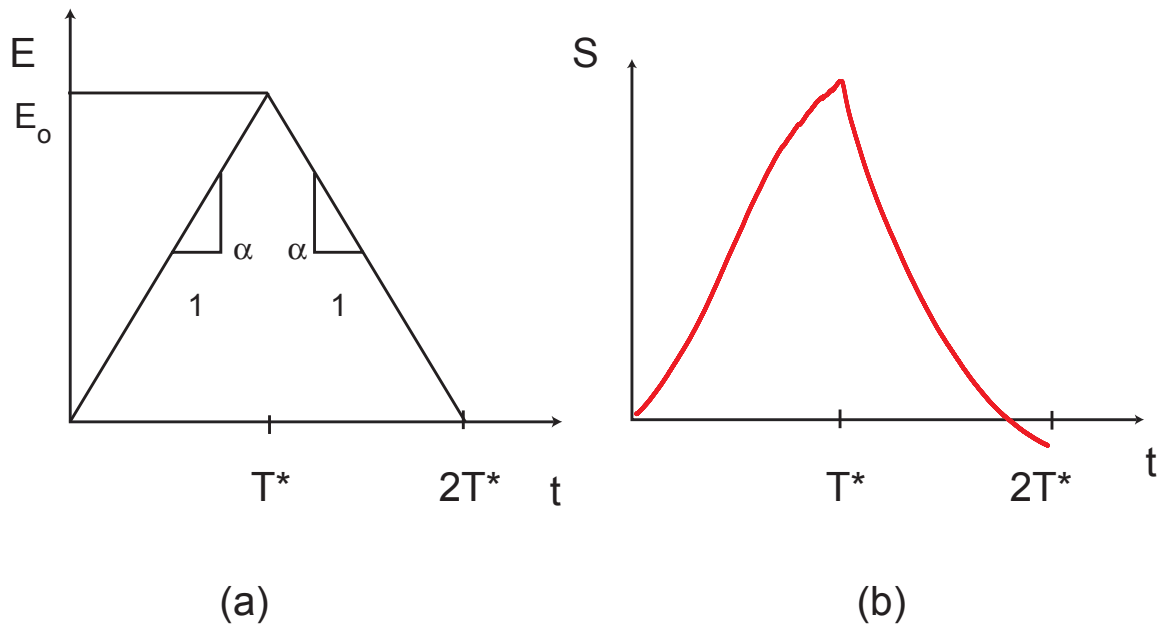
Constant Strain Rate Deformation and Recovery

This type of test involves a constant strain rate deformation to a time T^* , at which time the strain rate is reversed until the specimen is returned to its original shape at time $2T^*$. The strain at time T^* is E_0 . The strain history and corresponding stress response is depicted in figure 2.12, and is described by equation 2.25.

$$E(s) = \begin{cases} \alpha s & s \in [0, T^*] \quad (a) \\ 2\alpha T^* - \alpha s & s \in [T^*, 2T^*] \quad (b) \\ 0 & s \geq 2T^* \quad (c) \end{cases} \quad (EQ 2.25)$$

in which $\alpha = E_0/T^*$.

Figure 2.12 Constant strain rate deformation and recovery history



Sinusoidal Oscillations

A strain-controlled sinusoidal oscillation profile has the form:

$$E(t) = E_0 \sin \omega t \tag{EQ 2.26}$$

The corresponding stress oscillates at the same angular velocity ω , but with an amplitude and phase lag which depend on ω :

$$S(t) = E(\omega) \cdot E_0 \sin(\omega t + \delta(\omega)) \tag{EQ 2.27}$$

where $E(\omega)$ and $\delta(\omega)$ are material parameters.

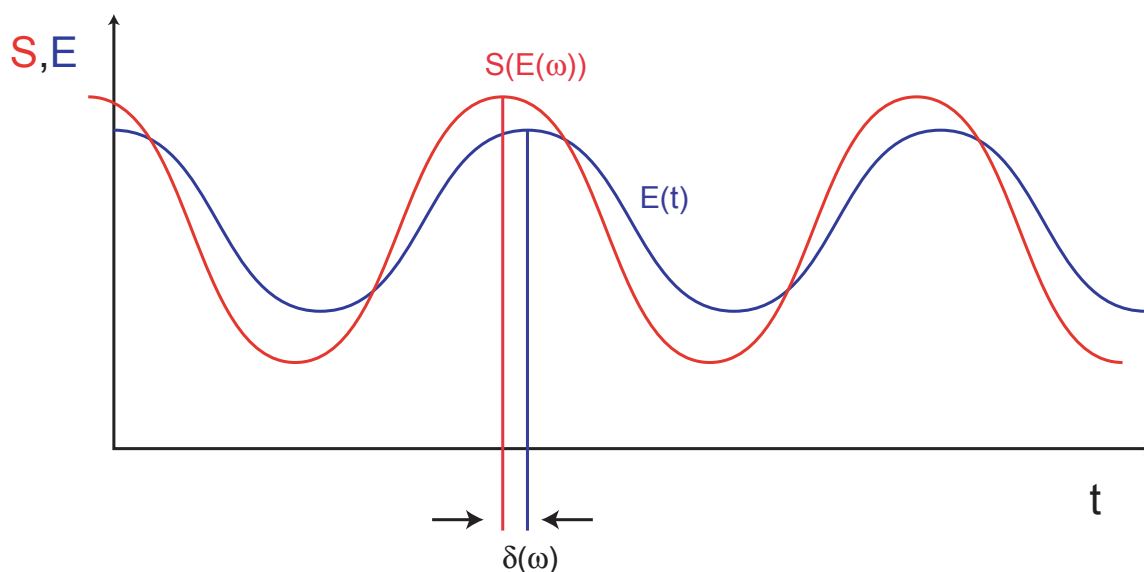
$$\delta = \Delta t \cdot \omega \tag{EQ 2.28}$$

Note that δ =phase lag in radians, Δt = phase lag measured as a time, and that

$$\omega = 2\pi f \quad (\text{EQ 2.29})$$

where f = frequency.

Figure 2.13 Response of ligament tissue subjected to sinusoidal oscillations. The stress function, S , is dependent on $E(\omega)$ and $\delta(\omega)$.



2.7.5 Response of a Linear Viscoelastic Material

Stress relaxation experiments can be designed to determine how the stress relaxation function $G(t, E_i)$ varies with E . The simplest to verify is linearity of response. There are two necessary conditions that must be met to determine the linearity of response of a material: (i) linear scaling, and the (ii) superposition of responses.

Linear scaling and superposition of responses are independent properties, therefore it is possible that experimental data satisfy the conditions for either scaling or superposition but not both. If experimental results show that linear scaling and superposition of response is possible, it is said that the material response is linear viscoelastic.

Linear Scaling

If the step strain is changed by a factor α , then the stress is changed at each time by the same factor α . In other words, all stress relaxation curves obtained experimentally are proportional to one reference curve at a specific strain. This can be expressed mathematically in the form :

$$G(t, \alpha E_0) = \alpha G(t, E_0) \quad (\text{EQ 2.30})$$

where E_0 is fixed.

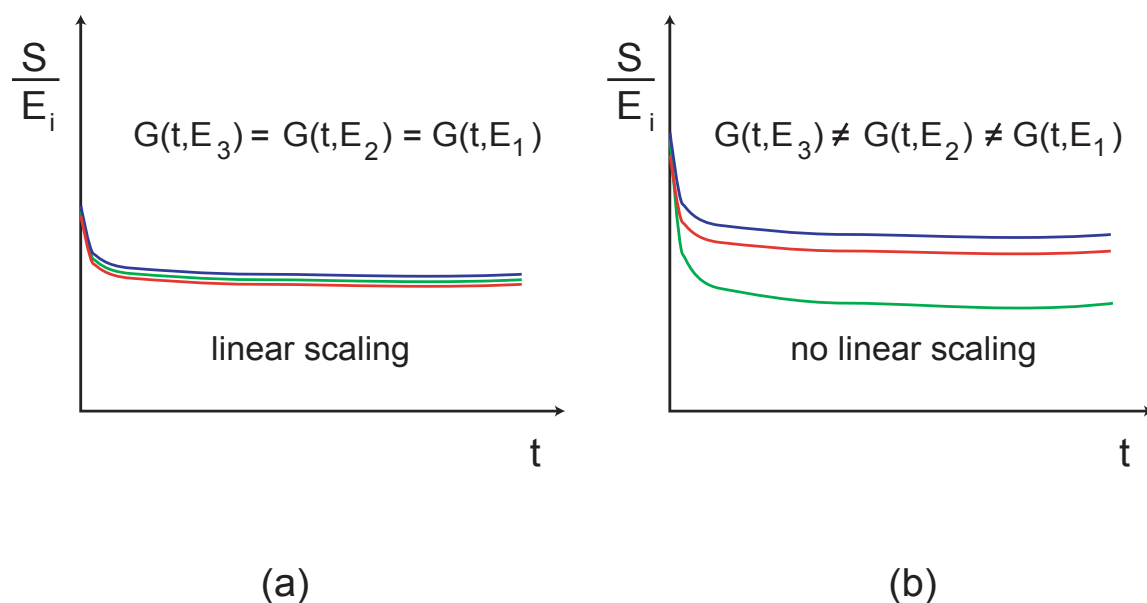
There are tests to determine whether the experimental data exhibits linear scaling. Figure 2.10 represents a set of stress relaxation responses to step strains. Suppose

$$E_3 = 3\alpha E_1 \quad E_2 = 2\alpha E_1 \quad (\text{EQ 2.31})$$

If each stress relaxation curve is scaled by its corresponding strain level, and if linear scaling is possible, all curves coincide to produce a single curve as in figure 2.14a. If the curves do not coincide, as is the case in figure 2.14b, then linear scaling is not possible [Wineman and Rajagopal 2000]

A method known as the hypothesis of variables separation is widely used in soft tissues biomechanics [Pioletti and Rakotomanana 2000; Pioletti and Rakotomanana 2000] and verifies this dependence of time and strain effects in the stress relaxation of soft tissue. This method, however, has not yet been applied to the PDL.

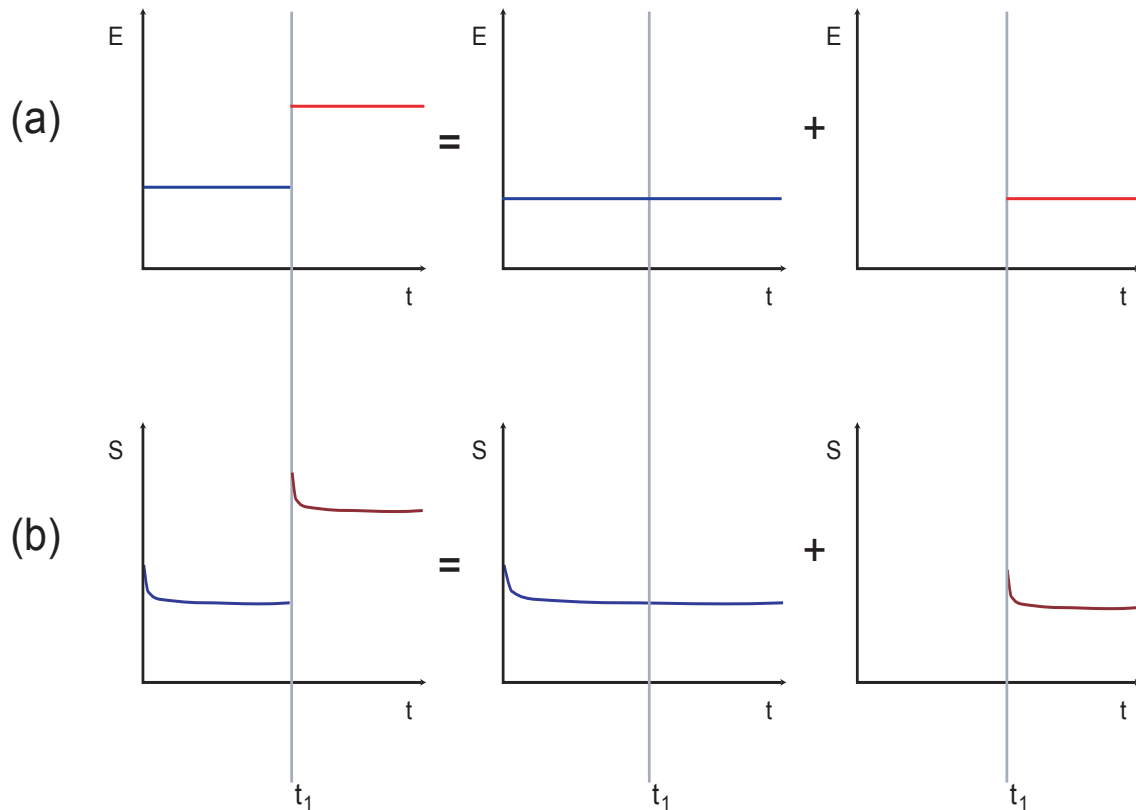
Figure 2.14 Linear scaling: step strains at different strain levels and corresponding normalised stress relaxation for when (a) linear scaling is observed and, (b) no linear scaling is observed.



Superposition of Separate Responses

Another condition that must be met in order to prove linearity of response of a material is the principle of superposition. If a given material is subjected to a series of n step strains, the corresponding material response has n distinctive parts. In order for the principle of superposition to be valid, it would be necessary that the material response curve be broken down into n independent single step strains, giving n independent material response curves. To illustrate this consider a two-step test and its decomposition into two one-step tests, as shown in figure 2.15a. When superposition of responses is possible, the stress response due to the step strain induced in separate tests can be constructed as shown in figure 2.15b.

Figure 2.15 Graphical representation of the use of superposition to construct a strain history response to two step-stress histories.



2.7.6 Preconditioning and Hysteresis of Soft Living Tissue

Preconditioning and hysteresis are features that are observed repetitively in living tissue that distinguish them from other viscoelastic materials.

Preconditioning

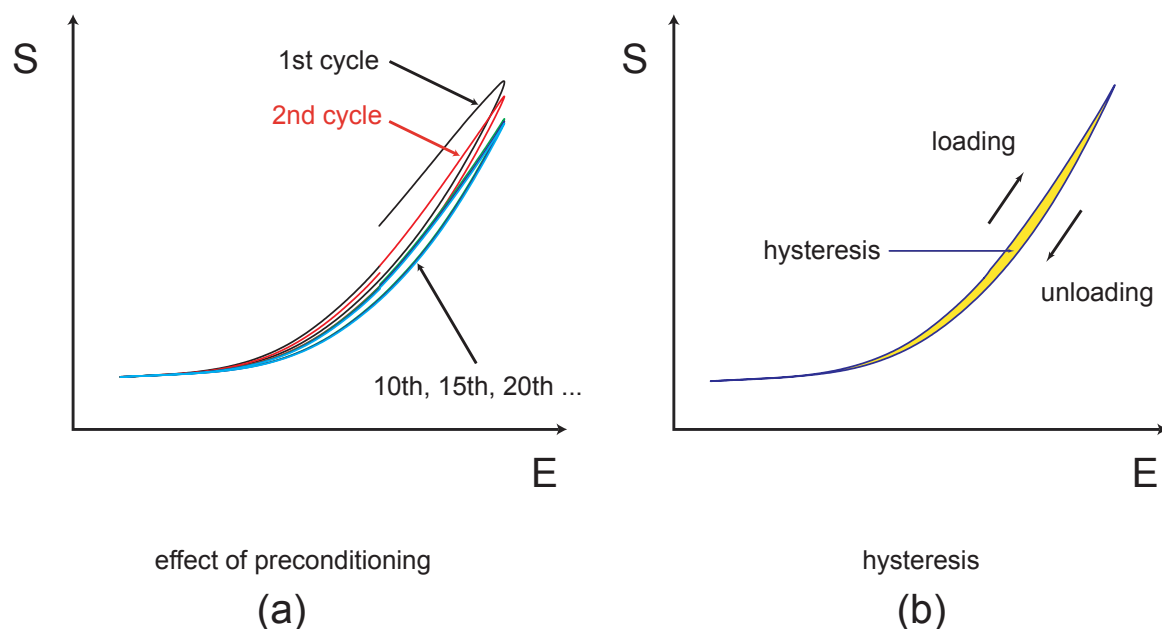
When testing soft tissues, generally only mechanical data of preconditioned specimens are presented. The notion of preconditioning can be understood by considering the variation in the mechanical behaviour of living tissue when loaded cyclically. If a tissue is subjected to deformation by a series of loading and unloading cycles at a constant rate, a difference will be observed in the load-elongation curves for the first three to ten cycles (see figure 2.16a). If cycling is repeated indefinitely, after a certain number of cycles the difference between successive cycles disappears. When this occurs, the specimen is said to have been preconditioned [Fung 1993].

Hysteresis

The phenomenon of hysteresis is observed in living tissue. If a tissue is subjected to a cyclic loading, the stress-strain relationship in the loading process is different from that in the unloading process. This difference is called hysteresis (see figure 2.16b) and represents the dissipated energy during the loading cycle.

The effect of loading rate and hysteresis in PDL has not been reported in the literature. It is possible that PDL behaves as most biological soft tissues, i.e. the hysteresis loop is almost independent of the strain rate within several decades of the rate variation. However, such a behaviour must be confirmed experimentally.

Figure 2.16 The effect of (a) preconditioning ligament tissue by subjecting it to cyclic loading, and (b) hysteresis: the difference in the loading and unloading stress-strain curves. The area between the loading and unloading curves quantifies the hysteresis of the material.



-
-
-

•

•

•

“Why does the eye see a thing more clearly in a dream
than the imagination when awake?”

Leonardo da Vinci

•

•

•

3

Materials and Methods

This chapter is divided into four sections and outlines techniques used to study the structure, morphology and mechanical behaviour of the PDL.

Section 3.1 discusses why bovine tissue was selected as the subject of study, where and how it was obtained, and criteria of selection of the animal. Section 3.2 presents the medical imaging diagnostic techniques used to determine the geometry of a bovine tooth-PDL-bone system. Section 3.3 deals with the methods used to investigate the physiology of the PDL, the histology and morphology on a microscopic scale. Sections 3.4 and 3.5 outline the techniques used to study the mechanical behaviour of the ligament.

3.1 Tissue Selection

3.1.1 Why not Human?

An important issue that must be addressed is the decision to use animal tissue as the subject to study. One may question the use of animal tissue when the ultimate long-term goal is to describe tooth mobility in humans. It is a clear advantage that human tissue would give the most realistic results in all aspects, however, when one weighs the advantages and disadvantages of handling human against the advantages and disadvantages of using animal tissue, it becomes clear that animal tissue must be used in order to establish methodology and the necessary tools of investigation.

The safety requirements in handling human tissue in a laboratory due to the possibility of transmission of disease in its improper handling cannot be ignored. There are strict standards that must be followed in handling post-mortem human tissue and in doing so, lengthy procedures are added to study protocols. In the planning stages of this thesis, it became clear

that a large number of samples would be required. With this in mind, it became clear that human tissue would not be practical in such a study.

The use of animal tissue also has the advantage that the researcher can select subjects more easily with respect to age, sex, dimensions etc.... by examining the animals immediately after their death rejecting several before accepting one into the study. For human cadavers, of course, this is much more difficult.

Minimising the time between death and testing is an important factor when working with tissue *in-vitro*. This time is difficult to control when using human cadaverous tissue, however, is possible with animals.

It must not be ruled out that testing human tissue be disregarded altogether. On the contrary, it is expected that once a refined methodology is developed for determining the mechanical behaviour of the PDL in an animal system, a more efficient and shorter study can be performed on human tissue.

3.1.2 Why Bovine?

With human tissue not practical for testing, the question that now arises is: which animal tissue should be selected?

In the literature, animals of all types have been used *in-vivo* and *in-vitro* experiments. Most animals used, however, have been: rat, rabbit, pig and monkeys. Few articles, however, exist on PDL mechanics of bovine tissue.

A primary reason why bovine is chosen is because of its large size. The experiments planned for this thesis ruled out the use of rats or rabbits. Unlike rats and rabbits, the teeth of bovine are not in continuous eruption. The teeth of pigs, although morphologically and physiologically more similar to humans than bovine, are still somewhat small. Bovine tissue is also readily available on short notice and easy to obtain at a local slaughterhouse with no special procedures when handled in the laboratory. Few studies as to the bovine's morphology have been performed, however, the few that have been made show that the biology of bovine PDL does not differ largely from human PDL. This point remains a subject of debate and has therefore been investigated in this thesis.

In terms of function, however, it can be argued that bovine are herbivores and chew almost continuously throughout the day on soft grass. The PDL width of bovine (see Table 2.1) is also much broader than that which is found in humans. These differences must be kept in mind when the data of mechanical behaviour is interpreted.

3.1.3 Why 1st Molar?

The first molar was chosen after several preliminary tests were performed on the other teeth of the bovine. In sum, the incisors have a broad PDL with a greater mobility than what is observed in humans. Moreover, only a small part of the root is embedded in the bone, which would in effect make it difficult to prepare samples from any bovine incisor. The canines and premolars, whose dimensions are comparable to human molars, the roots are not sufficiently long which would have, as with the incisors, complicated sample preparation. The long axes of canines and premolars were also more difficult to define due to the inherent shape of these teeth. During the developing stages of a bovine to maturity, of the six mandibular molars, the first to erupt are the first molars. First molars in all bovine, except in rare circumstances, have two well defined roots with no deformities: one distal root (more towards the back of the head) , and one mesial root (more towards the front of the head). This is not the case for second and third molars which can both develop anywhere between, depending on the animal, two to five different roots, many of which have a shape difficult to define.

3.1.4 Selecting and Obtaining Bovine Mandibles

Based on discussions with veterinarians at the slaughterhouse of Vulliamy SA (Cheseaux-sur-Lausanne, Switzerland), bovine were selected according to two criteria: their age, and after ensuring that no visible abnormalities were observed in all teeth of the mandible.

With regards to age, all animals used for *in vitro* experiments were between 3 and 5 years old. This age range was determined based on two factors:

- 1 the bovine brought in for slaughter are younger than 6 years of age.
- 2 the eruption of the third molar ensures that the animal is older than 3 years. Moreover, the presence of a fully erupted third molar implies that the first molar has reached physical maturity.

The selected mandibles were then placed into a plastic container and transported to the EPFL biomechanics lab for removal of soft tissue and sectioning. The mandible was then sectioned following specific procedures (see sections 3.4 & 3.5). The time from death to arrival of the mandible to the lab was less than 1 hour.

3.2 3D Reconstruction of First Molar from CT Scans

Studying problems in biomechanics consists of several steps. The first is to study the shape in order to define the geometric configuration of the object.

There are 3 goals to this study:

- 1 reconstruct the tooth, the ligament and the bone using CAD programs,
- 2 measure the geometry of the system, primarily of the ligament,
- 3 prepare the reconstruction of the tooth for use in finite element studies and conduct a stress analysis of the system using appropriate constitutive equations.

The reconstruction was done using the images obtained from μ -computerised tomography scans of the a first molar block specimen. Coreldraw, a software package, was used to transform the images into CAD file format and Rhinoceros, another software package, was used to convert these images into the 3D reconstruction.

3.2.1 Methodology

The goals of this study are met by following 5 principal tasks. These tasks are:

- 1 the acquisition of CT data from X-Ray of bovine first molar block,
- 2 the geometric reconstruction of the surface of the tooth,
- 3 obtaining the geometric measurements of the ligament,
- 4 the construction of the 3D mesh of the ligament-tooth-bone system and definition of boundary conditions, and
- 5 analysis of results.

These 5 tasks can be divided into 2 principal parts. The first part involved experimental aspects and make up tasks 1, 2 and 3. The second part involves an approach using numerical methods and makes up points 4 & 5.

3.2.2 Principles of X-Ray CT

In medical imaging, many non-invasive methods exist for determining the internal structure of biological tissues. These methods include the use of ultrasound, radiopharmaceuticals, and magnetic resonance imaging. The most common methods are based on the use of x-ray emissions such as radiology, tomodensitometry and vascular imaging. The method used in this study is x-ray computerised tomography.

The result obtained by x-ray tomography is an image plane in 2D, which accurately represents the cross-section of the specimen scanned. This technique is non-invasive and

is based on measuring the attenuation coefficients of a body that has been subjected to beams of x-ray photons. The level of attenuation depends on the physical and chemical properties of the body as well as the characteristics of the x-ray beams, i.e. frequency, wavelength and energy.

The experimental setup, shown in figure 3.1, is comprised primarily of an x-ray source, the positioning mechanisms and the x-ray detectors. The instrumentation is connected and controlled by computer which calculates and associates the corresponding acquisitions to the reconstruction unit. The reconstructed scan is then stored and visualised with the aid of a graphics processor and user interface.

Figure 3.1 Experimental setup of the μ -computerised tomography scanner

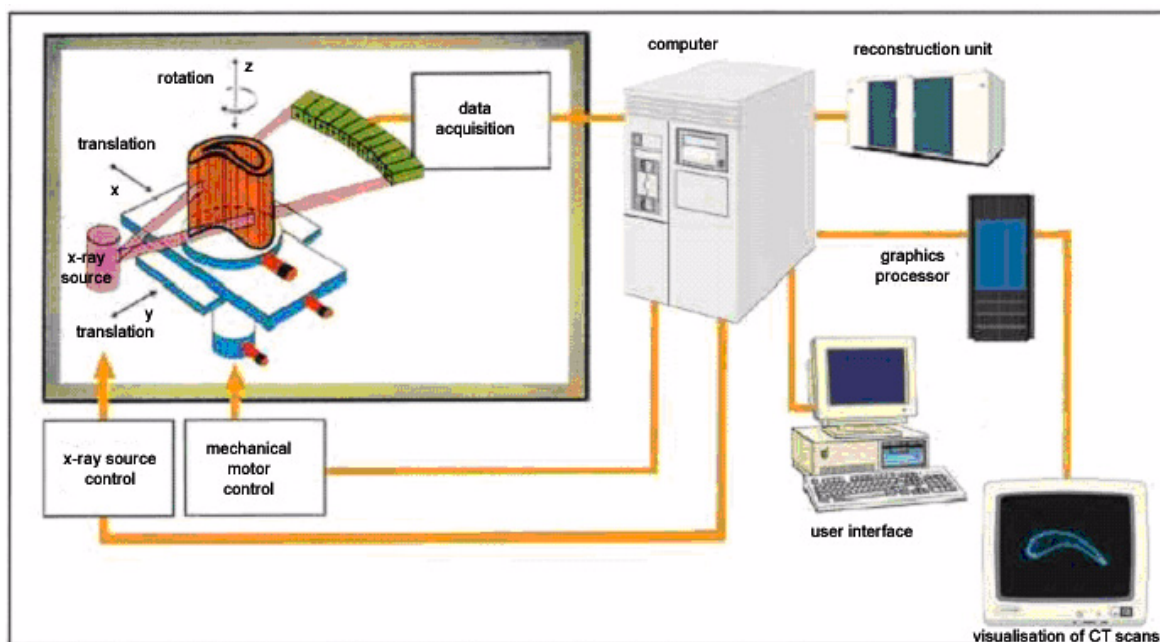


Table 3.1 CT Scanning characteristics

Specimen dimensions	70 x 50 x 40 mm
CT Machine	Micro CT Scan (μ CT 80 Scanco Medical)
Number of transverse scans	~700
Space between each scan	75 μ m
Resolution	75 μ m
Size of image	1024 x 1024 pixels
Size of pixel	13.3 pixels/mm

The μ CT device scans the intact first molar and produced approximately 700 scans, in order to ensure a resolution of 75 μ m. The PDL thickness being in the order of 500 μ m made it necessary to scan at this resolution.

3.3 Histology Studies

Histology is the study of the microscopic structure of biological tissues.

3.3.1 Research Methodology

Mandibular jaws from bovine ranging in age between 3 and 5 years are retrieved from the slaughterhouse and immediately transported to the laboratory. The first molars are horizontally sectioned into about 4 slices using a band and a manual saw. The slices are fixed either in 4% buffered formalin at room temperature or in 1% glutaraldehyde and 1% formaldehyde, buffered with 0.08 M sodium cacodylate (pH 7.3) at 4°C.

For the production of undecalcified ground sections, tissue samples fixed in 4% buffered formalin are rinsed in running tap water over night, trimmed and dehydrated in a graded series of increasing ethanol concentrations. They are embedded in methylmethacrylate (MMA) without being decalcified. Following polymerization, tissue blocks are exhaustively cut in the horizontal plane into 200 μ m-thick sections using a slow-speed diamond saw (Varicut® VC-50, Leco, Munich, Germany). The sections are ground and polished to a final thickness of 80-100 μ m (Knuth-Rotor-3, Struers, Rodovre/Copenhagen, Denmark), and surface stained with toluidine blue/McNeal (Schenk et al. 1984). The stained ground sections are observed in a Leica M3Z stereolupe and a Leica Dialux 22 EB microscope.

For the production of decalcified semi-thin sections, tissue samples fixed in 1% glutaraldehyde and 1% formaldehyde are further subdivided in an apico-coronal direction at the mesial, distal, lingual, and buccal aspects of the mesial and distal roots of the first molars.

After washing twice in 0.1 M sodium cacodylate containing 5% sucrose and 0.05% CaCl_2 , pH 7.3, the tissue samples are decalcified in 4.13% ethylenediaminetetra acetic acid (EDTA) for 10 weeks (Warshawsky & Moore 1967) at 4°C, and extensively washed again in washbuffer solution. The decalcified samples are trimmed and further subdivided. Some tissue samples are then post-fixed with potassium ferrocyanide-reduced osmium tetroxide (Neiss 1984) and processed for embedding in Taab 812 epoxy resin (Merck, Dietikon, Switzerland). The remaining tooth samples are osmicated or left unosmicated and processed for embedding in LR White resin (Fluka, Buchs, Switzerland). Semi-thin sections (1 μ m thick) are cut with glass and diamond knives on a Reichert Ultracut E microtome (Leica Microsystems, Glattbrugg, Switzerland), stained with toluidine blue, and observed in a Leica Dialux 22 EB microscope.

Some tissue samples are macerated in order to remove cells and noncollagenous proteins, leaving the collagenous matrix fairly intact (Kuroiwa et al. 1996). Fixed and decalcified tissue samples are immersed in a 10% aqueous solution of NaOH for 3-4 days at room temperature and then processed for embedding in epoxy or acrylic resins as described above.

3.3.2 Determination of Fibre Density

Fibre density is determined using an image analysis software program (*IMAQ Vision*, National Instruments). A digitized micrograph taken of a histological slide of a stained decalcified thin section with a thickness of approximately 1 μm is loaded into *IMAQ Vision* (see figure 4.20), and converted to a grayscale image. Contrast threshold values are measured in non collagenous zones repetitively to give an average contrast threshold. Applying this threshold value to the entire image with algorithms incorporated in *IMAQ Vision* resulted in transforming the noncollagenous zones to white, and the collagen zones to black. The transformed images of figure 4.20 produce figure 4.21. To calculate the density from the micrograph, a region of interest is chosen and the area representing the collagen (black) is divided by the area of the region of interest. Repeating this for several regions of interest would give an average value of the collagen fibre density.

3.4 Uniaxial Specimens

The majority of data obtained in this thesis is from experiments performed on uniaxial specimens. The different techniques for testing the mechanical properties of the PDL have been described in section 2.4.1.

3.4.1 Methodology and Specific Procedures

After selecting a bovine mandible as described in section 3.1.4, four steps are taken in preparing PDL uniaxial specimens:

- 1 cutting the first molar from the mandible,
- 2 sectioning the first molar into transverse sections
- 3 storing the specimens, and
- 4 cutting the uniaxial specimen from the transverse sections on the day of mechanical testing.

The specific procedures for each of these steps are described below in this section.

Note: about freezing

It is important to note that in preparing biological specimens, storage is a crucial step. The methodology developed for all biological samples for this thesis are designed to ensure that each sample was frozen and thawed once. Repetitive freezing, i.e. thawing cycles, affect the mechanical properties of the specimen, thus testing such a biological specimen would give unrepresentative results. [Quirina and Viidik 1991]

Removal of First Molar Site from Mandible

After selecting the bovine mandible at the slaughterhouse according to criteria outlined in section 3.1.4, the first step is to cut the right and left first molars from the mandible in such a way as to keep the PDL intact with as much alveolar bone as possible around the teeth. A flowchart of this procedure is given in figure 3.2.

The intact mandible is placed on a bench and, with the aid of a scalpel, all remaining soft tissue (skin, muscle etc...) is removed. Digital photographs of the mandible are also taken. These photographs are archived in the event that follow-up measurements need be made at a later time.

The first series of cutting involves separating the left and right sides of the mandibles containing the molars, premolars and canines. This is shown schematically in the images (ii) through (v) in figure 3.2.

The cuts made are indicated on images (ii) and (iii) and only the parts between cuts A and C, and cuts B and C were used in following steps. The other parts are disposed.

In order to obtain a block containing an intact first molar, further sectioning of the tooth is required. These cuts are shown in image (v). Note that in order to ensure that no damage to the first molar occurred, cuts D and E of image (v) are made along the long axes of the premolar and second molar respectively. A final cut F is made to reduce the size of the block. Image (vi) shows the intact block now ready for further sectioning to obtain the transverse sections.

All cutting is performed using a heavy industrial band saw (Magnum, Metabo, Germany) and took less than two hours after death of the animal.

Sectioning of Transverse Sections

The following step consists of obtaining transverse sections (i.e. slices perpendicular to the long axes of the teeth) from this block. The sectioning of this block into transverse sections is time consuming and takes approximately 2 hours per tooth. Since most often two mandibles are obtained after each visit to the slaughterhouse, a total of 4 first molar blocks would be sectioned. While one block is being prepared, the other blocks are stored in a refrigerator at 5°C to minimise tissue degradation.

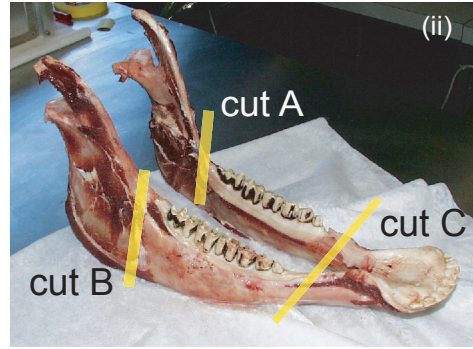
The schematic in figure 3.3 shows how the transverse sections are obtained from the first molar blocks. Transverse sections are obtained by first mounting the blocks into a custom-made chuck. The chuck is equipped with a 20 μm resolution dial gauge, thus ensuring a precise control of the thickness of the resulting sections. Cutting is performed at a low feed force (50g) using a 0.2 mm thick, diamond coated band saw (Exakt, Germany) under abundant saline irrigation. The first cut is placed approximately at the alveolar crest and the resulting section, the crown, is measured and discarded.

Subsequently, the second and third cuts are made giving the first two transverse sections. Only transverse sections containing distinct distal and mesial roots are kept for mechanical testing, and as a result, these first two sections are measured and discarded. It is important that the tooth be free of any enamel, which in bovine, unlike humans, can descend quite apically into the depth of the tooth. It is decided, thus, that samples be taken from the apical regions below the apex, as it is unlikely at this depth or below for the tooth surface to be made of enamel. The apex of a tooth with two roots is the point where the two roots meet.

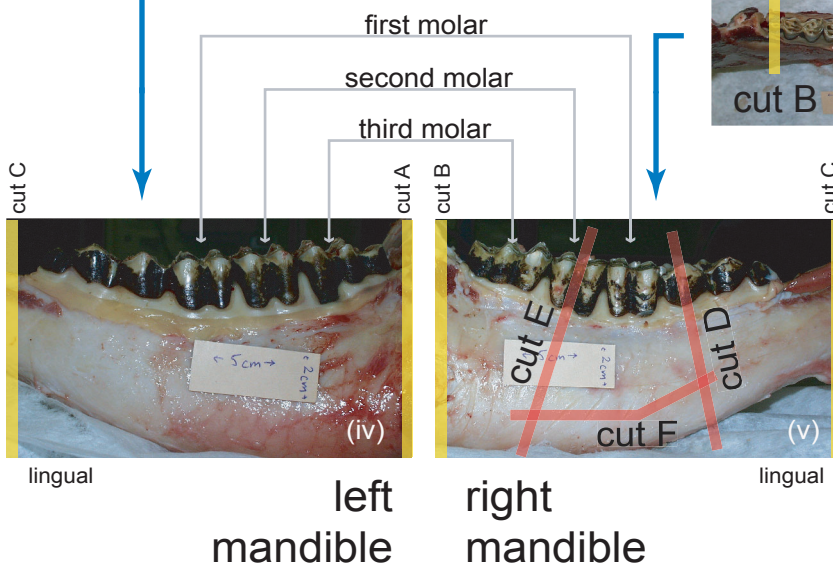
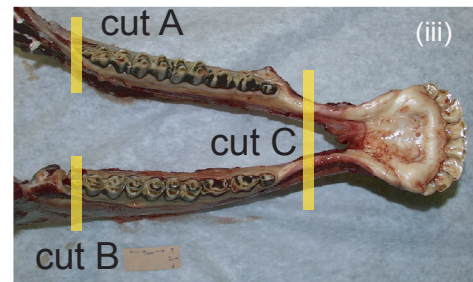
The transverse sections for mechanical testing are prepared by placing transverse cuts every 2 mm resulting in 5 to 6 sections (shown as A through F in figure 3.3). These are labelled as to their depth, placed in an airtight container and frozen to -21°C in a refrigerator equipped with a thermostat (Bosch, Germany).

Figure 3.2 Obtaining an intact first molar site from a bovine mandible

1. Select fresh bovine mandible from slaughterhouse



2. Cut mandible to obtain required regions.



3. Cut left and right mandibles to isolate intact left and right first molars.

4. first molar site sectioned from right mandible

*first molar site from left mandible is obtained following same cutting procedure

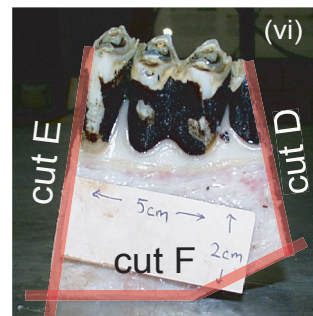
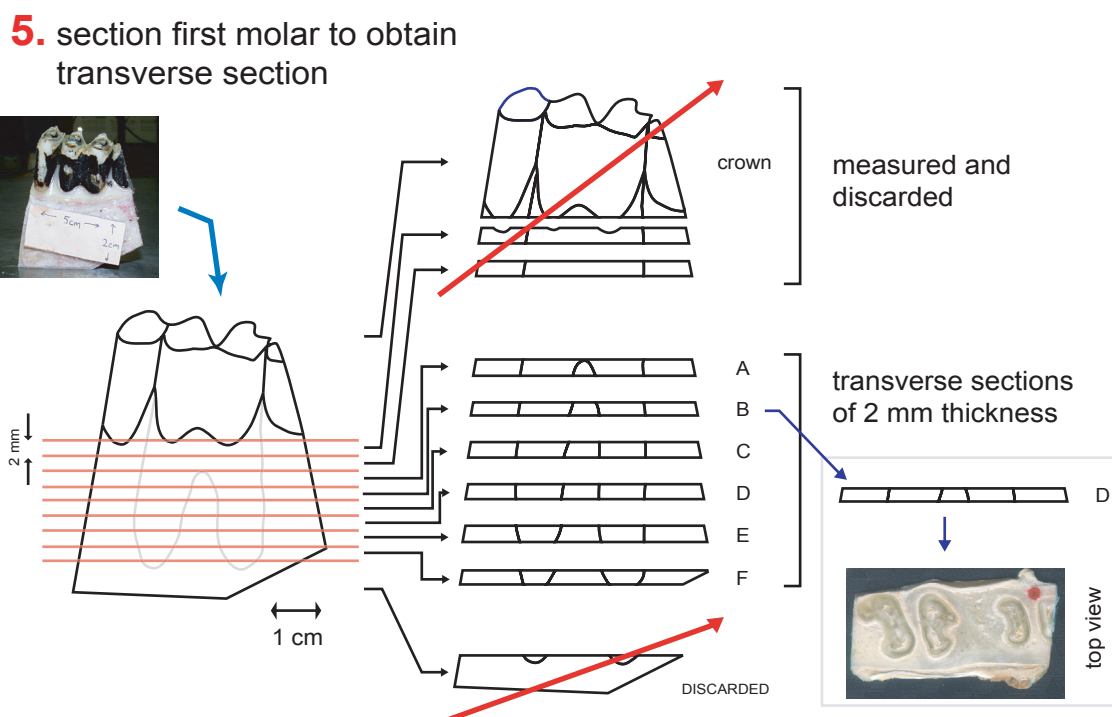


Figure 3.3 Schematic describing how transverse sections are cut from block containing first molar*.



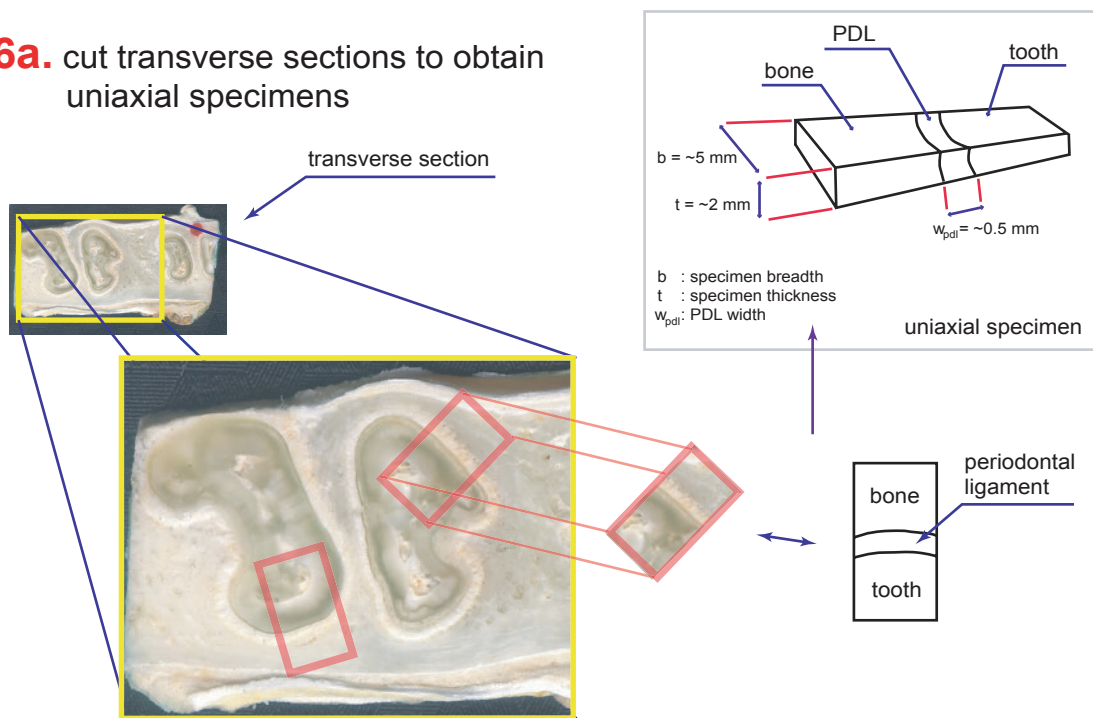
* this figure continues from figure 3.2.

Cutting the Uniaxial Specimen

On the day of testing uniaxial specimens are removed from the freezer and immediately cut from the sections as they thaw using the diamond-coated band saw and a custom made shape guide. Specimens are prepared from each section as shown in Figure 3.4. As it becomes available, each specimen is placed in a saline filled vial (9 g/l NaCl) and refrigerated to 5°C until testing. Saline is necessary to reduce the swelling of the tissue. Depending on the sample, a total of 5 - 6 uniaxial specimens are obtained from each transverse section.

The external dimensions of the each specimen as well as the PDL width are determined from digital images taken prior to mounting them into the testing machine. The thickness of the specimens is measured using a caliper.

Figure 3.4 Schematic describing the cutting of uniaxial specimens from transverse sections*.

6a. cut transverse sections to obtain uniaxial specimens

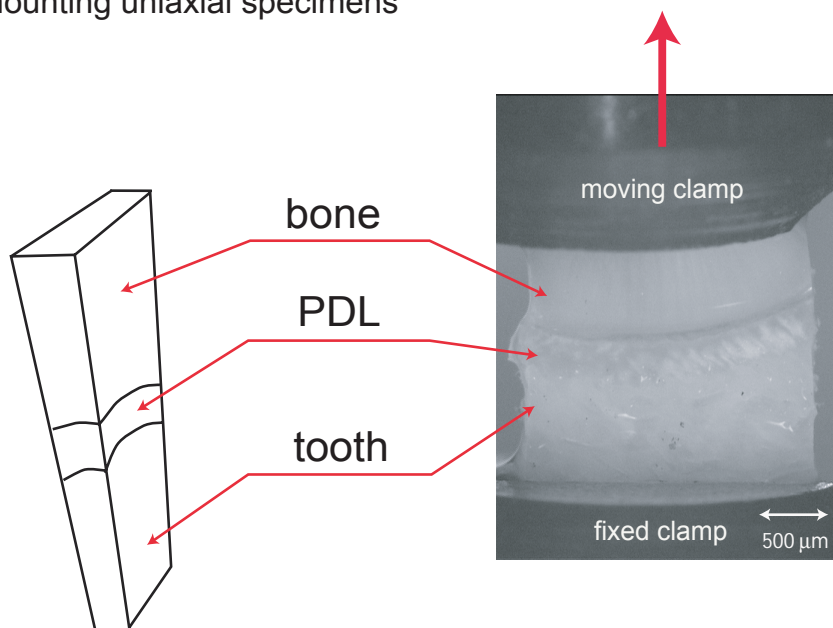
* this figure continues from figure 3.3.

Mounting the Uniaxial Specimen for Testing

The mounting of the uniaxial specimen, because of its small size, is a delicate procedure. With the aid of tweezers, the specimen is held into place. The clamps are closed over the bone and dentin portion of the sample leaving the ligament visible for observation. A saline bath is then raised to completely submerge the specimen. Tests are performed at room temperature.

Figure 3.5 Schematic showing how uniaxial specimen was clamped into the grips of the machine*.

6b. mounting uniaxial specimens



* this figure continues from figure 3.4

3.4.2 Initial Uniaxial Studies

In a study that involves testing a material of unknown properties such as the PDL, the experimental design stage is one with many uncertainties. As a result several mini-studies have been performed. Concerning the uniaxial testing of PDL, the preliminary studies can be divided into two groups.

- 1 preliminary studies with the custom-made Microtensile Machine (MTM)
- 2 preliminary studies with the commercial Instron Microtester.

Preparatory Uniaxial Studies with the Microtensile Machine

Before any comprehensive experimental work was planned, a series of pilot studies were launched using the custom-made microtensile machine and done in two stages.

- 1 Adapt the instrumentation for use with periodontium tissue.
- 2 Perform preliminary relaxation experiments to determine the time-dependent parameters for use in a more comprehensive study at a later time.

The first stage involved calibration of the MTM, determine which components could be improved and take the necessary steps to do so. First materials used in this stage included metal springs, polymers and foams.

The second stage involved reprogramming the machine to test, for the first time, the time-dependent behaviour of the PDL. Preconditioning, ramp and rupture tests (see section 2.7.4) were performed. Sinusoidal testing, however, was beyond the capacity of the microtensile machine. Although these tests were successful, the results have not been included in this thesis. These experiments were, however, an important milestone in the development of this thesis as it provided invaluable experience when it came to preparing specimens and designing testing protocols with the more advanced Instron Microtester obtained by the lab (LMAF-EPFL) in early 2002. Thus, all results reported in this thesis have been collected from the Instron Microtester (refer to Appendix A for the characteristics of this machine).

Preliminary Stress Relaxation Tests

It was realised that little information describing the time-dependent behaviour of PDL tissue existed. Most studies in literature had treated the PDL as a linear elastic material (see section 2.4). Preliminary experiments to test PDL time-dependency were therefore necessary to identify key parameters crucial to experimental design of the more comprehensive experimental procedures described later in this chapter.

3.4.3 Tests on Uniaxial Samples

As discussed in section 2.7.4, there are a number of tests that can be performed to identify the material properties of a viscoelastic material. It was necessary, therefore, that a specific testing protocol be developed.

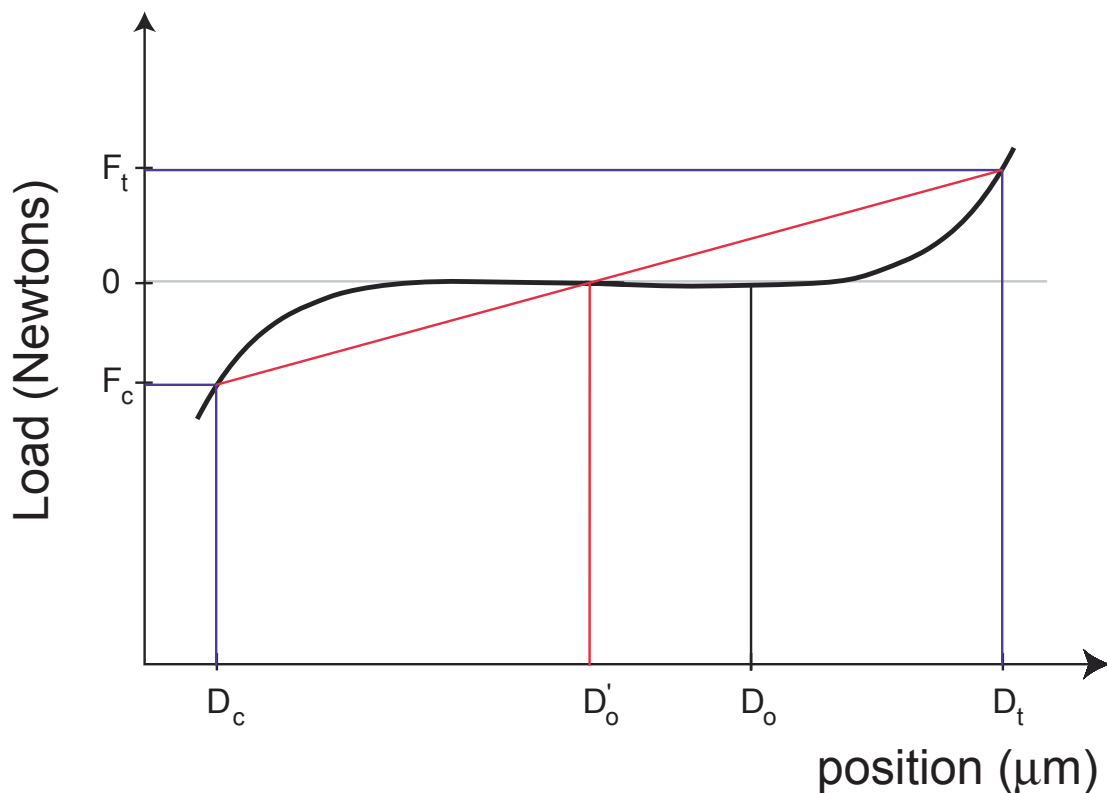
Zeroing

Defining the “zero” of the uniaxial specimen before testing was necessary in order to have a known reference point for interpretation of the data collected from the experiment. The zero is defined as the point at which stress and strain values are set to equal zero. When the PDL is pulled in tension it displays, as any soft tissue, a distinct “toe” region (Figure 2.6). It is in the toe region that the collagen fibres start to uncrimp and align along a preferential direction. In the literature, the beginning of the toe region is usually defined as the zero, though results presented in this manner can be misleading, especially when the uniaxial specimen is to be tested both in tension and compression. As a result, a method was developed to determine the zero of the specimen prior to testing.

$$D'_0 = \frac{D_t - D_c}{2} + D_c \quad (\text{EQ 3.1})$$

Placing the specimen into the grips, the position of the displacement sensor is recorded, D_0 . The zero is determined by slowly pulling the sample in tension to a load of $F_t = 5$ N. The position, D_t , at F_t is recorded, and the specimen is then compressed to a load of $F_c = -5$ N. The position, D_c , at F_c is recorded and the zero, D'_0 , obtained by equation 3.1. Determining the zero is shown graphically in figure 3.6.

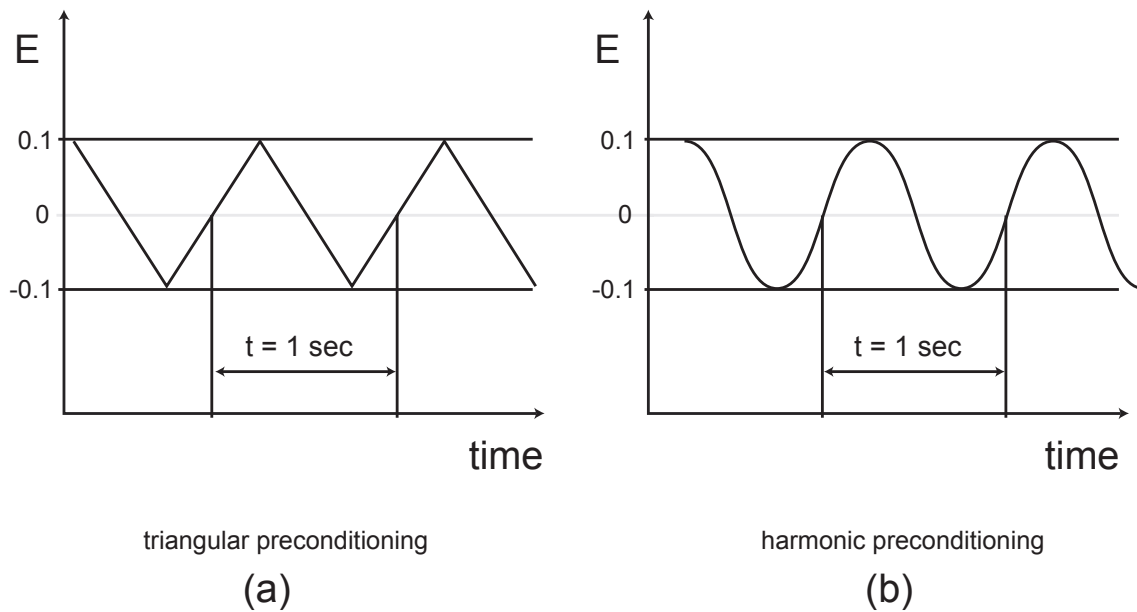
Figure 3.6 Defining the zero of a ligament specimen



Preconditioning

All uniaxial specimens are preconditioned by subjecting them to 10 harmonic cycles with an amplitude of 10% of the PDL width (or approximately 0.1 strain) at a frequency of 1 Hz. No damage to the tissue is assumed due to low E levels. It is also possible to precondition samples by using triangular waveforms. This is shown graphically in figure 3.7.

Figure 3.7 Triangular and harmonic preconditioning



Constant Strain Rate Deformation Tests

Also called ramp tests, constant strain rate deformation tests are performed to quantify the difference in the properties of the PDL with respect to the strain rate. Constant strain rate deformation is described in section 2.7.4.

Constant strain rate deformation and recovery tests (see figure 2.12) are also performed. The rates chosen in the studies of this thesis range from 0.002 to 1.4 s⁻¹ corresponding to displacement rates of 0.1 to 800 μm·s⁻¹.

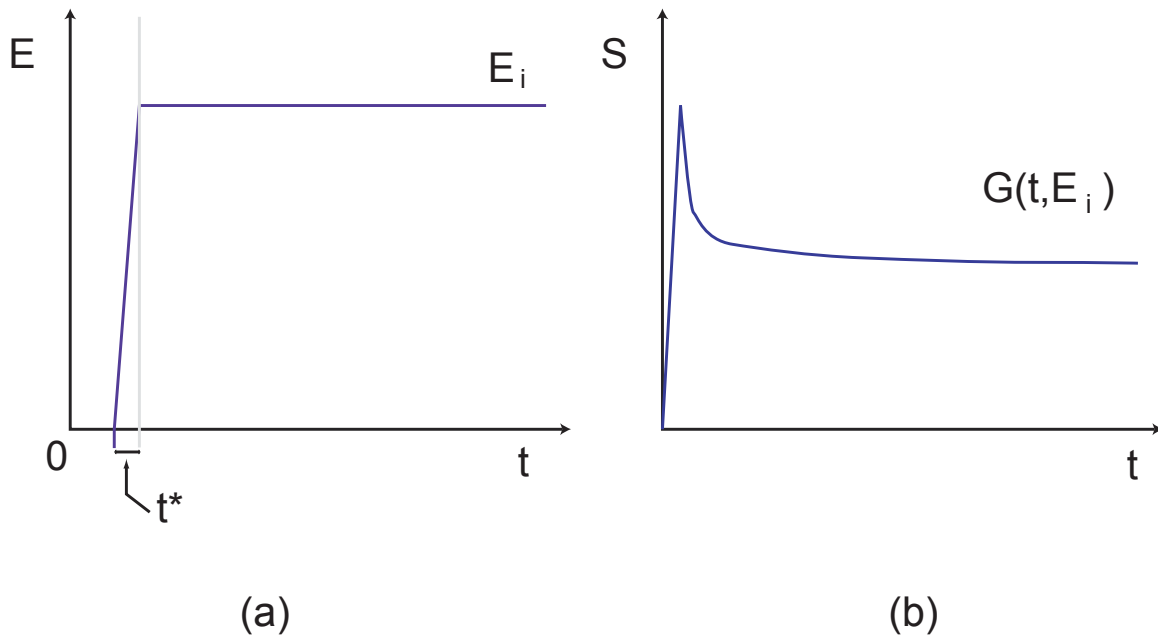
Relaxation Tests

When performing relaxation tests, theoretically there is an instantaneous strain jump at $t = 0$ (see section 2.7.4). Practically, this is not possible because a finite amount of time, t^* , is necessary to deform the specimen from $E = 0$ to $E = E_i$ to produce an appropriate relaxation response $G(t, E_i)$. This is shown graphically in figure 3.8. When preparing the machine for experimentation, the goal is to obtain, as much as possible, the step-displacement at time, $t=0$. In order to do this, one must minimise t^* . In other words, the strain rate over t^* must be sufficiently fast with respect to the fastest characteristic time of the PDL.

In preliminary relaxation tests, the fastest characteristic time observed when the ligament is deformed from $E = 0.20$ to $E = 0.40$ of the PDL width was 1 second. Having obtained this parameter, it was decided to set the maximum rate of deformation to one order of magnitude faster than the fastest observed characteristic relaxation time, which remained within the limit of the machine (see section 5.4.2).

Performing the step-relaxation tests faster than this speed, although possible, is not done to avoid vibrations of the instrumentation and to minimise error caused by the inertial effects of the gripping devices of the machine.

Figure 3.8 Step-strain Experimental Relaxation Response : Experimental



Sinusoidal Tests

Prior to subjecting specimens to sinusoidal loading, all specimens undergo the zeroing process as well as sinusoidal preconditioning. To remain in the physiological range of the specimen, oscillations have an amplitude to remain in the physiological range, selected based on an average PDL width of $535\mu\text{m}$ (see section 4.1), which corresponds to a displacement amplitude of 0.20 mm . The frequencies were limited to a range (from $f_{\min} = 0.01\text{ Hz}$ to $f_{\max} = 4\text{ Hz}$) due to the limitations of the testing system (see table 3.2).

Rupture Tests

The rupture curves of the PDL are similar between specimens at a defined strain rate. It is for this reason that the rupture test is a standard test for all experiments as a means to verify the validity of the experiments. The parameters that define each rupture curve, shown in figure 3.9, are:

- 1 maximum stress, S_{\max}
- 2 maximum strain at maximum stress, or maximiser strain, E_{\max}
- 3 maximum strain energy, Ψ

4 maximum tangent modulus, ε

The rupture of uniaxial specimens is performed at a strain rate of $20\mu\text{m} \cdot \text{s}^{-1}$. Uniaxial PDL samples are tested at a sufficiently slow rate in attempt to minimise the role of the viscous element during rupture, i.e. testing a dashpot sufficiently slow will have a negligible role in a viscoelastic material.

3.4.4 Sequential Testing of Uniaxial Specimens

A major problem in experiments with biological tissue involves the uniqueness of specimens. Otherwise said, reproduction of results is difficult. Testing sample A to rupture at a certain strain rate α would most likely give a different curve than sample B, even if each sample is prepared in the same manner, and section from the same depth. Accounting for this difference requires examining structural properties, histology and other parameters. However, since both specimens have already been tested to rupture, it is no longer possible to examine the initial structures of the specimens to quantify their differences. Even if the structural properties had been known, a sound understanding of the ligament's behaviour would be required to relate its structure to mechanical properties. One way to reduce the extent of non-reproducibility is to precondition the specimens before obtaining the S-E curve.

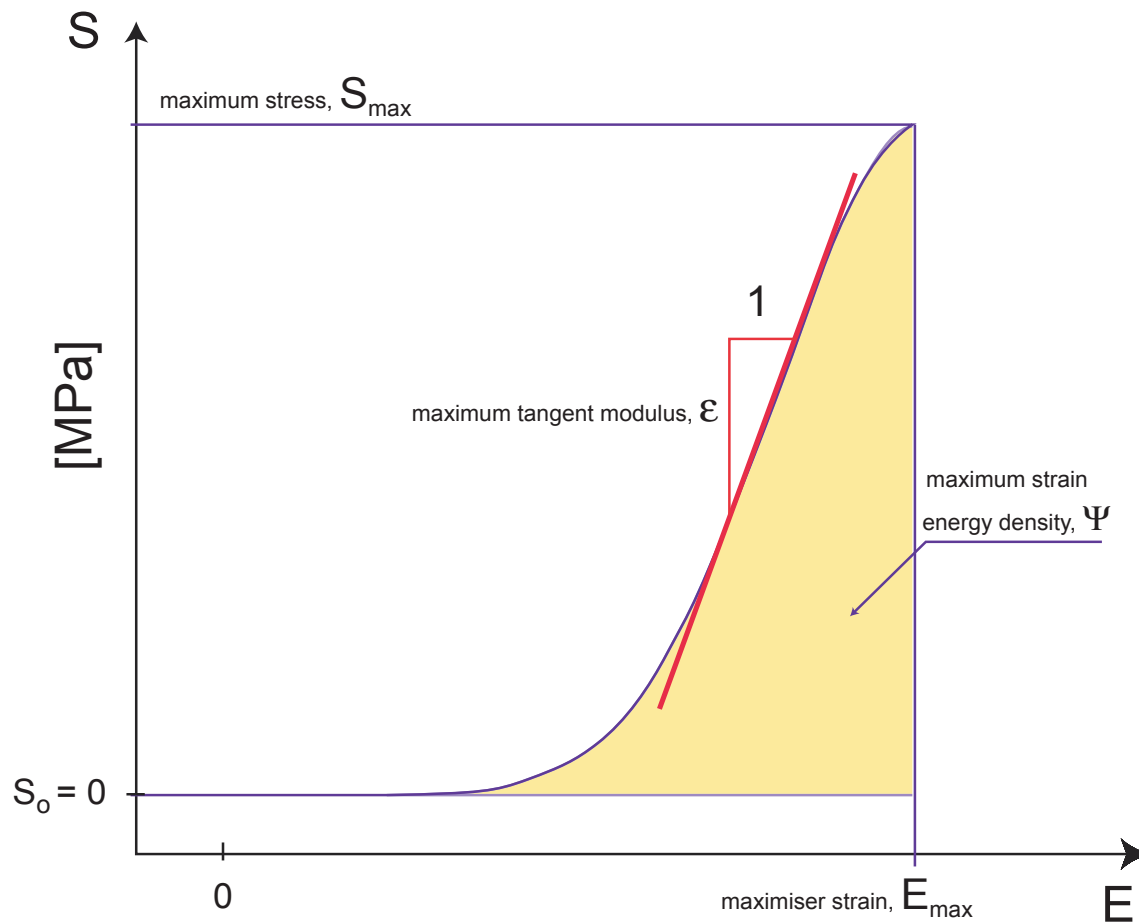
Sequential testing have been performed in studies reported in literature however not as extensively as in the studies of this thesis. Between each phase of the testing profile, it is necessary to wait a certain amount of time at the determined zero of the tissue in order that it recovers before executing the following stage of testing. This recovery is a direct consequence of the time-dependent properties of the PDL.

Sequential Testing Profile

The most extensive testing profile performed on the PDL that did not include sinusoidal oscillations is made up of four separate stages:

- 1 preconditioning, triangular-type
- 2 ramp tests, ramp tests at $\dot{E} = 0.002 \text{ s}^{-1}$, $\dot{E} = 0.04 \text{ s}^{-1}$, $\dot{E} = 0.4 \text{ s}^{-1}$ and $\dot{E} = 1.2 \text{ s}^{-1}$ to verify linear scaling criteria
- 3 step-relaxation tests, three separate tests to verify the superposition of response criteria
- 4 rupture test, at a strain rate, $\dot{E} = 0.04 \text{ s}^{-1}$ as a standard test to verify the validity of the specimen, and to obtain general parameters as a means to compare each specimen.

Figure 3.9 Rupture curve of uniaxial specimen with parameters obtained from each curve



Note: between each individual test, a wait time of 2 minutes is used to permit the specimen to ‘recover’ from the previous test.

When sequential testing is performed so as not to damage the tissue, different tests can be performed yielding different parameters. Because tests are performed on the same specimen, these parameters can be directly compared. The comparison of these parameters between different specimens is more difficult due to the biological variability of the tissue.

Sinusoidal Sequential Testing Profile

After sinusoidal preconditioning, the sinusoidal testing profile involve 17 separate harmonic oscillation cycles at frequencies ranging from $f=0.02$ Hz to $f=4$ Hz. Furthermore, a total of 4 step-relaxation tests are also performed, 2 in tension and 2 in compression, to observe how the behaviour of the tissue changed after successive tests. Each specimen was subjected to a series of 21 tests. A summary of these tests is given in table 3.2 and describes the control parameters of each test. The PDL is non-linear

viscoelastic, yet in experimental design, sine tests were designed around linear viscoelastic theory.

Table 3.2 Summary of sinusoidal sequential loading of uniaxial specimens.

test no.	Description	frequency	amplitude (mm)
1	step-relaxation test	-	0.2
2	Sine test 5 cycles	0.02 Hz	0.2
3	Sine test 30 cycles	0.2 Hz	0.2
4	Sine test 30 cycles	0.4 Hz	0.2
5	Sine test 30 cycles	0.6 Hz	0.2
6	Sine test 30 cycles	0.8 Hz	0.2
7	Sine test 30 cycles	1.0 Hz	0.2
8	step-relaxation test	-	-0.2
9	Sine test 30 cycles	1.2 Hz	0.2
10	Sine test 30 cycles	1.4 Hz	0.2
11	Sine test 30 cycles	1.6 Hz	0.2
12	Sine test 30 cycles	1.8 Hz	0.2
13	Sine test 30 cycles	2.0 Hz	0.2
14	step-relaxation test	-	0.2
15	Sine test 30 cycles	2.2 Hz	0.2
16	Sine test 30 cycles	2.4 Hz	0.2
17	Sine test 30 cycles	2.6 Hz	0.2
18	Sine test 30 cycles	2.8 Hz	0.2
19	Sine test 30 cycles	3.0 Hz	0.2
20	step-relaxation test	-	-0.2
21	Sine test 30 cycles	4.0 Hz	0.2

3.4.5 Treatment of Data

For all mechanical tests on performed on the PDL, whether in traction-compression or in shear, load data in Newtons and deformation in millimetres was obtained at a specific sampling frequency. These data were converted to stress and strain data in making specific assumptions about the system. Because the bone and tooth are virtually rigid compared to the properties of the PDL, they have been considered as rigid and can be considered as extensions of the gripping device.

Concerning the sine tests, the relaxation tests (see table 3.2) were compared. If a significant difference was observed among these four relaxation curves, the data for the specimen were not used. Moreover, if the rupture curve was found to greatly deviate from the average results, these data were not used.

Treatment of Uniaxial Data

With reference to Kirchhoff-St.Venant's linear elastic law for homogeneous isotropic materials (see section 2.6.3) stress is defined by :

$$\mathbf{S}[\mathbf{E}] = \lambda \text{tr}(\mathbf{E})\mathbf{I} + 2\mu\mathbf{E} \quad (\text{EQ 3.2})$$

Referring to the schematics of figure 3.10 where the ligament is shown to undergo a deformation

$$\Delta = L - L_0 \quad (\text{EQ 3.3})$$

and, the force measured by the load cell of the tensile testing machine is represented by \mathbf{q} . Note that in traction, only the element q_{RR} , denoted hereafter as q , is measured. It follows from equation 3.2 that the material stress, or Piola-Kirchhoff-II stress, in the testing direction, S_{RR} , (hereafter denoted as S) may then be calculated:

$$S = \frac{L_0}{L} \cdot \frac{q}{A_0} \quad (\text{EQ 3.4})$$

where L_0 is the initial length of the PDL (i.e. the PDL width), L is the extended width of the ligament and A_0 is the original cross-sectional area of the PDL calculated as

$$A_0 = \text{thickness} \cdot \text{breadth}. \quad (\text{EQ 3.5})$$

With regards to strain, recall the Green-Lagrange strain tensor

$$\mathbf{E} = \mathbf{E}(\mathbf{x}, t) \equiv \frac{1}{2}(\mathbf{F}^T \mathbf{F} - \mathbf{I}) = \frac{1}{2}(\mathbf{H} + \mathbf{H}^T + \mathbf{H}^T \mathbf{H}) \quad (\text{EQ 3.6})$$

from which the E_{RR} (denoted hereafter as E).

$$E = \frac{L^2 - L_0^2}{2L_0^2} \quad (\text{EQ 3.7})$$

for large deformations. Note that for small deformations where $\|\mathbf{E}\| \ll 1$, equation 3.7 can be rewritten by substituting equation 3.3:

$$\begin{aligned} E &= \frac{(\Delta + L_0)^2 - L_0^2}{2L_0^2} = \frac{(\Delta + L_0)^2 - L_0^2}{2L_0^2} = \dots \\ &\dots = \frac{\Delta^2 + 2\Delta L_0 + L_0^2 - L_0^2}{2L_0^2} = \frac{\Delta^2 + 2\Delta L_0}{2L_0^2} \end{aligned} \quad (\text{EQ 3.8})$$

Since Δ is small, i.e. $L \cong L_0$, equation 3.8 becomes:

$$E \cong \frac{\Delta}{L_0} \quad (\text{EQ 3.9})$$

which is the strain measure for a Hookean, linear elastic material.

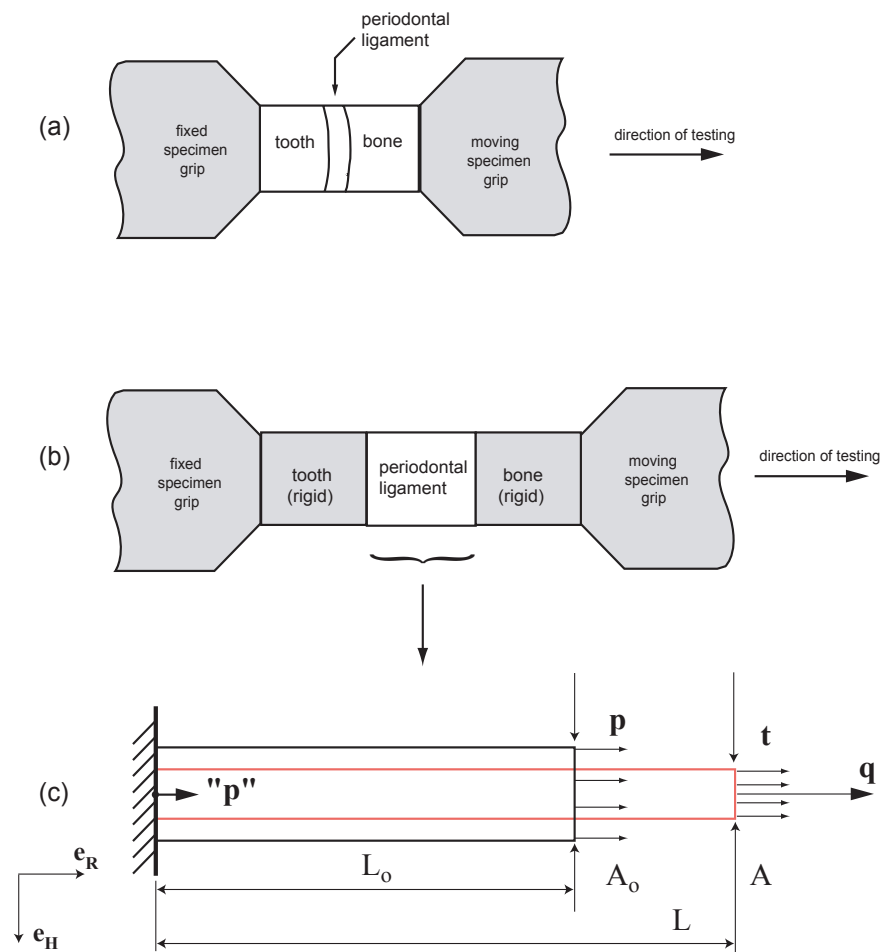
3.5 Shear Specimens

The novelty of the shear tests performed in this thesis lies in that specimens are pushed in the apical, or intrusive, direction as well as in the coronal, or extractive direction. A new shear testing machine is conceived and constructed for this purpose. Moreover, custom-made pieces ensured that they can be used to test the irregular-shaped specimens of the tooth in the socket of the bone.

Shear tests reported in the literature (see section 2.5) pull only in one direction and the methods fail to take into account the biological variability of the specimen manifested in the complex contour of the tooth in a transverse section.

The method to prepare transverse sections is identical to the method to prepare transverse sections for uniaxial specimens. From these sections, custom-made grips are made to hold the bone in place while the bone is moved apically-coronally.

Figure 3.10 Schematic of (a) PDL uniaxial sample in tensile machine showing (b) bone and tooth and (c) how the data is interpreted from simple traction tests.



3.5.1 Design of the Periodontal Ligament Shear Testing Machine

Preliminary studies were performed in order to determine the parameters necessary for the design of the machine. These parameters included:

- 1 **Dimensioning the machine:** shear samples were cut and weights of known mass were hung from the tooth portion of the transverse section to approximate the maximum load and maximum displacement that would need to be taken into account in the design. The geometry of several specimens was taken into account to size the support table.
- 2 **Mounting of the specimen** into the machine: a number of methods were considered to connect the machine to the shear specimen. The methods considered but rejected, included using glue and a spring to hold the specimen during pushing and pulling. The method chosen for preparing the grips is shown in figure 3.12.

3 Instrumentation: after determining the displacement and loading ranges of the machine based on (1), various commercially available components were evaluated and selected for use with the machine. The most important components were the instruments involved in data acquisition. A TTL (Transistor-Transistor Logic) digital displacement sensor as well as a piezoelectric load transducer were implemented into the design of the machine. The other components, i.e. linear screw with micron resolution, motor, gears etc... were also evaluated on an individual basis.

A photograph of the system is shown in figure 3.12.

3.5.2 Methodology and Specific Procedures

Transverse sections are obtained as shown in figures 3.2 and 3.3. Due to the biological variability, each specimen required custom made pieces used only once for each specimen. After obtaining the transverse sections, individual components are designed and fabricated using a selective laser sintering (SLS) rapid prototyping process. Though time-consuming, this procedure simplifies the design of the gripping device and solves many problems reported in the literature concerning the geometrical variability of transverse tooth-PDL-bone sections.

Obtaining Shear Specimens from Bovine First Molar Site

Section 3.2.1 describes how the transverse sections are obtained from bovine first molar sites for uniaxial specimens. The procedure for obtaining transverse sections for shear experiments follows the sample procedure up to this step. Afterwards, the transverse sections undergo a procedure that leads to the design and fabrication of the pieces to attach the section to the shear testing machine.

Design of the Grips for Shear Specimens

Figure 3.12 is a flowchart of the major steps in the conception and design of the grips for shear specimens. After obtaining the specimen, four holes are drilled in each specimen: two holes in the tooth portion of the specimen, and two holes in the bone portion of the specimen. The holes (screw-holes) in the tooth portion are made to allow the 2 mm screws to pass through the tooth to allow a connection between the lower head and the upper head, thus allowing the tooth to be held firmly in place during upwards or downwards motion. The holes drilled in the bone portion (the guideholes) are made to ensure precise horizontal alignment of the specimen when placed and loaded into the machine. The guideholes are made using a template, whereas the screw-holes are made arbitrarily, depending on the shape of the transverse tooth section.

After drilling the four holes in the transverse section, the specimen is scanned using a standard office scanner set at a scale of 1:1. With the digitized image of the transverse section, the contours of the four drillholes, as well as the irregular contour of the PDL region are traced with the aid of a computer aided design (CAD) program [Coreldraw].

Exporting these contours into a 3D CAD program [Solidworks], the pieces as shown in step 10 of figure 3.12 are made. The four pieces constitute a unique set for each specimen. Using 2 mm screws, the (a) upper head and (d) lower head are used to clamp the tooth part of the transverse section. The upper head is attached to the machine allowing the clamped tooth portion to be pulled and pushed. The (b) upper and (c) lower bone support are used to clamp the bone portion of the transverse section. Clamping of the bone supports to the fixed support table of the machine is done using 4 clamps as shown in figure 3.12f.

The 3D files are exported as .STL (Standard Template Library) files which are used directly by the selective laser sintering machine for the fabrication of the pieces.

3.5.3 Tests to determine the mechanical behaviour of PDL Shear Specimens

Zeroing the Shear Specimen

Defining the “zero” of the shear specimen before testing is necessary in order to have a known reference point for interpretation of the data collected from the experiment. The zero is defined as the point at which stress and strain values are set to equal zero. When the PDL is deformed in shear it displays, as any soft tissue, a distinct “toe” region (figure 2.6). It is in the toe region that the collagen fibres are said to uncrimp and align along a preferential direction. In the literature, the beginning of the toe region is usually defined as the zero, though results presented in this manner can be misleading, especially when the shear specimen is to be tested both in apical and coronal directions. As a result, a method was developed to determine the zero of the shear specimen prior to testing.

After placing the shear specimen into the grips, the position of the displacement sensor is recorded, D_0 . The zero is determined by slowly pulling the sample in the coronal direction to a load of $F_t = 10$ N. The position, D_t , at F_t is recorded, and then the specimen is sheared to a load of $F_c = -10$ N. The position, D_c , at F_c is recorded and the zero, D'_0 , is obtained by equation 3.1. Determining the zero is shown graphically in figure 3.6.

Figure 3.11 Technical drawing of the PDL Shear Testing Machine

Ligament
Shear
Testing
Mechine

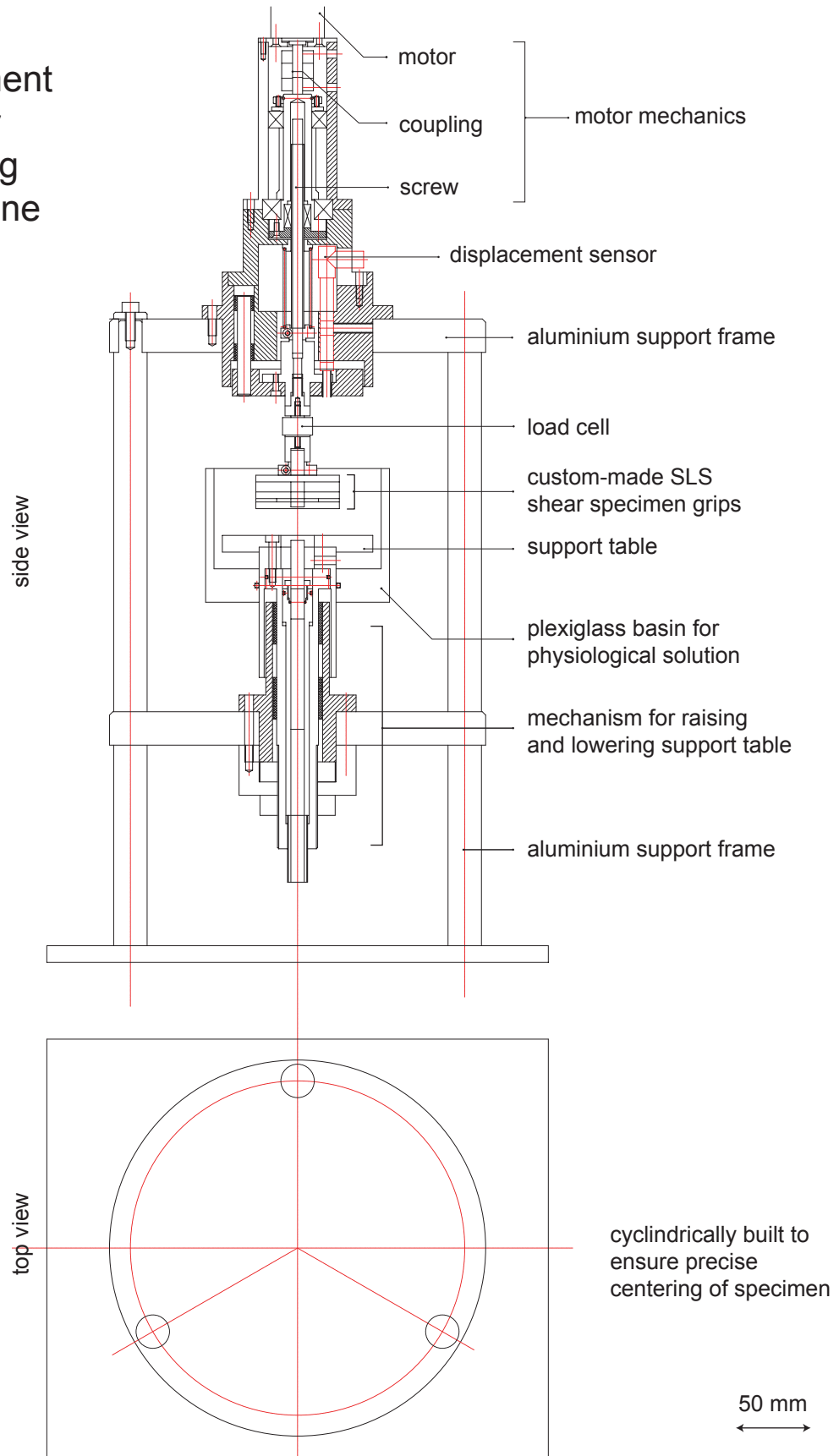
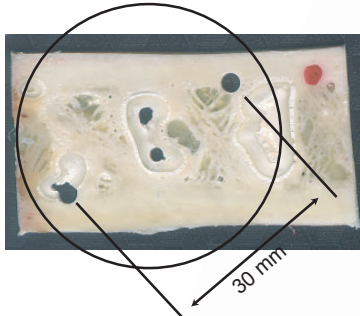
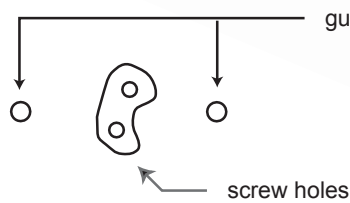


Figure 3.12 Design of the custom-made grips for PDL shear test specimens *

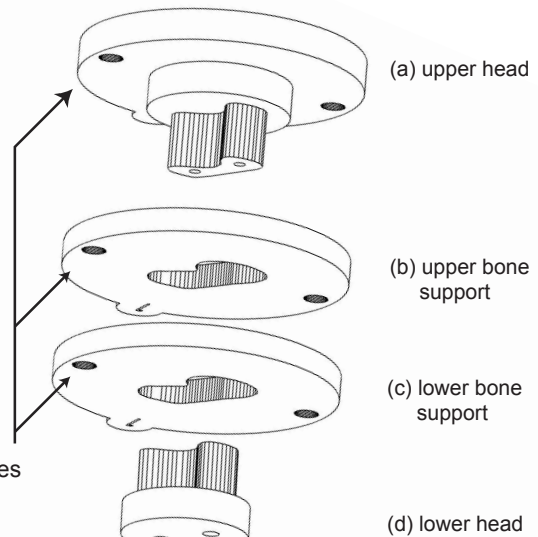
7. Drill holes in shear specimen for centering specimen into grips and onto machine



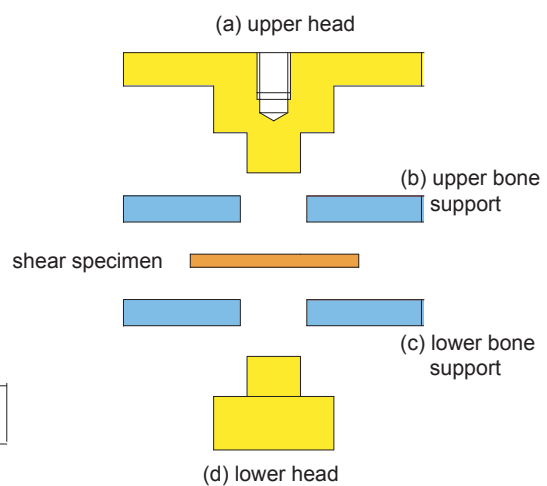
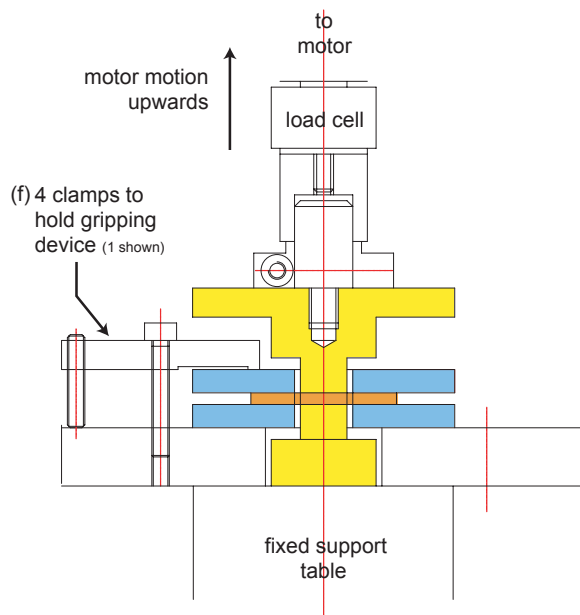
8. Draw contours of drillholes and tooth/bone contours from specimen geometry



9. Design and make pieces based on contours obtained from specimen dimensions



10. Load shear specimen into shear testing machine



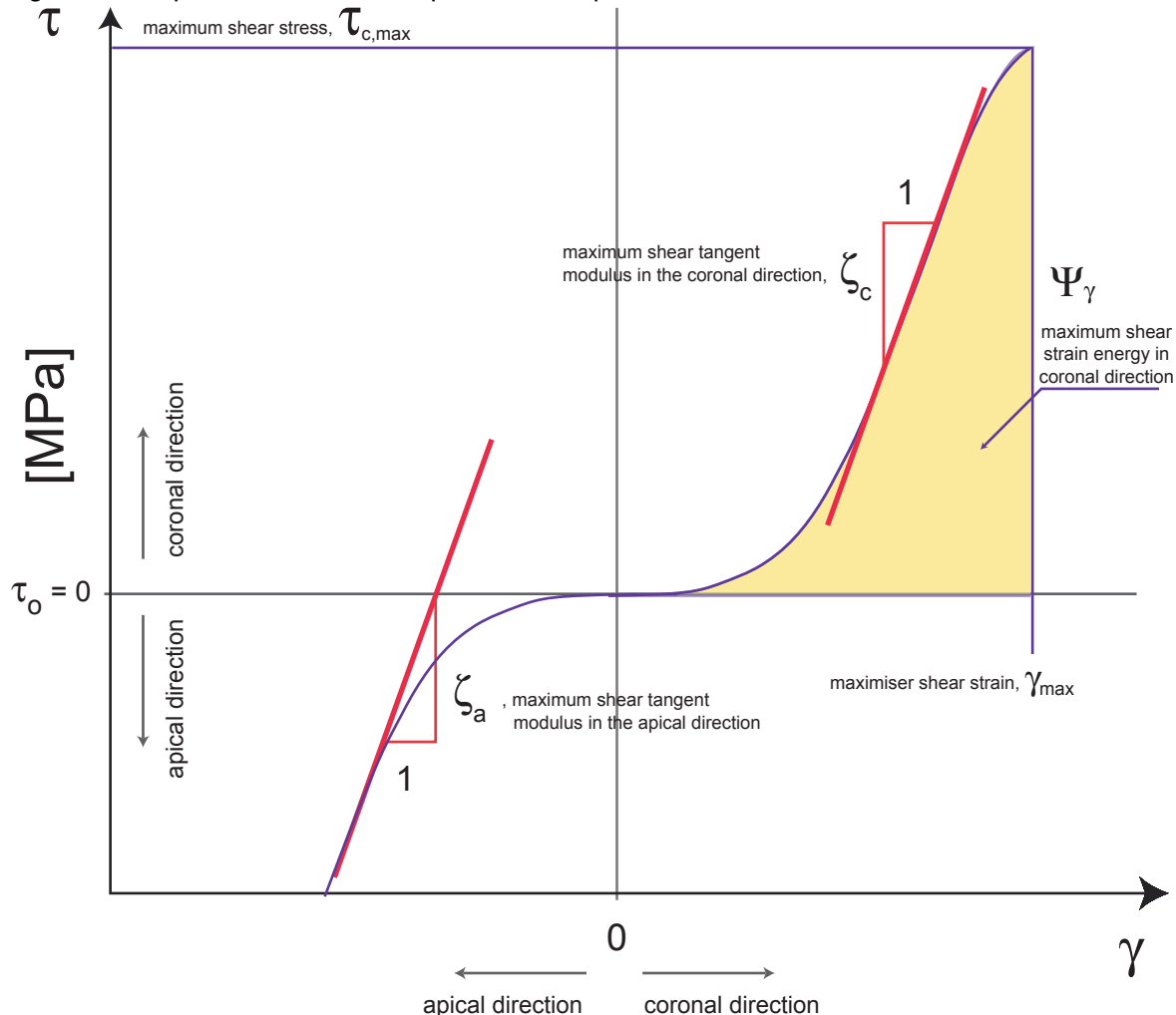
SLS custom-made pieces

* this figure continues from figure 3.3.

Figure 3.13 Photograph of Shear Testing Machine after construction



Figure 3.14 Rupture curve of shear specimen with parameters obtained from each curve



Preconditioning

All shear specimens are preconditioned by subjecting them to 10 harmonic cycles with a shear strain amplitude of 0.30 at a frequency of 1 Hz. It is also possible to precondition samples by using triangular waveforms. This is shown graphically in figure 3.7.

Relaxation Tests

When performing relaxation tests, theoretically there is an instantaneous strain jump at $t = 0$ (see section figure 2.7.4). Practically, this is not possible because a finite amount of time, t^* , is necessary to deform the specimen from $\gamma = 0$ to $\gamma = \gamma_i$ to produce an appropriate relaxation response $G(t, \gamma_i)$. Shear specimens are pulled to a shear strain, $\gamma_i = 0.50$ in both the coronal direction as well as in the apical direction.

Sinusoidal Tests

All shear specimens subjected to sinusoidal loading undergo the zeroing process as well as sinusoidal preconditioning. The amplitude of 0.3 mm for testing was established in a preliminary study (section 6.1).

Frequencies used ranged from $f_{\min} = 0.01$ Hz to $f_{\max} = 4$ Hz.

Rupture Tests

The rupture curve of a shear specimen is performed in the coronal direction, i.e. the same direction as the extractive direction of the tooth. Before rupture, however, the shear specimen is pushed in the apical direction to a shear strain of 0.3 before reversing the direction and rupturing in the coronal direction. The parameters obtained from each shear specimen in rupture are shown in figure 3.14 and are:

- 1 maximum shear stress in the coronal direction, $\tau_{c,\max}$
- 2 maximum shear strain at maximum shear stress, or maximiser shear strain, γ_{\max}
- 3 maximum shear strain energy at rupture in coronal direction,
- 4 maximum shear tangent modulus in the coronal direction, ζ_c
- 5 maximum shear tangent modulus in the apical direction, ζ_a

Sinusoidal Sequential Testing Profile in Shear

After sinusoidal preconditioning, the sinusoidal testing profile involve 17 separate harmonic oscillation cycles at frequencies ranging from $f=0.02$ Hz to $f=4$ Hz. Furthermore, a total of 4 step-relaxation tests are performed, 2 in the coronal direction and 2 in the apical direction, to observe relaxation behaviour and how the behaviour of the tissue changed after successive tests. Each specimen is subjected to a series of 21 tests. A summary of these tests is given in table 3.3 and describes the control parameters of each test.

Table 3.3 Summary of sinusoidal sequential loading of shear specimens.

test no.	Description	strain rate	amplitude (mm)
1	coronal step-relaxation	-	0.3
2	Sine test 5 cycles	0.02 Hz	0.3
3	Sine test 30 cycles	0.2 Hz	0.3
4	Sine test 30 cycles	0.4 Hz	0.3
5	Sine test 30 cycles	0.6 Hz	0.3
6	Sine test 30 cycles	0.8 Hz	0.3
7	Sine test 30 cycles	1.0 Hz	0.3
8	apical step-relaxation test	-	-0.3
9	Sine test 30 cycles	1.2 Hz	0.3
10	Sine test 30 cycles	1.4 Hz	0.3
11	Sine test 30 cycles	1.6 Hz	0.3
12	Sine test 30 cycles	1.8 Hz	0.3
13	Sine test 30 cycles	2.0 Hz	0.3
14	coronal step-relaxation test	-	0.3
15	Sine test 30 cycles	2.2 Hz	0.3
16	Sine test 30 cycles	2.4 Hz	0.3
17	Sine test 30 cycles	2.6 Hz	0.3
18	Sine test 30 cycles	2.8 Hz	0.3
19	Sine test 30 cycles	3.0 Hz	0.3
20	apical step-relaxation test	-	-0.3
21	Sine test 30 cycles	4.0 Hz	0.3

3.5.4 Treatment of Shear Data

For shear tests the $\text{tr}\mathbf{E} = 0$ therefore the Kirchhoff-St. Venant becomes

$$\mathbf{S}[\mathbf{E}] = 2\mu\mathbf{E} \quad (\text{EQ 3.10})$$

It is difficult to predict the structure of the ligament in a state of stress in relation to a homogeneous deformation. It is particularly true when the ligament undergoes a shear deformation. In order to interpret the results, one must assume that the state of stress remains planar, analogous to a pack of cards sheared in the principal loading direction. Indeed, the nominal stress tensor is not symmetric

$$[\mathbf{P}] = \begin{bmatrix} P_{HH} & P_{HR} & 0 \\ P_{RH} & P_{RR} & 0 \\ 0 & 0 & 0 \end{bmatrix} \quad (\text{EQ 3.11})$$

In the case of the shear test for the PDL the force being measured by the load cell is q_{HH} and allows for the definition of the shear stress, τ , to be defined

$$\tau = \frac{q_{HH}}{A} \quad (\text{EQ 3.12})$$

and A is the area subjected to shear defined by

$$A = \text{thickness} \cdot \text{perimeter}|_{\text{PDL}} \quad (\text{EQ 3.13})$$

The perimeter is calculated using

$$\text{perimeter}|_{\text{PDL}} = \frac{P_t + P_b}{2} \quad (\text{EQ 3.14})$$

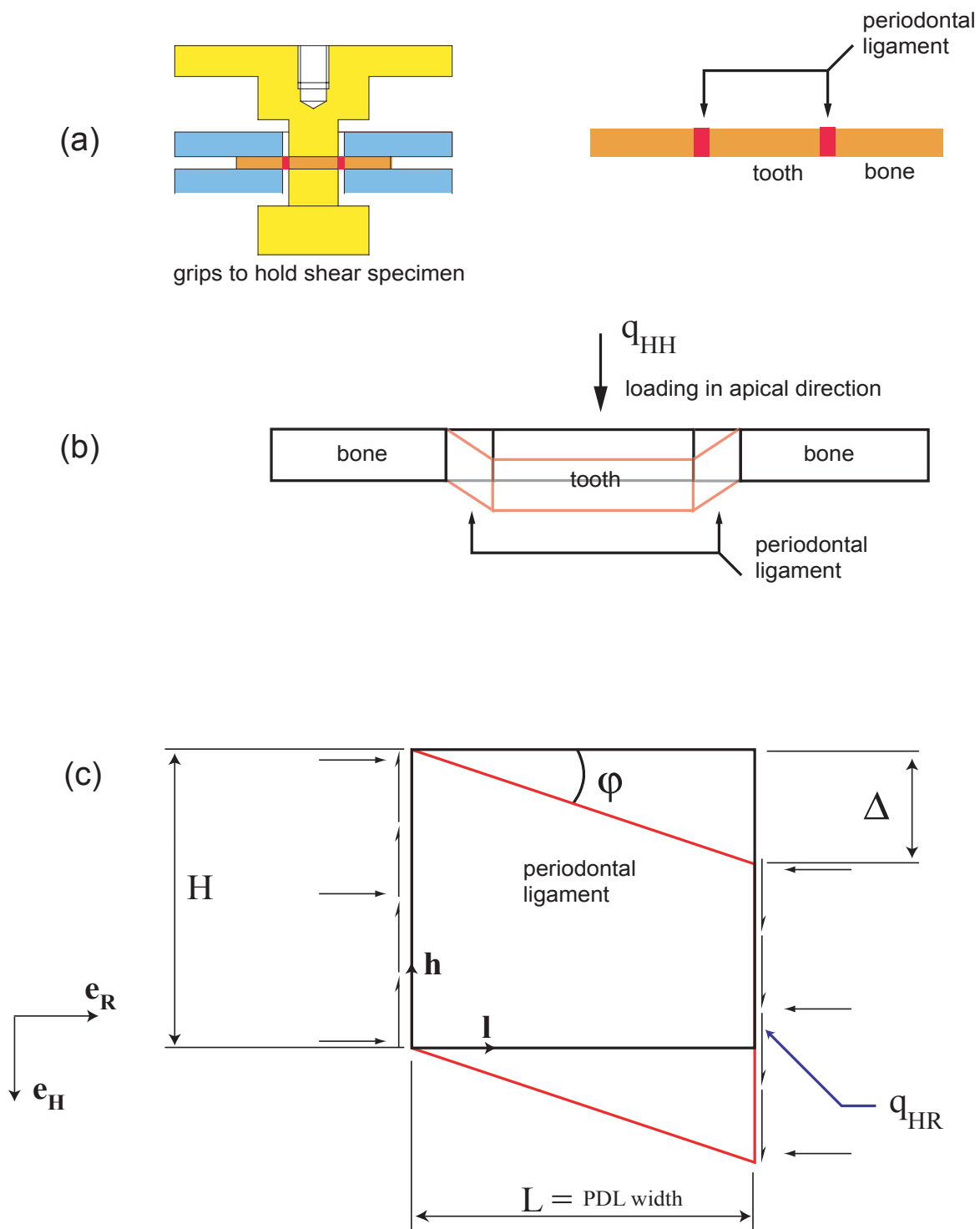
where P_t and P_b are measured from the specimen as shown in figure 4.2.

The shear strain, γ , is defined as

$$\tan \phi = \gamma = \frac{\Delta}{L} \quad (\text{EQ 3.15})$$

where Δ , ϕ and L are shown in figure 3.15c.

Figure 3.15 Schematic of (a) PDL shear specimen in machine showing (b) bone and tooth and how (c) the data obtained from the shear test is used to interpret results.



-
-
-

-
-
-

•

•

•

“The subtlest beauties in our life are unseen and unheard.”

Kahlil Gibran

•

•

•

4

Results: Geometry, Structure and Histology

Important in the study of problems in biomechanics is the understanding of the morphology, histology, the structure and ultrastructure in order to know the geometric configuration of the system under investigation. The work of this thesis has collected such information using a number of methods and techniques.

- 1 The first and simplest of the methods involves measuring the untreated and untested specimen with standard laboratory equipment to identify key dimensions (section 4.1).
- 2 A second technique obtains the dimensions non-destructively from an intact bovine first molar system fresh after slaughter using μ CT scans, and 3D reconstructive methods (section 4.2)
- 3 A third technique used optical microscopy to investigate the uniaxial specimen during deformation (sections 4.3 & 4.4).
- 4 The fourth technique studied the biology and ultrastructure of the PDL, alveolar bone and tooth using methods of histological investigation (section 4.5)

4.1 Geometrical Measurements taken from Specimens

Prior to testing the uniaxial and shear specimens, measurements were made with calipers, and through optical microscopic observation. A summary of the dimensions of these specimens is presented in this section.

4.1.1 Uniaxial Specimen Dimensions

After sectioning the uniaxial specimen to its final form, measurements are made of its (i) thickness, (ii) breadth, and (iii) PDL width. The dimensions of $n=67$ specimens are defined in figure 4.1. A summary of these measurements is presented in table 4.1.

Table 4.1 Average Dimensions of Uniaxial Specimens

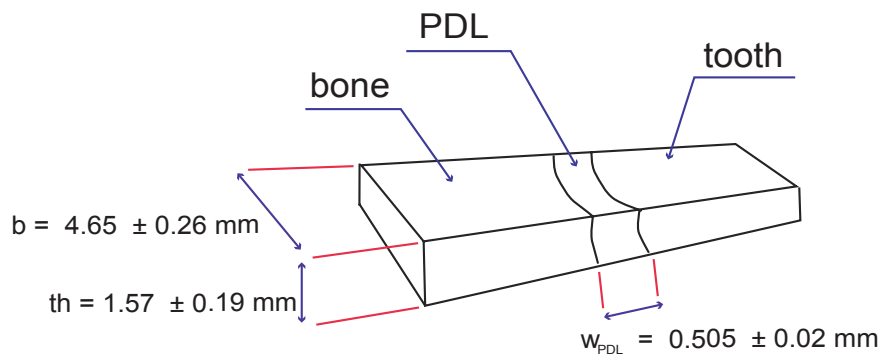
dimension	n = 67*
PDL width, w_{PDL}	0.505 ± 0.020 mm
Breadth, b	4.650 ± 0.260 mm
Thickness, th	1.570 ± 0.190 mm

averages based on measurements taken from 67 uniaxial specimens

The cross-sectional area of the PDL taken into account for the calculation of stress values is calculating using the relation

$$A = b \cdot th \quad (\text{EQ 4.1})$$

Figure 4.1 Dimensions of the PDL specimens



b : specimen breadth
th : specimen thickness
 w_{PDL} : PDL width

average dimensions of uniaxial specimens
(based on $n=67$ samples)

4.1.2 Shear Specimen Dimensions

After sectioning the shear specimen to its final form, measurements are made of its (i) thickness, (ii) perimeter of PDL at bone interface, (iii) perimeter of PDL at tooth interface, and (iv) PDL width. These dimensions are defined by figure 4.2. The typical P_t ranged from 36 to 44 mm (mean value = 40 mm) and the typical P_b range from 34 to 42 mm (mean value = 38 mm).

The PDL width is measured using an optical microscope and an image analysis software package (National Instruments Image Acquisition IMAQ Vision Builder). For each specimen, between 6-10 measurements are made to obtain the PDL width for the given specimen. The average PDL width for all shear specimens is 0.535 ± 0.027 mm.

The average thickness of the shear specimens is 1.81 ± 0.15 mm.

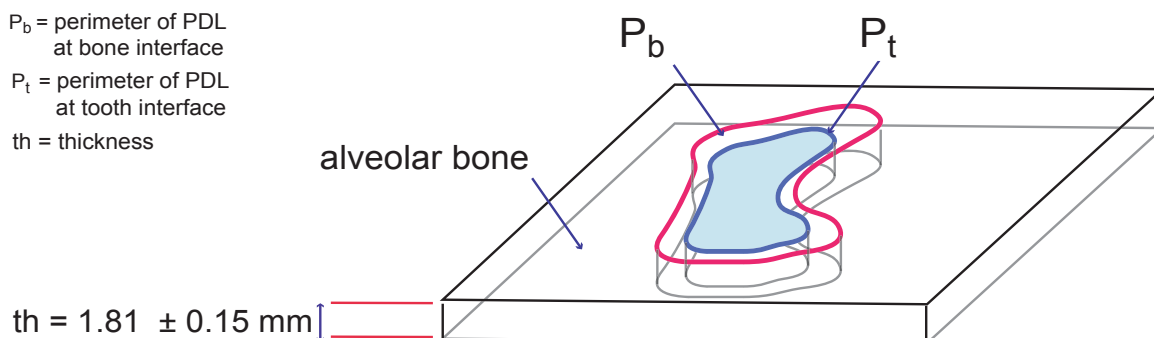
Table 4.2 Average Dimensions of Shear Specimens

dimension	n = 14
PDL width, w_{PDL}	0.535 ± 0.027 mm
Thickness, th	1.810 ± 0.150 mm
P_t	~40 mm
P_b	~38 mm

averages based on measurements taken from 14 shear specimens

Figure 4.2 Measured Dimensions of the Shear Specimens

P_b = perimeter of PDL
at bone interface
 P_t = perimeter of PDL
at tooth interface
th = thickness



4.2 Geometrical Measurements taken from μ CT scans

The μ CT scans of a first molar bovine tooth enables 3D reconstruction using certain software packages (see section 3.2). With the μ CT scans with a resolution of 75 μm , it is possible to take measurements of the system with a reasonable precision.

Different measurements are taken. Dimensions indicative of the dimensions of the tooth are presented, e.g. PDL width (w_{PDL}). Moreover, the relative volume of the ligament is estimated.

4.2.1 3D Reconstruction Method

Image Acquisition

The scans of the first molar tooth are performed transversally, i.e. planes defined by the long axis of the tooth. Of the 700 scans performed, six are presented in figure 4.3. Looking at each of these images in detail already gives an idea of the morphology of the tooth - ligament - bone system. On each of the images, a circle is seen at the extremities of the scan. This is the recipient in which the tooth is placed during the scanning process. The tooth is held in place by foam which cannot be seen in the image due to the low attenuation coefficient.

The most apical of the images in figure 4.3, *image a* shows 4 zones. Zone 1 represents the compact bone, zone 2 represents the trabecular bone, and zone 3 represents the tooth. The fourth zone is the PDL defined as the thin layer around the contour of the transverse sections of the teeth.

More coronal than *image a*, *image b* show the roots to be larger in diameter and in place of the trabecular bone as seen in *image a*, there is now compact bone. *Image c* represents the transverse section near the point at which the tooth becomes visible, seen by the thin thickness of bone around the tooth roots. *Image d* no longer shows any sign of bone, indicating that this section represents the region where the crown of the tooth is protruding from the mandible. *Image e* shows bright contours on the outer surface of the teeth. These represent the enamel of the tooth.

Contour Tracing

The 3D reconstruction of the tooth requires that a selection of transverse scans be traced. Using *ImageJ*, an imaging software program, and the original image in figure 4.4a, the negative of the image is produced (b), and the *find edges* tool is used to determine the contours of the scan. This image is then imported by a CAD program, CorelDraw. Using the supplied Bézier tools, the contours are traced and the original image is erased leaving image (c).

Figure 4.3 Image acquisition of bovine first molar using μ CT scanner.

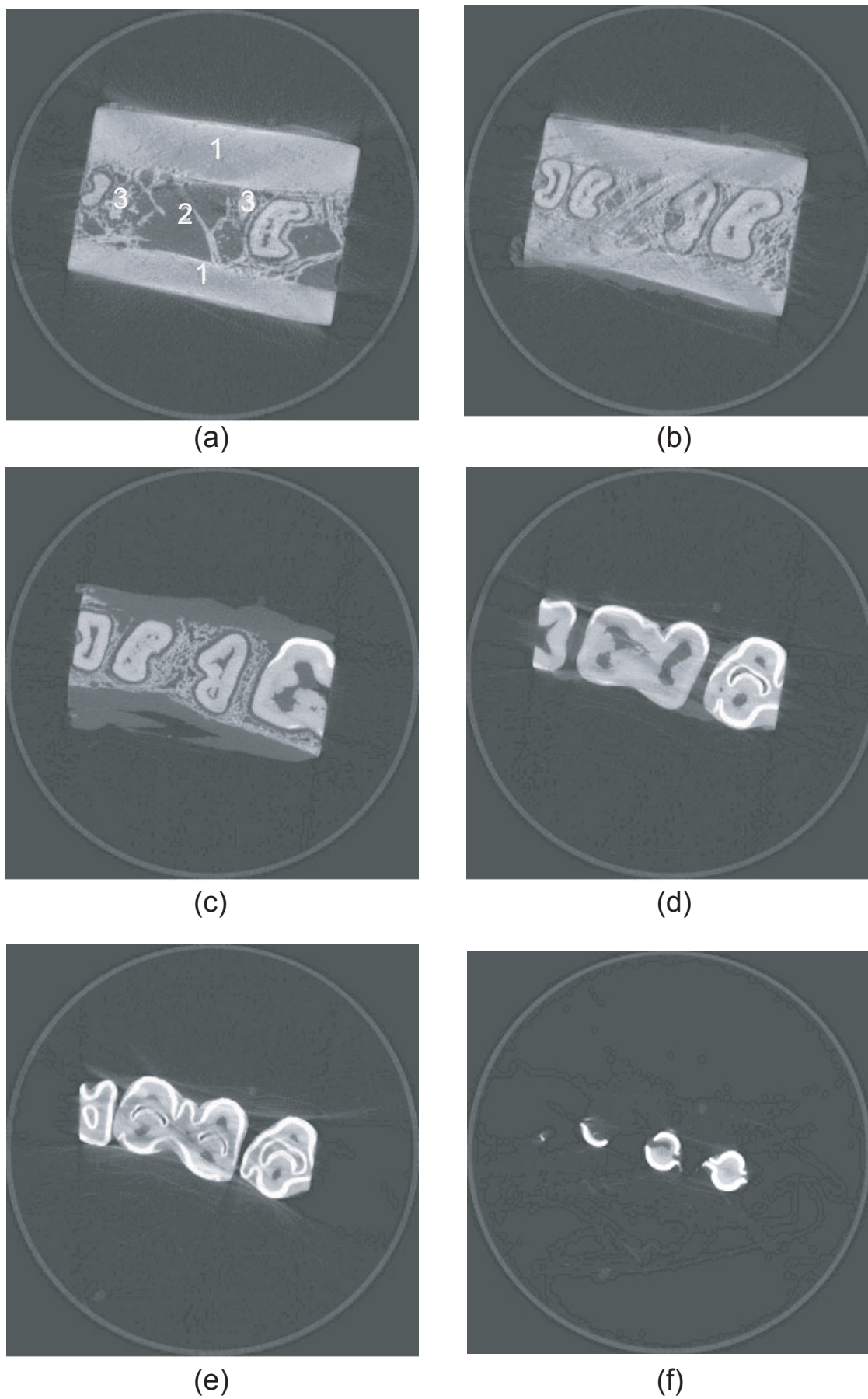
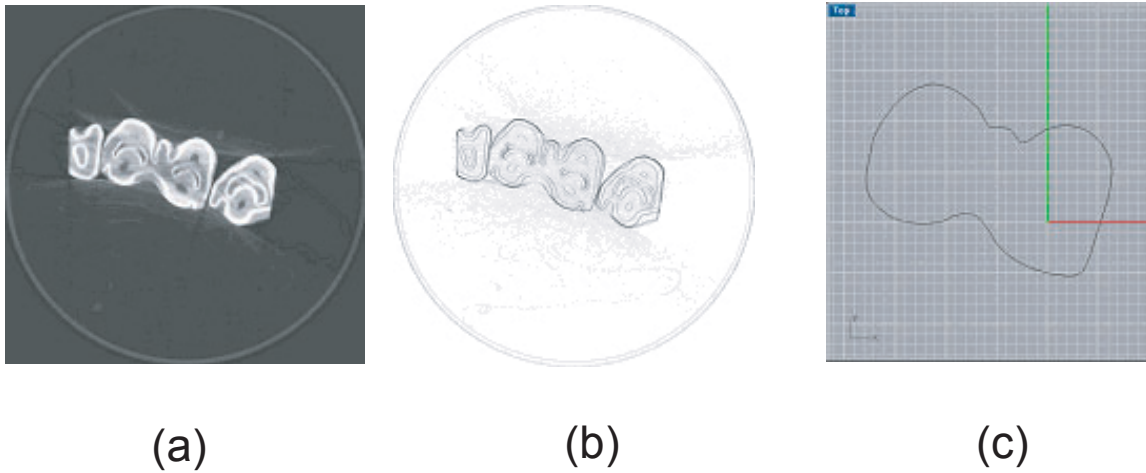


Figure 4.4 Tracing of the contours from (a) the original image, (b) the modified image to produce (c) the traced contour of the tooth.

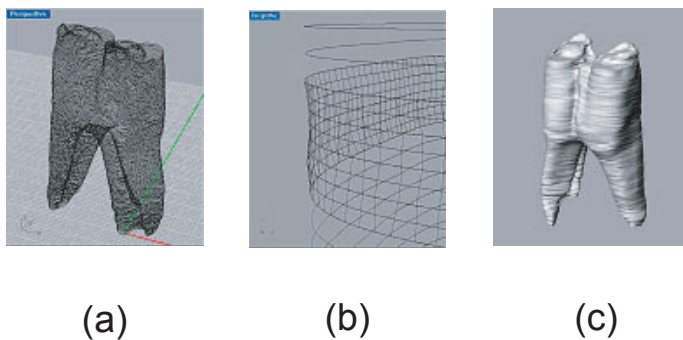


3D Reconstruction of the Tooth

The program selected to perform the reconstruction of the tooth in 3 dimensions was Rhinoceros. This program has powerful surfacing tools and was indispensable in the reconstruction of the complex geometry of the tooth. With the software tools available, three different methods are used to reconstruct the tooth from the traced contours.

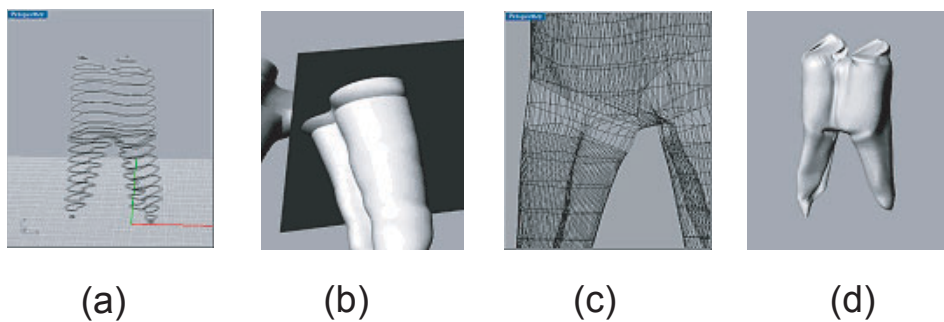
Method 1 : This method uses the contours in the most precise possible way, however, produces a tooth that is not realistic. Taking each pair of adjacent contours and joining and smoothing them create successive sections of the surface of the tooth as shown in figure 4.5b. Doing this creates three surfaces: the crown of the tooth, and the mesial and distal roots. Finally, all remaining surfaces can be joined as shown in figure 4.5c. Although precise, this method is not used due to the undulated surface demonstrated in the final reconstructed tooth.

Figure 4.5 The steps of method 1 (a) all the contours, (b) the successive joining of the surfaces, and (c) the joining of the different parts.



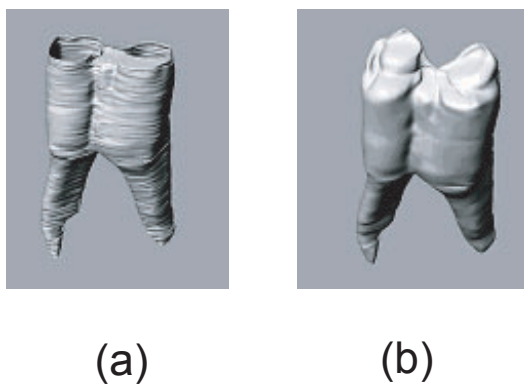
Method 2 : This method creates a seemingly realistic surface of the tooth, however, the resultant reconstruction is not precise. In order to reduce the undulated effect as obtained by method 1, the number of transverse sections used is significantly reduced. In reducing the number of contours used for the reconstruction of the surface, the smoothing program can generate smooth surfaces. This translates into an estimation, and does not properly represent the morphology of the tooth. This method is not used to reconstruct the tooth.

Figure 4.6 The steps of method 2 (a) import a reduced number of contours to (b) perform smoothing and then perform (c) blending to obtain (d) a reconstruction with a realistic form.



Method 3 : this reconstruction is similar to method 1 as it involves using all the contours, however, each contour is treated to reduce the undulated surface as experienced in method 1. Using a function incorporated in the software of Rhinoceros, the surfaces with a certain radius of curvature are smoothed. In doing so, a smoother, more realistic surface is obtained.

Figure 4.7 Method 3 involved creating the undulated surface (a) before using a smoothing function to produce (b).



4.2.2 General Dimensions of the Bovine First Molar

The general dimensions of the tooth are presented in table 4.3.

Table 4.3 General dimensions of the bovine first molar

	Tooth	PDL
Height	51 mm	28 mm
Breadth (mesial to distal)	27 mm	29 mm
Area	3481 mm ²	1727 mm ² *
Volume	8632 mm ³	1031 mm ³

* area of PDL calculated based on surface in contact with the tooth.

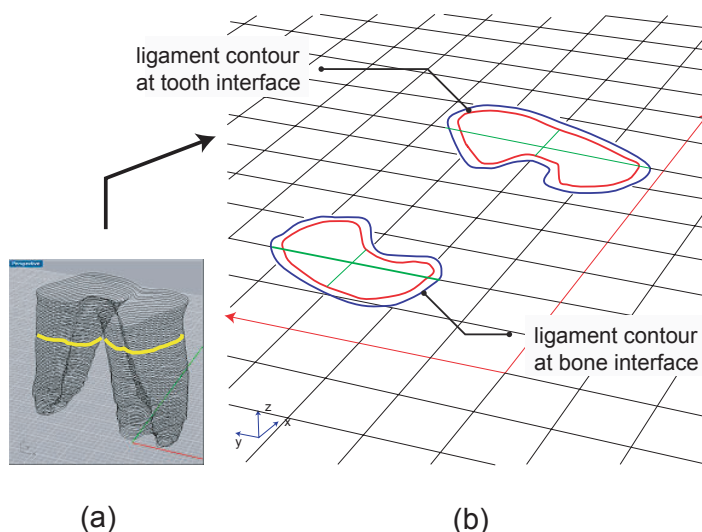
4.2.3 Periodontal Ligament Width from 3D Reconstruction

It is possible to measure the PDL width at different depths along the long axis of the tooth. For each contour corresponding to a specific depth, determining the PDL width consists of measuring (i) the contours defined by the PDL and the surface of the tooth giving the perimeter of the ligament at the tooth/PDL interface, P_t , and (ii) the contours defined by the PDL and the surface of the bone giving the perimeter of the ligament at the bone/PDL interface, P_b (see figure 4.8). It is also necessary to measure the area defined by P_t and P_b in the xy-plane giving A_t and A_b respectively. The average PDL width, w_{PDL} is calculated using the relation

$$w_{PDL} = \frac{A_b - A_t}{(P_b + P_t)/2} \quad (\text{EQ 4.2})$$

Measuring the PDL width in this manner gives an average dimension of $623 \pm 32 \mu\text{m}$

Figure 4.8 Measurement of PDL width from μ CT scans: (a) tooth showing the transverse sections used for measuring the PDL width, with yellow indicating the transverse section shown in (b).



4.3 Variation of PDL Width with Root Depth

From a single first molar tooth, approximately 30 uniaxial samples are obtained below the apex of the tooth. Measuring the PDL width, w_{PDL} , of each specimen and plotting this as a function of depth shows a dependence of the ligament width on tooth geometry.

Shown in figure 4.9 is a presentation of two sets of data; one set of data is obtained experimentally from specimens ($n=28$) of a single molar tooth, the other set of data is measured from the 3D reconstruction as described in section 4.2.3. The tendency shown by both plots in figure 4.9 is that w_{PDL} decreases as it is measured more apically, i.e. the w_{PDL} is thinner as you move deeper along the tooth.

Note, however, that the two curves show an average difference of PDL width of 10% ($\sim 55 \mu\text{m}$). This difference can be accounted for in comparing the methods of measuring w_{PDL} . First, the specimens are measured using an optical microscope, with which roughly five measurements are made in pixels. With the aid of a template of standard dimensions, pixels were converted to millimetres. Although precise measurements are obtained, the difficulty arises in the definition of the PDL interface with the bone and the tooth. This difficulty is seen in figure 4.10; the continuous (red) lines are arbitrary. Overcoming this difficulty comes with experience in manipulating specimens, and remains an excellent accurate method to quickly measure w_{PDL} . The second method, from the 3D reconstruction, is precise in that many measurements are made at any given depth, and the width is in fact an average of the whole PDL width around the contour of the tooth. The error, however, originates from the scan. All μ CT scans are taken with a resolution of $75 \mu\text{m}$ which falls into the range of the 10% difference in values mentioned above. Note how the error bars are larger in measurements made from μ CT scans.

Figure 4.9 PDL width with depth

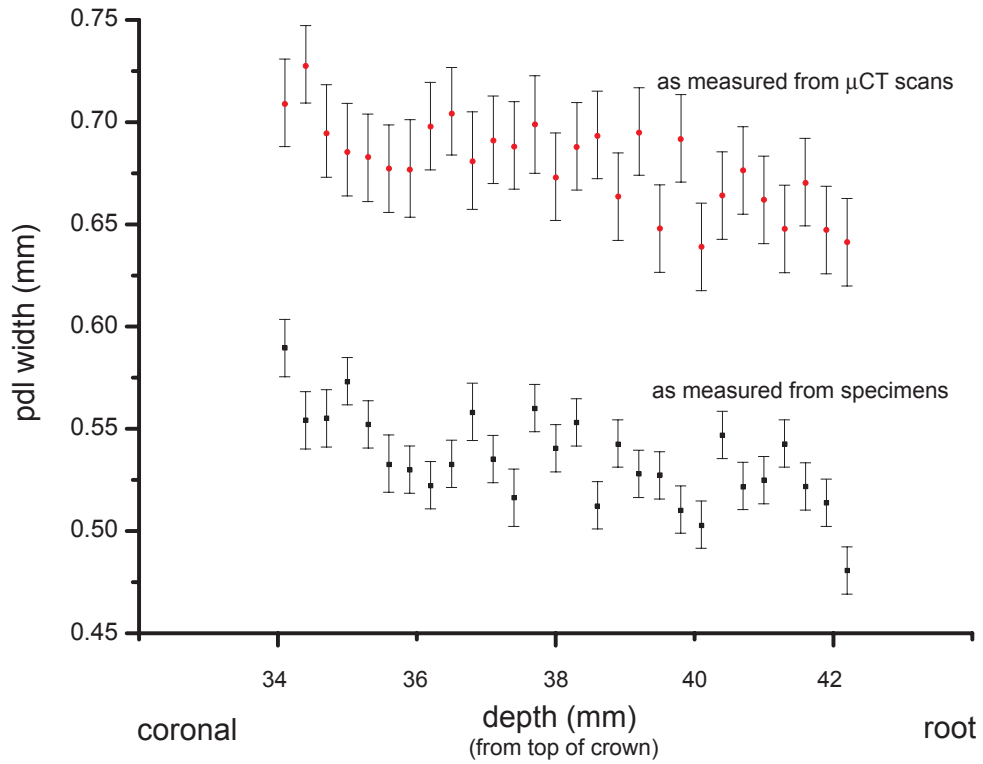
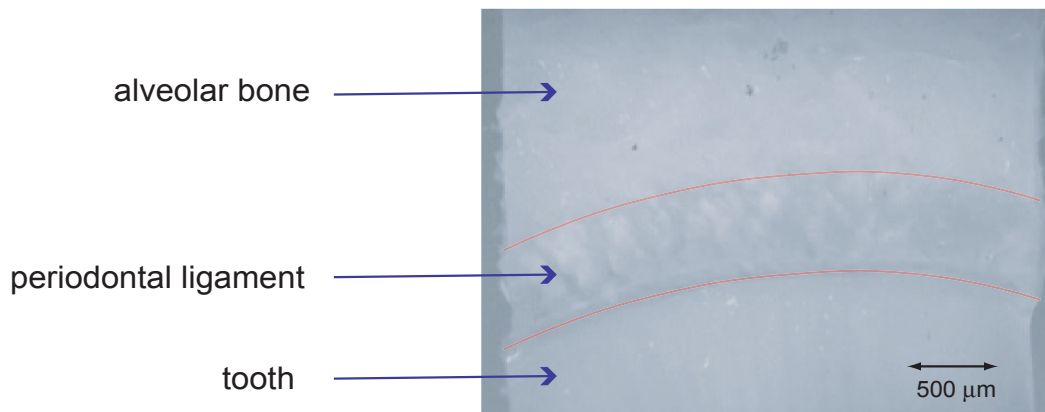


Figure 4.10 PDL, bone and tooth showing difficulty in defining interface for measurements (viewed by optical microscope at 4x magnification).



4.4 Morphology of Uniaxial Specimen During Loading

The morphology of uniaxial specimens is observed during loading and rupture with an optical microscope set up over the machine during the loading profiles. The initial goal of this study is to identify the variation in the structure of the collagen fibres during deformation in the physiological range. This method proved to be insufficient because no definite structure of the PDL could be identified at deformations less than the maximiser strain. These attempts, however, brought out three important findings that account for the mechanical behaviour of the PDL.

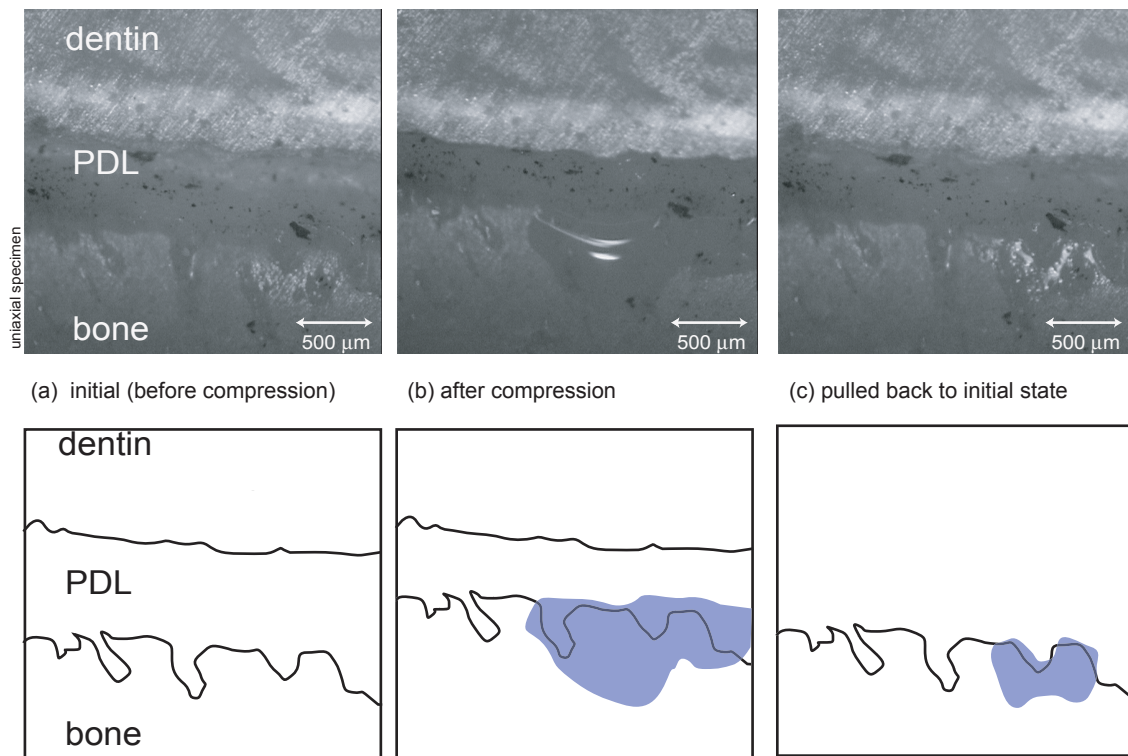
- 1 The first observation shows the expulsion of liquid when the PDL is compressed, with this liquid later being re-infiltrated into the ligament once pulled in tension back to its initial state.
- 2 The second observation shows the appearance of a void at $E = 0.75$ during the rupture of the ligament, through histological studies described in section 4.5, this void is in fact a blood vessel brought into evidence under loading.
- 3 The final observations involve the total failure of the ligament. Sequential images are taken during ligament rupture and provide useful data on the PDL.

4.4.1 Expulsion of Fluid from Periodontal Ligament in Compression

It is observed that uniaxial specimens subjected to compressive loads result in the PDL to expel fluid. When the ligament is pulled back to its initial state, the majority of the fluid, yet not all, is absorbed back into the tissue. This observation is recorded using a CCD camera to capture this phenomena in images. The images are presented in figure 4.11. *Image a* shows the ligament in its initial state, *image b* shows the ligament after being compressed $150\ \mu\text{m}$, or to 30% of the PDL width. The schematic of *image b* shows the region where fluid is expelled indicated by the shaded blue area. *Image c* shows how the majority of fluid is absorbed back into the tissue, however, clearly some fluid remains on the surface of the bone.

This is a significant finding in that it indicates that fluid flow within the tissue does play a role in the mechanical behaviour. To what degree fluid contributes to mechanical behaviour cannot be determined from these observations.

Figure 4.11 Uniaxial specimen in its initial state (a) pushed into (b) compression showing fluid expulsion from the PDL, with fluid resorption when pulled to initial state (c).



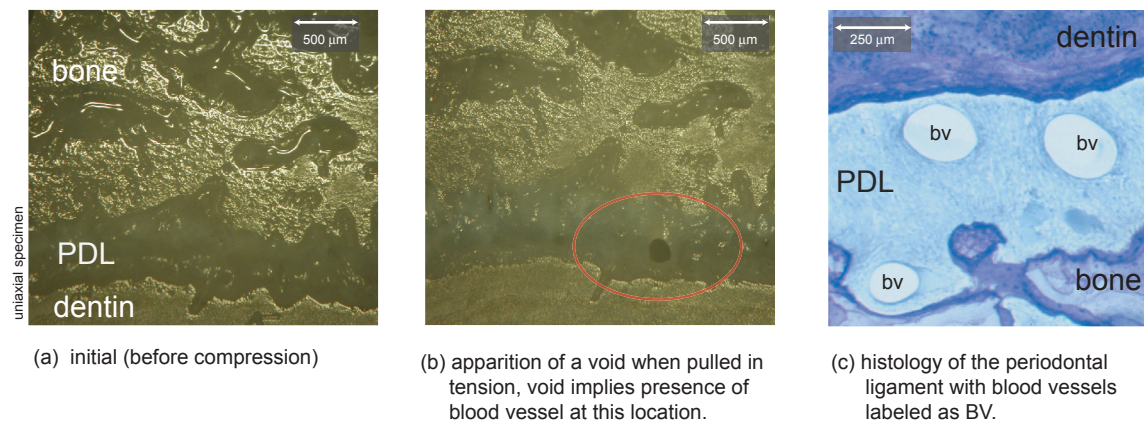
4.4.2 Apparition of Voids when PDL is Pulled in Tension

When uniaxial specimens are pulled in tension, voids appear in the middle region of the ligament between the tooth and the bone. This apparition of voids at first, was unexplained and was attributed to the gradual degradation and breakdown of the collagen fibre network. It was after obtaining histology slides of the PDL that the voids were explained by the presence of blood vessels in the tissue.

The three images in figure 4.12 show how a void comes into apparition when the ligament is pulled in tension. *Image a* shows the ligament in its unloaded initial state. The interfaces of the bone-ligament and dentin-ligament are clearly distinguishable. Pulling the specimen to approximately $E = 0.75$ results in the apparition of the first voids as indicated by on *image b*. Comparing this image to a histological slide of the PDL, it is clear that the void indicates that a blood vessel is present at that location. For more detail on the histology and biology results of the PDL see section 4.5.

As the ligament continues to rupture, more voids appear until complete rupture of the ligament occurs. This is described in the next section.

Figure 4.12 Apparition of voids when PDL is pulled in tension. The circular void appearing implies the presence of a blood vessel in the PDL at this location.



4.4.3 Rupture Tests with Sequenced Image Acquisition

In a series of experiments performed on uniaxial test specimens, load data, deformation data and image data are synchronized and collected simultaneously making it possible to relate the images of the ligament to the corresponding stress-strain curve. From optical microscope observations some observations regarding the structure of the PDL during deformation are made.

The images presented in figure 4.14 & figure 4.15 show a single uniaxial specimen at different strain stages from $E=0.25$ to $E=2.0$. The graph in figure 4.15 shows the strain and stress curve for this specimen, which indicate the values that correspond to the *images a - k*.

Image a shows the ligament at $E=0.3$; no information with regards to the structure of the ligament is obtained.

Image b shows the ligament at $E=0.7$; a first void appears (1) implying the presence of a blood vessel at that location. Darker circular areas begin to appear (2) at the surface of the ligament showing where the ground substance is thinning, and further voids are to form.

Image c shows the ligament at $E=0.9$; new apparition of voids (2) are observed. The void (1) has become oval-shaped indicating that the cylindrical blood vessel is being elongated non-uniformly in the direction of loading. An apparition of a darker region (3) indicate where a new void is forming.

Image d shows the ligament at $E=1.0$; The voids (1 & 2) become more difficult to distinguish as they are pulled to greater strain. A void (3) begins appears. New voids form (4 & 5).

Images e & f show the ligament at $E=1.2$ and $E=1.3$ respectively; the voids have now interconnected and the collagen fibre bundles (6, 7 & 8) become distinguishable. It is

noted that the ligament is rupturing in the middle regions, whereas the tissue near the interfaces of the bone and dentin remain relatively intact. The tissue in the background (9) shows that rupture is occurring throughout the depth of the ligament.

Image g shows the ligament at $E=1.4$; the fibre bundles are apparent (6, 7 & 8) and run almost perpendicular from bone to dentin. Moreover, the bundles are thinning as deformation increases.

Images h - k show the ligament from $E=1.6$ to $E=2.0$; note the further thinning of the fibre bundles (6, 7 & 8) and the dark zone (9) increasing in size indicating that no tissue remains in this area of the specimen.

4.4.4 Observation of a Single Collagen Fibre Bundle in Rupture

After *image k*, in figure 4.15, the magnification is increased to observe the remaining fibre bundles indicated by (8). Because no staining is possible to bring the collagenous substances into evidence, the detail of the fibre bundle is difficult to distinguish. Nevertheless, as the sample is pulled in traction there is indication that the fibrils of the fibre bundle stretch with a reduction in the diameter of the fibre bundle. As strain increases, fibrils rupturing at the surface of the fibre bundle are observed to quickly *peel away* from the body of the bundle, out of the view of the microscope. The stress values obtained after *image k* show to be significantly less than the maximum observed stress, yet they are not negligible, indicating the load-carrying capacity of collagen fibres.

Figure 4.13 Magnified view of a single collagen fibre bundle.



(a) OM 64.8x

Figure 4.14 Sequenced image acquisition during rupture of PDL (a - f) shown here at 5X magnification

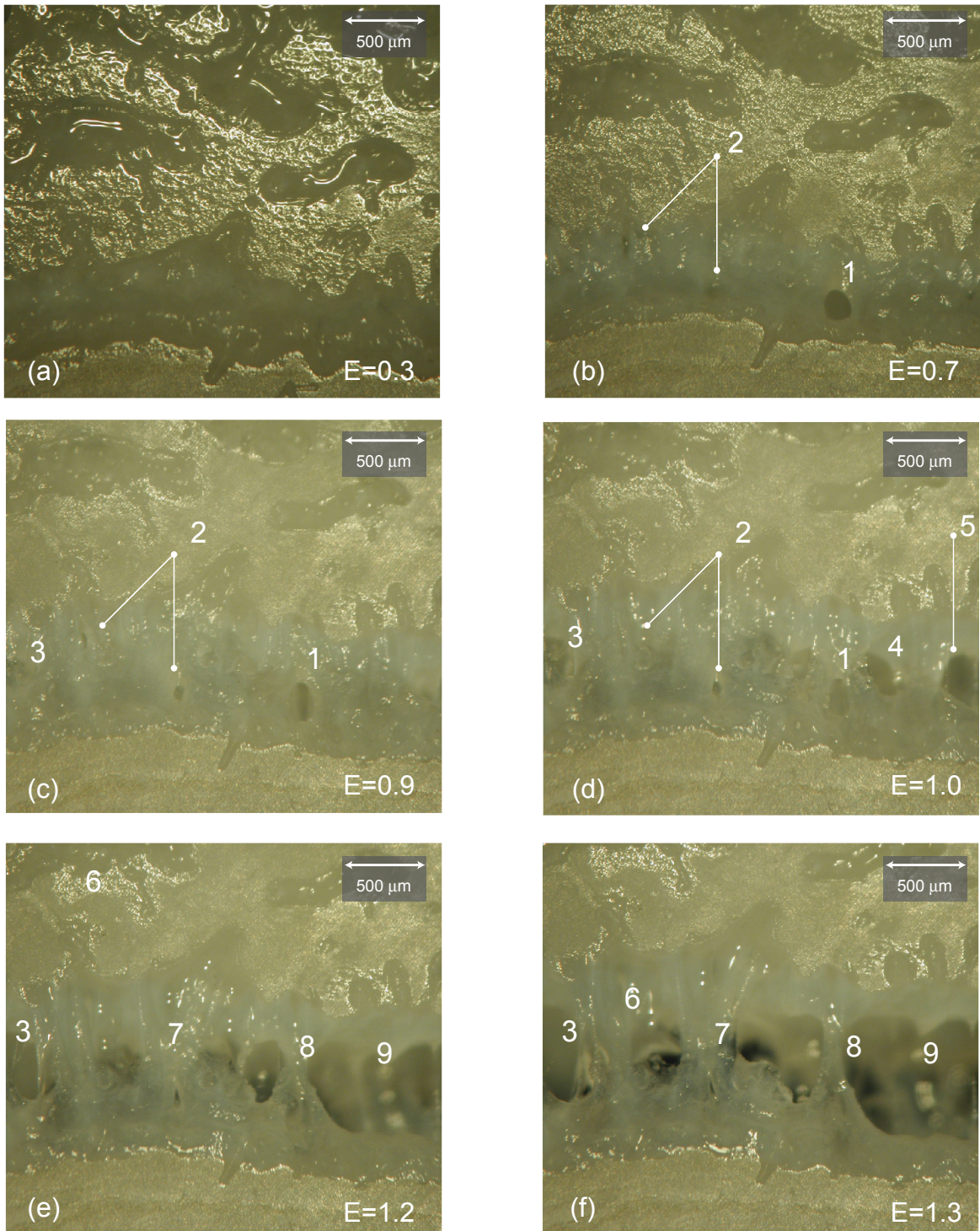
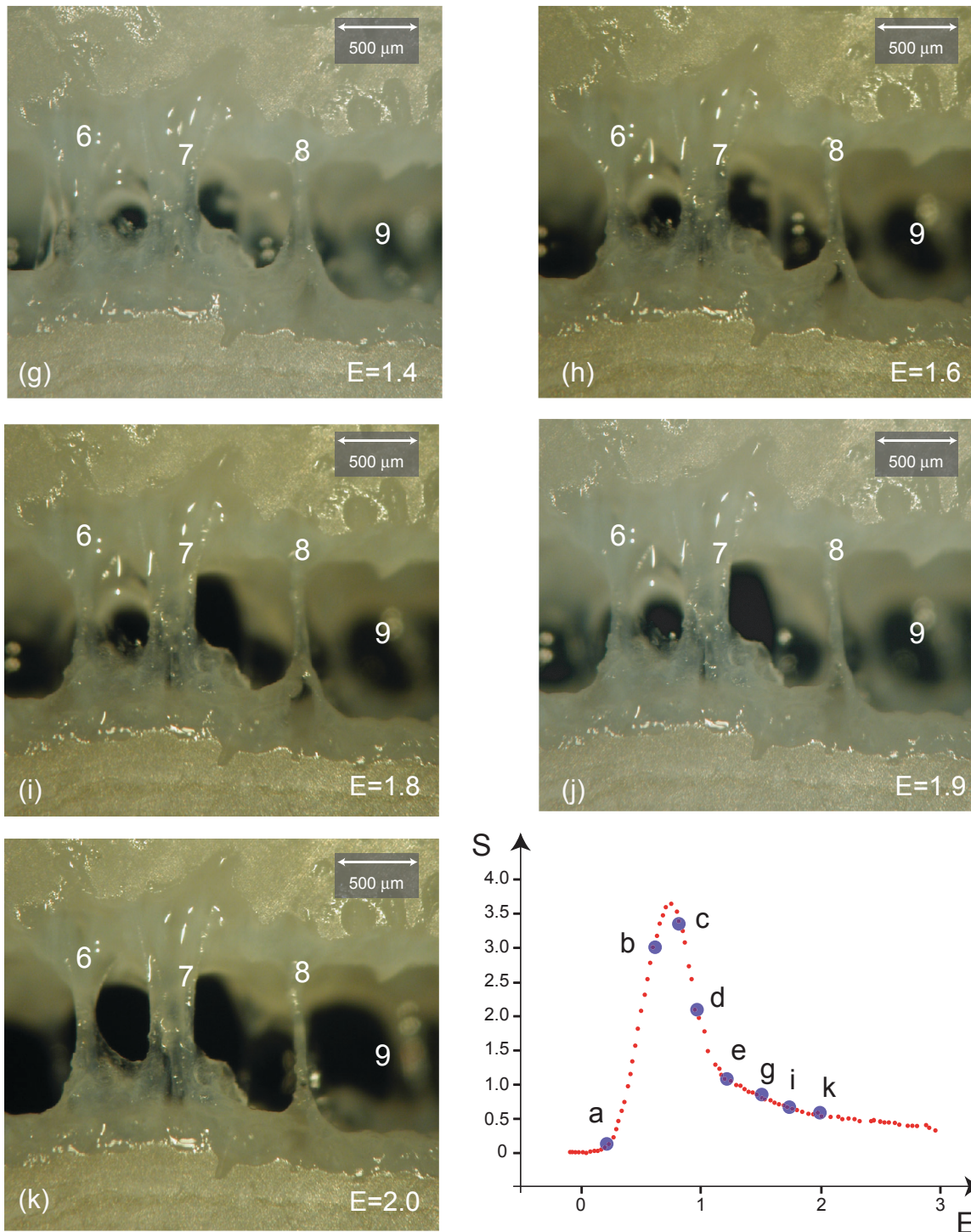


Figure 4.15 Sequenced image acquisition during rupture of PDL (g - k) with optical microscope shown here at 5X magnification and rupture curve .



4.5 Histology

Studying the structure of the biological tissue involves treating the tissue as described in section 3.3. From the time of death of the animal to viewing the slide under a microscope takes approximately 6 months. In 1999, when work on this thesis began, no information related to the structure of the PDL in bovine tissue was available in the literature.

The objective of the histology studies is to identify the circumferential axisymmetry, vertical and radial heterogeneity of the collagen fibres in the PDL and to identify key structural components of the PDL that play a role on its mechanical behaviour. Such structural information is related to the mechanical behaviour of the PDL. Studying the tissue, therefore, requires the selection of a technique that brings into evidence those parts of the ligament that interest the engineer in terms of structure and mechanics, instead of that which interests the biologist i.e. the composition and function of the tissue cells.

Three studies are performed in this thesis. First, a preliminary study is made to establish a procedure. Several whole tooth blocks (see figure 3.2) undergo different procedures and the final results are observed qualitatively by biologists to determine the best method to examine the structural components of the PDL, namely the collagen fibres. From this first study it is concluded that specimens are to be sectioned to a small size so as not to damage the tissue. A small sample size has the additional benefit of an accelerated dehydration of the tissue, and penetration of the fixative.

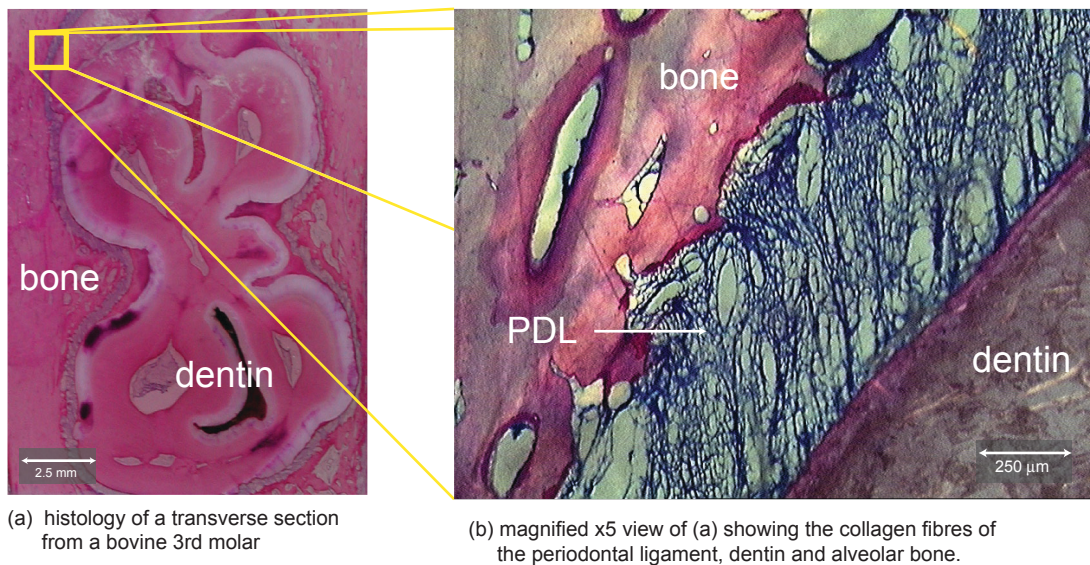
Once establishing a refined method specific for bovine tissue of a specific size, the second study is undertaken. This involves studying a single molar, however, in this study, a third molar is used. The results from this study are of moderate quality, and a selection of the data is presented in section 4.5.1. The sections are sufficient to quantify the preferential fibre direction of the ligament around the radius of the root, and to quantify the irregular contours of the alveolus junction using fractal geometry methods.

The third study involves taking a total of 8 first molars. Four right molars, and four left molars. For structural studies, two right teeth and two left teeth are prepared for histology. For mechanical studies, the remaining teeth are tested as uniaxial specimens keeping track at all times of the exact location of each specimen. (*note: This study was launched in February 2003 and unfortunately, the full extent of this work is not presented in this thesis due to the unavailability of histology data.*) A view of the structural components of the PDL is presented in detail in this work. The results are presented below in section 4.5.3.

4.5.1 Preliminary Histology Study

The third molar used in this study provide moderate results. In order to investigate the radial heterogeneity of the collagen fibre bundles around a transverse section. A presentation of the biology is not made here, please refer to section 4.5.3 for the biological components of the periodontium as seen in figure 4.16.

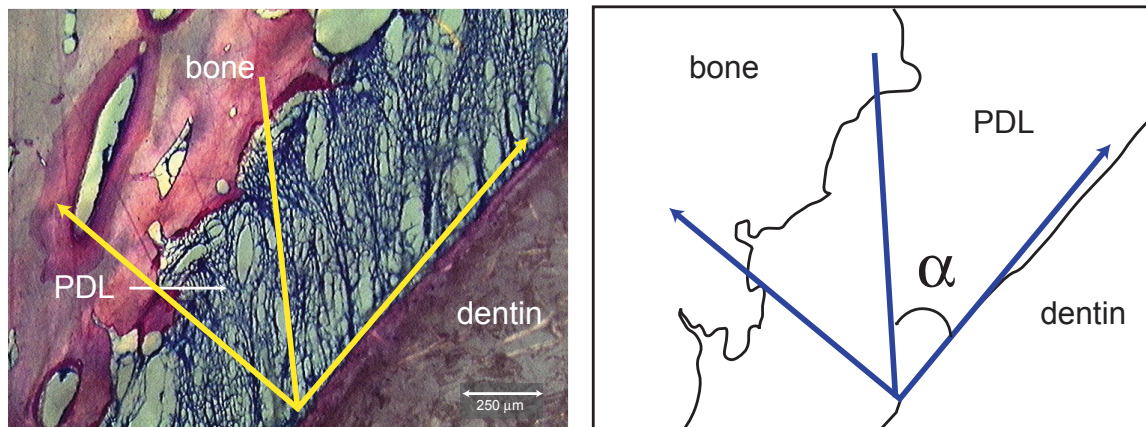
Figure 4.16 Micrographs of undecalcified ground sections showing (a) transverse section of a bovine third molar, and (b) the transverse section magnified on a section of the periodontium at a magnification of 5x.



A total of 51 images are taken, one is shown in figure 4.16b. For each specimen, the angle, α , is measured as a means to determine the distribution of the fibre direction. The method involves placing an xy-coordinate system such that the x-axis is parallel to the relatively smooth surface of the dentin. This has been shown schematically in figure 4.17. A line is drawn from the origin in such a way as to follow the preferential direction of the fibres. Doing this along the contour of the tooth gives a mean angle, $\alpha = 48 \pm 12^\circ$. A histogram showing the distribution of the angle α is given in figure 4.17.

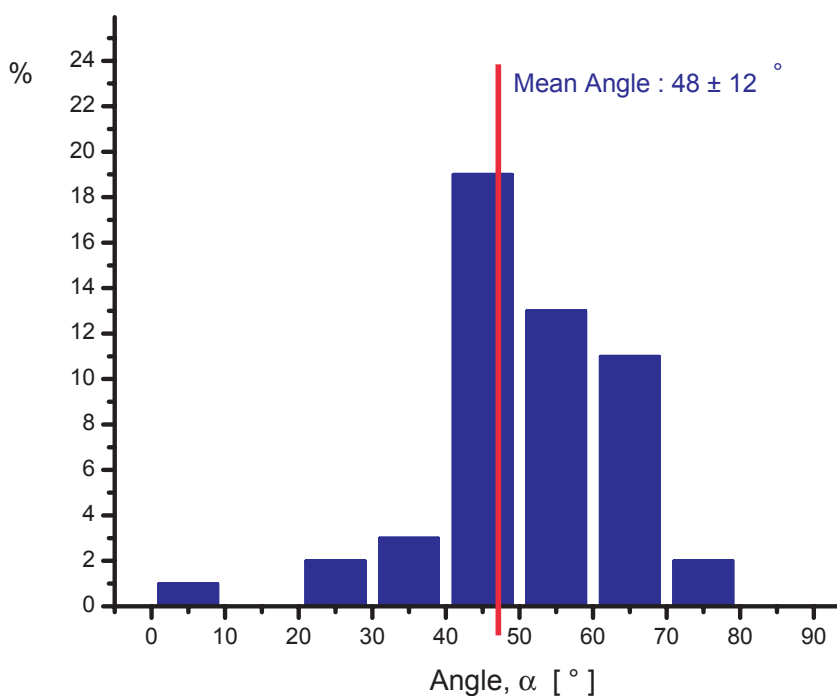
Figure 4.16a is a histological section of a transverse specimen obtained from bovine third molar. The tooth is joined to the bone by the PDL between the two. Looking at the periodontium at a higher magnification shows the ligament in detail (figure 4.16b). It is clear from figure 4.16b that there is a preferential direction of the collagen fibre bundles.

Figure 4.17 (a) Micrograph of an undecalcified ground section showing definition of xy-coordinate system to (b) measure an angle, α , to quantify the preferential fibre direction. Histogram (bottom) showing the distribution of fibre direction around the entire contour of the tooth.



(a) histology of a transverse section from a bovine 3rd molar

(b) schematic showing angle, α , that defines the direction of the collagen fibres



4.5.2 Fractal Measurements

Fractal geometry can be used as a tool to describe the non-smooth contour of bone. Following standard methods for analysis of crack profiles in ceramics, concrete or metal described in literature and shown schematically in figure 4.18, the fractal dimension of the contours of the periodontium is determined [Mandelbrot 1982; Mandelbrot et al. 1984; Kappraff 1986; Mecholsky et al. 1989; Borodich 1997; Borodich and Onishchenko 1999].

The measurements for the bone interface are made following the method described by Borodich [Borodich 1997].

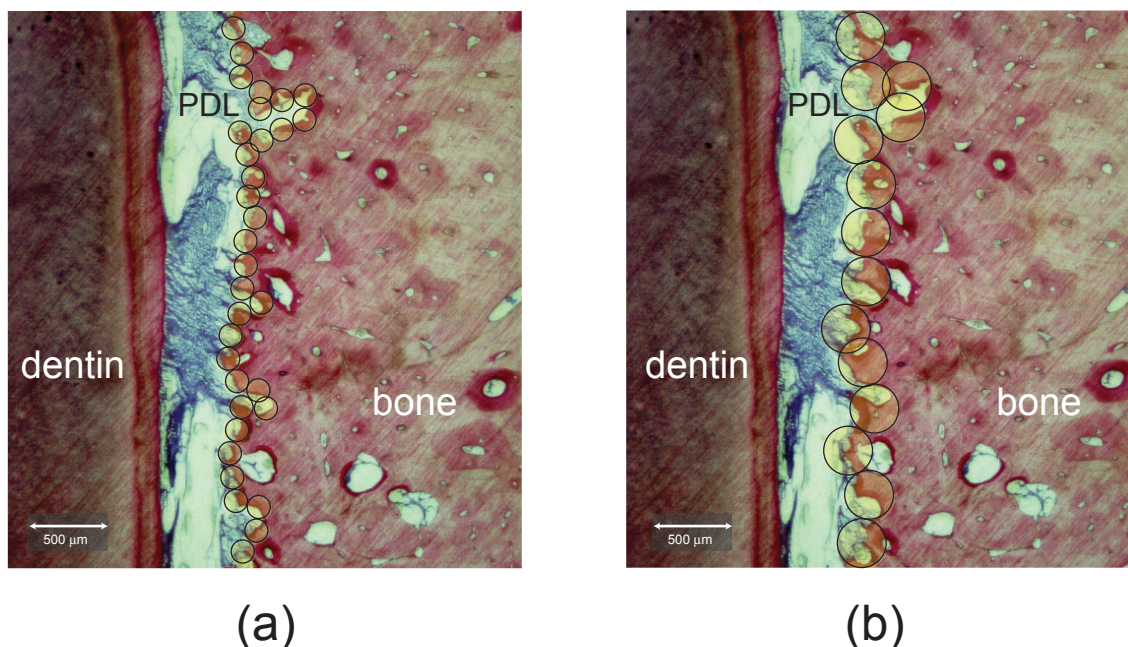
The bone-ligament contour is found to have a fractal dimension of

$$d = 1.17$$

whereas the fractal dimension of the smooth dentin-ligament contour was found to be

$$d = 1.0.$$

Figure 4.18 Micrographs of undecalcified ground sections showing the method to determine fractal dimensions of the bone-ligament junction using (a) circles of small radius, and (b) larger radius.



4.5.3 Advanced Histology Study

Sections obtained from bovine first molar sites are prepared using three different techniques: (i) undecalcified sections, (ii) decalcified sections, and (iii) macerated decalcified sections.

The undecalcified ground sections embedded in MMA are initially cut to 200 μm-thick specimens before being polished to a final thickness of 80-100 μm. These sections are stained using toluidine blue, a basic stain commonly employed on resin embedded specimens. The decalcified sections are cut, using a microtome, to 1 μm thick and also

stained with toluidine blue. The macerated tissues are macerated to remove cells and the noncollagenous matrix using NaOH. (for specific procedures refer to section 3.3).

Distal Root below Apex of a Bovine First Molar

Figure 4.19a shows a transverse section of the distal root of a bovine first molar below the apex. The dentin shown here forms the bulk of the crown and root, and is composed of a calcified organic matrix similar to that of bone. The inorganic component constitutes a larger proportion of the matrix of dentine than that of bone and exists mainly in the form of hydroxyapatite crystals [Young and Heath 2002]. It is for this reason that teeth are harder than bone. From the pulp cavity **P**, minute parallel tubules, called dentin tubules, radiate to the periphery of the dentine.

Figure 4.19b shows the morphology of the cells and organic components of bone in a decalcified section. The Haversian systems **H** are seen in this transverse section.

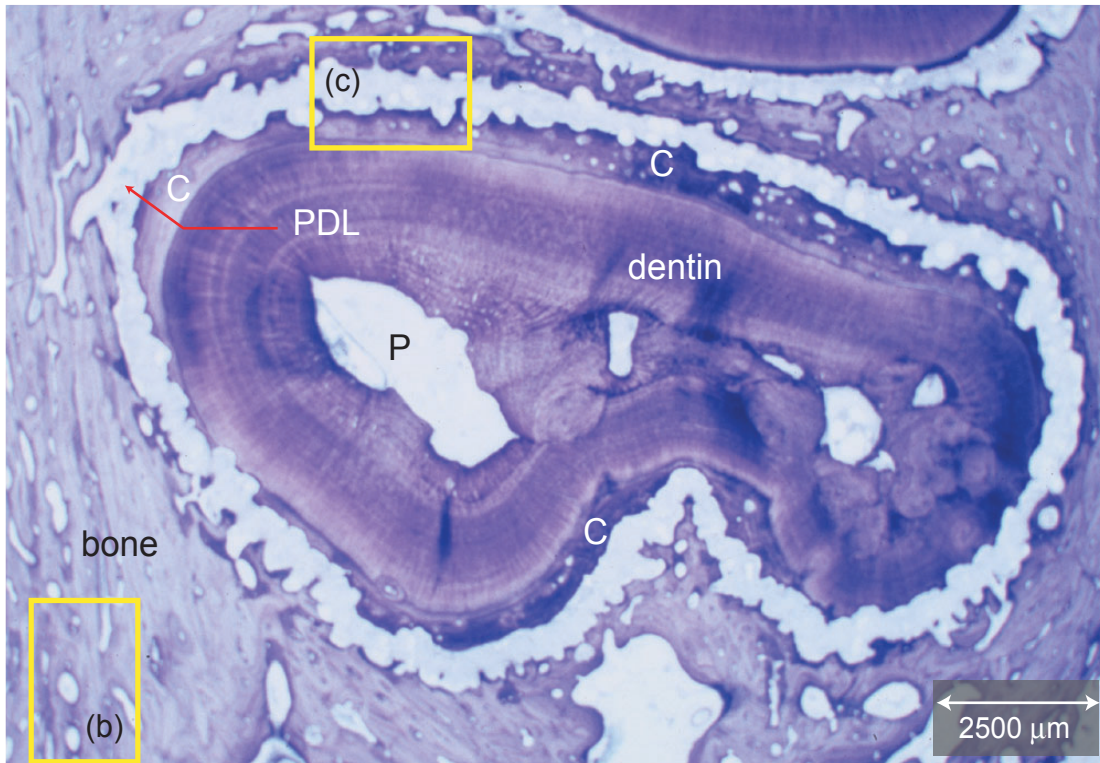
Figure 4.19c shows how the root is invested by a thin layer of cementum **C**, which is generally thicker towards the apex of the root. Cementum is an amorphous calcified tissue into which the fibres of the periodontal membrane are anchored. In the case of the cementum shown in this slide, it appears that remodeling is occurring.

The Periodontium, Collagen Fibres and Fibre Insertion Sites

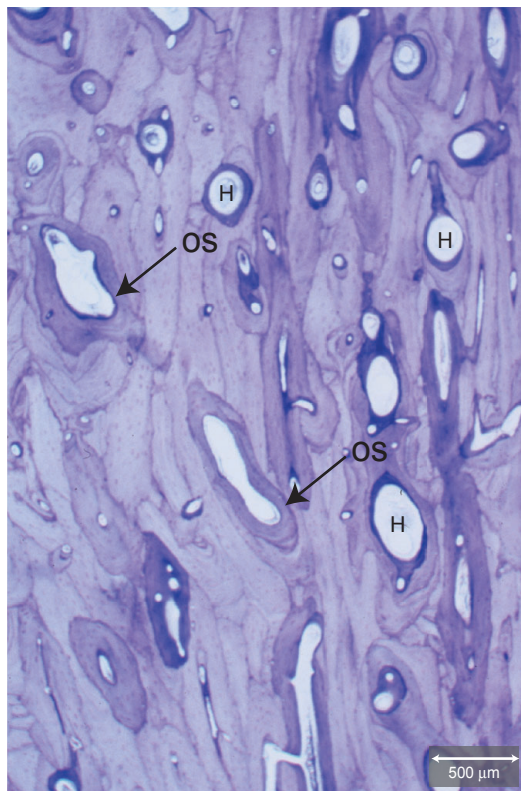
The images presented in figures 4.20, 4.21, 4.22 and 4.23 give detail on the structure and composition of the periodontium tissues and are discussed in this section.

Figure 4.20a is micrograph of a decalcified thin section, with a thickness of approximately 1 μm , showing the PDL forming a fibrous attachment between the tooth root and the alveolar bone. The dentin, comprising the root, is covered by a thin layer of cementum **C** which is elaborated by cells called cementocytes lying on the surface of the cementum. Cementum consists of a dense, calcified organic material similar to the matrix of bone, and is generally acellular. The bovine cementum shown in this micrograph, however, resembles bone in that it shows evidence of being cellular. Towards the root apex, the cementum layer becomes progressively thicker and irregular. The PDL consists primarily of dense collagenous tissue and the collagen fibres are in a constant state of reorganisation to accommodate changing functional stresses upon the teeth [Young and Heath 2002].

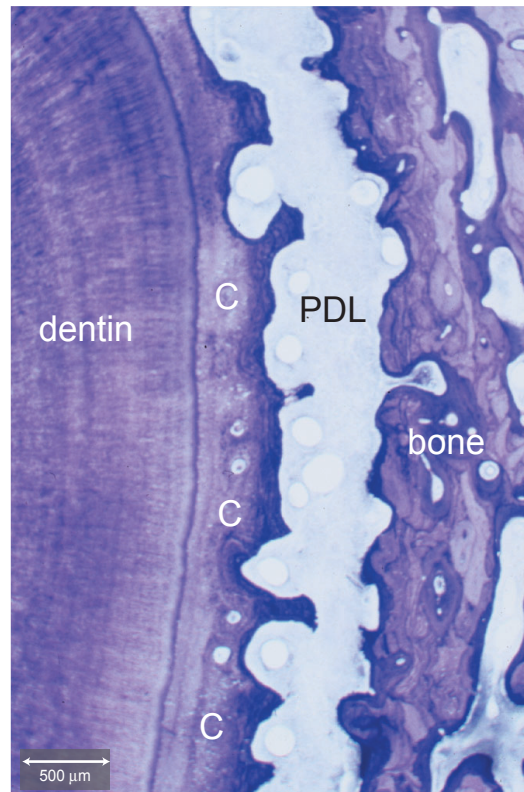
Figure 4.19 Micrographs showing transverse section of an undecalcified ground section (a) of a distal first molar root apical from apex of bovine first molar with (b) detail of alveolar bone and (c) periodontium.



(a) OM 2.1x



(b) OM 8x



(c) OM 8x

Figures 4.20b & c show the detail of the interface between the PDL and the cementum and bone surface respectively. Although somewhat difficult to see in this section, the insertion points of the Sharpey's fibres **Sh** investing into the cementum and bone are seen, however, the macerated decalcified sections shown in figure 4.23 better show the Sharpey's fibres. Fibroblast **fb**, cementoblasts **cb**, and osteoblasts **ob** are indicated by the arrows. The white spaces represent areas that would consist of interstitial fluid and cytoplasm. Figure 4.21 show the same micrographs of figure 4.20, however, they have been converted to black and white, i.e. details beyond the contrast level threshold as defined by the noncollagenous zones are eliminated as a means to measure the fibre density. For several images treated in this manner at a number of different magnifications, the fibre density is found to be between 55 and 74% by volume, comparable to what is reported in literature [Mühlemann 1967; Daly et al. 1974; Berkovitz et al. 1981].

Two micrographs of decalcified thin sections, with a thickness of approximately 1 μm , offer a magnification of the bulk of the collagen fibres and are presented in figure 4.22. Fibroblast are shown by **fb**. Density of the fibres and the waviness of the structure are seen well in these micrographs. The diameter of the fibre bundles are between 10-20 μm .

Figure 4.23 are decalcified thin sections as in the micrographs of figure 4.20, however, after being macerated with NaOH to remove cells and noncollagenous proteins. It is seen in both micrographs (a) and (b) that the collagen fibre bundles at the insertion points, Sharpey's fibres **Sh**, are bound to the hard calcified tissue of the root and the bone. Moreover, the Sharpey's fibres penetrate the whole thickness of the cementum and to a similar depth into the bone.

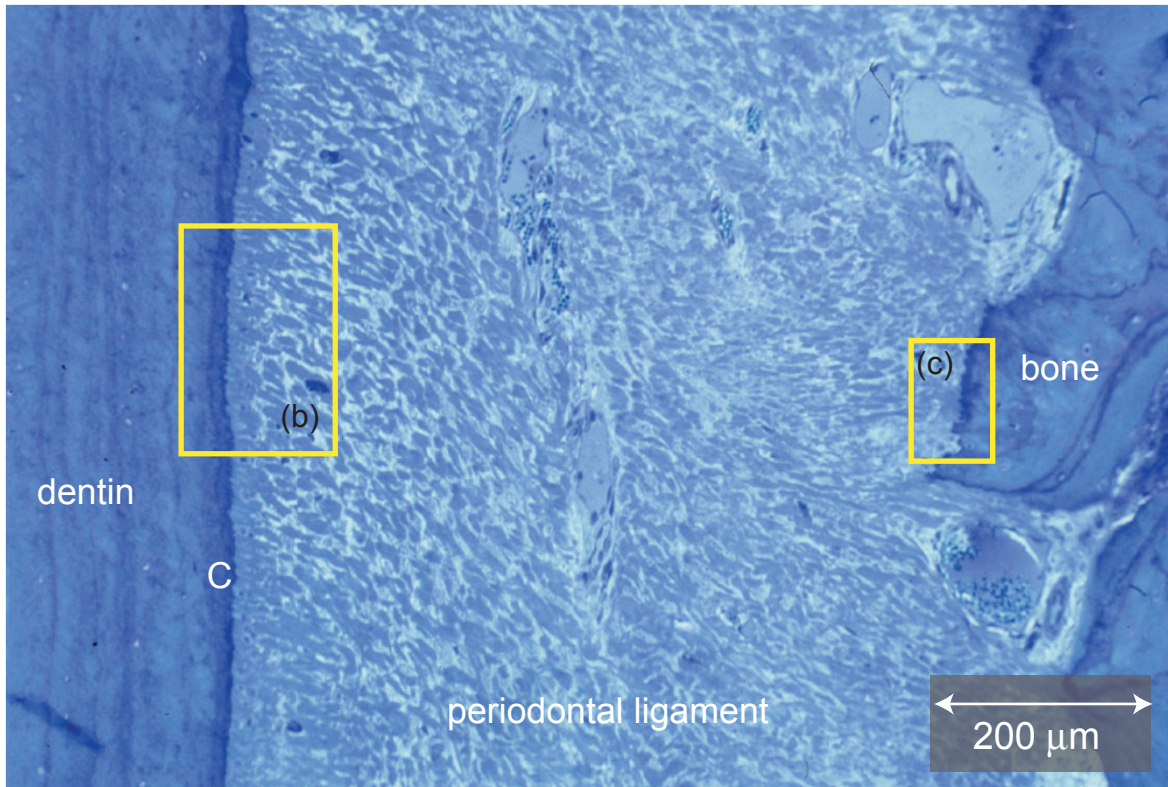
Vasculature

Figure 4.24 shows the PDL to be highly vascular with a large number of blood vessels **bv** apparent around the contour of the tooth.

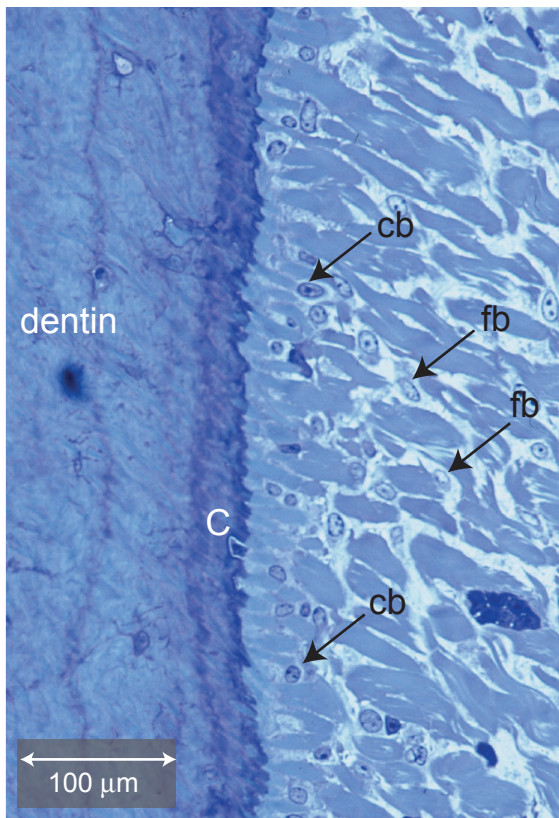
Ground Substance and Fluids

Besides collagen fibres and blood vessels, the extracellular matrix, i.e. the ground substance and fluids, make up a significant portion by weight of the PDL, however, quantification of the ground substance can not be done from this histological investigation of the PDL.

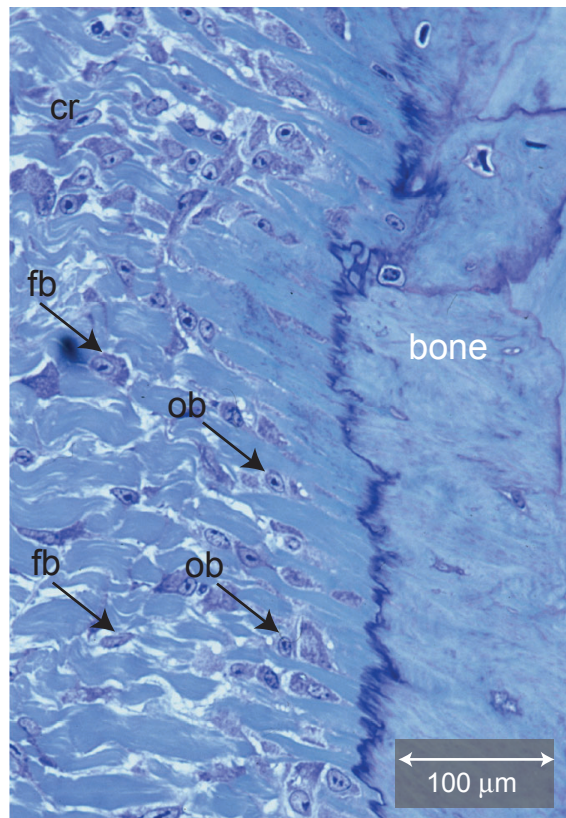
Figure 4.20 Micrograph of a decalcified thin section of periodontium showing insertion points at alveolus junction and cementum junction.



(a) OM 33x

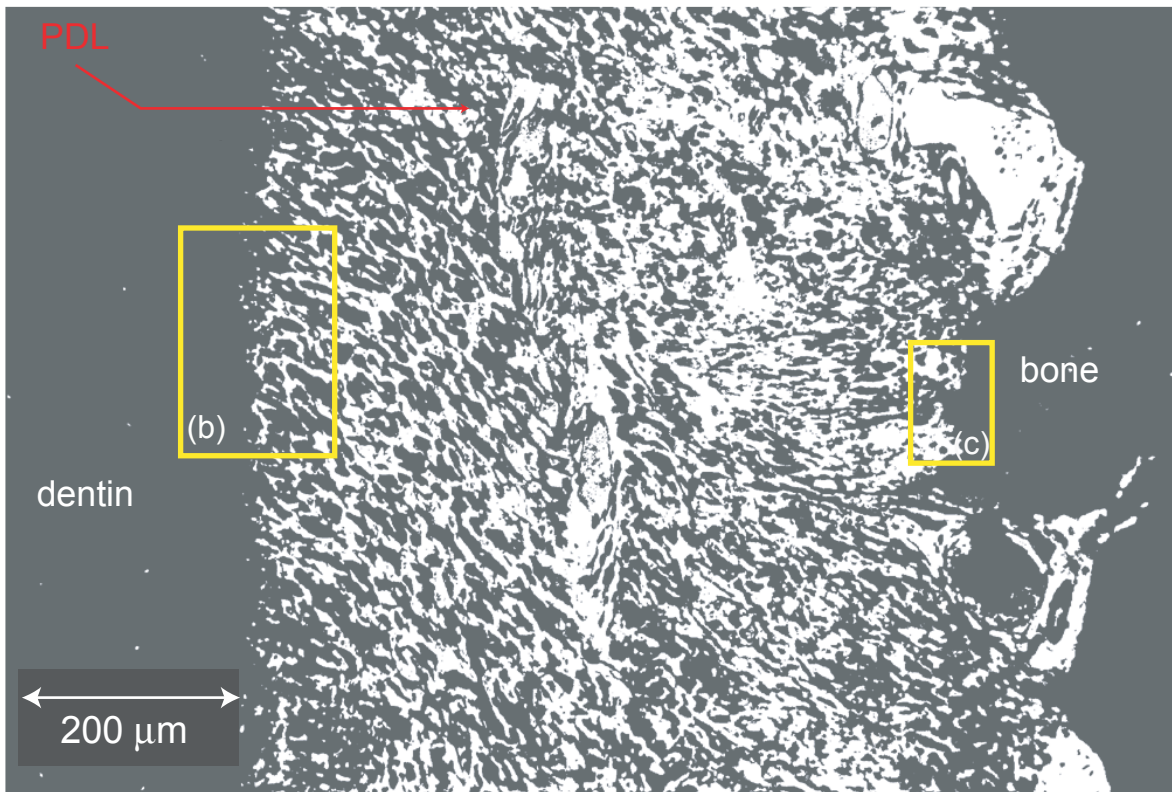


(b) OM 135x

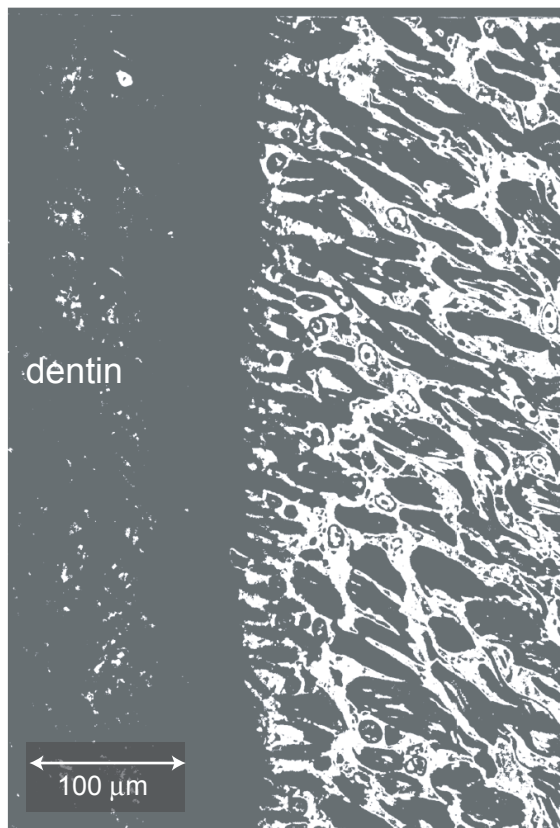


(c) OM 135x

Figure 4.21 Image analysis of periodontium showing decalcified thin section of periodontium and insertion points at alveolus junction and cementum junction to quantify fibre density



(a) 33x

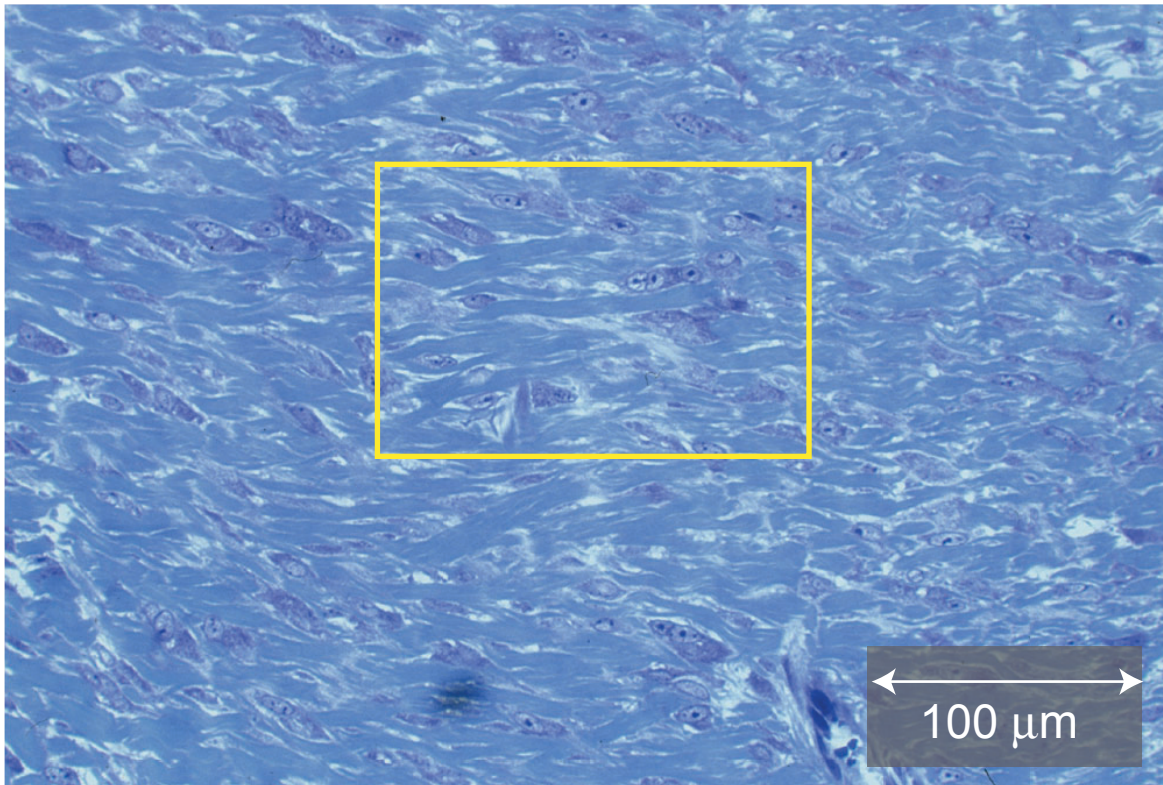


(b) 135x

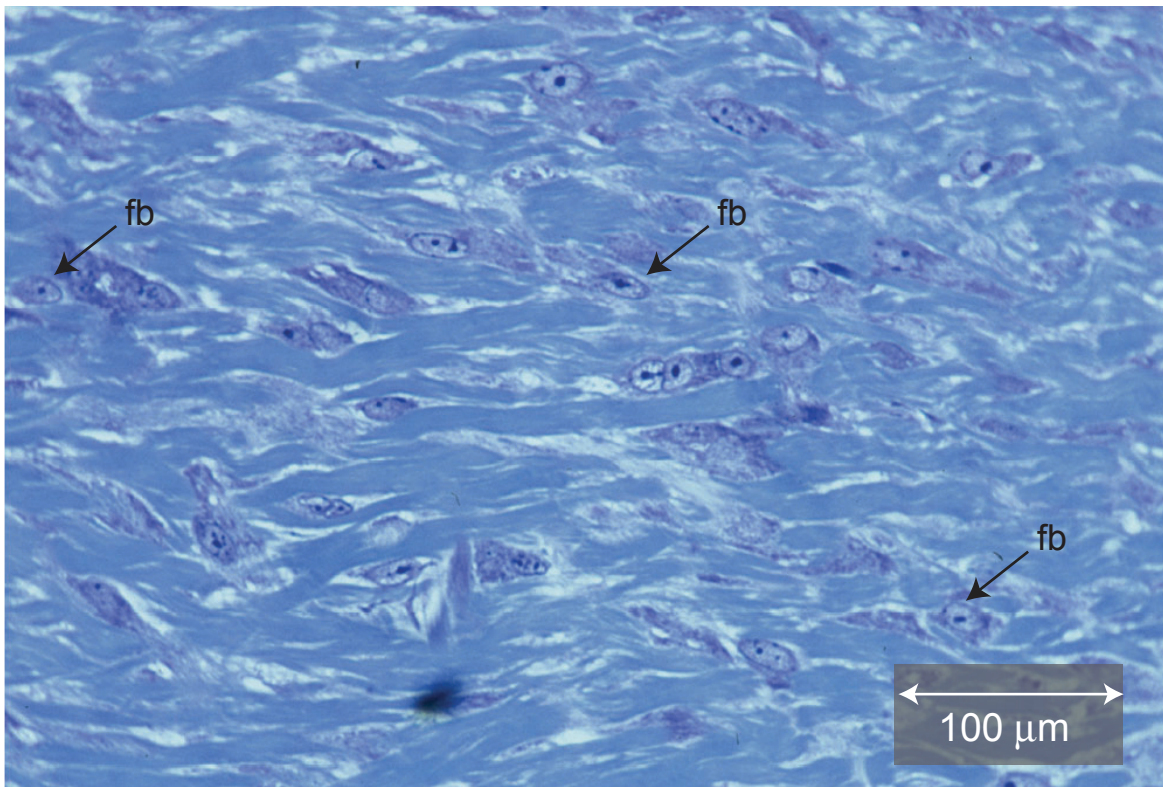


(c) 135x

Figure 4.22 Micrograph of a decalcified section showing the middle region of the PDL showing density and wavy structure of collagen fibres

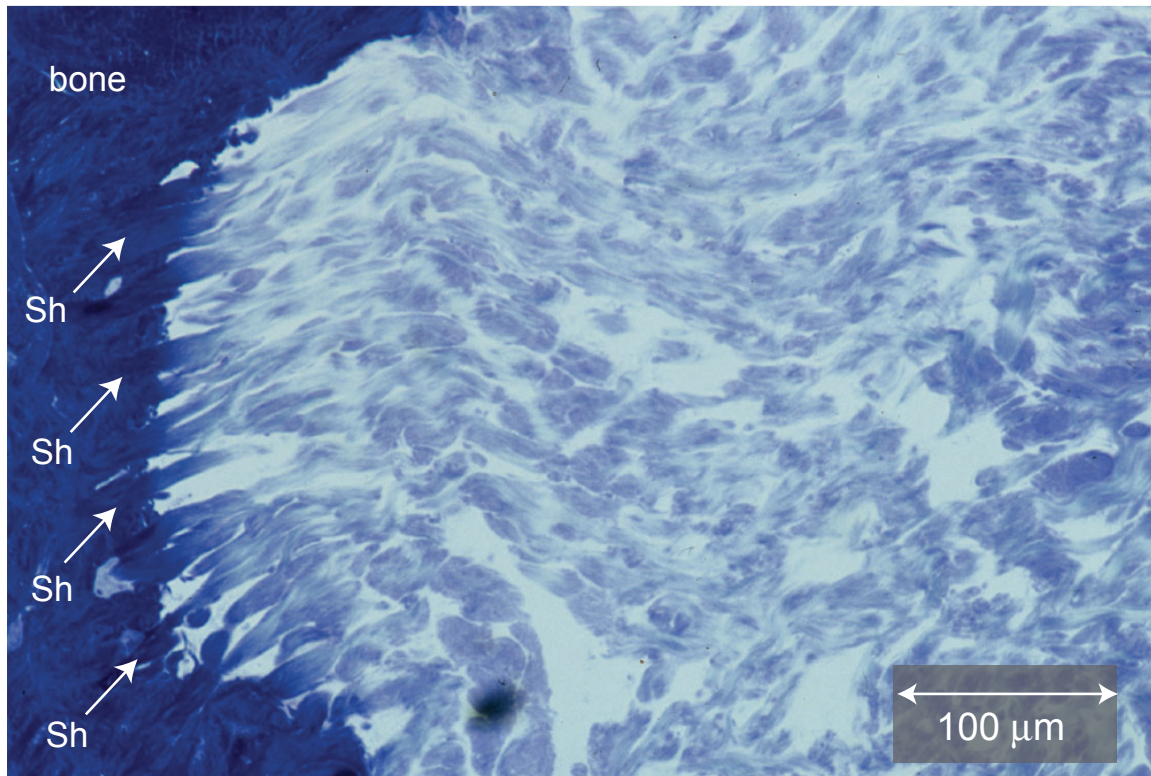


(a) decalcified thin section OM 83x

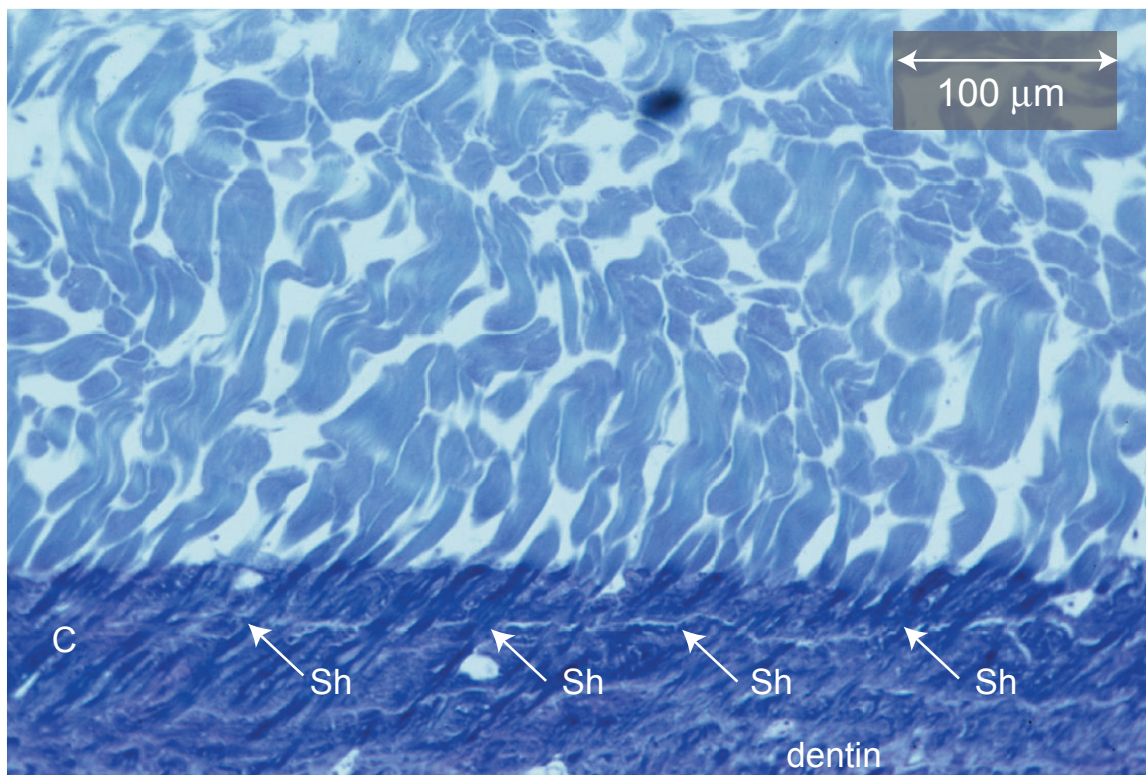


(b) magnification of periodontal ligament collagen fibres as defined by box in (a) OM 135x

Figure 4.23 Micrographs of macerated decalcified tissue showing intact collagen matrix and insertion points into bone and cementum.

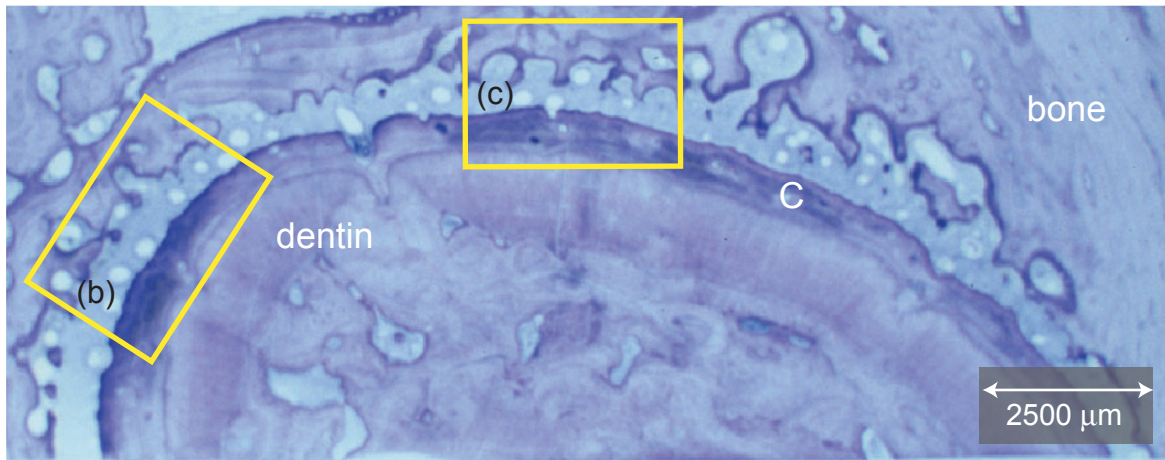


(a) micrograph of a macerated decalcified section OM 135x

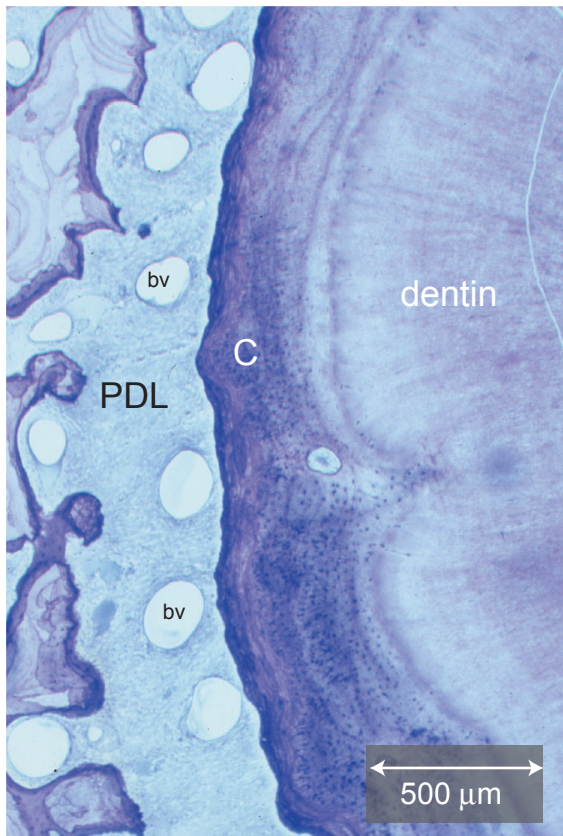


(b) micrograph of a macerated decalcified section OM 135x

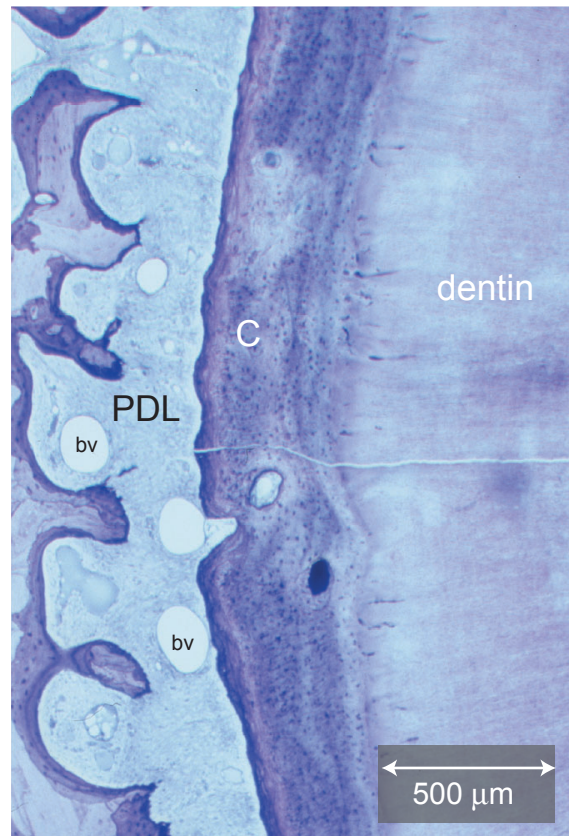
Figure 4.24 Micrograph of undecalcified ground sections showing vasculature of the PDL.



(a) OM 8x



(b) magnification of periodontal ligament as defined by box in (a) OM 12.5x



(c) magnification of periodontal ligament as defined by box in (a) OM 12.5x

4.6 Discussion of Geometry, Morphology and Histology Results

Heterogeneity-Anisotropy

The experimental results from mechanical experiments presented in Chapter 5 and Chapter 6 show a large degree of variability. Although experimental error and biological variability can account for, to a certain degree, the discrepancies from specimen to specimen, the complex structure of the PDL considerably affect the measured results. In this chapter, structural information obtained through a geometrical and histological investigation provides insight into the relevant anisotropies of the PDL.

The sequence of micrographs obtained during the rupture of the uniaxial PDL specimens, as shown in figures 4.14 and 4.15, support the hypothesis that such specimens are transverse isotropic (*transotropic*), i.e. the fibres are defined by a preferential direction. As the specimen is stretched to rupture, the fibre bundles are clearly distinguishable. Note, however, that this hypothesis is local to a sufficiently small region on the circumference of the tooth, as with the uniaxial specimens tested. That specimens are locally transotropic, however, does not explain the variability in the curves representing mechanical behaviour. A variation in density, an isotropic heterogeneity, or a variation in fibre-bundle orientation, an anisotropic heterogeneity, are factors that could contribute to the variation in mechanical results. A density by weight is not determined in this work, however, attempts to characterize the fibre-bundle orientation is part of a study on a transverse section. The fibre-bundle orientation was found to vary around the radius of the tooth (see section 4.5.1).

Role of the PDL Components on Mechanical Behaviour

The PDL is the only ligament in the body to span two distinct hard tissues, namely root cementum and bone, which make it unique. The PDL, therefore acts as a sling for the tooth within its socket, permitting slight movements which cushion the impact of mastication. Compared to other ligaments and tendons, the PDL is a cell-rich and highly vascularised soft connective tissue [McCulloch and Melcher 1983; Blaushild et al. 1992].

Fibres: The mechanical strength of ligaments in tension is largely due to the arrangement of type I collagen fibrils into fibre bundles, and their overall three dimensional structure [Liu et al. 1995]. The PDL is primarily made up of the same collagen I fibrils [Berkovitz et al. 1981; Berkovitz 1990; Berkovitz et al. 1997]. Pulling a PDL uniaxial specimen from its zero state results in a toe region followed by a linear region as strain is increased (see figure 2.6). The micrograph in figure 4.20 shows the wavy nature of the fibres, and is referred to as crimp [Gathercole 1987]. It has been suggested that fibres first uncrimp during initial straining which accounts for the toe region of the rupture curve [Pini et al. 2002]. Section 4.4 shows the rupture of the ligament with images at different strains

obtained synchronously. These images support the hypothesis that the main load carrying component in the ligament during tension are the collagen fibres. Moreover, these images also demonstrate the gliding of fibres as the ligament is pulled, especially when a single fibre bundle is observed at higher magnification. A more thorough explanation of the mechanisms of rupture in tension, combined with the histological techniques described in this thesis would give rise to the exact mechanisms of rupture of the PDL.

Ground Substance, Vasculature and Fluids: The presence of noncollagenous extracellular matrix (ground substance) constituents, interstitial fluid, blood vessels and cellular elements likely have an influence on the tooth support mechanism. It has been suggested that besides *uncrimping*, the toe region of the S-E curve is correlated to the shearing behaviour of the ground substance between the collagen fibres [Decraemer et al. 1980]. In a work by Mow [Mow et al. 1984] it is shown that molecules making up the ground substance exhibit viscous behaviour due to their resistance to flow under shear. Results in this thesis consistently show a more important viscous effect in compression than in tension. The expulsion of fluid from a compressed ligament (see section 4.4.1) support this hypothesis. The uniaxial specimens tested in this manner, however, were sectioned from the molar site resulting in a more *open* system allowing the fluid to escape. It is possible that under normal physiological conditions, the ligament is part of a closed system where a membrane would maintain an osmotic pressure that would reduce or inhibit any fluid expulsion. The mechanical results presented in section 5.5.2 also show the viscous influence to be greater in compression than in tension. Furthermore, relaxation tests performed at different ranges of strain (section 5.4.2) show that in the zero region of the S-E curve, the viscous elements dominate the mechanical behaviour of the PDL. In brief, the interaction of the extracellular components of the ligament are responsible for an internal mechanism, which defines the viscous properties of the tissue.

Fractal Geometry of Alveolus Junction

The irregular contour of the alveolus junction complicates interpretation of mechanical results, and the construction of a finite element (FE) model. In FE models, it is practical to consider the alveolus junction as a smooth surface, however, the micrographs in this section clearly show that this is not the case. The quantification of the irregular contour of the alveolus junction by a fractal dimension is a first approximation that could be useful in defining irregularities in a FE tooth-PDL-bone model.

-
-
-

•

•

•

“The important thing is not to stop questioning.”

Albert Einstein

•

•

•

5

Results: Uniaxial Behaviour

Uniaxial tests make up the most extensive part of this thesis. This chapter presents the results obtained from testing uniaxial PDL specimens. The behaviour of uniaxial specimens is tested under a variety of deformation profiles and are presented as follows:

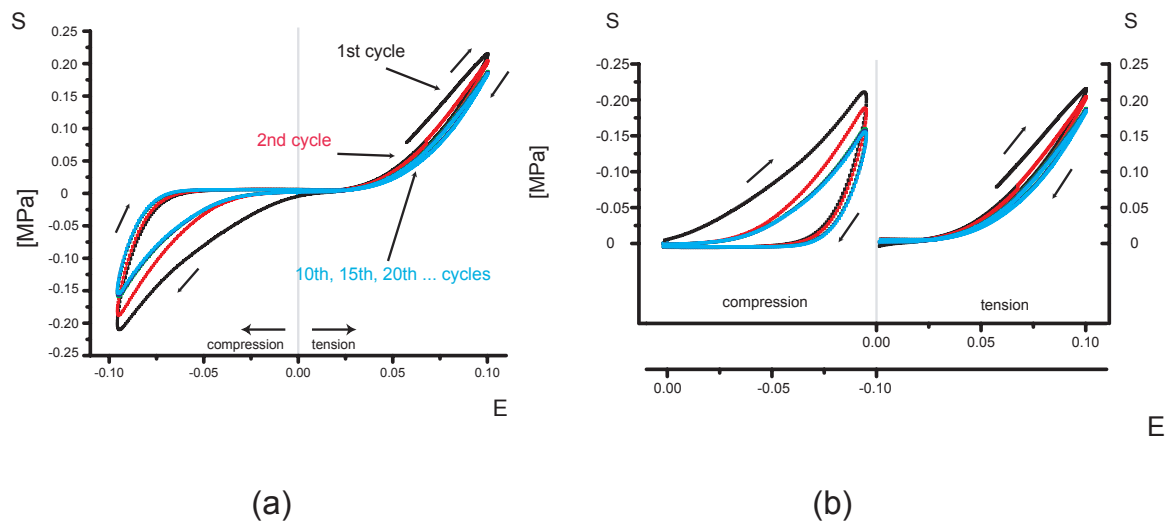
- Preconditioning on page 113,
- Constant Strain Rate Deformation Tests on page 115,
- Constant Strain Rate Deformation and Recovery History on page 121,
- Uniaxial Stress Relaxation of the Periodontal Ligament on page 124,
- Sinusoidal Response of the Periodontal Ligament on page 131,
- Rupture on page 142, and
- Regional Effects on Mechanical Behaviour of PDL on page 144.

A discussion of the results obtained from the uniaxial tests is discussed at the end of this chapter.

5.1 Preconditioning

When the PDL is preconditioned, i.e. the uniaxial specimen is subjected to 20 cycles at 1 Hz with a strain amplitude of approximately, $E=0.2$, a difference is observed in the stress-strain curves in tension as in compression for the first 10 cycles. After ten cycles, however, the difference between successive cycles disappears. It is at this point when the uniaxial specimen is said to have been preconditioned. (see figure 5.1)

Figure 5.1 Preconditioning

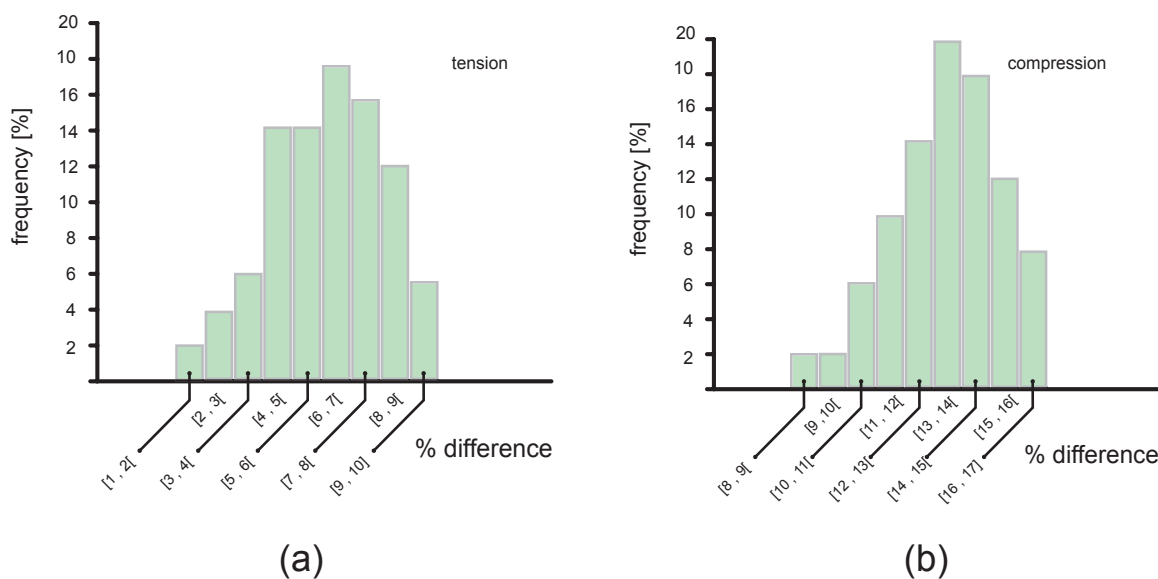


The effect of preconditioning is quantified in the relative change in maximum values in both tension and compression from cycle to cycle. Taking the typical preconditioning curve in figure 5.1, the stresses observed in tension at a strain, $E = 0.10$, show a maximum stress, $S = 0.23$ MPa for the first cycle, and $S = 0.215$ MPa for the second cycle. This corresponds to a 6.5% difference in the maxima stress values of the first and second cycles. Between the second and tenth cycle, a 6.2% difference in the maxima stress values is observed. The stresses observed in compression at a strain, $E = -0.10$, shows a minimum, $S = 0.23$ MPa for the first cycle, and $S = 0.20$ for the second cycle. This corresponds to a 13% change in the minima stress values of the first and second cycles. Between the second and tenth cycle, a 13% difference is also observed.

More importantly, the difference in hysteresis observed during the first cycles is large. Defined as the area between the loading and unloading curve of any specific cycle, a difference in hysteresis of 42% is observed between the first and second cycles. Between the second and tenth cycle, a 20% difference is observed. There is no significant difference in hysteresis observed in subsequent cycles.

When taking into account the 46 preconditioning curves, the difference between the first and second is summarised in the histograms in figure 5.2.

Figure 5.2 Histograms showing distribution of percent differences between first and second stress maxima in compression and tension



With regard to the shape of the preconditioning curves once stability is reached, the curve displays typical characteristics of a stress-strain curve of PDL tissue. With reference to Figure 2.6, the zero region, toe region, and the beginning of the linear region are readily identified. Furthermore, the hysteresis in compression is greater than in the tensile region by a factor of five.

Concerning the results of $n=67$ preconditioning curves obtained from uniaxial specimens, it is important to note that the zero region of the curves sometimes exceed the strain range in which preconditioning is performed. As a result, no response is observed. Of the 67 curves, 46 produced an interpretable stress response. The lack of stress response can be attributed to the biological variability of the specimen.

5.2 Constant Strain Rate Deformation Tests

If a single uniaxial specimen is tested non-destructively to a relative strain, $E_r = 0.30$, or actual strain, $E = 0.60$, at different strain rates, \dot{E} , a S-E curve is obtained for each strain rate. Each curve qualitatively has the same form with zero regions, toe regions and linear regions readily identifiable. The difference between these curves, however, can only be quantified by the maximum tangent modulus. Because the specimens are not tested to failure, the maximum stress, maximiser strain and strain energy density are not measured.

Concerning the form of the curve, the fact that the S-E curve is not a straight line cannot be taken as an indication that the material response is nonlinear. The shape of this S-E curve is the natural consequence of PDL time-dependency, and if it were to be linear

viscoelastic, the scaling and superposition properties of linearity of response would be valid. The tests performed at different strain rates are performed with two goals in mind:

- 1 to quantify the dependence of the maximum tangent modulus, ϵ , with strain rate, \dot{E} .
- 2 to verify the linear scaling criteria to determine if the PDL .

Pulling the PDL in tension to a relative strain, $E = 0.30$, at strain rates ranging from, $\dot{E} = 0.002 \text{ s}^{-1}$ to $\dot{E} = 1.2 \text{ s}^{-1}$ shows that the stress-strain curve is dependent on the rate at which the PDL is tested. This dependence is seen in figure 5.3a in which four curves are presented. Note that specimens are not tested to rupture, however, based on the rupture behaviour of the PDL (see section 5.6) it is possible to extrapolate (indicated as *projected* in figure 5.3a) the linear portion of the curves to estimate pertinent parameters. From each curve, the maximum tangent moduli, ϵ , are obtained and are summarised in table 5.1. It is seen that the maximum tangent modulus increases with increasing strain rate as shown graphically in figure 5.3b.

Regarding the curves in figure 5.3a, a total of 58 uniaxial specimens are tested at rates $\dot{E} = 0.002 \text{ s}^{-1}$, $\dot{E} = 0.4 \text{ s}^{-1}$ and $\dot{E} = 1.2 \text{ s}^{-1}$, and a total of 67 uniaxial specimens are tested at $\dot{E} = 0.04 \text{ s}^{-1}$.

Table 5.1 Summary of dependence of strain rate, \dot{E} , on the maximum tangent modulus, ϵ .

$\dot{E} [\text{s}^{-1}]$	$\epsilon [\text{MPa}]$
0.002	5 ± 2.1
0.04	12.5 ± 4.2
0.4	13.4 ± 4.7
1.2	19 ± 6.3

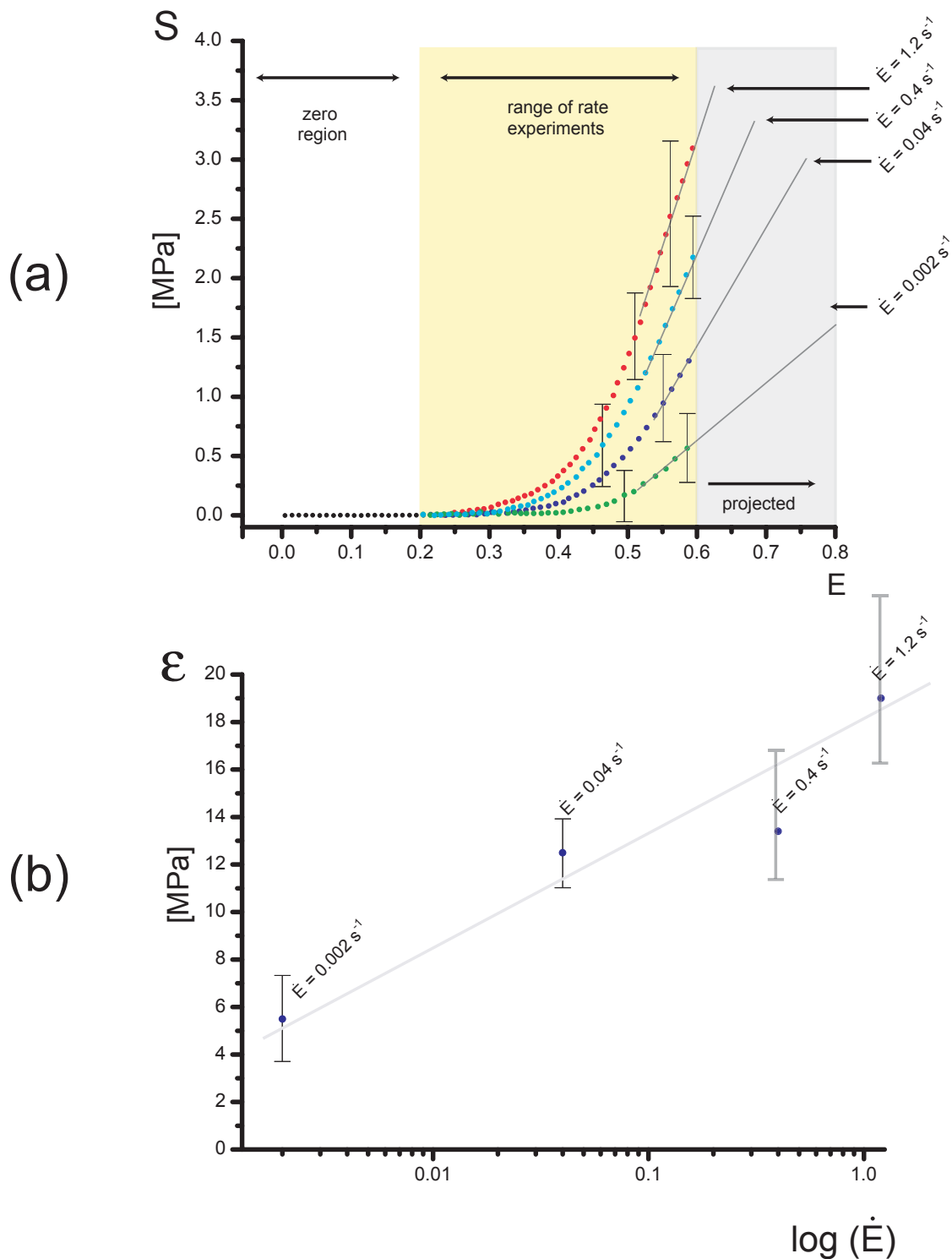
5.2.1 Verifying Linear Scaling Property

The constant strain rate deformation test is described by equation 2.24. Since the strain history has no jump discontinuity at $t=0$, as with the stress relaxation test, a convenient form of the constitutive equation for the design of the linear scaling experiment is given by equation 5.1:

$$S(t) = E(0)G(t) + \int_0^t G(t-s)\dot{E}ds \quad (\text{EQ 5.1})$$

where $G(t)$ is the relaxation function.

Figure 5.3 (a) 4 constant strain rate deformation curves at 4 different strain rates, and (b) showing the dependency of the maximum tangent modulus on strain rate.



The stress at time t is then found to be given by:

$$S(t) = \alpha \int_0^t G(s) ds \quad (\text{EQ 5.2})$$

Note that since

$$\frac{dS(t)}{dt} = \alpha G(t) \quad (\text{EQ 5.3})$$

the slope of the stress-time graph at each instant is proportional to the stress relaxation function.

Since $E(t)$ is proportional to time, t , the time scale can be converted into strain scale as has been done for figure 5.3a. This is done by setting $t=E/\alpha$ in figure 5.2.

$$S(t) = \alpha \int_0^{E/\alpha} G(s) ds \quad (\text{EQ 5.4})$$

Mathematically, the slope of the S-E curve is

$$\frac{dS}{dE} = \alpha \frac{dS}{d(E/\alpha)} \frac{d(E/\alpha)}{dE} = G(E/\alpha). \quad (\text{EQ 5.5})$$

According to equation 5.4, the S-E plot depends on the strain rate α . It is possible, however, to express equation 5.4 and equation 5.5 in terms of E/α and S/α . Doing this gives,

$$\frac{S}{\alpha} = \int_0^{E/\alpha} G(s) ds \quad (\text{EQ 5.6})$$

and

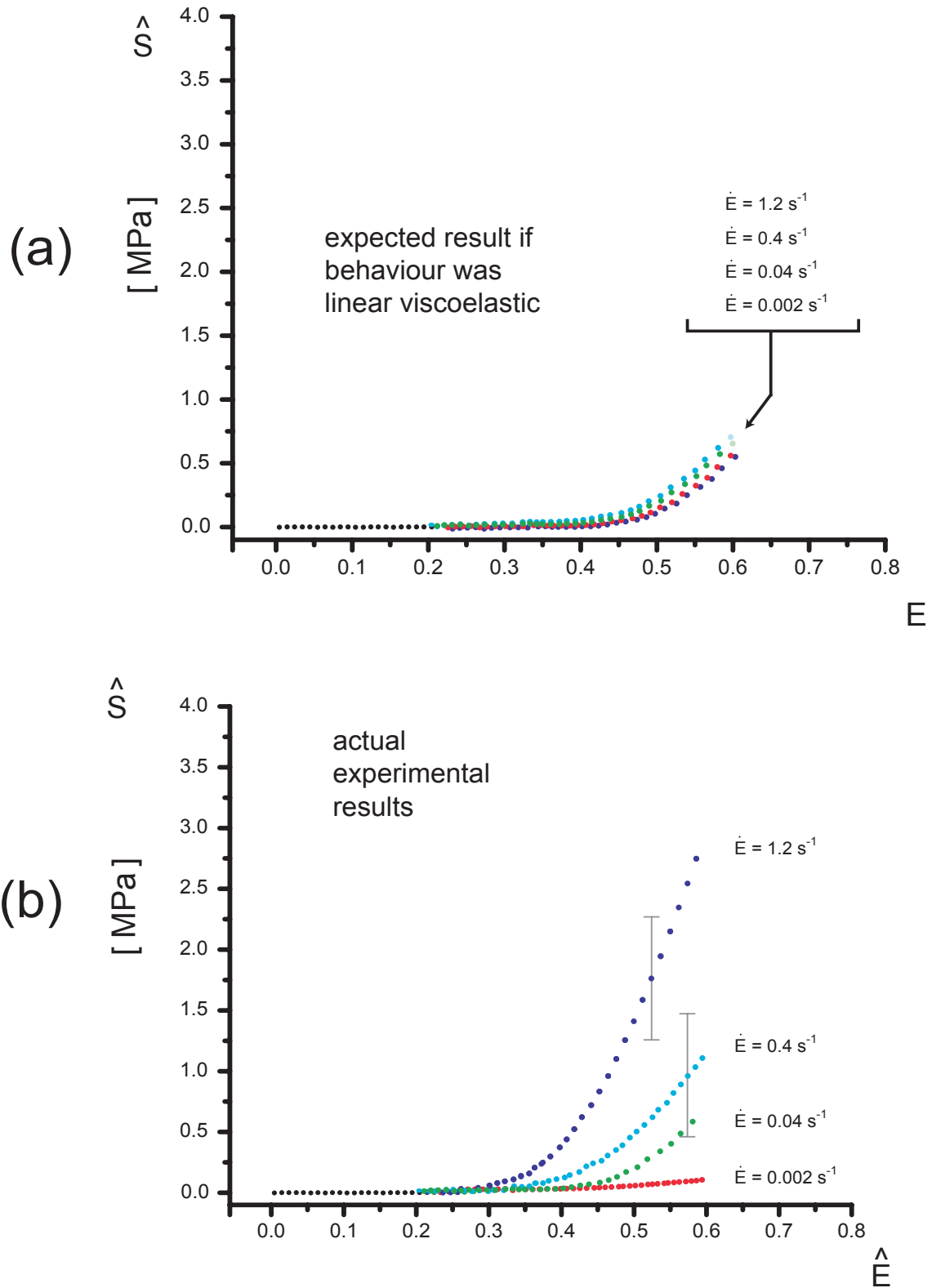
$$\frac{d(S/\alpha)}{d(E/\alpha)} = G(E/\alpha). \quad (\text{EQ 5.7})$$

These relations no longer depend explicitly on α . In other terms, the plot of

$$\hat{S} = \frac{S}{\alpha} \text{ vs. } \hat{E} = \frac{E}{\alpha} \quad (\text{EQ 5.8})$$

is independent of the strain rate. This is a direct consequence of the scaling property associated with linearity which is presented in section 2.7.3. It is this test which is in fact been performed on the PDL, and is used to determine whether it shows linearity of response. The plots of figure 5.3b are the experimental results obtained from constant strain rate deformation tests and are presented as described by equation 5.8. Because the plots of S/α versus E/α obtained from various strain rates differ, the PDL cannot be modeled as having linearity of response. If linearity of response were observed, the curves would not have differed, as shown in figure 5.3a.

Figure 5.4 Verification of linear scaling property: (a) the plot of equation 5.8 if the PDL displayed the linear scaling property, and (b) actual experimental results from testing linear scaling property.



5.3 Constant Strain Rate Deformation and Recovery History

This testing profile, as described by equation 2.25 and depicted in figure 2.12, is applied to the PDL at a strain rate of 0.04 s^{-1} . After defining the specimen zero, the adjusted zero is set at a strain of $E=0.3$ for loading and unloading. The results are presented in figure 5.5.

Interpreting the results presented in figure 5.5 is done through examining at mathematical relationships in their general form that describe linear viscoelastic materials. Although simplistic, this approach enables a first interpretation of how the PDL is behaving in such an experiment. The true behaviour cannot be described mathematically because the constitutive equations that describe PDL behaviour are currently unknown, i.e. no existing validated numerical model currently describes the behaviour of the PDL.

Any viscoelastic material will exhibit stress relaxation properties (see section 5.4). Typical stress relaxation is expressed as

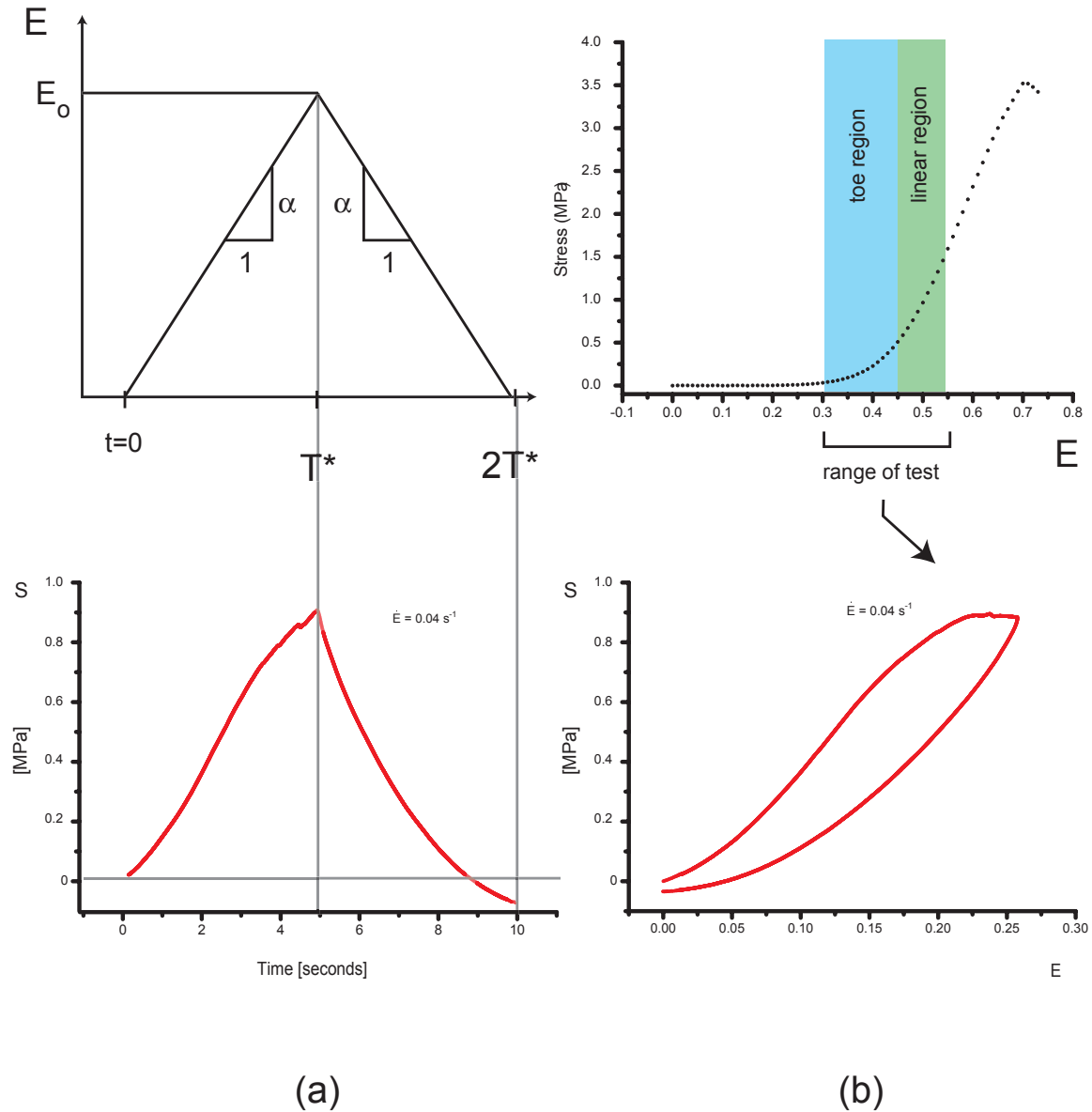
$$S(t) = E(0)G(t) + \int_0^t G(t-s)\dot{E}(s)ds. \quad (\text{EQ 5.9})$$

Substituting equation 5.9 into equation 2.25 gives the expressions for the stress at each time, t

$$S(t) = \begin{cases} \alpha \int_0^t G(s)ds & t \in [0, T^*] \quad (\text{a}) \\ \alpha \int_0^{T^*} G(t-s)ds - \int_{T^*}^t G(t-s)ds & t \in [T^*, 2T^*] \quad (\text{b}) \\ \alpha \int_0^{T^*} G(t-s)ds - \int_{T^*}^{2T^*} G(t-s)ds & t \geq 2T^* \quad (\text{c}) \end{cases} \quad (\text{EQ 5.10})$$

Since there is no jump discontinuity in the strain at T^* , there is no corresponding contribution to the stress. Likewise, the strain history has no jump discontinuity at $t = 0$, thus the most convenient form of the constitutive equation for $t \in [0, T^*]$ is given by equation 5.10a.

Figure 5.5 Results of Constant Strain Rate Deformation and Recovery History



The expression in equation 5.10b for $S(t)$ when $t \in [T^*, 2T^*]$ consists of two integrals. The first integral represents the strain increment contributions during the deformation interval $[0, T^*]$, and the second integral represents the contributions during the strain recovery interval $(T^*, 2T^*]$. Note that the upper limit of the first integral is fixed, but the time variable t in the integrand continues to increase. This represents the continuing stress relaxation of the stress responses to each of the strain increments during the interval

$[0, T^*]$). For the expression in equation 5.10c, the integration limits are also fixed, however, the presence of time t in the integrand represents the continuing stress relaxation of the stress responses to each of the previous strain increments.

Assuming $G(t)$ to be a general stress relaxation function, a stress versus strain plot (S vs. E) can be established, thus allowing a number of relationships to be established. These relationships are typical of viscoelastic material and give insight as to the viscoelastic nature of the PDL.

$t \in [0, T^*]$

The integral in equation 5.10a represents the area under the graph of $G(t)$ from 0 to t . Because the relaxation function, $G(t)$, decreases rapidly shortly after $t=0$ (see figure 5.8), the area is added in more slowly and the stress increases more slowly as t increases. This decrease in stress can be seen in the stress versus time curve shown in figure 5.5a.

$t \in [T^*, 2T^*]$

There is a change in the sign of the slope of the S vs. E plot at time T^* due to the change from increasing to decreasing deformation as shown in figure 5.5a. The first integral in equation 5.10b represents the area under $G(t)$ from time $t - T^*$ to time t . The second integral represents the area from time 0 to time $t - T^*$, and is considered negative. The positive area occurs under the smaller values of G for $t \in [t - T^*, t]$. The negative areas are under the larger values for $t \in [0, t - T^*]$. These areas can be visualised in looking at stress relaxation results presented in figure 5.8. As t approaches $2T^*$, the negative area becomes bigger than the positive area. Hence the stress becomes negative even though the strain is still positive as shown in the results presented in figure 5.5.

5.3.1 What does this say about the behaviour of periodontal ligament?

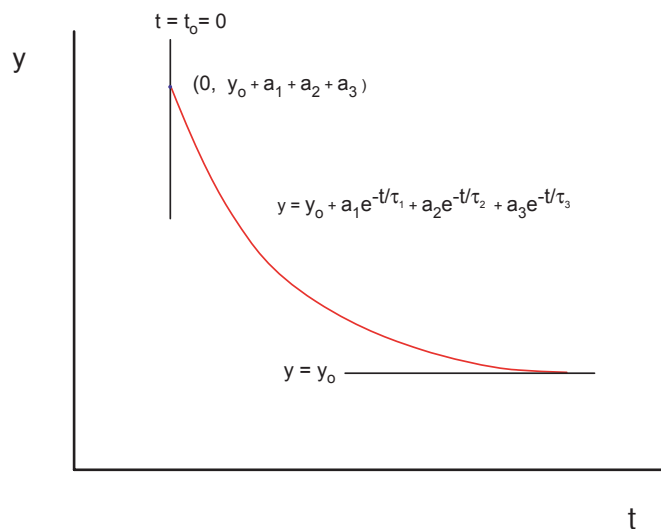
Constant strain rate deformation and recovery tests performed on PDL specimens show definite viscoelastic characteristics. The role played by the relaxation function in the shape of the S-E curve can be intuitively interpreted using linear viscoelastic theory. As the results of this thesis show, the PDL is not linear viscoelastic, such behaviour as shown in figure 5.5 gives an excellent starting-point for the development of a more advanced model that would take into account the nonlinearities of the PDL, i.e. non-linear dashpot, non-linear springs.

5.4 Uniaxial Stress Relaxation of the Periodontal Ligament

As a means to describe the stress relaxation observed in the PDL, some curves presented in this section are fit to a third order exponential decay function

$$y = y_0 + a_1 e^{(-t)/\tau_1} + a_2 e^{(-t)/\tau_2} + a_3 e^{(-t)/\tau_3} \quad (\text{EQ 5.11})$$

Figure 5.6 Third Order Exponential Decay Function



5.4.1 Zero Definition and Stress Relaxation

In performing any experiment on PDL tissue, it is critical that a zero is determined in order to have a reproducible frame of reference as a means to compare specimen to specimen. The results in this section show the dependence of where a zero is defined to the results obtained from stress relaxation experiments.

Two typical relaxation curves are presented in figure 5.7. The first curve obtained, figure 5.7a, is obtained by first zeroing the uniaxial specimen (see section 3.2.1) pulling the specimen to strain $E=0.30$, and recording the relaxation data for 60 seconds. It is important to note that this first test is performed with strain $0 < E < 0.30$, i.e. the specimen is tested in the zero region. The specimen is then unloaded submerged in saline and left to rest at $E=0$ for 5 minutes. The second stress relaxation test is then performed, however, the zero was adjusted by pulling the specimen slowly (strain rate $< 1 \text{ mm} \cdot \text{s}^{-1}$) to a strain value $E=0.20$, at which point the sample was left for 5 minutes. It is from this point that

the second relaxation test is performed, the strain range being $0.20 < E < 0.50$. Note that this relaxation test was performed in the zero, toe and linear regions.

Modifying the variables of the third order exponential decay function given in equation 5.11 to comply with the relaxation curves presented in figure 5.7 gives

$$G = G(\infty) + a_1 e^{(-t)/\tau_1} + a_2 e^{(-t)/\tau_2} + a_3 e^{(-t)/\tau_3} \quad (\text{EQ 5.12})$$

Fitting both these curves to a third order exponential decay function described by equation 5.12 yields the parameters presented in table 5.2.

Table 5.2 Parameters describing the relaxation curves in figure 5.7 fit to a third order exponential function

parameter	$G(0 < E < 0.3, t)$	$G(0.2 < E < 0.5, t)$
$G(\infty)$	0.00 ± 0.01	1.71 ± 0.01
t_1	0.14 ± 0.01	1.15 ± 0.01
t_2	2.49 ± 0.36	5.65 ± 0.04
t_3	43.32 ± 3.41	63.63 ± 0.53
a_1	0.03 ± 0.00	0.13 ± 0.03
a_2	0.08 ± 0.01	0.33 ± 0.05
a_3	0.80 ± 0.00	0.72 ± 0.06
R^2	0.9817	0.999

PDL Behaves as a Fluid and as a Solid depending on Zero Definition

Expressions have been presented in table 5.2 according to the 3rd order decay function in equation 5.12. In more general terms, equation 5.12 can be rewritten as the superposition of its asymptotic value as $t \rightarrow \infty$ and a time-dependent part which decays to zero

$$G(t) = G(\infty) + \Delta G(t) \quad (\text{EQ 5.13})$$

If $G(\infty) \neq 0$ the material acts as a solid. Viscoelastic fluid response can be accounted for by setting $G(\infty) = 0$. Demonstrated graphically in figure 5.7a the PDL behaves as a fluid, i.e. $G(\infty) \cong 0$. Figure 5.7b on the other hand, shows the same specimen to behave as a solid, i.e. $G(\infty) \neq 0$. This remarkable result indicates the importance of defining the

zero of the specimen. Moreover, in modeling such behaviour respective boundary limits must be defined for fluid-like and solid-like behaviour of the ligament.

5.4.2 Relaxation Tests of PDL at Different Strain Levels

To determine the role of varying the strain level when performing step-strain stress relaxation experiments on the PDL, two strains are chosen. A first strain $E_1 = 0.20$, is chosen to remain in the physiological range of the tissue, i.e. the strains did not exceed the strains in the toe region of the specimen. A second strain $E_2 = 0.40$, is chosen to exceed the physiological range, and enter into the linear region of the specimen.

The relaxation responses are defined by the G functions:

$$G_1 = G(E_1, t)|_{E_1 = 0.20} \quad (\text{EQ 5.14})$$

and

$$G_2 = G(E_2, t)|_{E_2 = 0.40} \quad (\text{EQ 5.15})$$

Specific Procedures

The stress relaxation curves G_1 and G_2 are obtained by following a specific procedure: the zero is determined as described in section 3.3.1. Once the zero is determined, the specimen is subjected to the first step strain E_1 , relaxation is observed over a period of 60 seconds during which the data for G_1 are obtained. After obtaining this data, the specimen is unloaded and left to recover for a period of 5 minutes before subjecting it to a step strain E_2 . The data for G_2 are hence obtained.

Results of Stress Relaxations G_1 and G_2

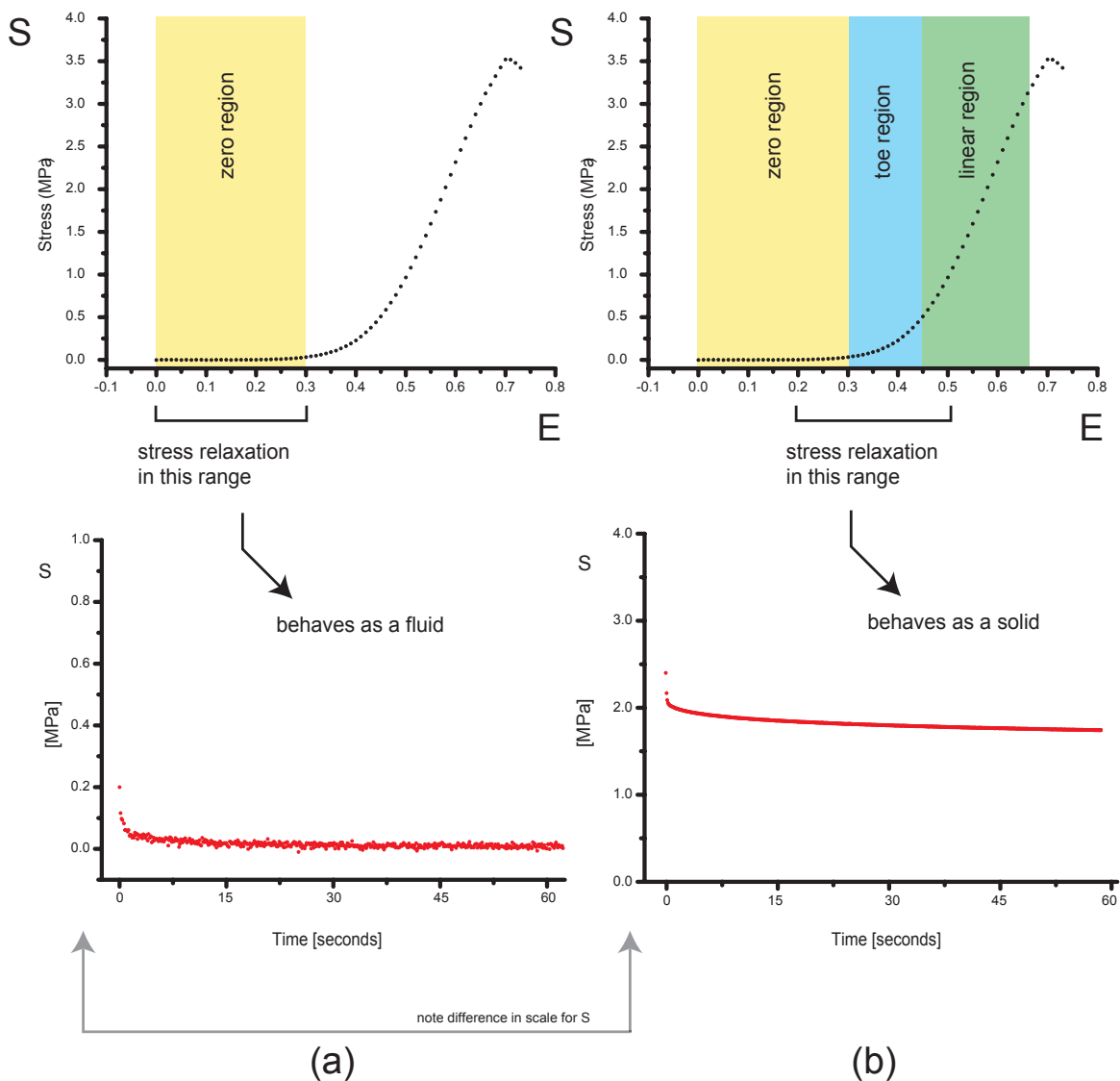
The maximum stress in a stress relaxation curve of the PDL is observed at time $t=0$. The corresponding stress for this maximum is S_0 . In order to compare these relaxation curves, it is necessary to normalise relaxation curves G_1 and G_2 . The normalised curves, \hat{G}_1 and \hat{G}_2 are obtained by dividing the G_1 and G_2 by their respective maximum stress S_0 and are plotted in figure 5.8.

$$\hat{G}_1 = \frac{G_1}{S|_{t=0}} \quad (\text{EQ 5.16})$$

and

$$\hat{G}_2 = \frac{G_2}{S|_{t=0}} \quad (\text{EQ 5.17})$$

Figure 5.7 Relaxation at zero



Modifying the variables of the third order exponential decay function given in equation 5.11 to comply with the curves presented in figure 5.8 gives

$$\hat{G} = \hat{S}_0 + a_1 e^{(-t)/\tau_1} + a_2 e^{(-t)/\tau_2} + a_3 e^{(-t)/\tau_3} \tag{EQ 5.18}$$

Fitting \hat{G}_1 and \hat{G}_2 to a third order exponential decay function described by equation 5.18 yields the parameters presented in table 5.3.

Table 5.3 Parameters describing \hat{G}_1 and \hat{G}_2 in figure 5.8 fit to a third order exponential function

parameter	$G(E_1, t) _{E_1 = 0.20}$	$G(E_2, t) _{E_2 = 0.40}$
s_0	0.91 ± 0.00	0.72 ± 0.00
t_1	0.96 ± 0.11	1.15 ± 0.01
t_2	5.31 ± 0.33	5.65 ± 0.04
t_3	52.86 ± 3.68	63.63 ± 0.53
a_1	0.01 ± 0.00	0.03 ± 0.00
a_2	0.03 ± 0.01	0.08 ± 0.00
a_3	0.05 ± 0.00	0.17 ± 0.00
R^2	0.9987	0.999

5.4.3 Verification of the Linear Scaling Property of Relaxation Response

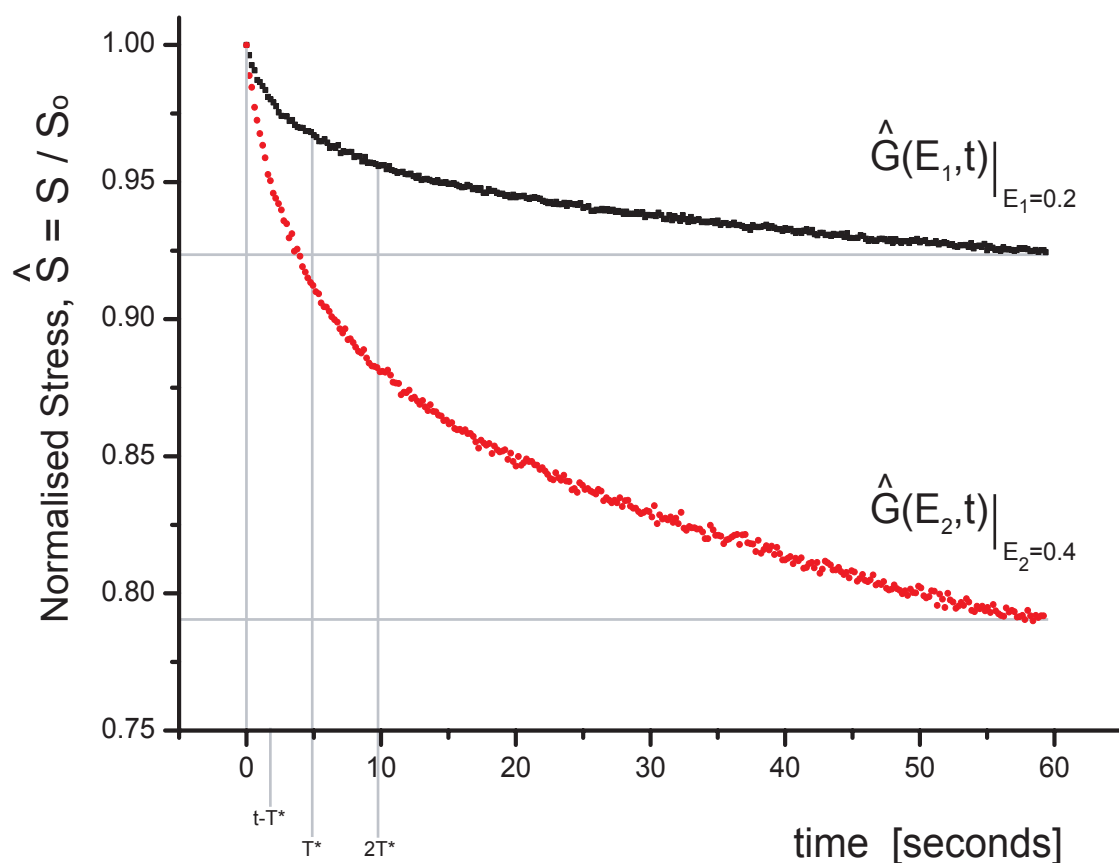
The relaxation curves shown in figure 5.8 show the typical response of a uniaxial specimen. These curves show that linear scaling is not a property of the PDL. If it were so, the curves in figure 5.8 would collapse to a single curve as shown in Figure 2.14a.

Examining the parameters in table 5.3 also support that the PDL does not show linear scaling in that no single factor exists to relate \hat{G}_1 and \hat{G}_2 as demonstrated by equation 2.30. In other terms, the column of parameters for \hat{G}_1 in table 5.3 are not equal to the parameters for \hat{G}_2 .

It can be seen from the curves in figure 5.8 and the parameters in table 5.3 that \hat{G}_1 and \hat{G}_2 differ. This difference implies that stress relaxation depends on the level to which the periodontal is strained. \hat{G}_1 is pulled in tension to a strain of $E_1=0.20$ and after 60 seconds, the PDL relaxes to 91% of its maximum stress at $t=0$. \hat{G}_2 , on the other hand, is pulled in tension to a strain of $E_2=0.40$ and after the same amount of time, the PDL relaxes to 71%. This shows that the rate of relaxation of the PDL depends on the strain-level.

A total of 58 specimens are tested in this manner and each consistently demonstrate the behaviour described above.

Figure 5.8 Relaxation at different strain levels



The characteristic times τ_1 , τ_2 and τ_3 are fairly similar, the fastest time, τ_1 being around 1 second, τ_2 being roughly 5 times greater than τ_1 , and τ_3 being around 50-60 times greater than τ_1 . The fastest characteristic time, τ_1 , is used as the basis of selecting the control parameters for testing the PDL experimentally. Obtained first experimentally in preliminary experiments, the value for τ_1 consistently produces a value of ~ 1 second.

5.4.4 Verification of the Hypothesis of Variables Separation

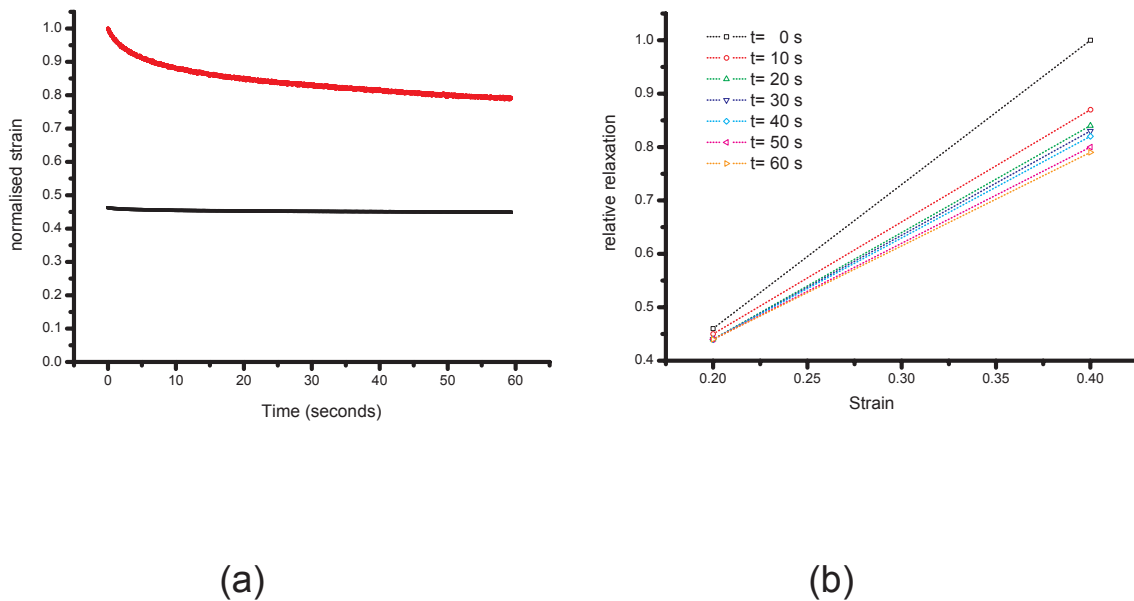
Another method to verify the dependence of time and strain effects in the stress relaxation data presented above is in verifying the hypothesis of variables separation. This hypothesis is widely used in soft tissue biomechanics [Pioletti and Rakotomanana 2000; Pioletti and Rakotomanana 2000]. Ideally, stress relaxation should be observed at several different strain values, and not just at two levels (i.e. $E=0.2$ & $E=0.4$), however, as a first indication of the time dependence of the PDL, this analysis proves useful.

If the hypothesis of variables separation is justified, (i.e. linear scaling is possible, equation 2.30) the relative relaxation function (equation (5) [Pioletti and Rakotomanana 2000]) should be independent of the strain E , however, this is not shown to be the case (figure 5.9). If it were the case, the relative relaxation observed at different strains E

should be constant at any specific time value, thus giving a horizontal line. The relative relaxation curves are obtained by normalising initial relaxation data by:

$$S_{\text{normalised}} = \frac{S_{\text{experimental}}}{S(t = 0, E = 0.4)} \quad (\text{EQ 5.19})$$

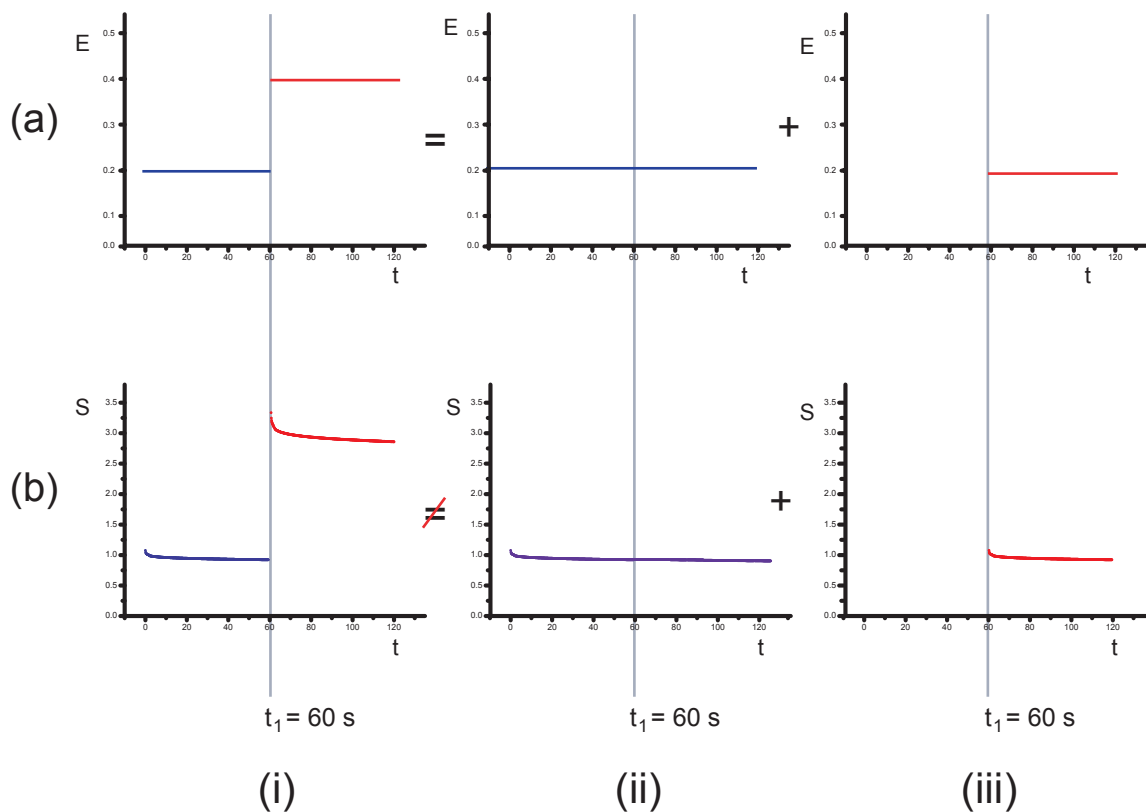
Figure 5.9 (a) normalised stress relaxation curves at 2 strains ($E=0.2$ & $E=0.4$) for bovine PDL uniaxial specimens.



5.4.5 Verification of Superposition Property of Relaxation Responses

The notion of the superposition property of a viscoelastic material is discussed in section 2.7.5. The verification of this property for the relaxation responses directly follows the results presented in section 5.4.2 in which relaxation curves G_1 and G_2 are presented. A third experiment, however, is performed to permit this verification, producing compounded relaxation curves $G_3 = [G_{3,a} \text{ and } G_{3,b}]$. The non-normalised relaxation curves G_1 , G_2 and G_3 are shown in figure 5.10. and graphically show that this linear superposition is not a property of the PDL.

Figure 5.10 Superposition of Relaxation Responses



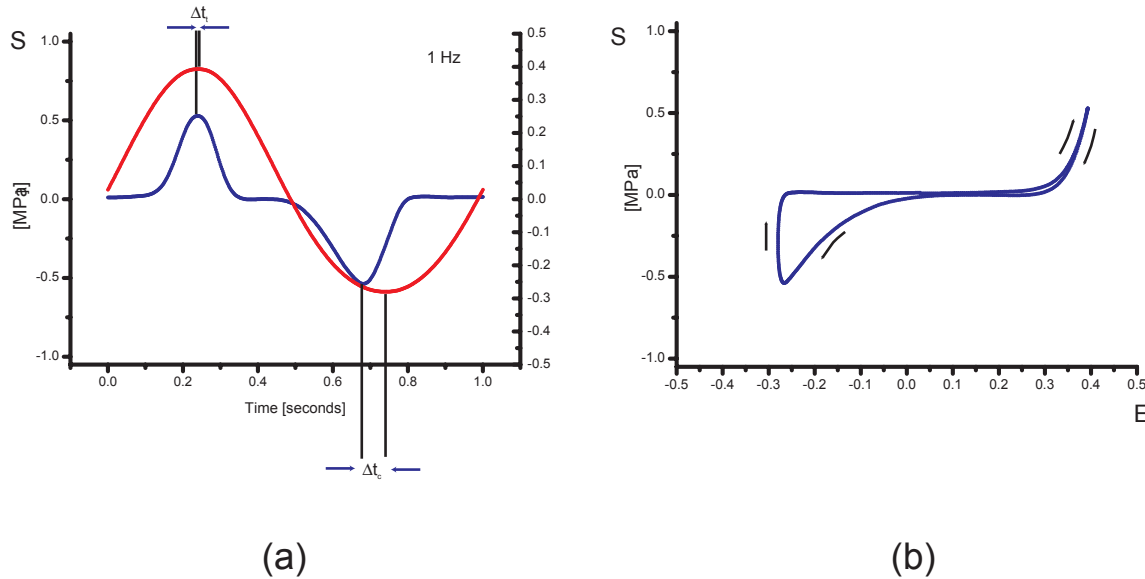
5.5 Sinusoidal Response of the Periodontal Ligament

To this point, the time-dependent mechanical properties of the PDL have been presented as a relaxation modulus G , which is a function of time. Although this relaxation modulus is most useful in characterizing the time-dependent material response of the ligament, the large variation of results depending on zero definition, strain level in stress-relaxation experiments and biological variability make it difficult to attribute definite parameters to ligament behaviour. Subjecting the ligament to sinusoidal strain histories give rise to other material response functions which are related to the relaxation modulus G . The results obtained from subjecting uniaxial specimens to sinusoidal strain histories give valuable insight into how the PDL behaves.

A total of 43 specimens are subjected to sinusoidal oscillations and many hundreds of cycles are performed for each given uniaxial specimen. Processing the data with the aid of custom-made MATLAB programs enabled a thorough investigation of the PDL when subjected to harmonic oscillations. As described in this sections, the parameters of primary interest are the phaselags. In compression denoted as δ_c and in tension as δ_t . The

phaselag measurement is shown graphically in figure 5.11, and mathematically in equation 5.27 and equation 5.28.

Figure 5.11 Sine Test : stress/strain vs. time 1 cycle and corresponding stress strain curve at 1 Hz of a typical specimen.



5.5.1 Transient Stress Response to Sinusoidal Strain History

Each uniaxial specimen used for sinusoidal testing is subjected to a total of 30 cycles. Figure 5.14 is a stress versus strain curve of the first ten cycles of a uniaxial specimen and clearly demonstrates the initial transient phase evolving into a steady stress response. No phaselag difference from cycle to cycle is observed in the compression nor in tension, however, as shown in figure 5.14, a variation in the stress response amplitude in compression is observed. No variation in the tensile stress response amplitude is observed.

After the tenth cycle, no further change to the stress response is observed. This supports viscoelastic theory in that as time increases, the coefficients become independent of time and depend only on frequency.

Consider the sinusoidal strain history

$$E(s) = E_0 \sin \omega s \quad s \in [0, \infty) \quad (\text{EQ 5.20})$$

For the sake of interpreting the results, the amplitude E_0 is said to be considered for small deformations where linearity is assumed, however, for the PDL this is not the case. The constitutive equation for calculating the stress history can be expressed as

$$S(t) = E(0)G(t) + \int_0^t G(t) \dot{E}(t-s) ds. \quad (\text{EQ 5.21})$$

The stress relaxation function can be expressed as the superposition of its asymptotic value as $t \rightarrow \infty$ and a time dependent part which decays to zero

$$G(t) = G(\infty) + \Delta G(t). \quad (\text{EQ 5.22})$$

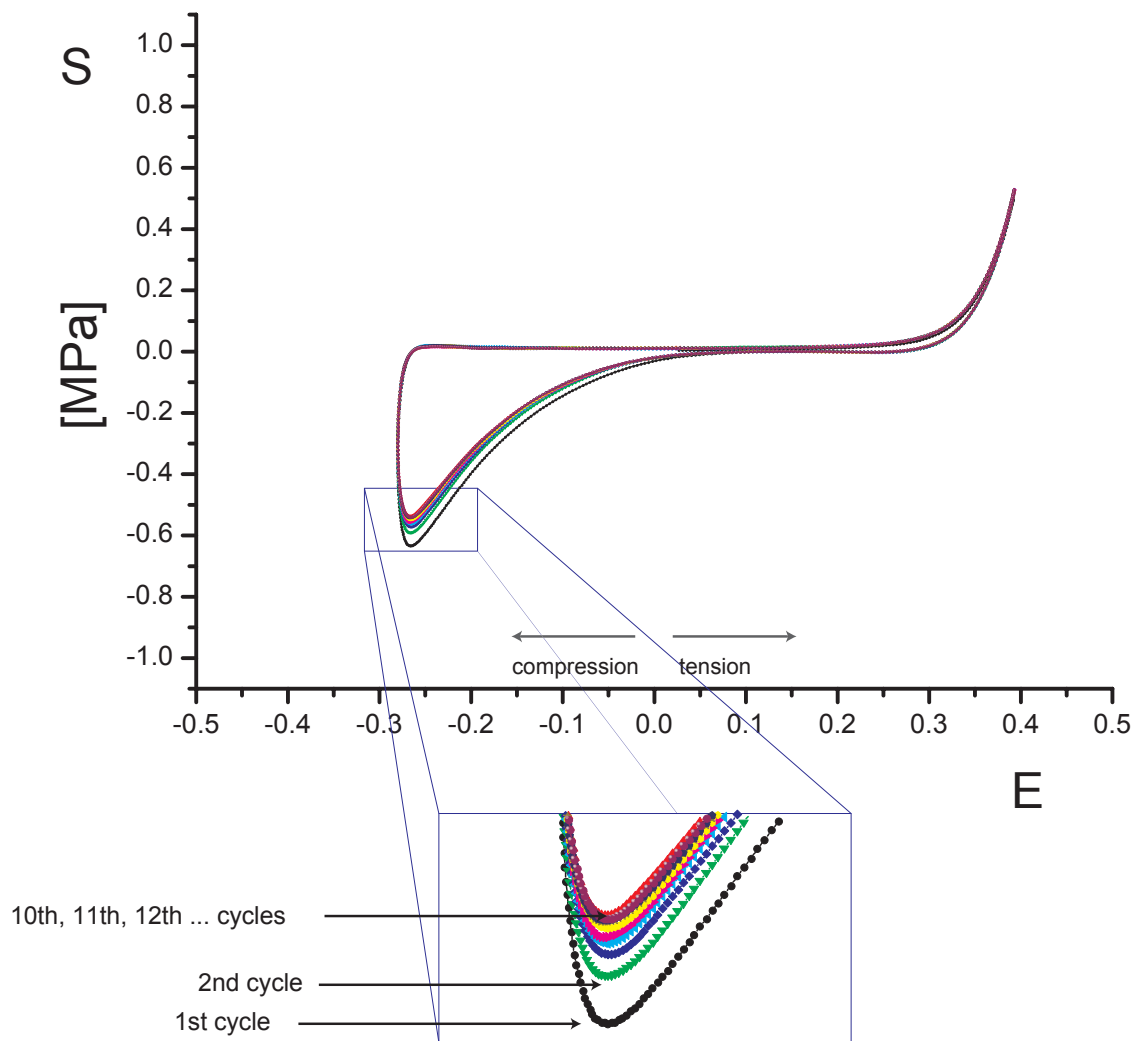
Substituting equation 5.22 into equation 5.21 gives

$$\begin{aligned} S(t) &= E(0)[G(\infty) + \Delta G(t)] + \int_0^t (G(\infty) + \Delta G(t)) \dot{E}(t-s) ds \\ &= G(\infty)E(t) + E(0)\Delta G(t) + \int_0^t \Delta G(s) \dot{E}(t-s) ds \end{aligned} \quad (\text{EQ 5.23})$$

Substituting the sinusoidal strain history given by equation 5.20 gives

$$\begin{aligned} S(t) &= E_0 \left[G(\infty) \sin \omega t + \omega \int_0^t \Delta G(s) \cos(t-s) ds \right] \\ &= E_0 \left\{ \left[G(\infty) + \omega \int_0^t \Delta G(s) \sin \omega s ds \right] \sin \omega t + \left[\omega \int_0^t \Delta G(s) \cos \omega s ds \right] \cos \omega t \right\} \end{aligned} \quad (\text{EQ 5.24})$$

Figure 5.12 Transient state to stable state of PDL under sinusoidal oscillations



Let

$$G'(\omega, t) = G(\infty) + \omega \int_0^t \Delta G(s) \sin \omega s ds \tag{EQ 5.25}$$

$$G''(\omega, t) = \omega \int_0^t \Delta G(s) \cos \omega s ds$$

Then equation 5.24 can be rewritten as

$$S(t) = E_0 [G'(\omega, t) \sin(\omega t) + G''(\omega, t) \cos \omega t]. \tag{EQ 5.26}$$

It can also be written in the form

$$S(t) = E_0[G'(\omega, t)^2 + G''(\omega, t)^2] \sin(\omega t + \delta(\omega, t)). \quad (\text{EQ 5.27})$$

where

$$\tan \delta(\omega, t) = \frac{G''(\omega, t)}{G'(\omega, t)} \quad (\text{EQ 5.28})$$

While the strain is sinusoidal in time, the stress is not because of the time-dependent coefficients in equation 5.26 and equation 5.27. In order to study the effect of stress response as $t \rightarrow \infty$ it can be assumed that there is a finite area under the graph of $\Delta G(s)$. That is, for some number M ,

$$\int_0^{\infty} \Delta G(s) ds = M. \quad (\text{EQ 5.29})$$

This ensures that the time integrals in equation 5.25 approach finite values as $t \rightarrow \infty$. It is now possible to define

$$G'(\omega) = \lim_{t \rightarrow \infty} G'(\omega, t) \quad G''(\omega) = \lim_{t \rightarrow \infty} G''(\omega, t) \quad (\text{EQ 5.30})$$

then by equation 5.25 and equation 5.30,

$$G'(\omega) = G(\infty) + \omega \int_0^{\infty} \Delta G(s) \sin \omega s ds \quad (\text{EQ 5.31})$$

$$G''(\omega) = \omega \int_0^{\infty} \Delta G(s) \cos \omega s ds$$

and there is dependence only on the frequency of oscillation. As a result, equation 5.26 can be rewritten as

$$S(t) = E_0[G'(\omega) \sin(\omega t) + G''(\omega) \cos \omega t] \quad , \quad (\text{EQ 5.32})$$

equation 5.27 as

$$S(t) = E_0[G'(\omega)^2 + G''(\omega)^2] \sin(\omega t + \delta(\omega)) \quad . \quad (\text{EQ 5.33})$$

and equation 5.28 as

$$\tan \delta(\omega, t) = \frac{G''(\omega)}{G'(\omega)} \quad . \quad (\text{EQ 5.34})$$

These results show that initially the stress is not sinusoidal because of the time-dependent coefficients in equation 5.26. As time increases, the coefficients become independent of time and depend only on frequency. The stress response then develops the form in equation 5.32 and equation 5.33. In other terms, the initial transient response dies out, after which the stress undergoes an oscillation at the same frequency as the strain with amplitude

$$\sqrt{E_0[G'(\omega)^2 + G''(\omega)^2]} \quad (\text{EQ 5.35})$$

and phase difference $\delta(\omega)$.

What does this transient to steady state say about the Periodontal Ligament?

The behaviour PDL as described by the Stress versus Strain curve in figure 5.12 varies with time, i.e. the S-E response varies from cycle to cycle during initial loading, however, after a certain number of cycles, a steady state is reached. In essence, this demonstrates that the PDL behaves in a viscoelastic behaviour, and based on the equations above it is possible to describe this phenomenon by linear viscoelastic theory. This does not imply that the PDL is linear viscoelastic, as no linear viscoelastic model could describe the form of the S vs. E curve.

5.5.2 Effect of Frequency on the Sinusoidal Response of the PDL

Figure 5.14 shows a series of graphs of stress and strain plotted on a common axis of time and summarise the role frequency plays on the sinusoidal response of the PDL. The graphs (a) through (f) have been obtained from the same specimen at different frequencies of oscillation. Note that the control parameter, i.e. the strain amplitude, did not vary from frequency to frequency.

It can be seen in figure 5.14 that the magnitude of the stress response amplitude in tension, i.e. the absolute value of the maximum stress value, increases with increased frequency. Likewise, the magnitude of the stress response amplitude in compression, i.e. the absolute value of the minimum stress value, increases with increased frequency. The increase in compression, however, is relatively more significant than in tension.

As shown by figure 5.11, the phaselags between the strain and the stress were measured for each corresponding frequency. The phaselags were measured as a time, and converted to radians using the angular velocity imposed on the ligament using

$$\delta = \Delta t \cdot \omega \quad (\text{EQ 5.36})$$

where δ =phaselag in radians, Δt = phaselag measured as a time, and

$$\omega = 2\pi f \quad (\text{EQ 5.37})$$

where f = frequency.

With respect to the measured phaselags, two conclusions can be drawn from the data presented in figure 5.14. First, the phaselag in compression, δ_c , is greater than the phaselag in tension, δ_t . And second, there is no significant effect of frequency on δ_c nor on δ_t . A table of the results of phaselags and frequency is presented in table 5.4 and a plot

showing the independence of frequency in the range of 0.02 Hz to 4 Hz is presented in figure 5.16.

Another method to study the effect of frequency can be done in examining plots of stress versus strain at different frequencies. This has been presented in figure 5.15 and it can be seen that hysteresis is observed primarily in compression. Superimposing each stress versus strain curve into a single graph (see figure 5.13) shows the significant difference in the curves with variations in frequency.

Figure 5.13 Frequency effect on Stress versus Strain Curves

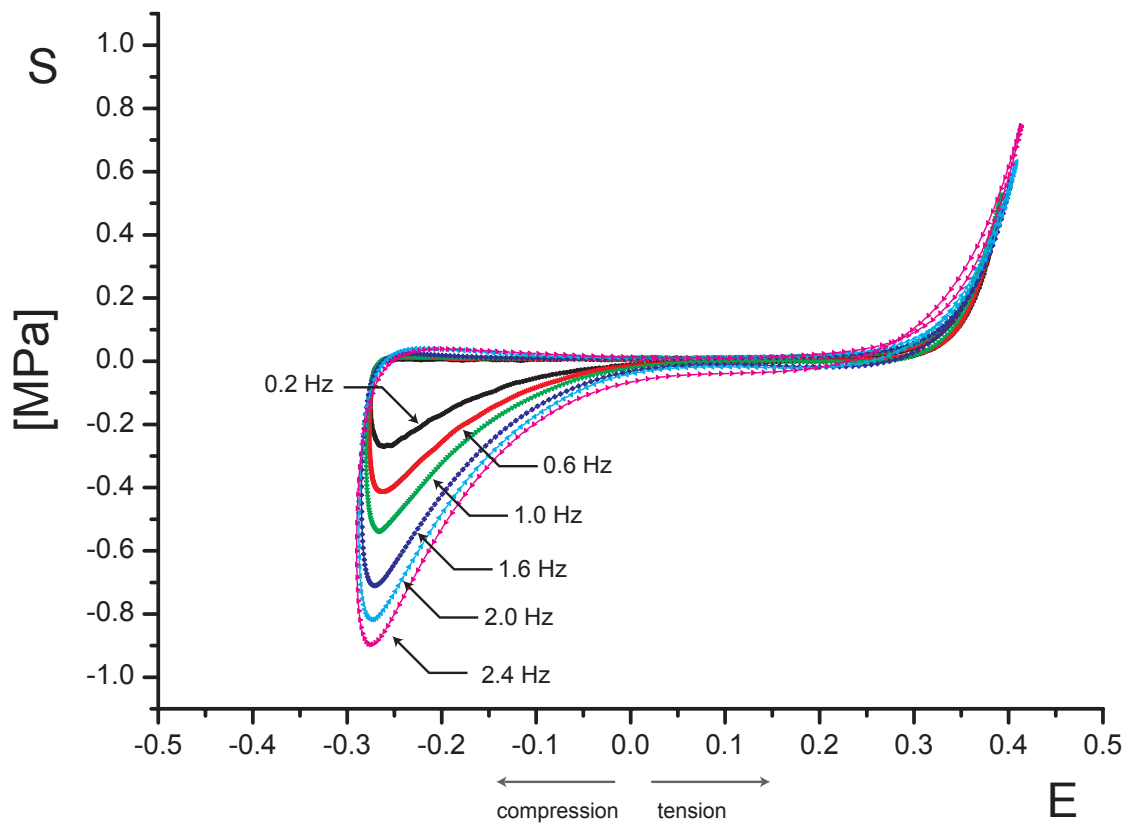


Figure 5.14 Stress and strain as functions of time for a selection of frequencies

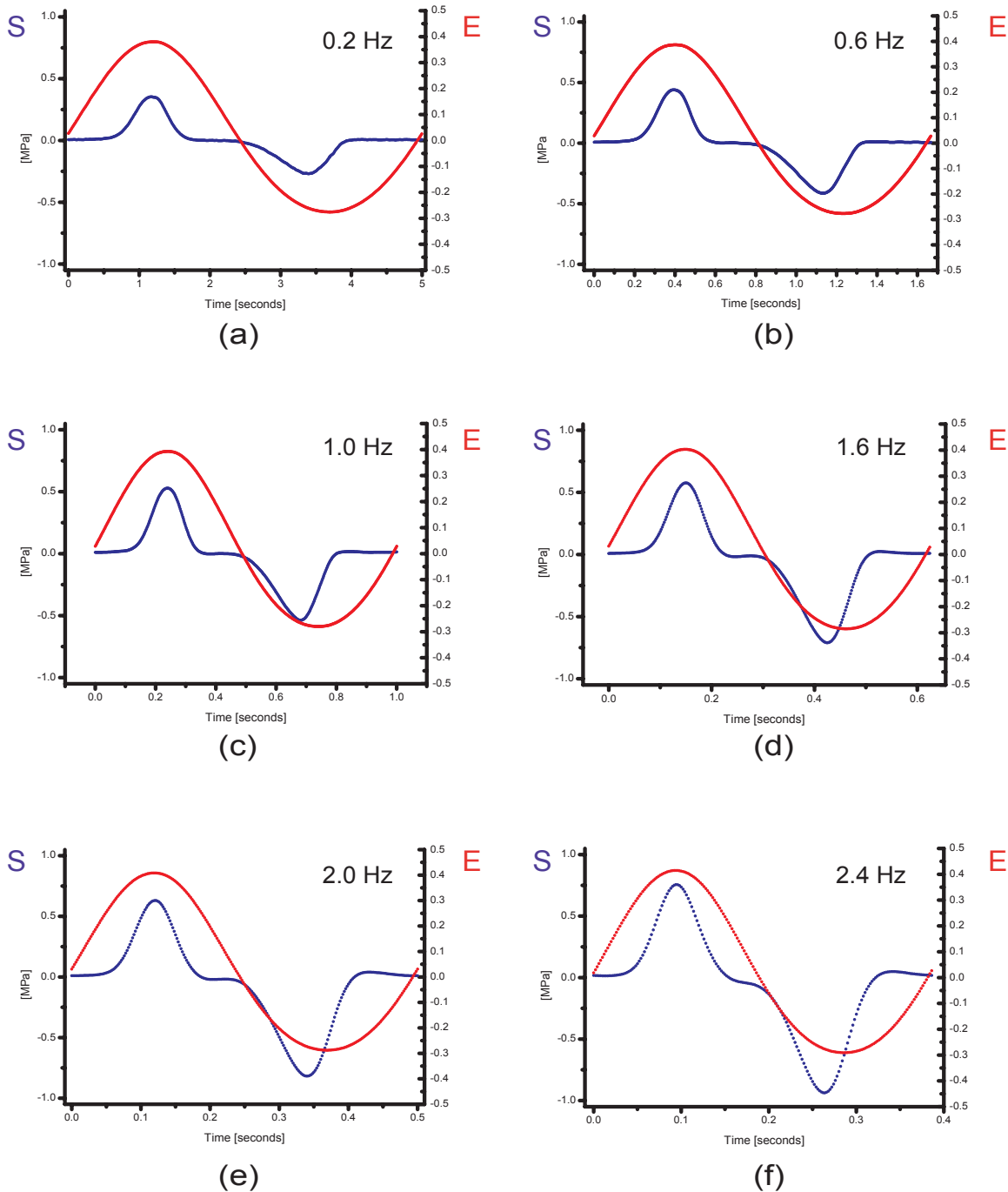


Figure 5.15 Stress as a function of strain for a selection of frequencies

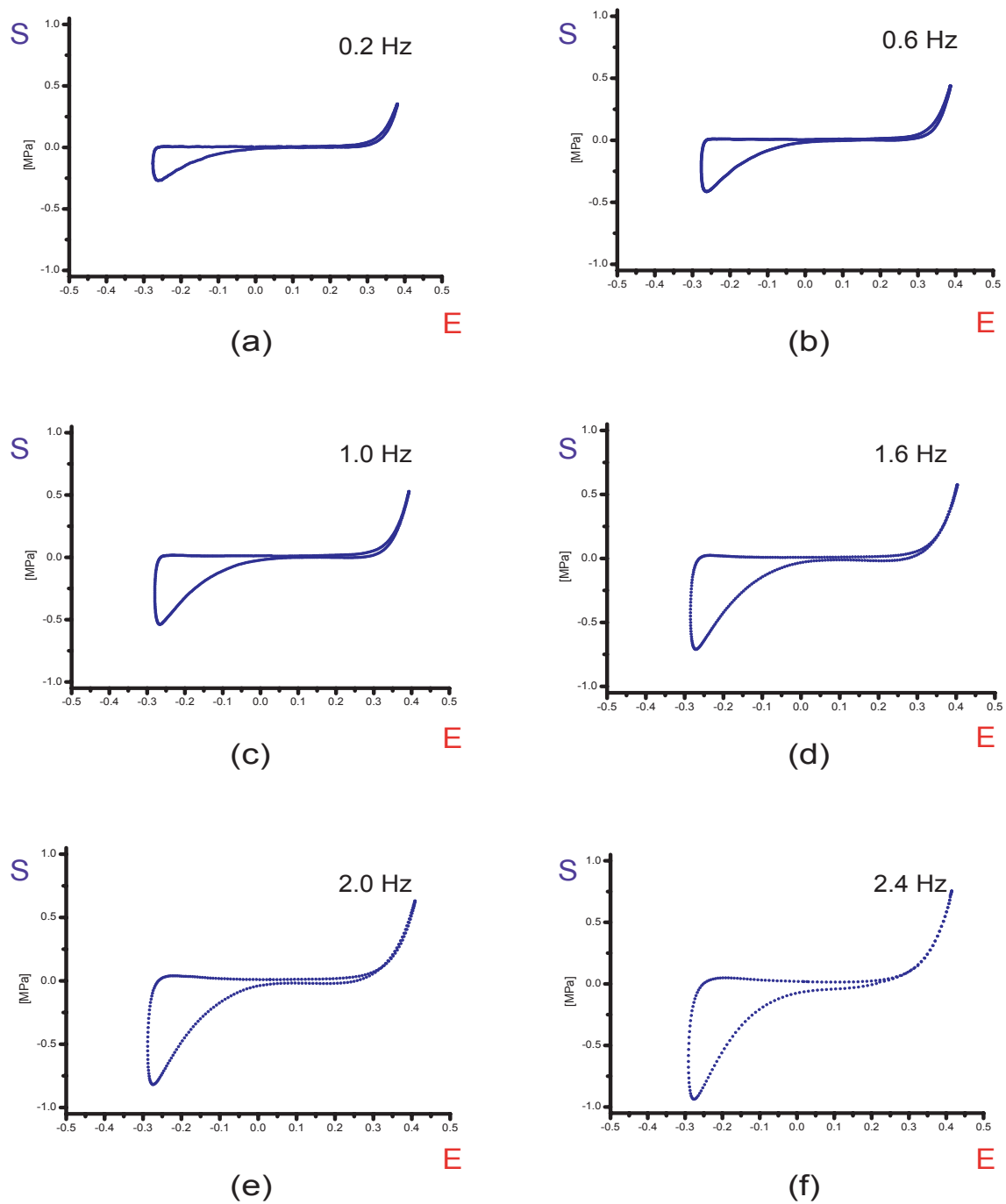


Figure 5.16 Effect of frequency on phaselag expressed as $\tan \delta$ versus frequency

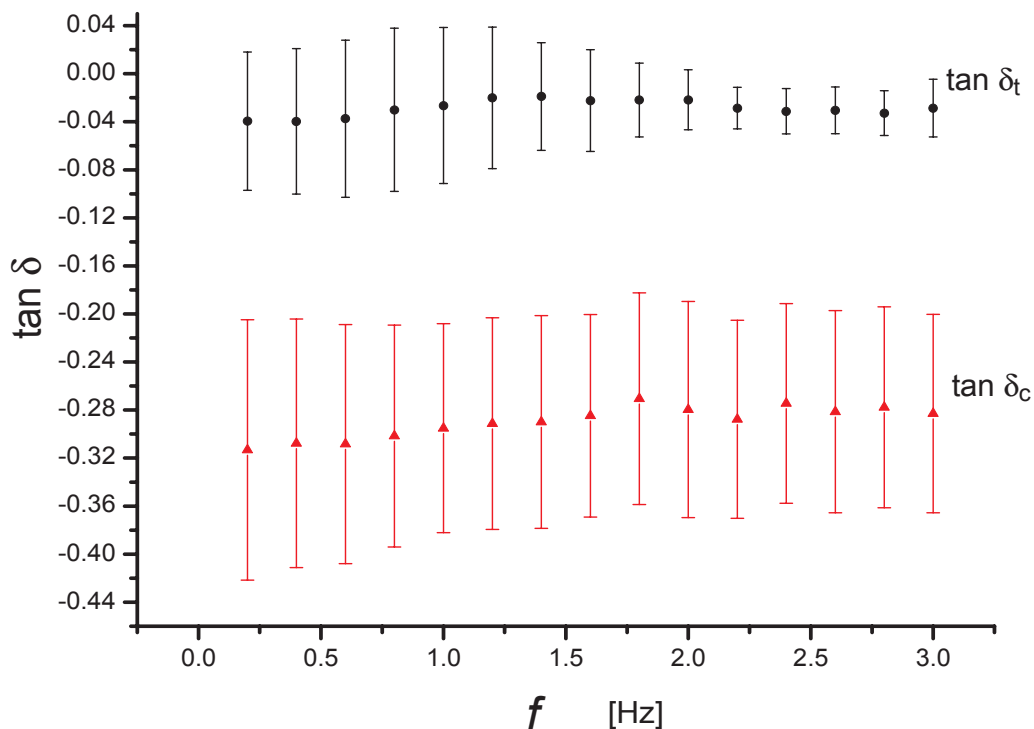


Table 5.4 Data of Effect of frequency on phaselags, δ_c & δ_t

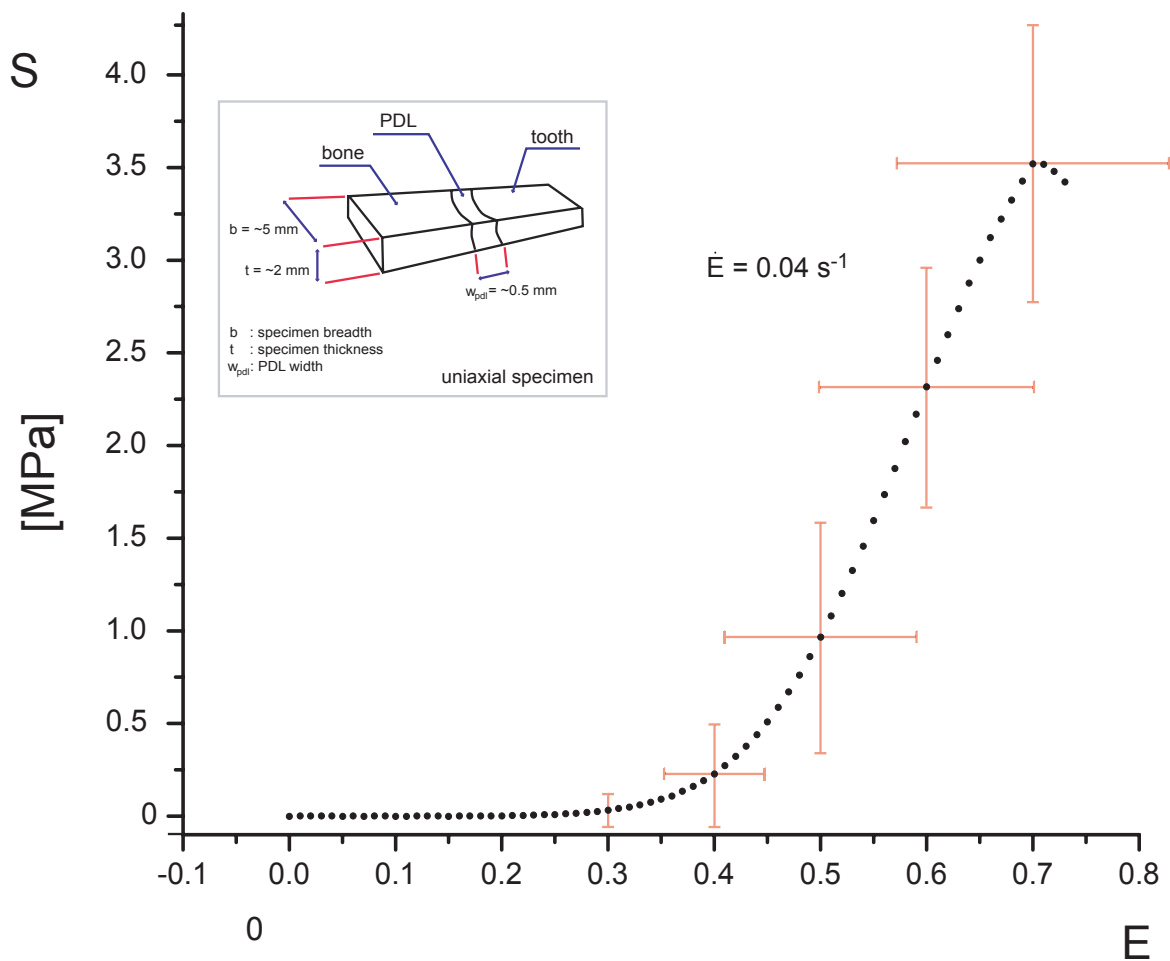
f [Hz]	$\tan \delta_t$	$\tan \delta_c$
0.2	-0.039 ± 0.06	-0.313 ± 0.14
0.4	-0.040 ± 0.06	-0.310 ± 0.13
0.6	-0.038 ± 0.06	-0.309 ± 0.13
0.8	-0.030 ± 0.06	-0.301 ± 0.12
1.0	-0.027 ± 0.07	-0.295 ± 0.12
1.2	-0.020 ± 0.06	-0.291 ± 0.12
1.4	-0.019 ± 0.05	-0.290 ± 0.12
1.6	-0.022 ± 0.04	-0.285 ± 0.11
1.8	-0.022 ± 0.04	-0.271 ± 0.11
2.0	-0.022 ± 0.03	-0.280 ± 0.11
2.2	-0.029 ± 0.03	-0.288 ± 0.11
2.4	-0.031 ± 0.02	-0.275 ± 0.11
2.6	-0.030 ± 0.02	-0.281 ± 0.11
2.8	-0.033 ± 0.02	-0.278 ± 0.11
3.0	-0.029 ± 0.02	-0.282 ± 0.11

5.6 Rupture

The rupture curve shown in section Figure 5.17 is the average of 67 specimens. The average dimensions and relevant geometry of the specimens ruptured are presented in figure 4.1 and the parameters that describe its behaviour are given in table 5.5.

It is seen that the PDL behaves as a typical soft tissue with an identifiable zero region, toe region, linear region and rupture region. The rate of deformation, or strain rate, was chosen to be $\dot{E} = 0.04 \text{ s}^{-1}$ in order to minimise the viscosity effect; the strain rate is a factor of approximately 5 slower than the fastest relaxation time, τ_1 (see section 5.4.2).

Figure 5.17 Rupture curve of Uniaxial Periodontal performed on Uniaxial Specimen



5.6.1 Rupture Tests at Different Strain Rates

To investigate the role of strain rate on the rupture behaviour of the PDL, a series of experiments are performed to determine this dependence. Three rates are chosen for this study ranging from $\dot{\epsilon} = 0.002 - 1.2 \text{ s}^{-1}$.

In addition to the 67 rupture tests performed at $\dot{\epsilon} = 0.04 \text{ s}^{-1}$, an additional 37 specimens are ruptured at $\dot{\epsilon} = 0.002 \text{ s}^{-1}$, and $\dot{\epsilon} = 1.2 \text{ s}^{-1}$. After zeroing, each specimen is preconditioned and then ruptured. The results are summarised in the Table 5.5.

Table 5.5 Summary of dependence of strain rate on the PDL rupture parameters.

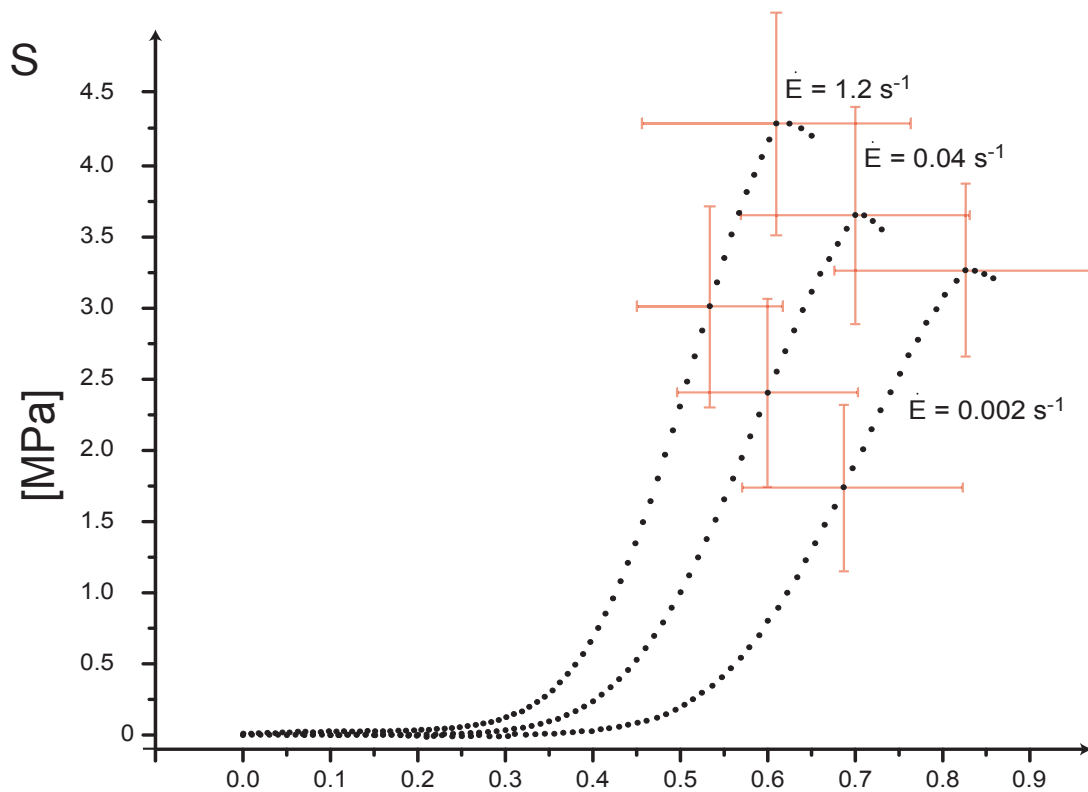
$\dot{\epsilon}$	0.002 s⁻¹	0.04 s⁻¹	1.2 s⁻¹
ϵ [MPa]	5.5 ± 2.1	12.5 ± 4.2	19 ± 6.3
E(S _{max})	0.82 ± 0.19	0.78 ± 0.23	0.61 ± 0.17
S _{max} [MPa]	3.2 ± 0.66	3.7 ± 0.70	4.3 ± 0.75
Ψ [MPa]	0.71 ± 0.20	0.73 ± 0.23	0.77 ± 0.25

The general form of the rupture curves at different strain rates does not differ, however, the individual regions do. The following observations can be made in this respect:

- 1 the strain range of the zero region decreases with increased strain rate,
- 2 the strain range of the toe region increases with increased strain rate,
- 3 the maximum tangent modulus, ϵ , increases with increased strain rate,
- 4 the maximiser strain, E(S_{max}), decreases with increased strain rate,
- 5 the maximum stress, S_{max}, increases with strain rate.
- 6 the strain energy density, Ψ

These observations are similar to those reported in a study by Komatsu [Komatsu and Chiba 1993].

Figure 5.18 Rupture curve at different Strain Rates



5.7 Regional Effects on Mechanical Behaviour of PDL

Figures 5.21 - 5.20 give an extensive summary of specific properties of the PDL and how these properties vary with location and depth. For this study, two entire first molars from two animals are used. Each tooth is sectioned following the protocol for uniaxial specimens and tested sinusoidally and to rupture. A total of 43 samples are obtained; 27 from animal A, and 16 from animal B. For each uniaxial specimen, information as to its depth (following the notation as shown in 3.3), and location on the transverse section are noted. The parameters compared are:

- 1 from sinusoidal testing, the phaselag, δ , in compression and tension figure 5.19 & figure 5.20
- 2 maximum stress, S_{\max} , figure 5.21
- 3 maximiser strain, $E(S_{\max})$, figure 5.22
- 4 strain energy density, Ψ , figure 5.23
- 5 maximum tangent modulus, ϵ , figure 5.24

Regional Effects on Phaselag

The location of the specimen plays no significant role in the observed phaselag when the PDL uniaxial specimen is loaded sinusoidally. The general trend that $\delta_c > \delta_t$ is clearly demonstrated when figures 5.21 & 5.20 are compared.

Graphs (a) and (b) in figures 5.21 & 5.20 show no identifiable trend with respect to location of specimen on the transverse section. Moreover, graphs (c) and (d) shown no significant effect of depth on the results. In comparing the mesial and distal roots, as shown by graphs (e) and (f), no difference is observed.

Regional Effects on Maximum Stress

The location of the specimen plays no significant role in the observed maximum stress when the PDL specimen is loaded to rupture. A difference in maximum stress between animal A (3.1 ± 1.7 MPa) and animal B (1.5 ± 1.3 MPa) is observed, and indicates that large variations occur from animal to animal.

Graphs (a) and (b) in figure 5.21 show that for a given animal, the location of the specimen on the transverse section does play a role, however, this dependence is animal specific. In animal A, for example, the maximum stress is greater in the buccal regions, than what is observed in the proximal and lingual regions of the transverse section. For animal B, however, the opposite is observed. A similar observation can be made with regards to graphs (e) and (f).

From graphs (c) and (d), it is observed that the maximum stress is independent of depth of the periodontal uniaxial specimen.

Regional Effects on Maximiser Strain

The location of the specimen plays no significant role in the maximiser strain when the PDL specimen is loaded to rupture. A percent difference of 30% in maximiser strain between animal A ($E(S_{\max}) = 0.75 \pm 0.24$) and animal B ($E(S_{\max}) = 1.1 \pm 0.6$) does indicate that a large variation occur from animal to animal.

Graphs (a) and (b) in figure 5.22 show no identifiable trend with respect to the location of the specimen on the transverse section and maximiser strain. Furthermore, graphs (c) and (d) indicate that depth does not have any significant effect on the maximiser strain. Graphs (e) and (f) also show no significant difference between the distal and mesial roots.

Regional Effects on Strain Energy Density, Ψ

The location of the specimen plays no significant role in the strain energy density when the uniaxial PDL specimen is loaded to rupture. A percent difference of 51% in Ψ is observed between animal A ($\Psi_A = 0.760 \pm 0.40$ MPa) and animal B ($\Psi_B = 0.375 \pm 0.15$ MPa).

Graphs (a) and (b) in figure 5.23 show no identifiable trend with respect to the location of the specimen on the transverse section and the strain energy density. Furthermore, graphs (c) and (d) indicate that depth does not have any significant effect on Ψ . Graphs (e) and (f) also show no significant difference between the distal and mesial roots.

Regional Effects on Maximum Tangent Modulus, ϵ

The location of the specimen plays no significant role in the maximum tangent modulus when the uniaxial PDL specimen is loaded to rupture. A percent difference of 55% in ϵ is observed between animal A ($\epsilon_A = 11 \pm 7$ MPa) and animal B ($\epsilon_B = 5 \pm 4$ MPa).

Graphs (a) and (b) in figure 5.24 show that for a given animal, the location of the specimen on the transverse section does play a role on the maximum tangent modulus, however, this dependence is animal specific. . Furthermore, graphs (c) and (d) indicate that depth does not have any significant effect on ϵ . Graphs (e) and (f) also show that there is somewhat of a difference between ϵ in the distal and mesial roots.

Figure 5.19 Effect of location of specimen on compression phaselag

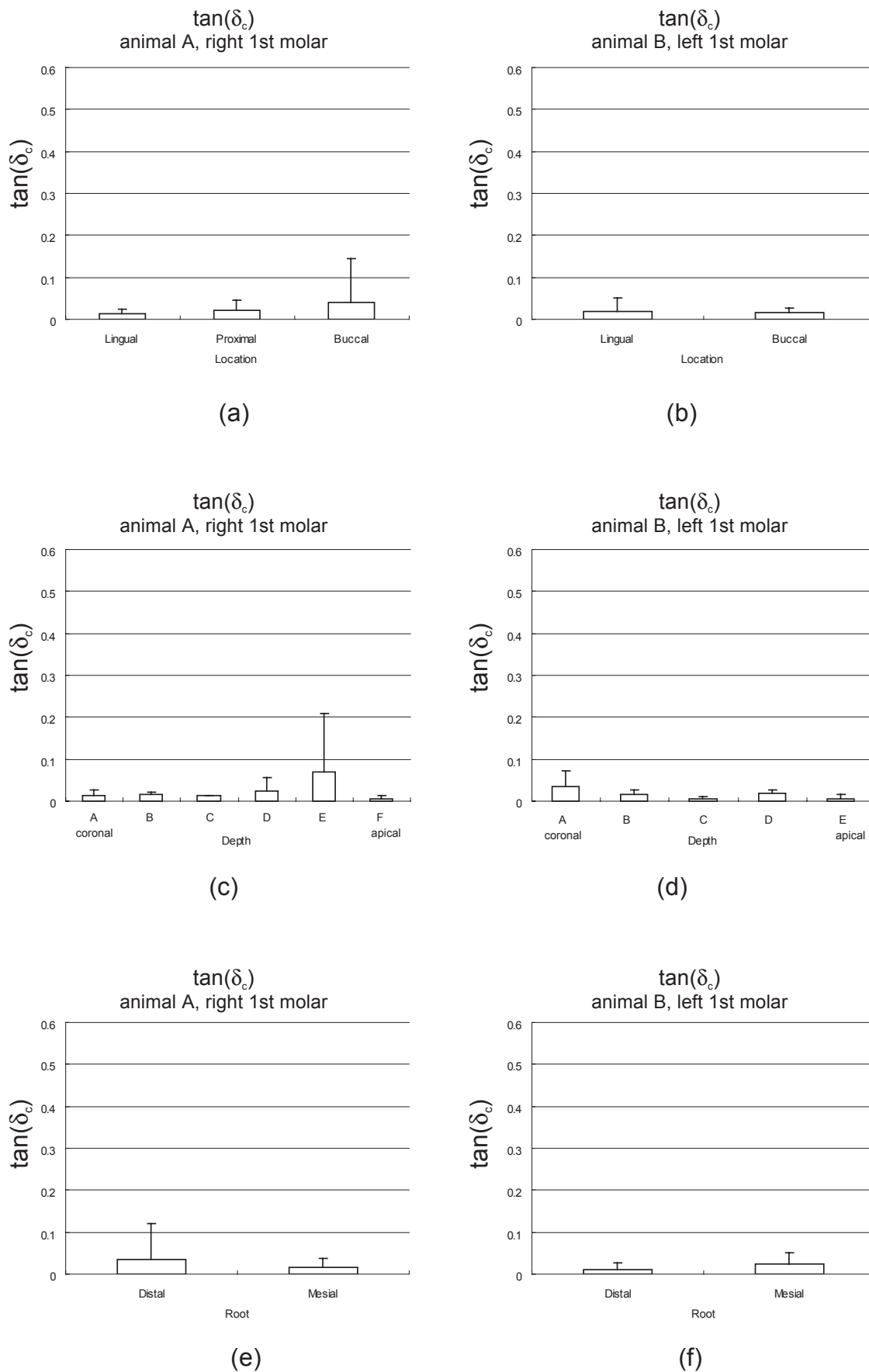
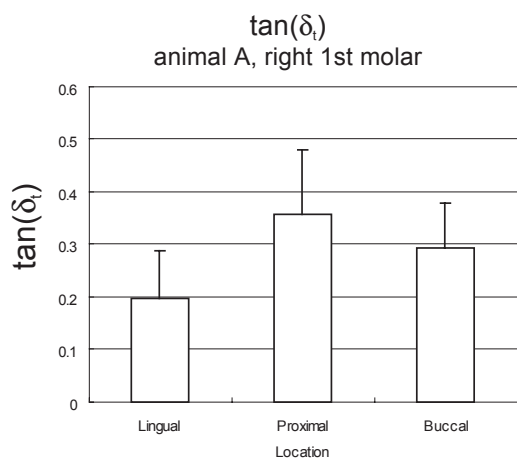
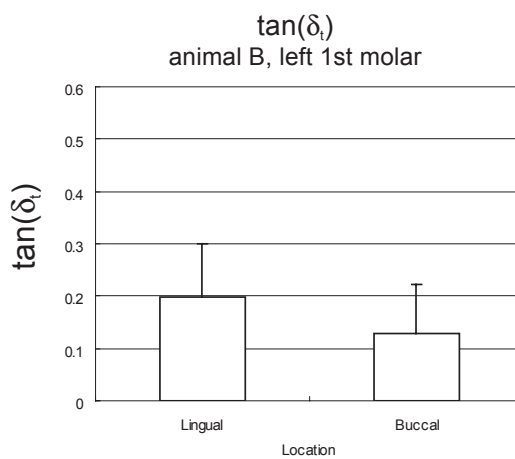


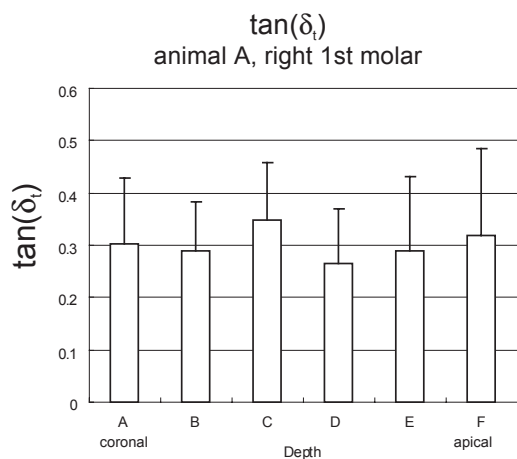
Figure 5.20 Effect of location of specimen on tension phaselag



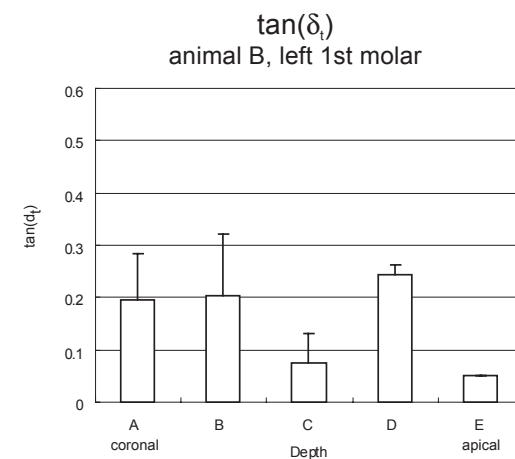
(a)



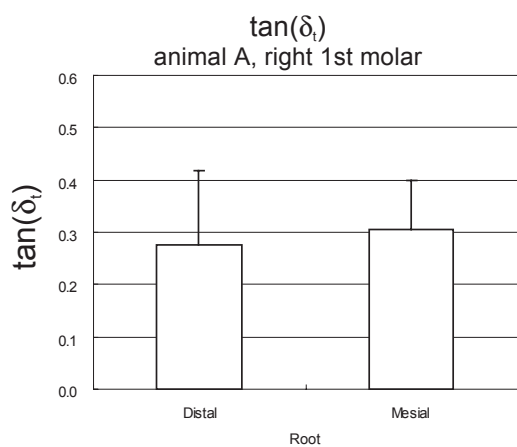
(b)



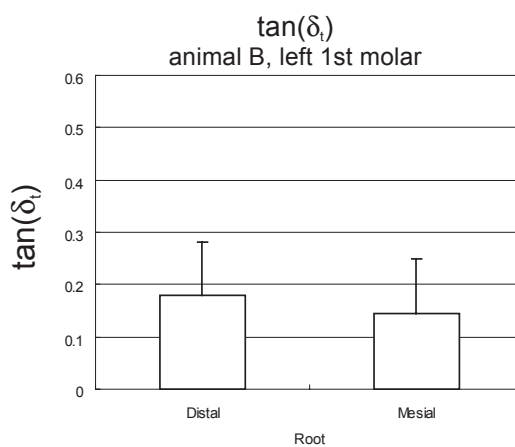
(c)



(d)

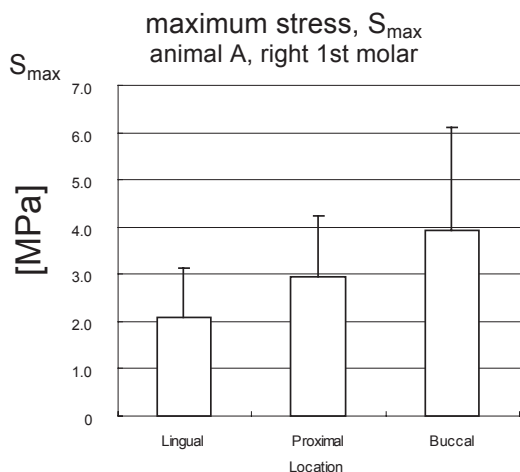


(e)

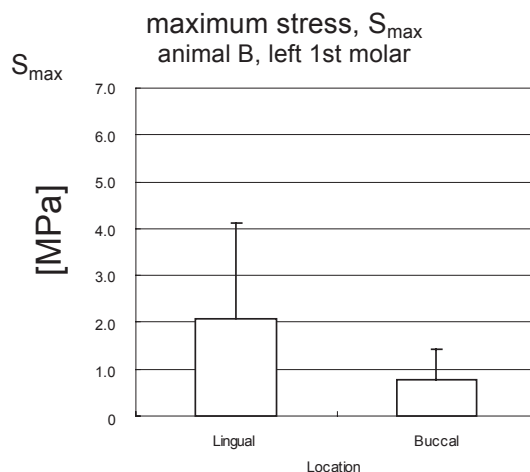


(f)

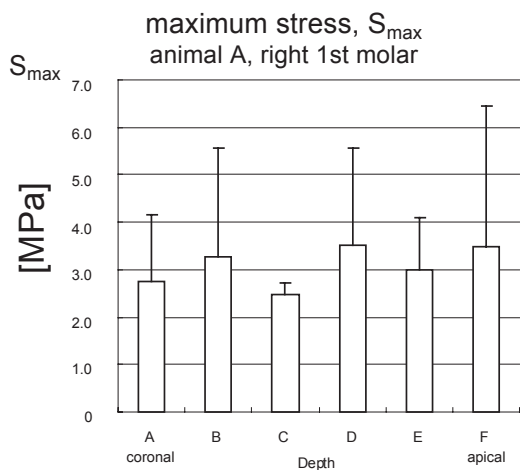
Figure 5.21 Regional Effects of PDL on Maximum Stress



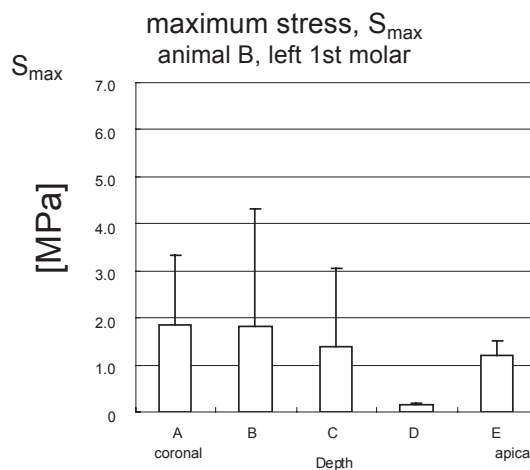
(a)



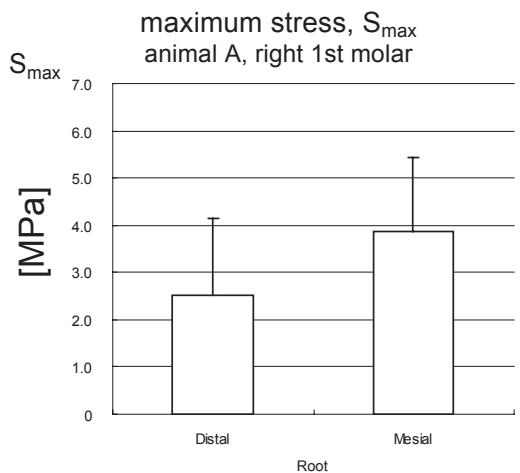
(b)



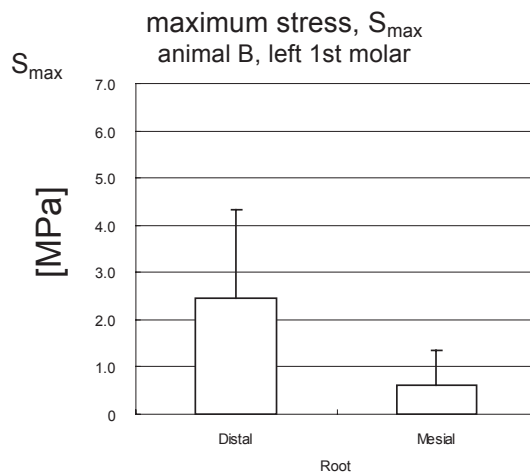
(c)



(d)



(e)



(f)

Figure 5.22 Effect of specimen location on Maximiser strain

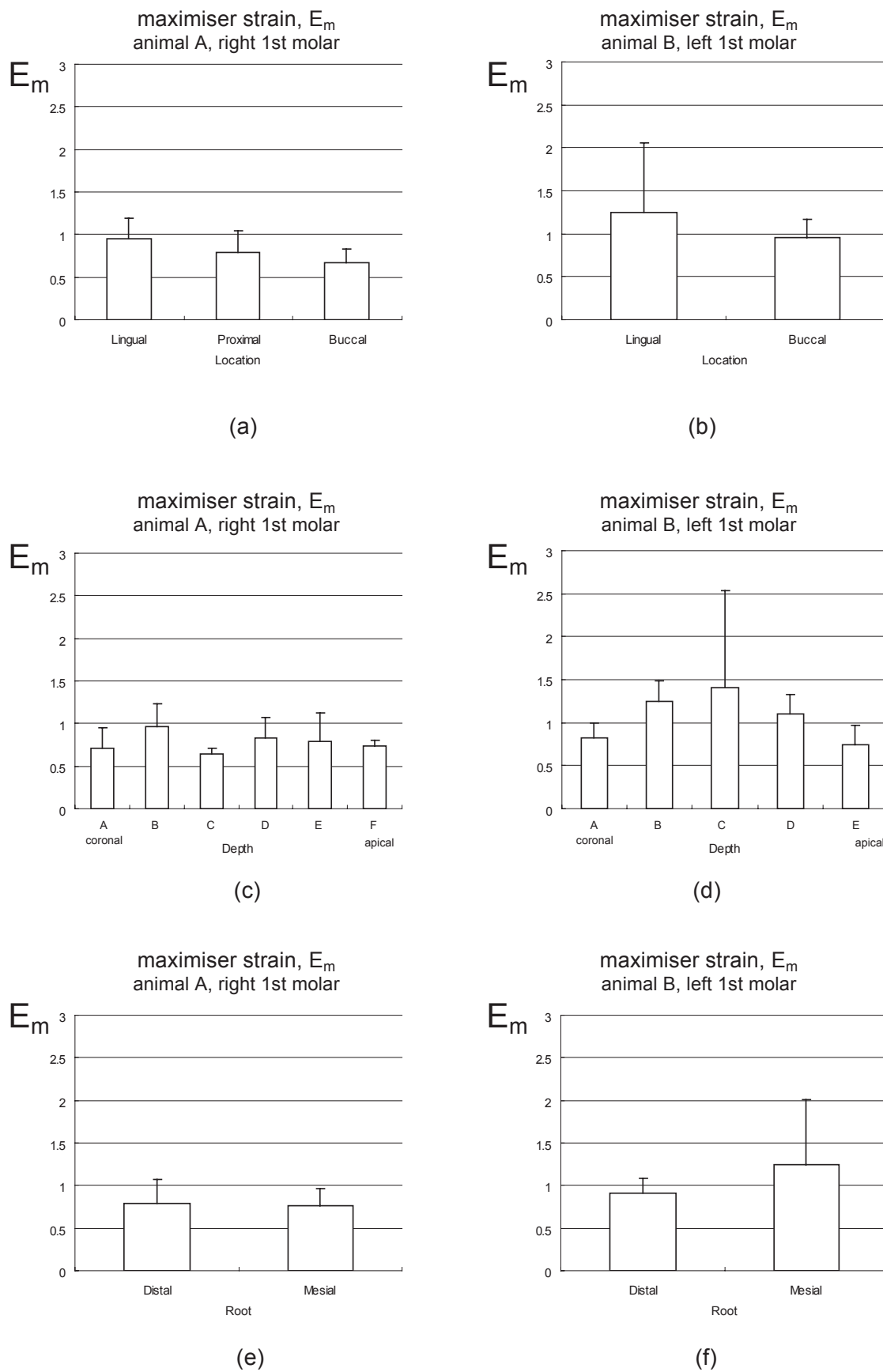


Figure 5.23 Effect of specimen location on strain energy density

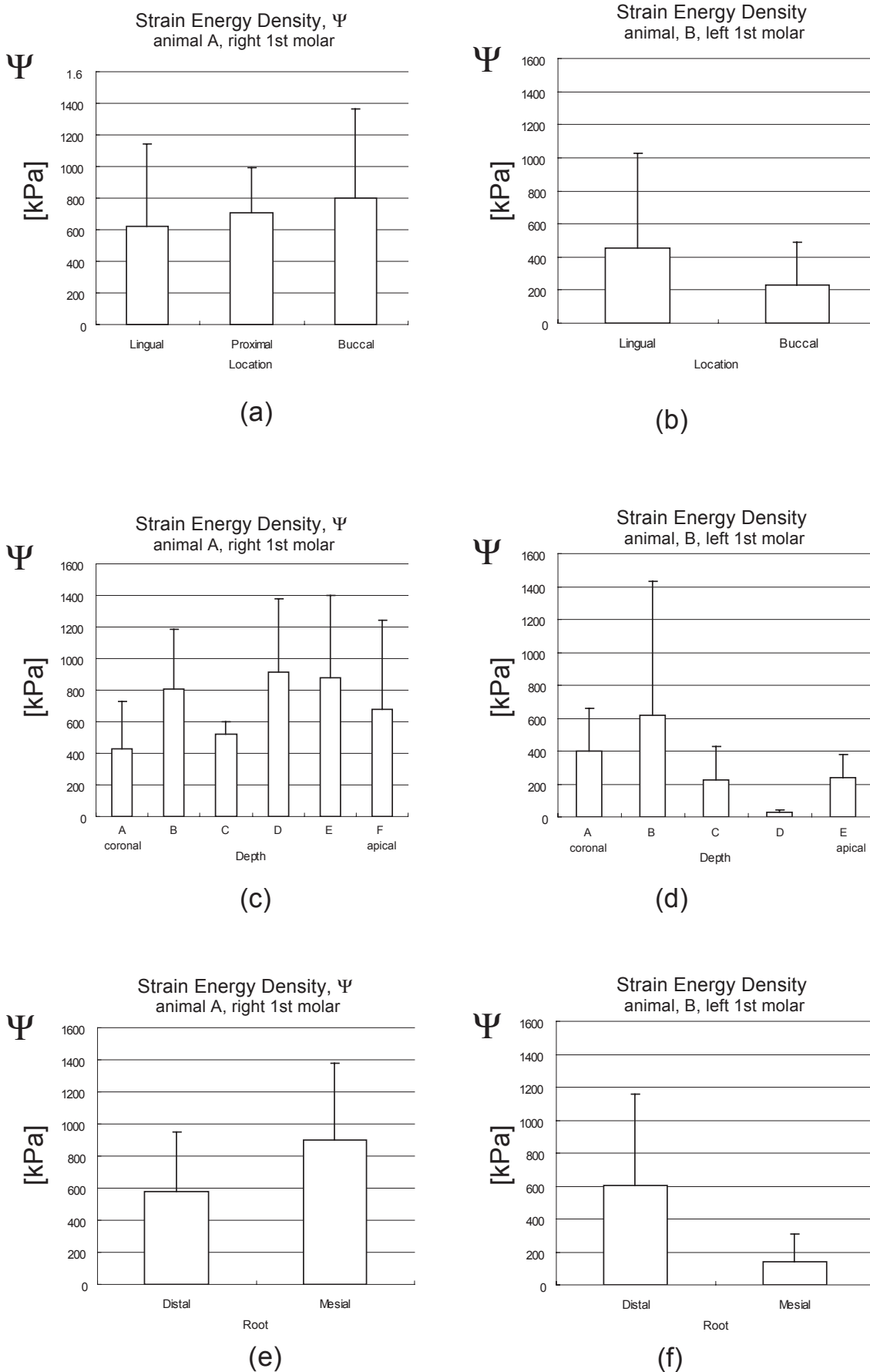


Figure 5.24 Effect of specimen location on maximum tangent modulus

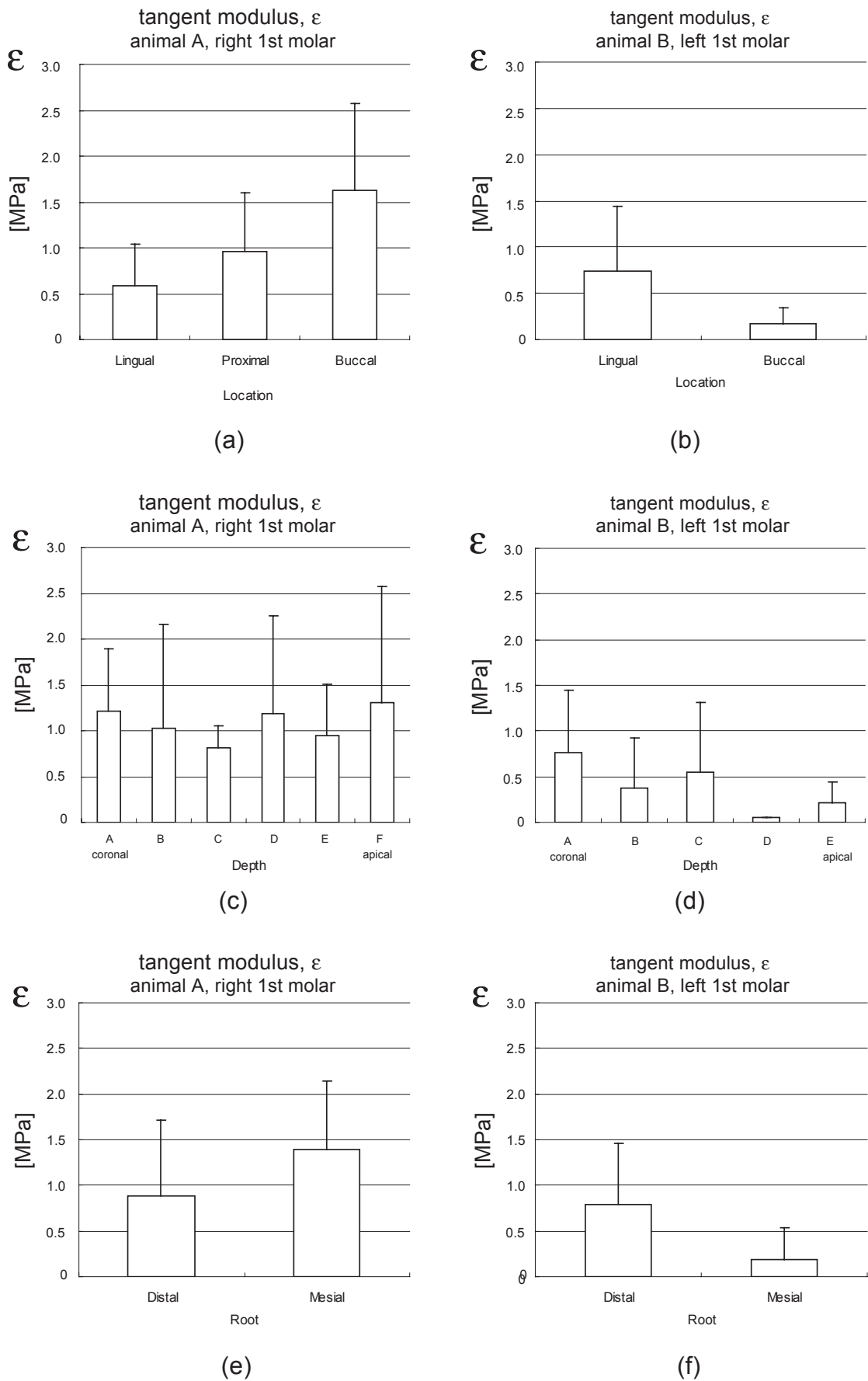
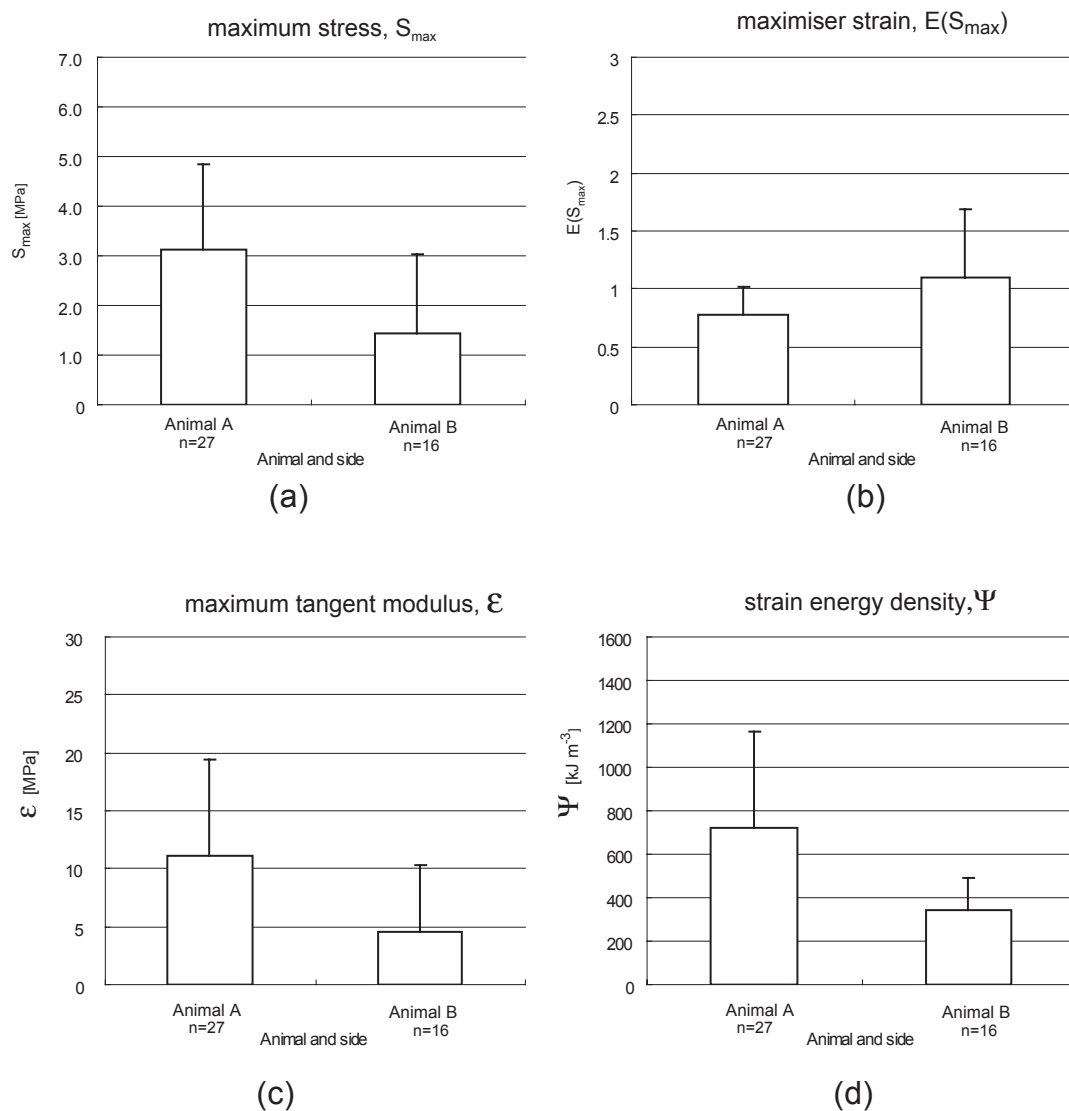


Figure 5.25 Summary of parameters obtained from rupture curves for animal A and animal B



5.8 Discussion of Uniaxial Results

Elasticity

The results presented in this chapter show the PDL to be nonlinear elastic. Past works related to the elastic nature of the PDL tissue are compared with the results presented throughout this chapter.

In past works, load-displacement curves of the PDL have shown a highly nonlinear behaviour. Tensile uniaxial (i.e. traction-elongation) tests on radial sections of animal or human tooth-ligament-bone systems [Daly et al. 1974; Atkinson and Ralph 1977; Ralph 1980; Durkee 1996; Pini 1999; Komatsu and Chiba 2001; Pini et al. 2002; Pini et al. in

press] have consistently shown a highly nonlinear stiffening pattern upto the damage threshold, or maximiser strain, of the specimens. The typical stress-strain curve demonstrating elastic stiffening takes the form of the cubic function $y=x^3$, whereas elastic softening takes the form of the cubic-root function $y=x^{1/3}$. Compressive uniaxial (i.e. traction-compression) tests yield a similar response, yet the stiffening is steeper ([Durkee 1996; Pini 1999; Pini et al. 2002; Pini et al. in press]. Note also that whole tooth studies [Parfitt 1960; Moxham and Berkovitz 1989; Picton 1990; Giargia and Lindhe 1997] have also shown this same stiffening phenomenon.

It was expected, and is the case, that this same stiffening behaviour observed in the literature be observed in results presented in this chapter. All S-E curves presented in this chapter consistently show this nonlinear elasticity. The next step, and overall objective of which this thesis work is part, is to model the PDL. As such, it is essential to quantify this stiffening behaviour from a nonlinear elastic perspective, in order to use these experimental data to, on one hand, develop a theoretical constitutive law for the PDL, and on the other hand, validate this law using these same data. The theoretical aspects are being addressed in the thesis by Justiz [Justiz 2004] which is being performed in parallel with the present work.

It has also been suggested that the elastic properties of the PDL vary with the depth along the root of each tooth [Pini 1999; Pini et al. 2002; Pini et al. in press], however, the data that took into account the regional differences of each specimen failed to lead to any conclusion of this type.

In sum, the experimental data presented in this chapter has lead to a first step in quantifying PDL elastic behaviour. More specifically, the data obtained from uniaxial tests show the PDL to follow a stiffening, nonlinear elastic law.

Viscosity

The many works found in literature that test the PDL under quasi-static conditions justify the hypothesis that the elasticity of the PDL is nonlinear stiffening. However, the few works that have tested the PDL cyclically and to observe its creep or stress relaxation give little insight into its viscoelastic behaviour.

A few works in the literature do demonstrate definite time dependent effects. Creep experiments on whole teeth, where tooth displacement increases with time under a constant load, has been observed, and upon unloading, the tooth slowly returns to its original rest position, rather than instantaneously [Brosh et al. 2002]. Furthermore, recent relaxation experiments on uniaxial specimens [Komatsu and Chiba 1993; Durkee 1996; Bourauel et al. 1999; van Driel et al. 2000; Toms et al. 2002; Toms et al. 2002] further confirm a viscoelastic response. An important hysteresis, greater in compression than in

tension for uniaxial specimens, is also observed [Pini 1999; Pini et al. 2002; Pini et al. in press]. Note, however, that in the few cases where time-dependent characteristics of the PDL have attempted to be modeled, the assumption that it is linear viscous is made. The results in this chapter support the hypothesis that the PDL is, in fact, nonlinear viscous.

With the linearity or non-linearity of viscosity unknown, a study was designed to determine whether the PDL displays a linear or non-linear viscous behaviour. The conditions for a material to be linear viscoelastic were tested; the first condition tested was linear scaling (see section 5.4.3), and the second tested was the superposition of separate responses (see section 5.4.5). Both conditions were not met, thus it was determined that the viscous behaviour of the PDL can be said to be nonlinear. It appears, from these data, that the nonlinear viscosity is pseudo-plastic or *thinning*. The typical stress-strain curve demonstrating viscous thinning would be of the form of the cubic-root function $y=x^{1/3}$, whereas viscous *thickening* would be of the form of the cubic function $y=x^3$. The viscous effects, therefore, show that the S- \dot{E} viscous curvature is opposite to the S-E elastic curvature. The mechanical results presented in section 5.5.2 show the viscous influence to be greater in compression than in tension. The viscous effect increases, i.e. hysteresis increases, increases with increased frequency, however, this is not the case in tension.

Relaxation tests performed at different ranges of strain (section 5.4.2) show that viscosity dominates and the PDL behaves as a fluid when tested in the zero region of the S-E curve, probably because the collagen fibres are still *crimped* (see Chapter 4). Testing in the linear portion of the S-E curve, where collagen fibres are *uncrimped*, show that the PDL behaves as a viscoelastic solid.

It should be noted that experimental values for maximum tangent moduli for the PDL in the literature span 2 orders of magnitude, and the elastic moduli used in numerical studies spans 4 orders of magnitude (see section 2.4.2). This huge variation in parameters can be attributed to the viscous behaviour of the ligament. Such a time-dependent behaviour implies a dependence of the S-E curve on the strain rate in quasi-static tests. This dependence was verified and observed in the results of this chapter (see section 5.2 & section 5.6). Examining the literature more closely yield an interesting observation: the maximum tangent moduli observed in literature span 2 orders of magnitude, yet the strain rates used in these same experiments span 4 orders of magnitude.

In sum, the experimental data obtained in this chapter have lead to a better understanding of the viscous nature of the PDL. More specifically, the data of obtained from uniaxial tests converge to show the PDL to follow a currently unknown thinning, nonlinear viscous law.

-
-
-

-
-
-

•

•

•

“The basis of optimism is sheer terror.”

Oscar Wilde

•

•

•

6

Results: Shear Behaviour

In this chapter, the results from testing the PDL in shear are presented. The results from initial pilot studies are presented. The experiments performed include subjecting the shear specimen to:

- 1 triangular loading profiles, see section 6.2.2,
- 2 shear stress-relaxation tests, see section 6.2.3,
- 3 sinusoidal loading profiles, see section 6.2.4, and
- 4 rupture tests, see section section 6.2.5. A discussion of shear results is presented in section 6.3.

6.1 Initial Studies

Many questions had to be asked in order to plan experiments. How does the ligament behave in coronal/apical shear? Does behaviour differ in the apical and coronal directions? At what load does the shear specimen rupture? What range of shear stress and shear strain should be chosen for future experiments?

6.1.1 Amplitude

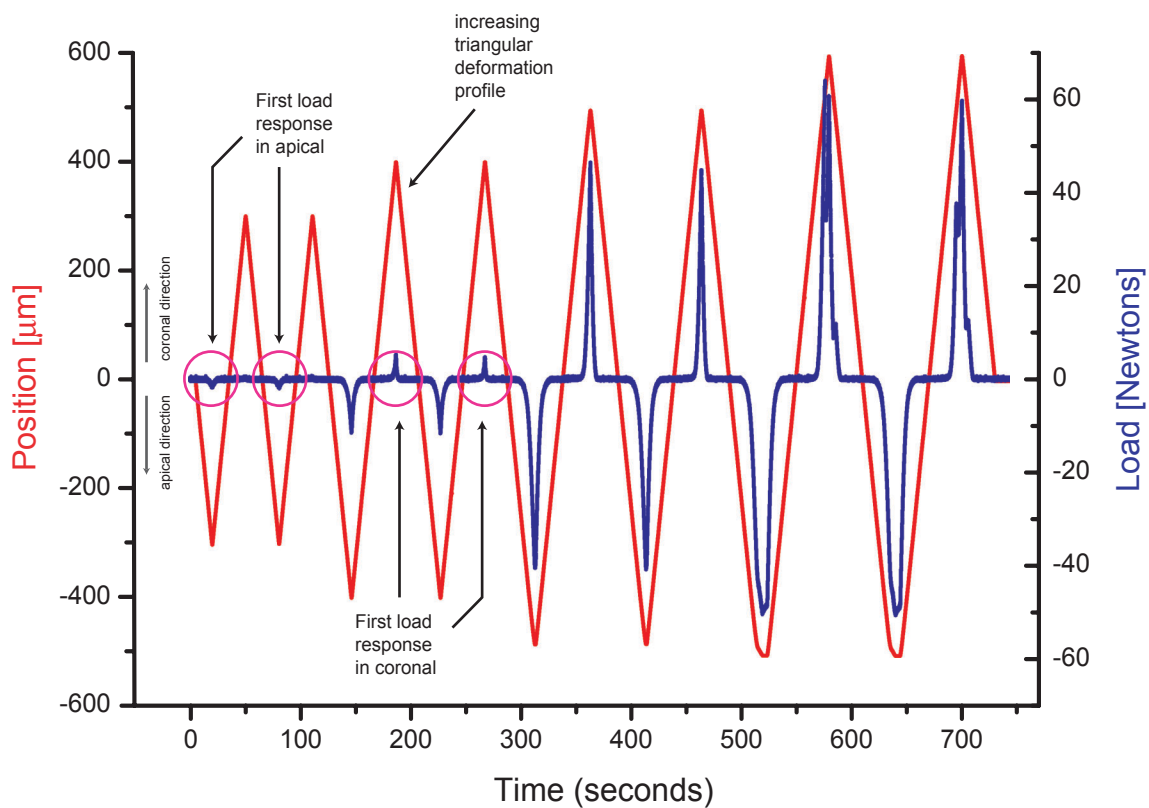
In order to determine an amplitude of loading, a pilot study is involved taking shear specimens, and subjecting them to cycles of an increasing triangular deformation function (see figure 6.1). An initial amplitude of 50 μm is chosen, and two cycles are performed at a rate of 20 $\mu\text{m s}^{-1}$. This profile is repeated after incrementing the amplitude by 50 μm . This is repeated automatically until a response is observed.

A first apical response is observed at an amplitude of 250 μm , corresponding to a load response of 2 N. The first coronal response is observed at an amplitude of 300 μm

corresponding to a load response of 5 N. Continuing to increase the deformation amplitude results in an increase in shear stress response amplitude.

These preliminary tests give rise to two important conclusions upon which experimental design parameters for the shear testing of transverse ligament samples are chosen. First, the amplitude is chosen to be greater than 250 μm to observe shear stress response. And second, a zero region observed over a range of almost 500 μm require that future specimens be zeroed prior to testing in order to ensure that testing begins at the midpoint of the zero region of the curve (see figure 3.6).

Figure 6.1 Preliminary increasing triangular profile



6.2 Mechanical Response of the Periodontal Ligament in Shear

A number of testing profiles are used to investigate the shear behaviour of the PDL. The bulk of shear specimens are subjected to 30 triangular cycles with an amplitude of 350 μm . Shear stress relaxation is determined both apically and coronally, and specimens are also subjected to sinusoidal oscillations. A number of specimens are also pulled to rupture. No shear specimens were preconditioned prior to testing.

6.2.1 Zeroing

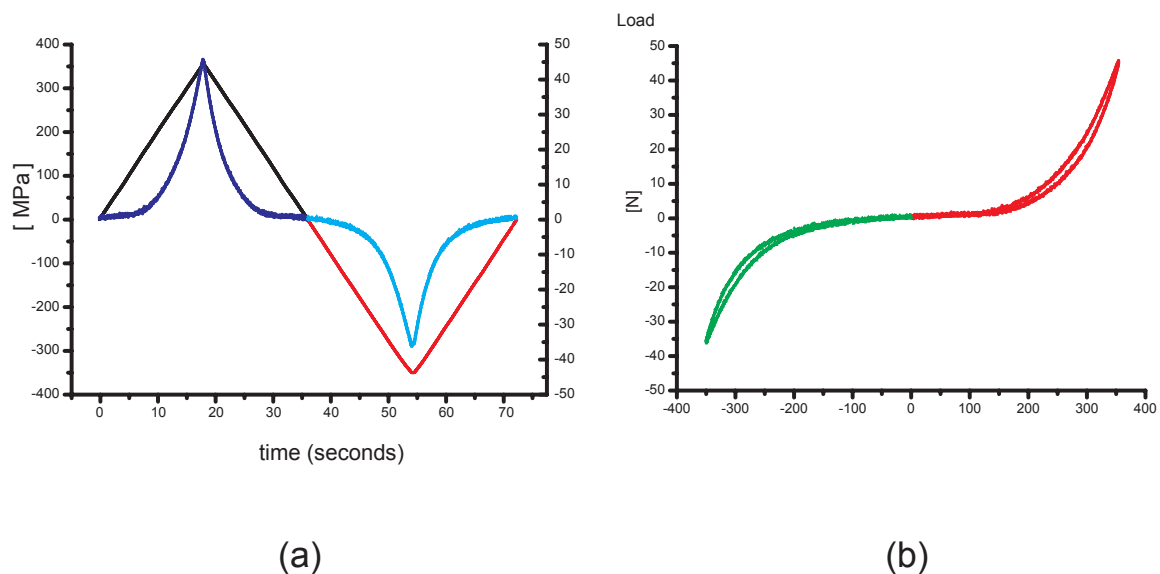
Based on the preliminary results, zeroing is performed before subjecting shear specimens to any motion profile as described in section 3.4.4.

6.2.2 Shear Response of PDL Subjected to Triangular Cycles

Subjecting 10 shear specimens to triangular cycles examine the ligament within a range of shear strain values so as to simulate the shear stress response of the ligament during mastication. After zeroing, the specimen is oscillated to amplitudes of $350\ \mu\text{m}$ at a rate of $20\ \mu\text{m}\ \text{s}^{-1}$. The resulting curve of a typical specimen is shown in figure 6.2a with its corresponding load deformation curve shown in figure 6.2b.

A number of remarks can be made regarding the resultant form of this curve. First, it shows that the PDL in shear displays typical soft tissue behaviour with the zero region, toe region and linear region clearly distinguishable. Second, the ligament shear behaviour in the apical direction is symmetrical to its behaviour in the coronal direction. And Third, the hysteresis observed in both the apical and coronal directions are minimal.

Figure 6.2 Results of a typical sample showing (a) the response of a shear specimen subjected to a triangular deformation profile with (b) load deformation curves.



6.2.3 Shear Stress Relaxation of Periodontal Ligament

Because the relaxation behaviour of the PDL is unknown, a third order exponential decay function expressed in equation 5.11 is used to fit the data obtained from shear stress relaxation experiments.

The shear stress relaxation is examined coronally and apically enabling an analysis of the shear behaviour in these directions. Modifying equation 5.11 for analysing shear stress relaxation can be expressed by

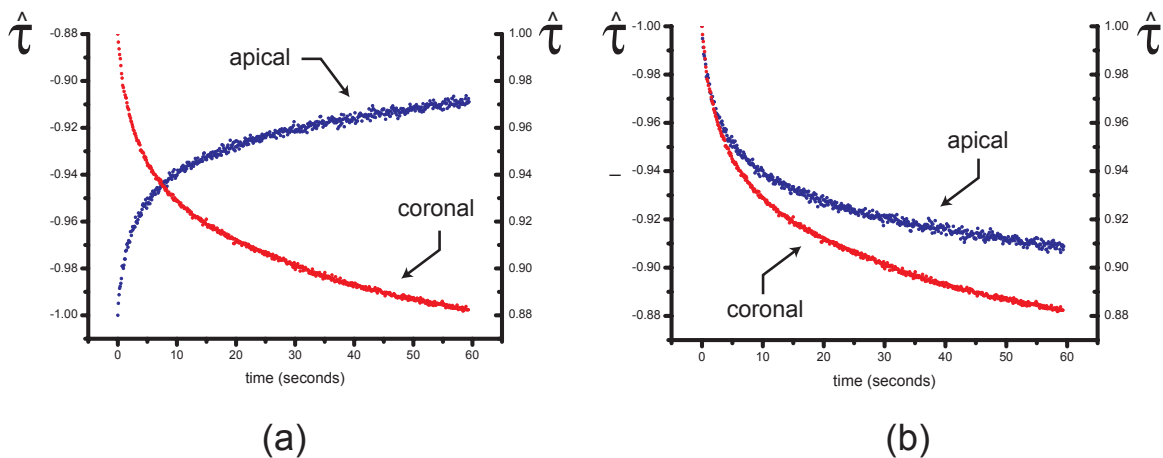
$$G_\gamma = G_0 + a_1 e^{(-t)/\tau_1} + a_2 e^{(-t)/\tau_2} + a_3 e^{(-t)/\tau_3} \quad (\text{EQ 6.1})$$

Data obtained from shear stress relaxation experiments were normalised by dividing all shear stress values by the shear stress at time $t = 0$. Doing this for both apical and coronal data is presented graphically in figure 6.3. Fitting the relaxation curves shown in figure 6.3 to equation 6.1 gives the parameters given in table 6.1.

Table 6.1 Parameters describing a normalised G_γ in figure 6.3 fit to a third order exponential function

parameter	$G_\gamma(\gamma, t) _{\text{apical}}$	$G_\gamma(\gamma, t) _{\text{coronal}}$
G_0	-0.89 ± 0.00	0.87 ± 0.00
t_1	0.92 ± 0.13	0.63 ± 0.07
t_2	4.87 ± 0.54	3.63 ± 0.12
t_3	40.23 ± 4.38	36.11 ± 0.71
a_1	-0.02 ± 0.00	0.01 ± 0.00
a_2	-0.03 ± 0.00	0.04 ± 0.00
a_3	-0.05 ± 0.00	0.08 ± 0.00
R^2	0.9951	0.999

Figure 6.3 Normalised relaxation curves in coronal and apical directions



6.2.4 Shear Behaviour of Periodontal Ligament subjected to Sinusoidal Oscillations

The shear properties of the PDL have been presented thus far as a relaxation modulus G_γ , which is a function of time. As with the uniaxial specimens, this relaxation is useful to describe, with limitations, the time dependent characteristics of the ligament in shear. Nevertheless, the shear specimens are subjected to sinusoidal shear strain histories in an attempt to give rise to other material response functions which could be related to G_γ , and ultimately to the behaviour of the PDL.

As with uniaxial specimens, the shear specimens display a transient shear stress response when oscillations commence, however, after approximately 10 cycles, a stable state is achieved (see section 5.5).

6.2.4.1 Effect of Frequency on the Sinusoidal Response of the PDL in Shear

The shear strain-controlled sinusoidal oscillation profile subjected to the ligament is

$$\gamma(t) = \gamma_0 \sin \omega t \quad (\text{EQ 6.2})$$

and gives rise to the corresponding shear stress response

$$\tau(t) = \gamma(\omega) \cdot \gamma_0 \sin(\omega t + \delta(\omega)) \quad (\text{EQ 6.3})$$

where γ is shear strain, ω is the angular velocity dependent on frequency, t is time, and δ is the phaselag between the shear strain control parameter and the shear stress response. Measuring the phaselag is done by plotting shear stress, τ , versus shear strain, γ , to give the plots as shown in figure 6.5, and measuring the phaselag as shown by figure 2.13.

It can be seen in figure 6.5 that the magnitude of the shear stress response amplitude in the coronal direction, i.e. the absolute value of the maximum shear stress value, does not vary significantly with increased frequency. Likewise, the magnitude of the shear stress response amplitude in the apical direction, i.e. the absolute value of the minimum shear stress value, increases somewhat with increased frequency.

As shown by figure 5.11, the phaselags between the shear strain and the shear stress are measured for each corresponding frequency. The phaselags are measured as a time, and converted to radians using the angular velocity imposed on the ligament using

$$\delta = \Delta t \cdot \omega \quad (\text{EQ 6.4})$$

where δ =phaselag in radians, Δt = phaselag measured as a time, and

$$\omega = 2\pi f \quad (\text{EQ 6.5})$$

where f = frequency.

With respect to the measured phaselags, two observations can be made. First, the phaselag in the apical direction, $\delta_{\gamma,a}$, does not vary with the phaselag in the coronal direction $\delta_{\gamma,c}$. And second, there is no significant effect of frequency on $\delta_{\gamma,a}$ nor on $\delta_{\gamma,c}$. A table of the results of phaselags and frequency is presented in table 6.2.

Shear Stress versus Shear Strain

It is clear from the phaselag results presented in this section that the PDL shear specimens have the same properties when sheared in the apical direction or the coronal direction. Moreover, the small variation in the stress-response amplitude with frequency is also observed. These observations are well exemplified in figure 6.6 which show several *shear stress* versus *shear strain* plots at different frequencies. These curves show how little the response of the ligament varies with the frequency at which the specimen is tested. The plots of figure 6.6a-e are superimposed upon one another on the same graph and are shown in figure 6.6f.

Figure 6.4 Phaselag with frequency

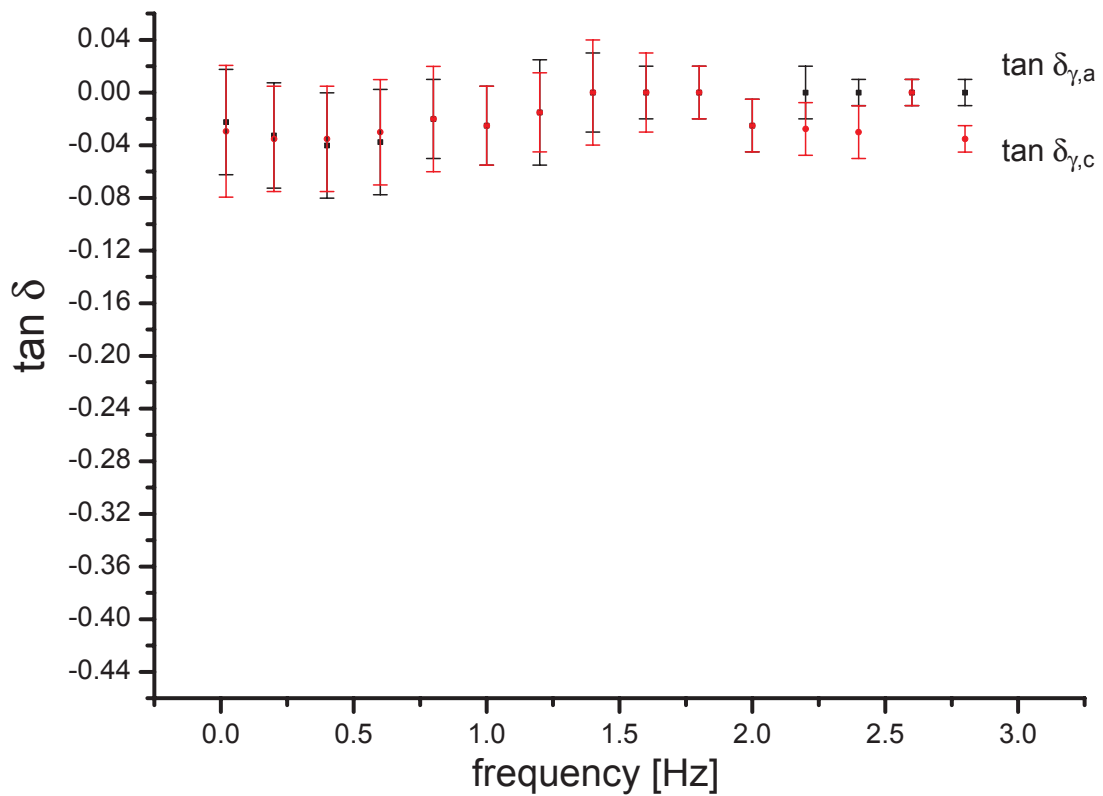


Table 6.2 Shear data of effect of frequency on phaselags in shear

f [Hz]	$\tan \delta_{\gamma,t}$	$\tan \delta_{\gamma,c}$
0.2	-0.022 ± 0.04	-0.029 ± 0.05
0.4	-0.032 ± 0.04	-0.035 ± 0.04
0.6	-0.040 ± 0.04	-0.035 ± 0.04
0.8	-0.038 ± 0.04	-0.030 ± 0.04
1.0	-0.020 ± 0.03	-0.020 ± 0.04
1.2	-0.025 ± 0.03	-0.025 ± 0.03
1.4	-0.015 ± 0.04	-0.015 ± 0.03
1.6	0 ± 0.03	0 ± 0.04
1.8	0 ± 0.02	0 ± 0.03
2.0	0 ± 0.02	0 ± 0.02
2.2	-0.025 ± 0.02	-0.025 ± 0.02
2.4	0 ± 0.01	-0.028 ± 0.02
2.6	0 ± 0.01	-0.030 ± 0.01
2.8	0 ± 0.01	-0.035 ± 0.01
3.0	0 ± 0.01	0 ± 0.01

Figure 6.5 Sinusoidal curves of shear specimen

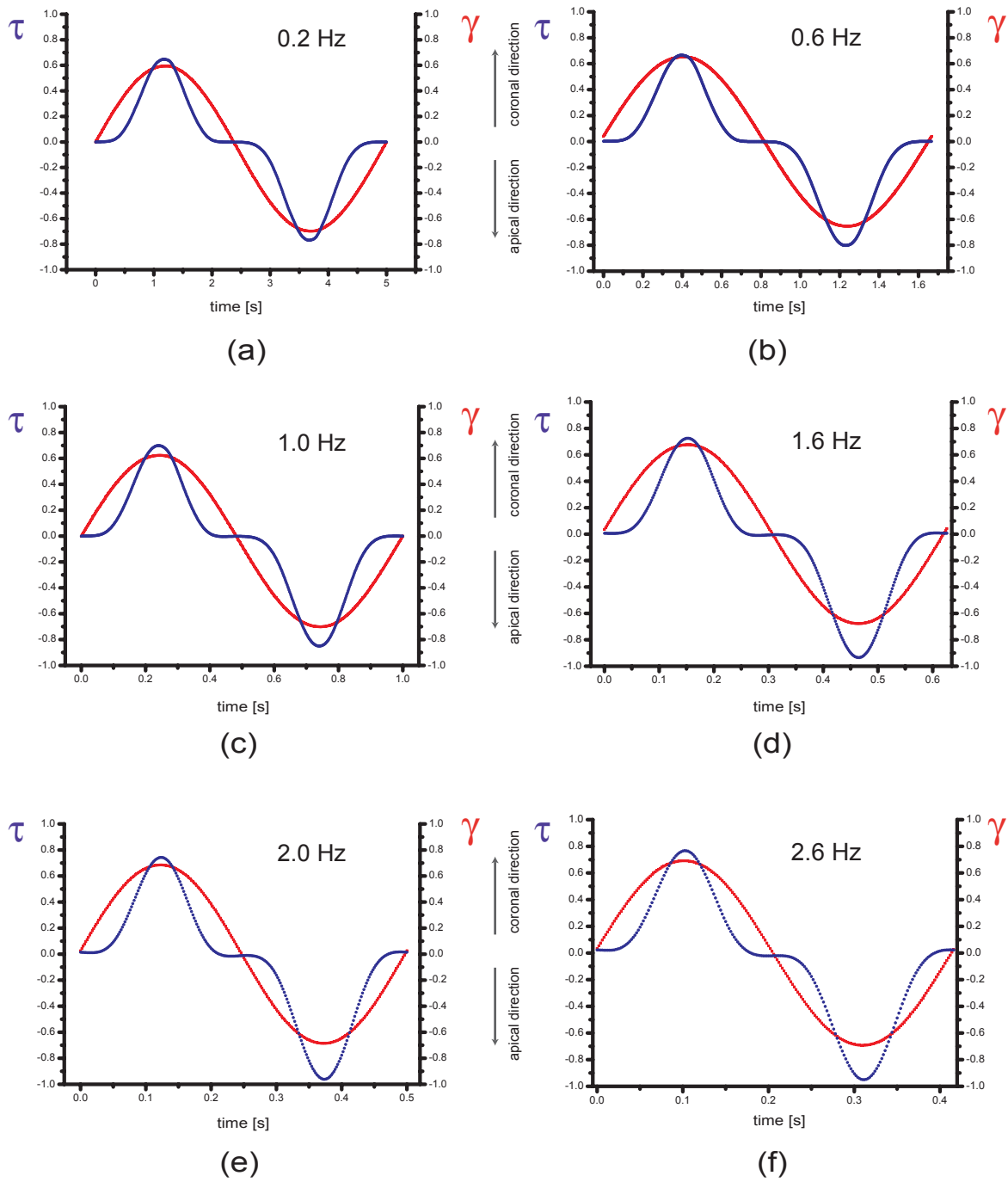
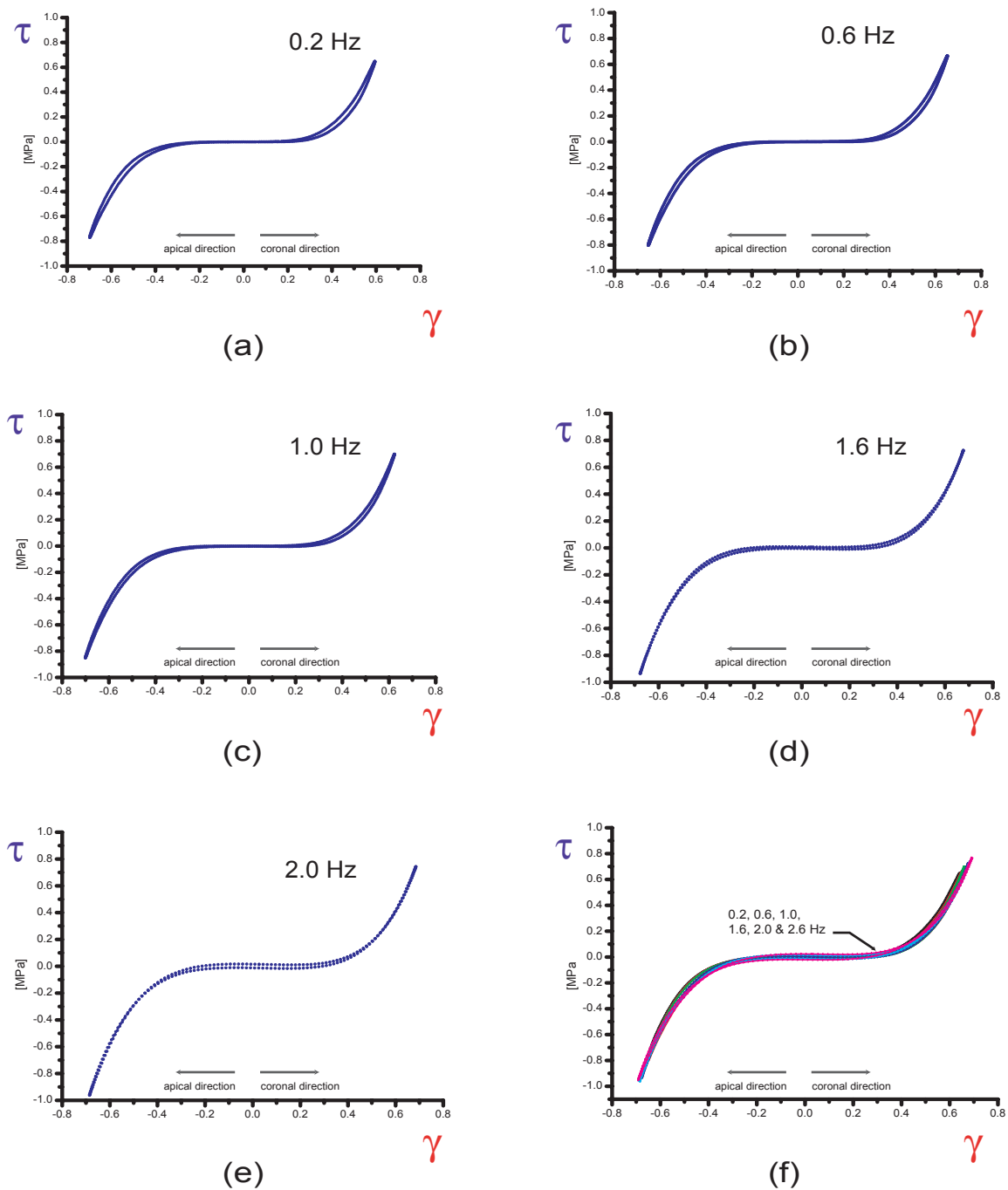


Figure 6.6 Shear Strain versus Shear Stress curves obtained from harmonic oscillations of PDL



6.2.5 Shear Rupture of Periodontal Ligament

The rupture data are non-conclusive. A total of 15 specimens are prepared and only 4 are ruptured successfully due to technical difficulties. Because of this small sample size, it is difficult to draw any definite conclusions regarding the rupture behaviour of the ligament in shear. From a qualitative perspective, however, it is clear that the ligament that ruptures in shear displays the typical behaviour as observed in any soft tissue with the

zero region, toe region, linear region and rupture region clearly identifiable (see the curves in figure 6.7).

The following parameters are measured following the method shown in Figure 3.13.

The maximum shear stress, $\tau_{c,max}$, in the direction of rupture is found to be:

$$\tau_{c,max} = 1.60 \pm 0.36 \text{ MPa}$$

The maximum shear strain energy density in the coronal direction, $\Psi_{\gamma,c}$, is measured to be:

$$\Psi_{\gamma} = 1,40 \pm 0.26 \text{ MPa}$$

The maximum shear tangent modulus, ζ_c , in the coronal direction is measured to be:

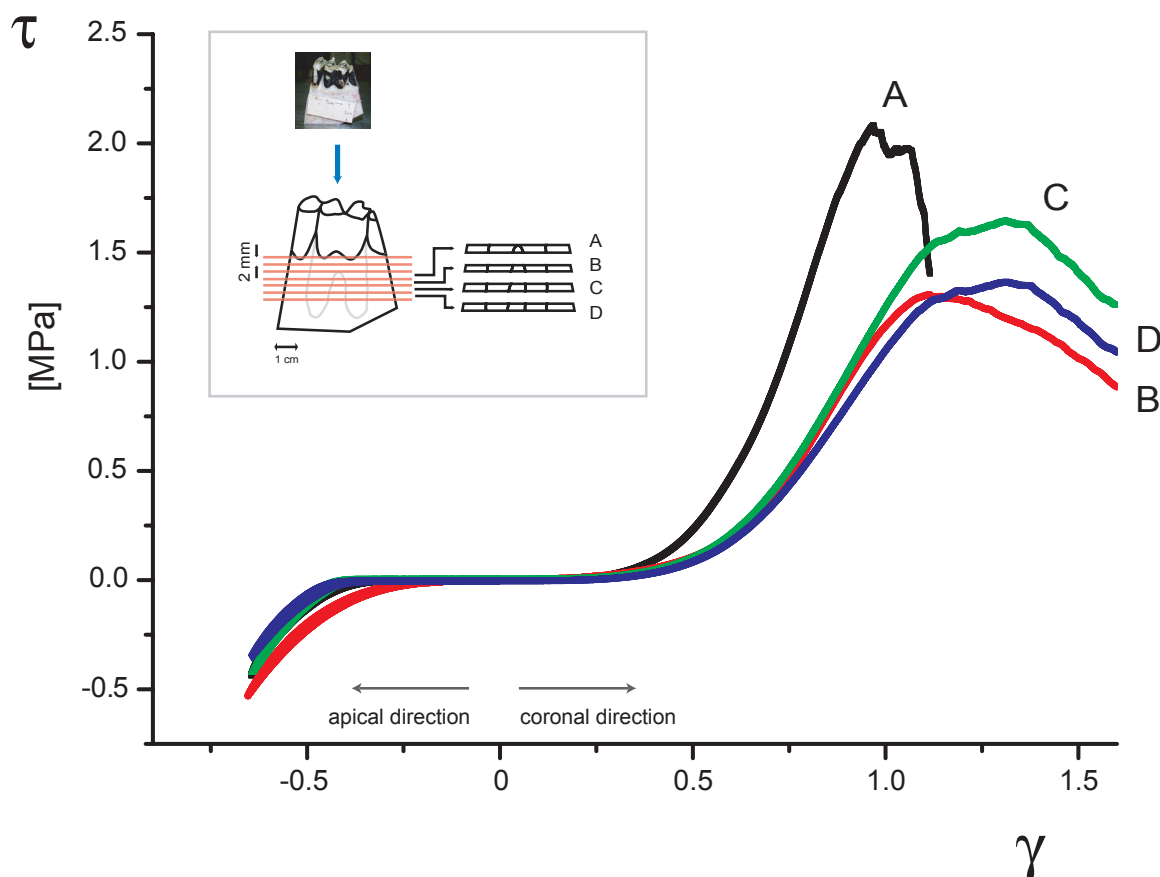
$$\zeta_c = 1.89 \pm 0.24 \text{ MPa}$$

and in the apical direction

$$\zeta_c = 1.54 \pm 0.17 \text{ MPa.}$$

Note that these parameters describe the curves obtained from the shear test experiments, however, due to the insufficient number of samples these results are inconclusive and can only be used to describe the PDL behaviour in shear from a phenomenological point of view.

Figure 6.7 Rupture curves



6.3 Discussion of Shear Results

Elasticity

The results presented in this chapter further show the PDL to be nonlinear elastic. Past works related to the elastic nature of the PDL tissue in shear are compared with the results presented throughout this chapter.

Shear tests, of the type presented in this thesis, in the literature are few [Ralph 1982; Mandel et al. 1986; Chiba et al. 1990; Komatsu and Chiba 1993]. These published works give shear information only in the extrusive (apical-coronal) direction. These data show, however, that in terms of elasticity the same nonlinear stiffening elastic response is to be expected (see section 5.8). All S-E curves presented in this chapter consistently show nonlinear elastic stiffening behaviour in the extrusive and intrusive directions.

The behaviour in extrusion was similar to in intrusion, which implies a isotropy along the apical-coronal axis, or vertical isotropy. No significant variation was found at different depths of the tooth root.

Most importantly, shear tests were performed in order to obtain the Poisson's ratio of the ligament. Section 7.2.1 shows how the Poisson's ratio can be determined, based on the Power Law.

In sum, the experimental data presented in this chapter has lead to a first step in quantifying PDL elastic behaviour in shear. More specifically, the data obtained from shear tests show the PDL to follow a stiffening, nonlinear elastic law. This behaviour was found to be symmetrical in the extrusive and intrusive directions implying a certain vertical isotropy.

Viscosity

One recent article [Toms et al. 2002] has tested shear specimens of PDL to determine its viscosity in shear. To our knowledge, no dynamic tests have been performed on the PDL to investigate its viscoelastic behaviour.

Examining the τ - γ curves it is evident that the PDL demonstrates time dependent effects. Extrusive and intrusive shear stress-relaxation experiments further confirms a viscoelastic response. A hysteresis, though minimal, is also observed, yet note that this hysteresis is similar in extrusion and in intrusion. Sinusoidal tests and the presence of a phaselag, though small, shows the ligament to be viscoelastic. The phaselag is the same in intrusion as in extrusion further justifies the notion of vertical isotropy. Moreover phaselags observed in shear are similar to phaselags observed in uniaxial tests *in tension* implying that viscosity mechanisms in shear are similar to those in uniaxial test tension.

With regards to linearity, these results are inconclusive. No relaxation experiments at different shear strain levels were performed, therefore linear scaling (hypothesis of variables separation) and the superposition of response properties (see section 2.7.5) could not be verified. It is expected, however, that such a study would show the PDL to be viscously nonlinear.

In sum, the experimental data obtained in this chapter have lead to a better understanding of the viscous nature of the PDL. More specifically, the data of obtained from shear tests implies that the PDL in shear follows a currently unknown thinning, nonlinear viscous law. However in view that the viscous effects observed are minimal, the PDL behaviour in shear could be approximated by a nonlinear elastic law.

Vertical Isotropy

Caution must be heeded in interpreting the observed vertical isotropy from shear results in this chapter. The chosen zero definition (see section 3.4.4) may have induced this observed isotropy. It is unlikely that this symmetry represents the actual behaviour of the ligament in shear because it is commonly reported that a fibre direction with respect to the vertical axis of the tooth exists [Young and Heath 2002], i.e. the Sharpey's fibres run

obliquely downwards from their attachment in the alveolar bone to their anchorage in the cementum at a more apical position on the root surface. If such a fibre direction exists, and is determined, the shear strain data can be shifted correspondingly. Defining the zero was therefore a necessary step to establish a known and reproducible reference point for interpretation of these results once more information with regards to the fibre structure becomes known.

-
-
-

-
-
-



“A pessimist sees the difficulty in every opportunity;
an optimist sees the opportunity in every difficulty.”

Sir Winston Churchill



7

Application to Numerical Models

In this chapter the reconstructed molar described in section 4.2 is used in a preliminary study that attempts to predict tooth mobility under simple loading conditions (see section 7.1).

7.1 Stress Analysis Applied to Reconstructed 3D Bovine Molar

A bovine tooth is reconstructed to study the dimensions of the tooth-PDL-bone system. Preparing this 3D tooth for finite-element studies, this system is used further as means to perform a preliminary stress analysis.

7.1.1 Problem Definition

All static problems in solid mechanics can be defined by the addressing three general points:

- 1 the geometry of the components,
- 2 the mechanical behaviour of these components, and
- 3 the boundary conditions.

7.1.1.1 Geometry

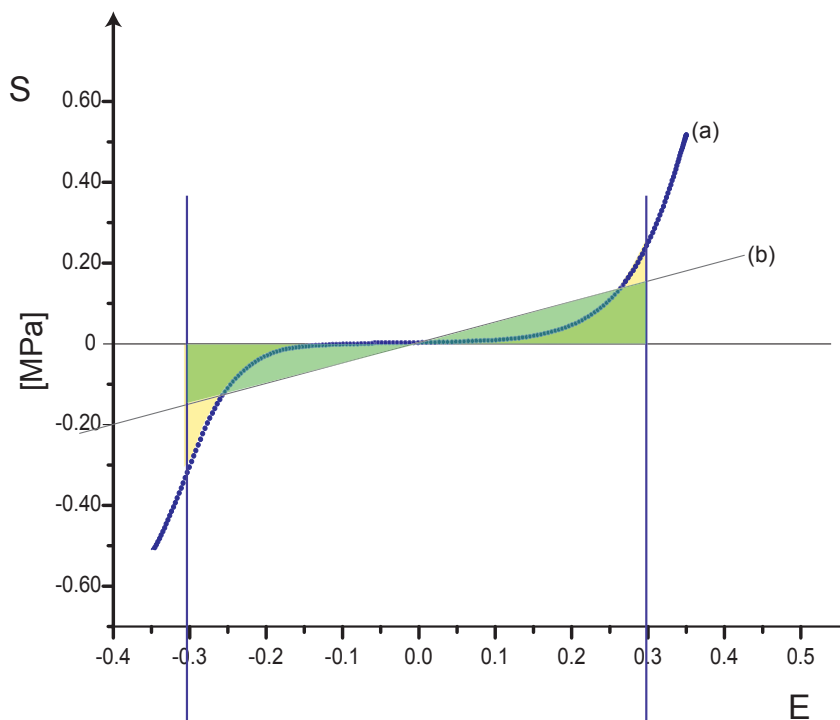
The geometry of the periodontium is broken into three components: the tooth, the ligament and the alveolar bone. Refer to section 4.2 for details on how these components are constructed.

7.1.1.2 Selection of Constitutive Equations

The tooth: the tooth is composed primarily of 3 materials: the dentin, the enamel, the cementum. These materials are intrinsically anisotropic, non-linear elastic. Nevertheless, within the scope of this study, they are considered to be isotropic, linear elastic. The cementum represents a considerably small volume of the tooth and is assimilated into the volume of the dentin. The PDL being a highly soft material, the hard dentin and the hard enamel deform little with respect to the PDL when the periodontium is loaded. Despite their anisotropic structure on the microscopic scale, the dentin and enamel are considered to be isotropic, as it is the macroscopic scale that this analysis is considering.

The ligament: the behaviour of the PDL is non-linear viscoelastic. As a preliminary study, a linear elastic law and a non-linear time-independent elastic law are chosen to represent its behaviour. These laws are based on experimental results, and a strain range is set as $-0.3 < E < 0.3$ to simulate the physiological conditions of mastication.

Figure 7.1 Actual experimental results shown by (a) used to define the non-linear elastic law, and (b) the linear law estimated based on curve (a).



The non-linear elastic law is defined based on experimental results as defined by figure 7.1a. Subjecting a uniaxial specimen to sinusoidal oscillations at a frequency of 1 Hz yields this stress-strain data that can describe its behaviour (see section 5.5). The linear elastic law is obtained by drawing a straight line such that the strain energy below curve

(a) is the same as the strain energy below the strain line (b). Doing so results in a Young's modulus of 0.625 MPa.

The alveolar bone: the bone is composed of cortical bone with a Young's modulus of around 20 GPa, and trabecular bone with a Young's modulus of around 2 GPa. The properties of cortical bone is chosen for analysis of the stress in the PDL under load.

Table 7.1 Summary of components and their mechanical behaviour parameters

	Constitutive Equation	Elastic Modulus (MPa)	Poisson ratio
Tooth	isotropic linear elastic	20000	0.3
PDL	isotropic non linear elastic	0.625 defined by experimental results	0.49 defined by experimental results
Alveolar bone	isotropic linear elastic	15000	0.3

7.1.1.3 The Boundary Conditions

In order to define the boundary conditions, a 3D coordinate system is defined by three forces in the coronal-apical direction, lingual-buccal direction and mesial-distal direction.

For the boundary conditions, 3 zones are presented:

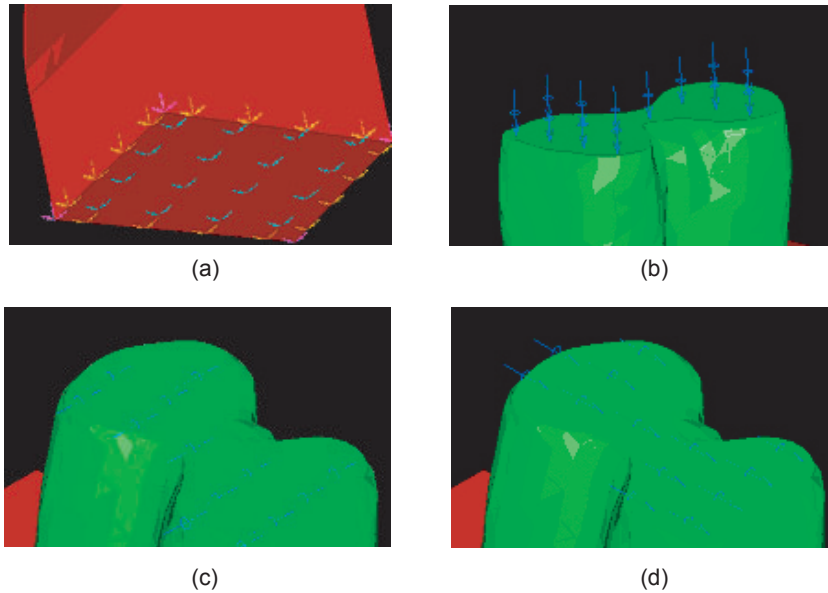
- 1 The inferior plane of the bone is defined as having zero displacement.
- 2 The most coronal plane of the tooth is subjected to a load of 10 N in either the coronal-apical, lingual-buccal or mesial-distal directions.
- 3 The other surfaces are treated as free surfaces, i.e. zero load.

7.1.2 Mesh

The mesh of the components is simplistic and consists of linear tetrahedron elements with 4 nodes. This method is chosen because the software package, IDEAS, does not allow the automatic meshing of complex geometries with elements other than the linear tetrahedron element. The elements chosen have the disadvantage of having a poor rate of convergence and therefore are more sensitive to produced non-representative results. A hexahedron element offers more precise results, however, for a preliminary investigation of the tooth-

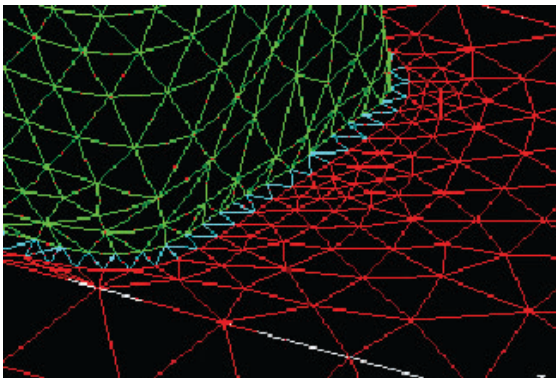
ligament-bone system, it is sufficient to use the tetrahedron elements. Moreover, the elements chosen resulted in a reduced number of nodes, and hence the calculation time for each analysis. The mesh is performed individually for each component of the system..

Figure 7.2 Boundary conditions (a) zero displacement, (b) coronal-apical load, (c) lingual-buccal load, and (d) mesial-distal load.



Since the ligament experiences the largest deformations under load, it is necessary to mesh this volume into small elements. This is done using the built-in algorithm *TriQuaMesh*. This algorithm initially discretizes the surfaces of the ligament and utilises an iterative subdivision routine to generate the interior mesh between the external surfaces. The tooth and the bone are meshed with increasingly larger elements as the distance from the ligament increases, with the size of elements in contact with the ligament being defined by the elements of the ligament mesh. The mesh of the components is verified for use in a finite element stress analysis.

Figure 7.3 Meshing of the tooth, ligament and bone showing how the elements in the bone increase in size as the distance increases from the ligament.

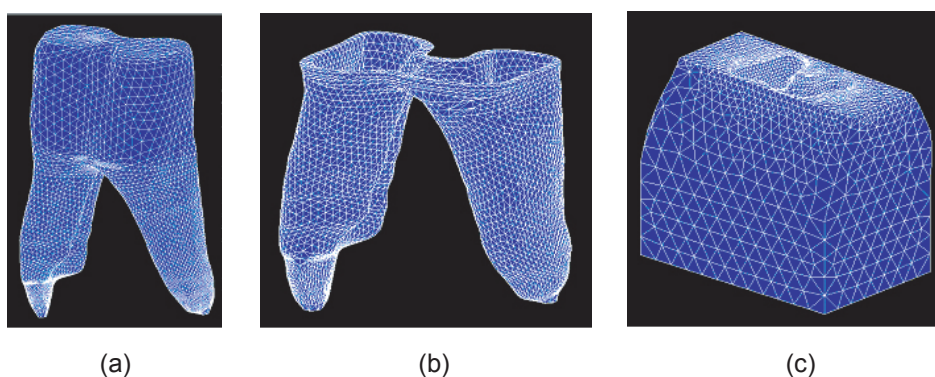


The characteristics for the meshes of each component are presented in table 7.2.

Table 7.2 Mesh characteristics for each component

Component	size of element (mm)	no. of elements	no. of nodes
Ligament	0.8	28,937	9,502
Tooth	2.0	85,270	17,283
Bone	4.0	178,193	33,320

Figure 7.4 Mesh using linear tetrahedron elements of (a) the tooth, (b) the ligament and (c) the alveolar bone



7.1.3 Analysis of Stress Distributions: Linear Elastic PDL

In this section a number of cases are examined to determine on a phenomenological level what occurs when the tooth system is subjected to specific loads. For the linear mesh described in the previous section, a number of loading conditions are imposed on the tooth-ligament-bone system and the corresponding stress distributions are calculated. The cases studied are outlined in table 7.3.

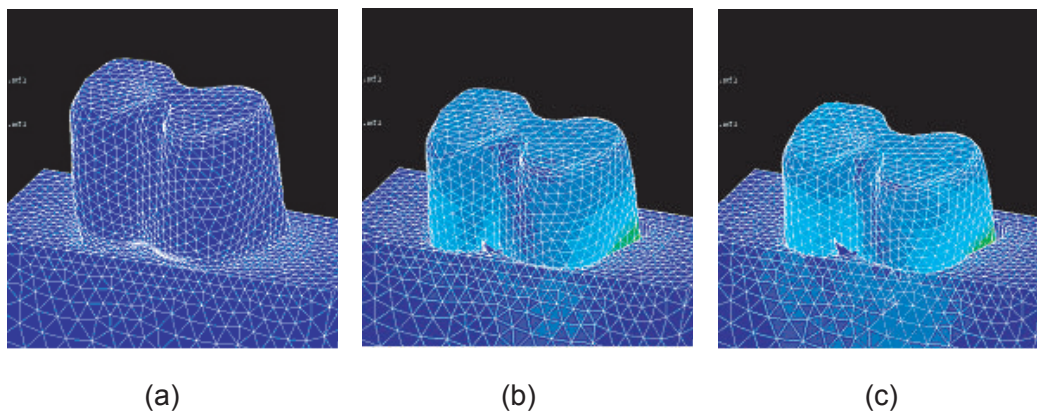
Table 7.3 Force application cases studied

	coronal-apical force	lingual-buccal force	mesial-distal force
isotropic, linear elastic ligament	✓	✓	✓
isotropic, non-linear elastic ligament	✓	✓	✓

7.1.3.1 Application of a Coronal-Apical Load

When a force of 10 N is applied in the coronal-apical direction to the crown of the tooth, a deformation response is observed as described by figure 7.5a-c. With regards to deformation, it is observed that the tooth experiences not only a deformation in the coronal-apical direction, but also in the lingual direction. This movement in the lingual direction, although small compared to the degree of deformation in the intrusive direction, indicates that the asymmetrical geometry of the tooth gives rise to an asymmetrical response to load.

Figure 7.5 Amplified movements of the tooth when subjected to an coronal-apical load of 10 N showing tooth (a) before loading, (b) during partial loading, and (c) fully loaded.



The colours represent the range of Von Mises stress experienced by the tooth as seen from the buccal side, with blue being the colour representing zero stress, and red representing maximum stress. Figure 7.6 shows the role the ligament plays in absorbing the stress. The stress distribution in the tooth is shown to be concentrated in the mesial and distal roots and at the surface of the tooth in contact with the ligament. The ligament deforms to a large extent and absorbs the load. This is demonstrated by the small magnitude of stresses observed in the bone.

Figure 7.6 Sagittal section of the discretized first molar subjected to a coronal-apical load of 10 N showing the Von Mises stress distribution. Maximum value, in red, 0.43 MPa)

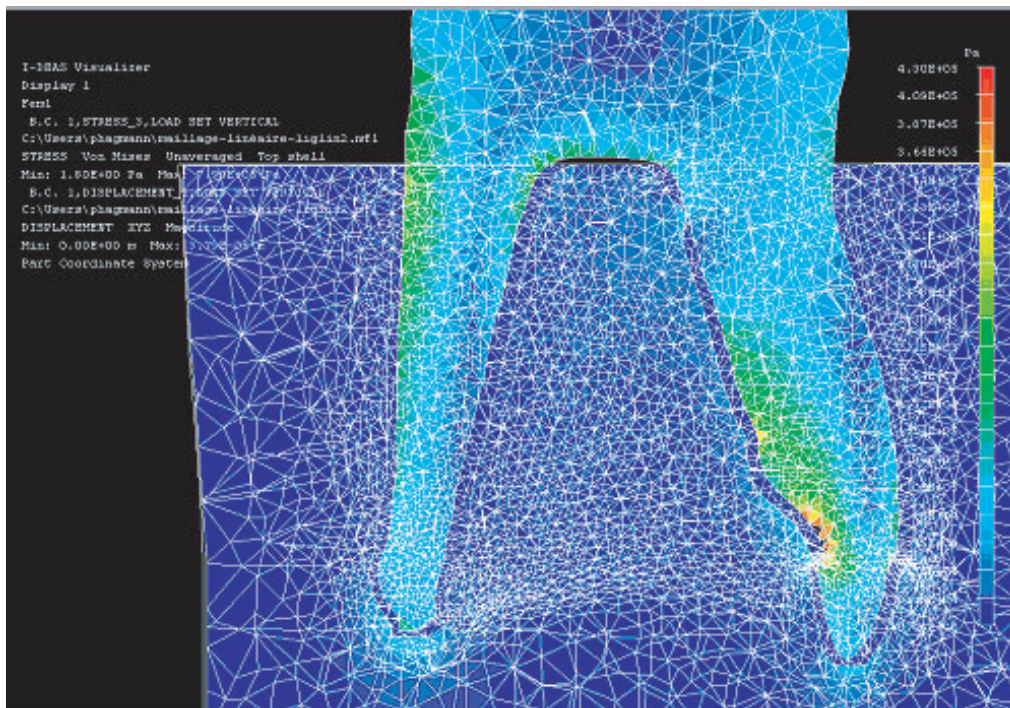
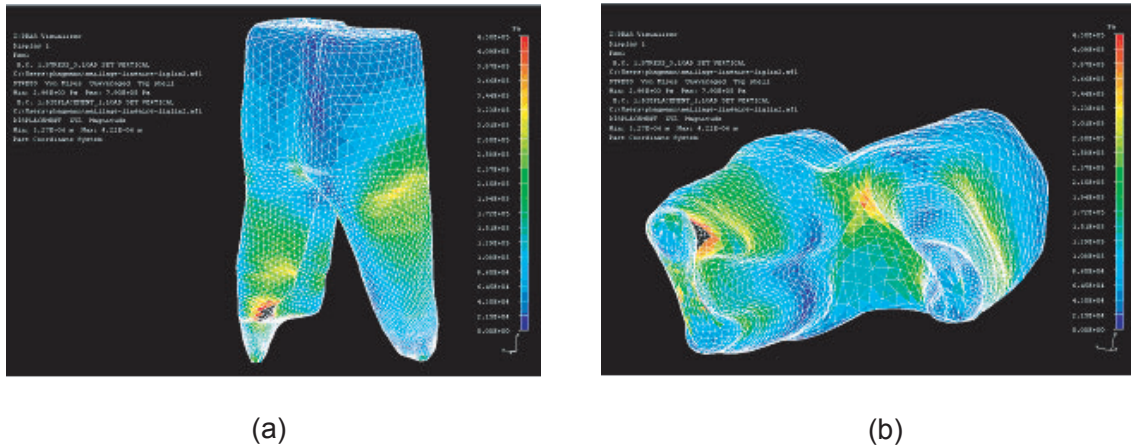


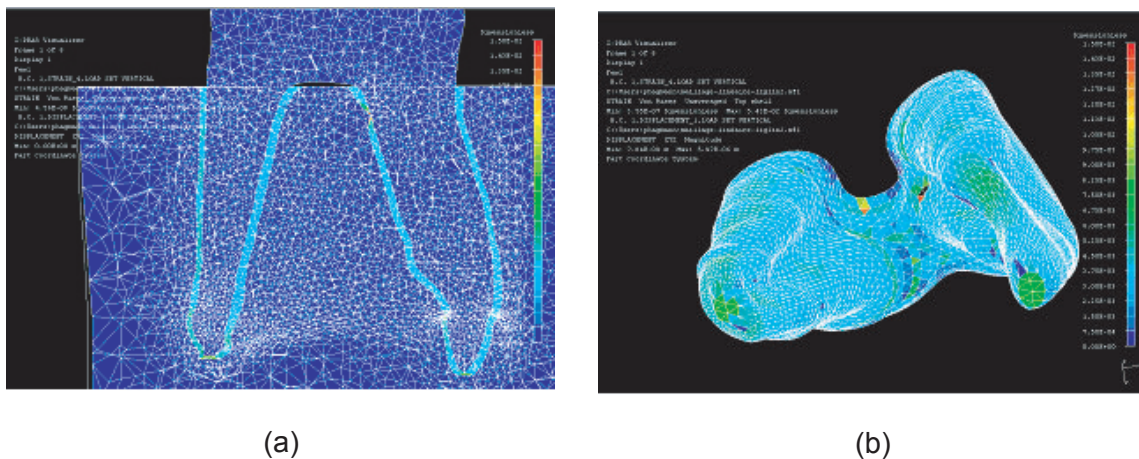
Figure 7.7 shows the distribution of Von Mises stress at the surface of the tooth. The crown is relatively free of stress whereas in the roots, the stresses are more concentrated, particularly near the most apical regions and at zones where geometric irregularities are observed.

Figure 7.7 Von Mises Stress at the surface of the tooth when the tooth is subjected to a coronal-apical load of 10 N (maximum stress, in red, 0.43 MPa). Seen here is the tooth without the surrounding bone and ligament viewed (a) from lingual-buccal and (b) from apical-coronal.



The Von Mises strain of the PDL shown in figure 7.8a indicates that it is principally the ligament that undergoes strain deformation. The tooth and bone, however, deform only marginally. In the apical-coronal view shown in figure 7.8b the strain field at the surface of the ligament is relatively homogeneous, and no region undergoes a particular deformation.

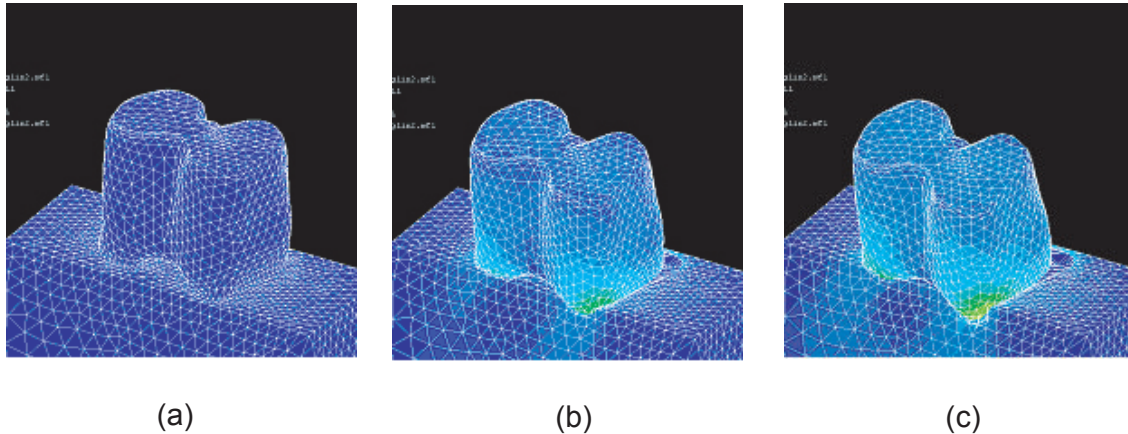
Figure 7.8 Von Mises Stress of the PDL when the tooth is subjected to a coronal-apical load of 10 N (maximum strain, in red, $E=0.015$). Seen in (a) is a sagittal section of the system clearly showing the relatively large deformation of the ligament with respect to the bone and tooth, and (b) the ligament seen in the apical-coronal direction.



7.1.3.2 Application of a Lingual-Buccal Load

When a force of 10 N is applied in the lingual-buccal direction to the crown of the tooth, the primary observations are similar to what is observed in the coronal-apical case: the stresses are high in the tooth, the ligament deforms relatively more than the surrounding tooth and bone and absorbs the stress, thus minimising the stress observed in the bone.

Figure 7.9 Amplified movements of the tooth when subjected to an lingual-buccal load of 10 N showing tooth (a) before loading, (b) during partial loading, and (c) fully loaded



Examining figure 7.9a-c, it is seen that the tooth is undergoing a movement of rotation that is asymmetric. The movement of the distal portion of the tooth (shown as the right portion of the tooth in figure 7.9) is greater than the deformation of the mesial root. This difference can be explained by the geometry of the tooth, the mesial root being longer and having a sudden change in its diameter near the most apical region of the root. This is seen clearly in figure 7.10

Figure 7.10 The result of applying a 10N lingual-buccal load showing (a) the field of Von Mises stress on the tooth (maximum, in red, 1.2 MPa) and (b) the field of Von Mises strain on the ligament (maximum, in red, $E=0.012$)

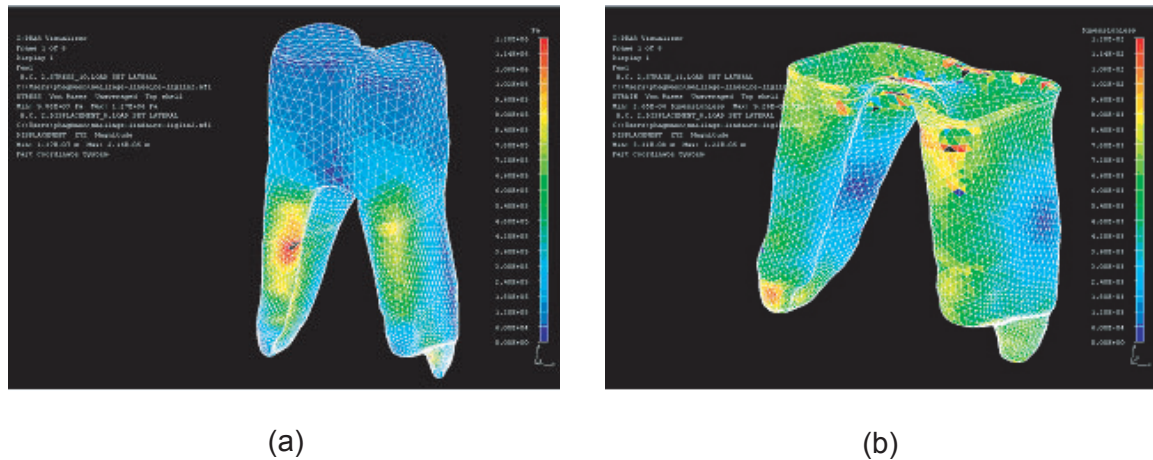


Figure 7.10a shows that the Von Mises stresses of the tooth are concentrated on the surfaces facing the alveolar bone. It is also observed that the stresses are greater in the zones of compression than in the zones of tension. The strain distribution observed in the ligament is less homogeneous than in the coronal-apical case, and deforms primarily on the surfaces in contact with the bone.

7.1.3.3 Application of a Distal-Mesial Load

When a force of 10 N is applied in the lingual-buccal direction to the crown of the tooth, the primary observations are similar to what is observed in the coronal-apical and lingual-buccal cases: the stresses are high in the tooth, the ligament deforms relatively more than the surrounding tooth and bone and absorbs the stress, thus minimising the stress observed in the bone.

Figure 7.11 Amplified movements of the tooth when subjected to a distal-mesial load of 10 N showing tooth (a) before loading, (b) during partial loading, and (c) fully loaded

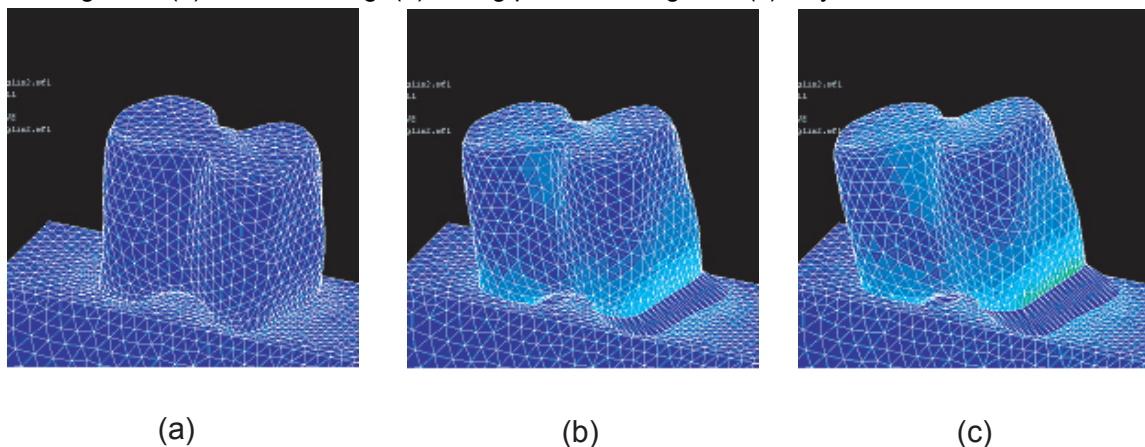


Figure 7.11 shows the amplified movements of the tooth when subjected to a distal-mesial load of 10 N applied to the crown. Unlike the previous two cases, this type of loading did not lead to any asymmetries due to the difference in length of the distal and mesial roots.

Figure 7.12 The result of applying a 10N distal-mesial load showing (a) the field of Von Mises stress on the tooth (maximum, in red, 1.3 MPa) and (b) the field of Von Mises strain on the ligament (maximum, in red, $E=0.01$)

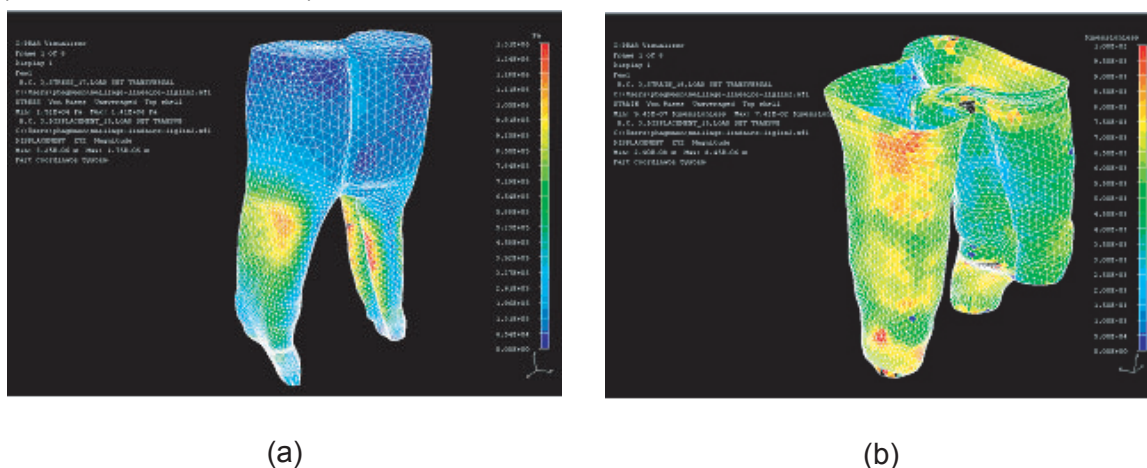


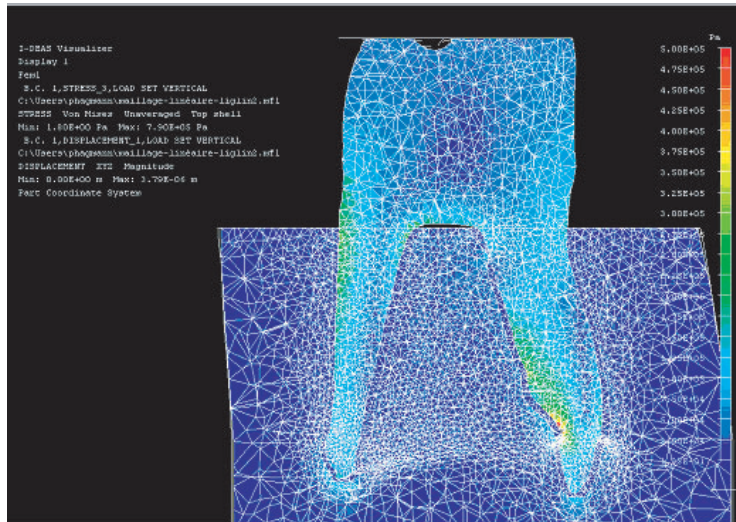
Figure 7.12 demonstrates the localised stresses in the zones where the tooth is facing the bone. The ligament undergoes localised deformation, primarily in the regions facing the tooth.

7.1.4 Implementing Non-Linear Experimental Data of the PDL

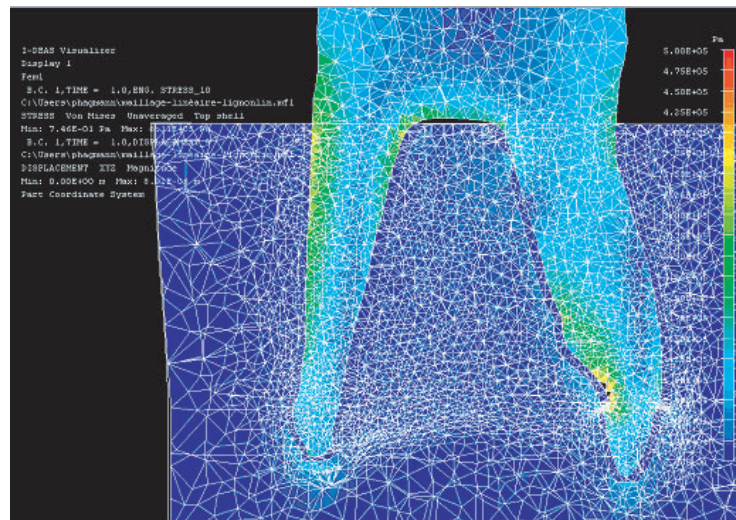
It is interesting to compare the effects of considering the ligament to be a linear elastic solid as opposed to non-linear elastic. Analysing the behaviour of the tooth is done simplistically in section 7.1.3, and through using the same 3D reconstructed tooth, non-linear experimental data obtained from subjecting the PDL to sinusoidal oscillations was introduced into the analysis of the tooth-PDL-bone system. Comparing the linear and non-linear results when a coronal-apical load is applied can then be performed.

In comparing figure 7.13a and figure 7.13b, it is seen that considering the ligament to be non-linear elastic has only a slight effect on the form and stress distribution in the tooth. The stresses are slightly greater in the non-linear case.

Figure 7.13 Comparing sagittal sections showing the Von Mises Stresses of the same tooth where PDL is (a) linear elastic, and (b) non-linear elastic ligament using experimental data. Maximum values, in red, 0.5 MPa.



(a)



(b)

Figure 7.14a and figure 7.14b further show the similarity in the stress distribution at the surface of the tooth for the linear and non-linear PDL. Again, the magnitude of the stresses is somewhat greater in the non-linear case.

Figure 7.14 Comparing the Von Mises Stresses at the surface of the same tooth when a coronal-apical load of 10 N is applied and considering the PDL to be (a) linear elastic, and (b) non-linear elastic ligament using experimental data. Maximum values, in red, 0.5 MPa.

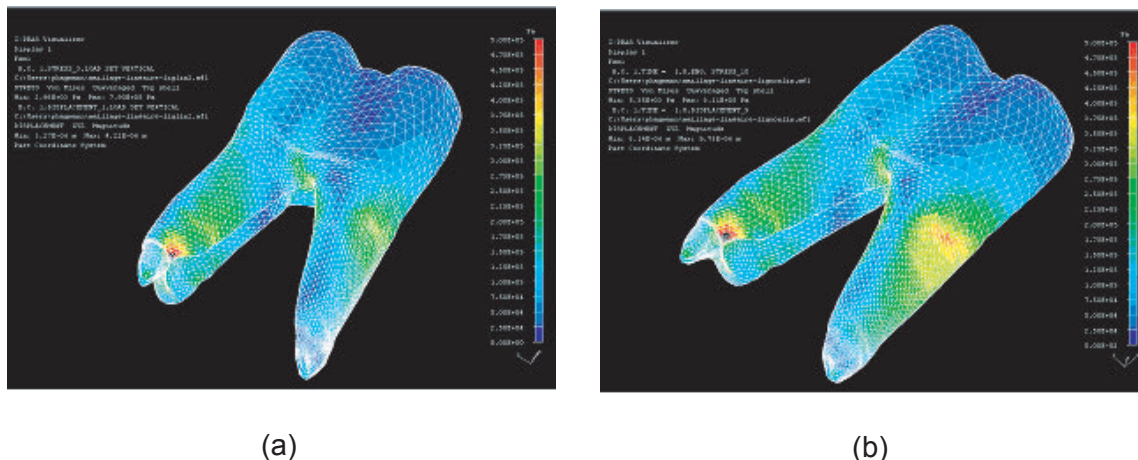
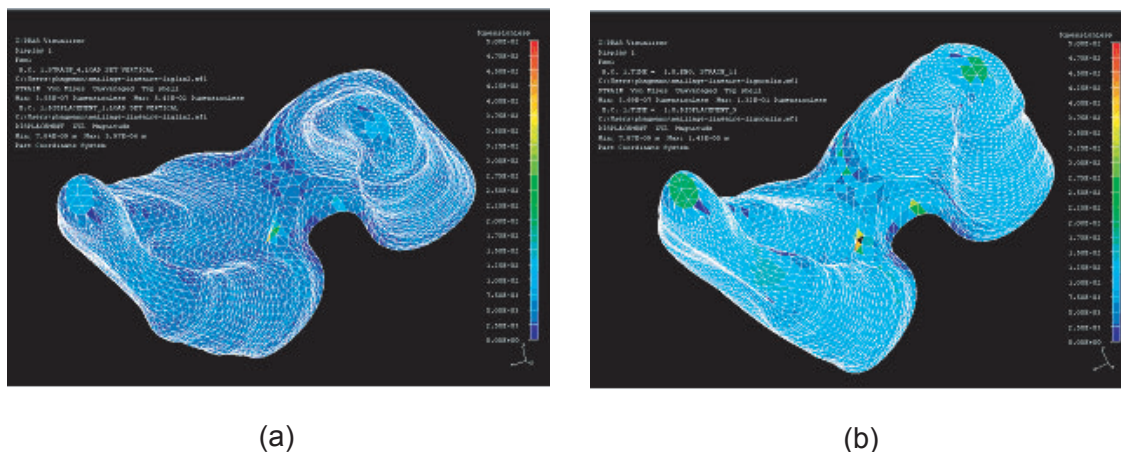


Figure 7.15 shows that the introduction of a non-linear ligament modifies the Von Mises strain distribution. This large difference is somewhat arbitrary since the method by which the linear curve was defined induces this effect. What this states, however, is that defining the ligament to be linear elastic is not justifiable, and that a more sophisticated method to model the behaviour of the PDL, that encompasses its nonlinearities, both elastic and viscous, is necessary.

Figure 7.15 Comparing the Von Mises Strain of the PDL when a coronal-apical load of 10 N is applied to the crown of the tooth, and considering the PDL to be (a) linear elastic, and (b) non-linear elastic ligament using experimental data. Maximum values, in red, $E=0.05$



-
-
-

-
-
-

•

•

•

“We are generally more convinced by the reasons we discover on our own than those given to us by others.”

Marcel Proust

•

•

•

8

Summary, Conclusion and Perspectives

8.1 Summary

8.1.1 Structure, Morphology and Histology of PDL

Geometry

Direct measurement: Using standard methods to measure sectioned shear and uniaxial specimens before subjecting them to a specific loading profile, key dimensions of the specimens' size and given periodontal widths are obtained.

3D tooth reconstruction: An advanced technique is used to investigate the geometry of a typical bovine first molar by reconstructing, in three dimensions, the tooth based on μ CT scans. Measurements are made by interpreting the reconstructed tooth system with the aid of a software programs (ImageJ, Rhinoceros, CorelDraw, IDEAS).

Through both direct measurement and 3D tooth reconstruction methods, it is observed that the PDL width decreases in the apical direction. The perimeter of the PDL at the midpoint between the bone and tooth interfaces are also measured, and found to decrease in the apical direction.

Morphology during Loading

Fluid expulsion in compression: It is observed that when the ligament is compressed, fluid is expelled onto the surface of the ligament. This fluid is absorbed back into the ligament once the specimen is pulled to its initial state.

Apparition of voids during rupture: When uniaxial specimens are pulled in tension, voids appear in the middle region of the ligament between the tooth and the bone. Based on the histology of the ligament, it is suggested that the apparition of voids at $E=0.75$ is attributed to the presence of blood vessels at that location.

Ligament morphology during rupture: Load, deformation and image data of the PDL are collected simultaneously enabling the observation of certain rupture mechanisms.

Structure and Histology of PDL

Preliminary study: The preferential fibre direction of the ligament around the radius of a third molar root is quantified, and the irregular contours at the alveolar bone interface are analysed using a fractal geometry technique.

Advanced Histology Study: A presentation of the biological components of the tooth, alveolar bone and periodontium is given. The structure is also displayed in a series of light microscope micrographs. Treating specific micrographs with the aid of an image analysis program, an estimation of the fibre density is obtained. Macerated decalcified specimens show the insertion points of Sharpey's fibres in the cementum and the alveolus junctions. The ligament is also shown to be highly vasculature, however, little information is obtained about the ground substance and extracellular matrix of the system.

8.1.2 Uniaxial Behaviour of PDL

Preconditioning

Preconditioning the sample cyclically shows a difference between initial and successive cycles, however, after the tenth cycle the difference between successive cycles is negligible. As such, in order to test the uniaxial specimen representatively, preconditioning is performed prior to any subsequent testing profiles.

Constant Strain Rate Deformation

Constant strain rate deformation tests on uniaxial specimens brings into evidence the dependence of the behaviour of the PDL at different strain rates. It is observed that increasing the strain rate increases the maximum tangent modulus measured from the stress-strain curve. Moreover, the constant strain rate test data are analysed to examine, as a first approximation, the linear scaling property; the first of two properties inherent to linear viscoelastic materials. It is observed that the PDL does not meet this criterion. Additional tests subject the PDL to constant strain rate deformation and recovery history profiles, which demonstrate that the PDL behaves in a viscoelastic manner.

Stress Relaxation

The PDL behaves as a fluid in the zero region, and as a viscoelastic solid in the toe and linear regions. The results from stress relaxation tests elucidate the importance of zero definition in performing any experiment. Step-relaxation experiments performed in the zero region of the stress-strain curve results in a stress-relaxation response analogous to a fluid, i.e. stress relaxes to zero. Shifting the zero to test in the toe and linear regions of the

S-E curve show the stress relaxation response to relax as would a solid. Relaxation tests are also performed to verify the superposition of responses property, the second of two properties inherent to linear viscoelastic materials. It is shown that superposition of separate responses is not a property of the PDL.

Response to Sinusoidal Oscillations

Subjecting the uniaxial specimens to sinusoidal responses gives rise to a number of material parameters. First, a transient stress response is observed and it is shown that this transient stress response is expected according to viscoelastic theory. It is noted, however, that the stress response curve is not sinus in its shape, and thus further supports that the ligament is nonlinear viscoelastic. Second, the frequency effects are examined; (i) the phaselag does not vary with increased frequency both in compression and in tension, and (ii) hysteresis increases with increased frequency. Third, the difference in behaviour in compression and tension are remarked; (i) the phaselag in tension is less than the phaselag in compression, and likewise (ii) the hysteresis in tension is less than in compression.

Rupture

Rupture data is used as a means to establish that no damage is caused to the specimen during the loading profiles (preconditioning, relaxation, constant strain rate and sinusoidal) prior to rupture. Rupturing the specimens at different strain rates show time-dependent behaviour. Moreover, the location of specimen plays a role in the maximum tangent modulus, maximum strain and strain energy density measured from S-E curves. No trends are observed for phaselag and maximum stress. It is possible that variation in experimental results is due to the biological variability of animals.

8.1.3 Shear Behaviour of PDL

Initial Studies

Preliminary experiments help determine a specific amplitude of testing in order to obtain a shear-load response. Because of the relatively large toe region observed when testing in shear, the shear strain amplitude for subsequent tests is rather elevated. A zeroing step is necessary to standardize the collected data in order to compare the results of different specimens. Zeroing the shear specimen follows the same method as with uniaxial specimens.

Triangular Cyclic Loading

The PDL's shear behaviour in the coronal direction is symmetrical to its shear behaviour in the apical direction. Moreover, the hysteresis observed is minimal. The curves show

typical soft tissue behaviour with the zero, toe and linear region clearly present. In addition, the hysteresis observed in shear is minimal when tested at a rate of $20 \mu\text{m s}^{-1}$.

Shear Stress Relaxation

Relaxation is observed in the PDL shear specimens both in the apical and coronal directions. In both directions the observed stress relaxation are similar, further supporting apical-coronal vertical symmetry at the selected amplitude

Shear Response to Sinusoidal Oscillations

The phaselags observed in tension and in compression are similar, and do not vary with frequency. Increasing the frequency at which the shear specimen is oscillated does not affect its mechanical response. The observed phaselags are similar to those observed in uniaxial tests in tension implying that viscosity mechanisms in shear are similar to those in tension.

Rupture

The data obtained are interpreted on a phenomenological level due to the small number of specimens tested successfully. Specimens tested in the apical-coronal direction, i.e. the same direction as one would extract a tooth, show typical soft tissue behaviour. The zero, toe, linear and rupture regions are clearly distinguishable. Due to the symmetry observed in shear stress relaxation and sinusoidal tests, it is probable that the ligament ruptured in the coronal-apical direction would yield similar results, though this remains to be determined in a future study.

8.1.4 Summary of Numerical Modeling Results

Stress Analysis Applied to Reconstructed 3D Bovine Molar

Using a FE-model reconstructed from μCT scans of a bovine first molar, different cases of tooth mobility are examined. In the first case, the PDL is considered to be a time-independent linear elastic material. The second case uses experimental data obtained from sinusoidal tests to describe PDL behaviour. A difference between these cases is observed with regard to the stress distributions in the system. The inadequacy of the linear assumption, and the inaccuracy of using experimental data used to model behaviour implicate the necessity of more viable constitutive equations to describe PDL behaviour.

The Power Law: A nonlinear viscoelastic model

A nonlinear viscoelastic law is proposed based on the standard linear viscoelastic model (Zener-Poynting). The viscous and elastic elements, however, are represented by nonlinear power functions, hence the name *Power Law* (PL). The reader is asked to refer

to the thesis by Justiz [Justiz 2004] for elaborate details of this model. Fitting this model to experimental data shows the adequacy of such a model to predict PDL behaviour. Determining the Poisson's ratio of the PDL is not trivial due to its inherent nonlinearities. A method, based on PL, to determine the Poisson's ratio is presented. The Poisson's ratio, for the PDL, is a function of its material parameters defined by the PL.

8.2 Conclusions

Geometry, Morphology and Histology of the PDL

- Fibre-bundle orientation varies around the radius of the tooth.
- Fibre-bundle orientation of PDL observed locally on a transverse section is transverse isotropic, i.e. transotropic.
- The movement of fluid within the ligament during compression and tension contributes to the viscous behaviour of the PDL.
- The viscous effects are greater in compression than in tension.

Elasticity of the PDL

- S-E curves of PDL uniaxial samples exhibit stiffening, nonlinear elastic behaviour in tension and in compression. Stiffening in compression is steeper than in tension.
- τ - γ curves of transverse PDL shear specimens exhibit stiffening, nonlinear elastic behaviour in extrusive and intrusive directions. Stiffening in extrusion is symmetrical to that in intrusion around the chosen *zero* of the specimen.

Viscosity of the PDL

- Stress relaxation of the PDL exhibit nonlinear viscous behaviour.
- S-E curves of PDL uniaxial samples are strain rate dependent.
- Harmonic oscillation of PDL tissue yields (i) a stress phaselag to strain that is independent of frequency, and (ii) a stress amplitude dependent on frequency.
- Phaselag for PDL is (i) greater in compression than in tension for uniaxial specimens, (ii) the same in intrusion as in extrusion.
- Viscous effects of the PDL are greater in compression than in tension.
- The PDL is a nonlinear pseudo-plastic, or *thinning*, viscous material.

8.3 Recommendations

Histology and Structure

A great hindrance to the progression in PDL research lies in that its structure, from a mechanical point of view, is unknown. Further studies must be performed to quantify the constituents of the PDL, and its structure with reference to a coordinate system defined for the tooth. Mechanisms that occur during mechanical deformation would require extensive histological work performed in two parts. First, a thorough investigation must be made that would identify structural components, and quantify the role of these components on mechanical behaviour. Second, mechanical tests must be performed in conjunction with histological studies to identify the structure of the PDL at rest and its structural changes during deformation.

Mechanical Tests

The uniaxial tests already provide valuable information as to the mechanical behaviour of the PDL. A preferential fibre orientation exists in uniaxial specimens, however, it may not be practical to define such a preferential fibre orientation for transverse sections, nor for whole tooth experiments. Nonetheless, information regarding the structural components of the PDL is vital to any accurate simulation of tooth movement. The shape of the shear specimens presented in this thesis, where transverse isotropy can no longer be assumed, makes interpreting results approximative. As a future study, it is proposed that an experimental setup be designed to test uniaxial specimens in shear, i.e. the uniaxial specimen would be placed into a machine as describe in this thesis, however, instead of testing in traction-compression, the test would be performed perpendicular to this direction. Such a test would provide a better representation of the PDL in shear, compared with the testing of whole transverse sections.

Tests in this thesis-work have been *in vitro*. Developing a system that tests the PDL *in vivo* would be an advantage in understanding the actual mechanics of the system. *In vivo* tests, however, are not practical, so it is recommended that an experimental setup be developed that would reproduce *in vivo* conditions as much as possible. Incorporating a membrane around the periodontium, or testing the periodontium in a closed system under pressure are possible solutions.

Once a numerical model that describes the nonlinear viscoelastic behaviour of the PDL is created based on results from uniaxial and shear experiments, it would be necessary to verify such a model. To do so, an experimental testing apparatus would be required to test an intact tooth connected to the alveolar bone.

References

- Andersen, K. L., H. T. Mortensen, E. H. Pedersen and B. Melsen (1991). Determination of stress levels and profiles in the periodontal ligament by means of an improved three-dimensional finite element model for various types of orthodontic and natural force systems. *J. Biomed. Eng.* 13(July): 293-303.
- Andersen, K. L., E. H. Pedersen and B. Melsen (1991). Material Parameters and stress profiles within the periodontal ligament. *Am. J. Orthod. Dentofac. Orthop.* 99(5): 427-40.
- Atkinson, H. F. and W. J. Ralph (1977). In Vitro Strength of the Human Periodontal Ligament. *J Dent Res* 56(1): 48-52.
- Atmaram, G. H. and H. Mohammed (1981). Estimation of Physiological Stresses with a Natural Tooth Considering Fibrous PDL Structure. *J Dent Res* 60(5): 873-877.
- Berkovitz, B. (1990). The Structure of the Periodontal Ligament: An Update. *Euro J Orthod* 12: 51-76.
- Berkovitz, B., B. Moxham and H. Newman, Eds. (1995). The Periodontal Ligament in Health and Disease. London, Mosby-Wolfe.
- Berkovitz, B., M. Weaver, R. Shore and B. Moxham (1981). Fibril Diameters in the Extracellular Matrix of the Periodontal Ligament. *Conn Tissue Res* 8(2): 127-132.
- Berkovitz, B. K. B., R. Whatling, A. W. Barrett and S.S. Omar (1997). The Structure of Bovine Periodontal Ligament with Special Reference to the Epithelial Cell Rests. *J Periodontology* 68(9): 905-913.
- Bien, S. M. and H. D. Ayers (1965). Responses of rat maxillary incisors to loads. *J Dent Res* 44: 517-520.
- Blaushild, N., Y. Michaeli and S. Steigman (1992). Histomorphometric study of the periodontal vasculature of the rat incisor. *J Dent Res* 71: 1908-12.
- Borodich, F. M. (1997). Some Fractal Models of Fracture. *J Mech Phys Solids* 45(2): 239-259.
- Borodich, F. M. and D. A. Onishchenko (1999). Similarity and fractality in the modelling of roughness by a multilevel profile with hierarchical structure. *International Journal of Solids and Structures* 36: 2585-2612.
- Bourauel, C., D. Freudenreich, D. Vollmer, D. Kobe, D. Drescher and A. Jäger (1999). Simulation of Orthodontic Tooth Movements: A Comparison of Numerical Models. *J Orofac Orthop* 60(2): 136-51.
- Brosh, T., I. H. Machol and A. D. Vardimon (2002). Deformation/recovery cycle of the periodontal ligament in human teeth with single or dual contact points. *Arch Oral Biol* 47: 85-92.
- Chiba, M. and K. Komatsu (1980). Measurement of the Tensile Strength of the Periodontium in the Rat Mandibular First Molar. *Archs oral Biol* 25: 569-572.

- Chiba, M. and K. Komatsu (1988). In vitro estimation of the resisting force of tooth eruption and the zone of shear in the rat incisor periodontal ligament. *The Biological Mechanisms of Tooth Eruption and Root Resorption*: 193-205.
- Chiba, M. and K. Komatsu (1993). Mechanical Responses of the Periodontal Ligament in the Transverse Section of the Rat Mandibular Incisor at Various Velocities of Loading in vitro. *J Biomechanics* 26(4/5): 561-570.
- Chiba, M., A. Yamane, S. Ohshima and K. Komatsu (1990). In vitro Measurement of Regional Differences in the Mechanical Properties of the Periodontal Ligament in the Rat Mandibular Incisor. *Archs oral Biol* 35(2): 153-161.
- Cobo, J., A. Sicilia, J. Arguelles, D. Suarez and M. Vijande (1993). Initial Stress Induced in Periodontal Tissue with Diverse Degrees of Bone Loss by Orthodontic Force: Tridimensional Analysis by Means of the Finite Element Method. *Am J Orthod Dentofac Orthop* 104(5): 448-454.
- Cook, S. D., J. J. Klawitter and A. M. Weinstein (1982). The Influence of Implant Geometry on the Stress Distribution Around Dental Implants. *J Biomed Mater Res* 16: 369-379.
- Cook, S. D., J. J. Klawitter and A. M. Weinstein (1982). A Model for the Implant-Bone Interface Characteristics of Porous Dental Implants. *J Dent Res* 61: 1006-1009.
- Cook, S. D., A. M. Weinstein and J. J. Klawitter (1982). Parameters Affecting the Stress Distribution Around LTI Carbon and Aluminum Oxide Dental Implants. *J Biomed Mater Res* 16: 875-885.
- Coolidge, S. D. (1937). The Thickness of the Human Periodontal Membrane. *J Am Dent Assoc* 24: 1260-1265.
- Daly, C. H., J. I. Nicholls, W. L. Kydd and P. D. Nansen (1974). The Response of the Human Periodontal Ligament to Torsional Loading - I. Experimental Methods. *J Biomechanics* 7: 512-522.
- Davy, D. T., G. L. Dilley and R. F. Krejci (1981). Determination of Stress Patterns in Root-Filled Teeth Incorporating Various Dowel Designs. *J Dent Res* 60: 1301-1310.
- Decraemer, W. F., M. A. Maes, V. J. Vanhuyse and P. Vanpeperstraete (1980). A non-linear viscoelastic constitutive equation for soft biological tissues, based upon a structural model. *J Biomechanics* 13: 559-564.
- Durkee, M. C. (1996). The Non-Linear Stress-Strain Behavior of the Periodontal Ligament and its Effect on Finite Element Models of Dental Structures. Department of Orthodontics. Newark, University of Medicine & Dentistry of New Jersey: 283.
- Dyment, M. L. and J. L. Syngé (1935). The Elasticity of the Periodontal Membrane. *Oral Health* 25: 105-109.
- Farah, J. W., R. G. Craig and D. L. Sikarskie (1973). Photoelastic and Finite Element Stress Analysis of a Restored Axisymmetric First Molar. *Journal of Biomechanics* 6: 511-520.
- Ferrier, J. M. and E. M. Dillon (1983). The water binding capacity of the periodontal ligament and its role in mechanical function. *Journal of Periodontal Research* 18: 469-473.

- Fung, Y. C. (1993). *Biomechanics: Mechanical Properties of Living Tissues*, Springer-Verlag.
- Gathercole, L. J. (1987). *Biophysical Aspects of the Fibres of the Periodontal Ligament. The Periodontal Ligament in Health and Disease*. B. Berkovitz, B. Moxham and H. Newman. Oxford, Pergamon Press: 103-117.
- Giargia, M. and J. Lindhe (1997). Tooth mobility and periodontal disease. *J Clin Periodontol* 24: 785-95.
- Imamura, N., S. Nakata and A. Nakasima (2002). Changes in periodontal pulsation in relation to increasing loads on rat molars and to blood pressure. *Archives of Oral Biology* 47: 599-606.
- Jones, S. and A. Boyde (1972). A Study of Human Root Cementum Surfaces as Prepared for and Examined in the Scanning Electron Microscope. *Z Zellforsch* 130: 318-337.
- Jones, S. and A. Boyde (1974). The Organization and Gross Mineralization Patterns of the Collagen Fibres in Sharpey Fiber Bone. *Cell Tiss Res* 158: 83-96.
- Justiz, J. (2004). A Nonlinear Large Strain Viscoelastic Law with Application to the Periodontal Ligament. STI-I2S-LMAF. Lausanne, Swiss Federal Institute of Technology (EPFL).
- Kappraff, J. (1986). The Geometry of Coastlines: A Study of Fractals. *Comp & Maths with Appls* 12B(3/4): 655-671.
- Katona, T., N. Paydar, H. Akay and W. Roberts (1995). Stress Analysis of Bone Modeling Response to Rat Molar Orthodontics. *Journal of Biomechanics* 28(1): 27-38.
- Khera, S. C., V. K. Goel, R. C. S. Chen and S. A. Gurusami (1988). A 3-D Finite Element Model. *Operative Dent* 13: 128-137.
- Khera, S. C., V. K. Goel, R. C. S. Chen and S. A. Gurusami (1991). Parameters of MOD Cavity Preparations: A 3-D FEM Study, Part II. *Operative Dent* 16: 42-54.
- Kitoh, M., T. Suetsugu and Y. Muakami (1977). Mechanical Behaviour of Tooth, Periodontal Membrane, and Mandibular Bone by the Finite Element Method. *Bull Tokyo Med Dent Univ* 25: 81-87.
- Komatsu, K. (1988). In vitro Mechanics of the Periodontal Ligament in Impeded and Unimpeded Rat Mandibular Incisors. *Archs oral Biol* 33(1): 783-791.
- Komatsu, K. and M. Chiba (1993). The Effect of Velocity of Loading on the Biomechanical Responses of the Periodontal Ligament in Transverse Sections of the Rat Molar in vitro. *Archs oral Biol* 5(5): 369-375.
- Komatsu, K. and M. Chiba (1996). Analysis of stress-strain curves and histological observations on the periodontal ligament of impeded and unimpeded rat incisors at low velocities of loading. *Japanese Journal of Oral Biology* 38(2): 192-202.
- Komatsu, K. and M. Chiba (2001). Synchronous recording of load-deformation behaviour and polarized light-microscopic images of the rabbit incisor periodontal ligament during tensile loading. *Archs oral Biol* 46: 929-937.

- Komatsu, K. and A. Viidik (1996). Changes in the fibre arrangement of the rat incisor periodontal ligament in relation to various loading levels in vitro. *Archs oral Biol* 41(2): 147-159.
- Liu, S. H., R. S. Yang, R. al-Shaikh and J. M. Lane (1995). Collagen in tendon, ligament, and bone healing. A current review. *Clin Orthop*: 265-178.
- Mandel, U., P. Dalgaard and A. Viidik (1986). A Biomechanical Study of the Human Periodontal Ligament. *J Biomechanics* 19(8): 637-645.
- Mandelbrot, B. B. (1982). *The Fractal Geometry of Nature*. New York, W.H. Freeman.
- Mandelbrot, B. B., D. E. Passoja and A. J. Paullay (1984). Fractal character of fracture surfaces of metals. *Macmillan Journals Ltd*.
- McCulloch, C. A. and A. H. Melcher (1983). Cell migration in the periodontal ligament of mice. *J Periodontal Res* 18: 339-52.
- McGuinness, N., Wilson AN, Jones M, Middleton J and NR Robertson (1992). Stresses induced by edgewise appliances in the periodontal ligament--a finite element study. *Angle Orthod* 62: 15-22.
- McGuinness, N. J., A. N. Wilson, M. L. Jones and J. Middleton (1991). A Stress Analysis of the Periodontal Ligament Under Various Orthodontic Loadings. *Eur J Orthod* 13(3): 231-242.
- Mecholsky, J. J., D. E. Passoja and K. S. Feinberg-Ringel (1989). Quantitative Analysis of Brittle Fracture Surfaces Using Fractal Geometry. *J Am Ceram Soc* 72(1): 60-65.
- Meroueh, K. A., F. Watanabe and P. J. Mentag (1987). Finite Element Analysis of Partially Edentulous Mandible Rehabilitated with an Osteointegrated Cylindrical Implant. *J Oral Implantology* 13(2): 215-238.
- Middleton, J., M. Jones and A. Wilson (1990). Three-dimensional analysis of orthodontic tooth movement. *J Biomed Eng* 12: 319-27.
- Middleton, J. and A. N. Wilson (1996). The Role of the Periodontal Ligament in Bone Modeling: The Initial Development of a Time-Dependent Finite Element Model. *Am J Orthod Dentofac Orthop* 109(2): 155-162.
- Mow, V. C., A. F. Mak, W. M. Lai, L. C. Rosenberg and L.-H. Tang (1984). Viscoelastic Properties of Proteoglycan subunits and Aggregates in Varying Solution Concentrations. *J Biomechanics* 17(5): 325-338.
- Moxham, B. J. and B. K. Berkovitz (1989). A comparison of the biomechanical properties of the periodontal ligaments of erupting and erupted teeth of non-continuous growth (ferret mandibular canines). *Arch Oral Biol* 34(763-766).
- Mühlemann, H. R. (1967). Tooth Mobility: A review of Clinical Aspects and Research Findings. *J Periodontology* 38: 686-713.
- Nagerl H, Burstone CJ, Becker B and Kubein-Messenburg D (1991). Centers of rotation with transverse forces: an experimental study. *Am J Orthod Dentofacial Orthop* 99: 337-345.
- Nigg, B. M. and W. Herzog (1994). *Biomechanics of musculo-skeletal system*. Chichester.

- Parfitt, G. (1960). Measurement of physiological mobility of individual teeth in an axial direction. *J Dent Res* 39: 608-618.
- Picton, D. C. (1990). Tooth mobility--an update. *Eur J Orthod* 12: 109-115.
- Picton, D. C. A. (1984). Changes in axial mobility of undisturbed teeth and following sustained intrusive forces in adult monkeys (*Macaca fascicularis*). *Arch Oral Biol* 29: 959-64.
- Picton, D. C. A. (1986). Extrusive mobility of teeth in adult monkeys (*Macaca fascicularis*). *Arch Oral Biol* 31: 369-72.
- Picton, D. C. A. (1989). The periodontal enigma: eruption versus tooth support. *Eur J Orthod* 11: 430-9.
- Picton, D. C. A. and W. I. R. Davies (1967). Dimensional changes in the periodontal membrane of monkeys (*Macaca irus*) due to horizontal thrusts applied to the teeth. *Arch Oral Biol* 12: 1635-1643.
- Picton, D. C. A. and J. Slatter (1972). The effect on horizontal tooth mobility of experimental trauma to the periodontal membrane in regions of tension and compression in monkeys. *J Periodont Res* 7: 35-41.
- Picton, D. C. A. and D. J. Wills (1978). Viscoelastic properties of the periodontal ligament and mucous membrane. *J Prosthet Dent* 40: 263-272.
- Pietrzak, G., A. Curnier, J. Botsis, S. S. Scherrer, H. W. A. Wiskott and U. C. Belser (2002). A nonlinear elastic model of the periodontal ligament and its numerical calibration for the study of tooth mobility. *Computer Methods in Biomechanics and Biomedical Engineering* 5(2): 91-100.
- Pini, M. (1999). Mechanical Characterization and Modeling of the Periodontal Ligament. Graduate School in Material and Structural Engineering. Trento, Università degli Studi di Trento.
- Pini, M., J. Botsis, P. Zysset and R. Contro (in press). Tensile and compressive behaviour of the bovine periodontal ligament. *J Biomechanics*.
- Pini, M., H. W. A. Wiskott, S. S. Scherrer, J. Botsis and U. C. Belser (2002). Mechanical characterization of bovine periodontal ligament. *Journal of Periodontal Research* 37: 237-244.
- Pioletti, D. P. and L.R. Rakotomanana (2000). On the independence of time and strain effects in the stress relaxation of ligaments and tendons. *J Biomechanics* 33: 1729-1732.
- Pioletti, D. P. and L. R. Rakotomanana (2000). Non-linear viscoelastic laws for soft biological tissues. *Eur J Mech A/Solids* 19: 749-759.
- Provatidis, C. G. (2000). A comparative FEM-study of tooth mobility using isotropic and anisotropic models of the periodontal ligament. *Medical Engineering & Physics* 22: 359-370.
- Putz, R. and R. Pabst (1994). Sobotta, Atlas d'anatomie humaine. Paris.
- Quirina, A. and A. Viidik (1991). Freezing for Postmortal Storage Influences the Biomechanical Properties of Linear Skin Wounds. *J Biomechanics* 24(9): 819-823.

- Ralph, W. and C. Thomas (1988). Tooth Support in the Human Mandible. *J Oral Rehab* 15: 499-503.
- Ralph, W. J. (1980). The In Vitro Rupture of Human Periodontal Ligament. *J Biomechanics* 13: 369-373.
- Ralph, W. J. (1982). Tensile behaviour of the periodontal ligament. *J Periodontal Res* 17: 423-426.
- Rees, J. and P. Jacobsen (1997). Elastic modulus of the periodontal ligament. *Biomaterials* 18: 995-999.
- Rees, J. S. (2001). An investigation into the importance of the periodontal ligament and alveolar bone as supporting structures in finite element studies." *Journal of Oral Rehabilitation* 28: 425-432.
- Reinhardt, R. A., R. F. Krejci, Y. C. Pao and J. G. Stannard (1983). Dentin Stresses in Post-Reconstructed Teeth with Diminishing Bone Support. *J Dent Res* 62(9): 1002-1008.
- Reinhardt, R. A., Y. C. Pao and R. F. Krejci (1984). Periodontal Ligament Stresses in the Initiation of Occlusal Traumatism. *J Periodontal Res* 19(3): 238-246.
- Selna, L. G., H. T. Shillingburg and P. A. Kerr (1975). Finite Element Analysis of Dental Structures- Axisymmetric and Plane Stress Idealizations. *J Biomed Mater Res* 9: 237-252.
- Shimada, A., T. Shibata, K. Komatsu and M. Chiba (2003). The effects of intrusive loading on axial movements of impeded and unimpeded rat incisors: estimation of eruptive force. *Archives of Oral Biology* 48: 345-351.
- Sims, M. R. (1987). A model of the anisotropic distribution of microvascular volume in the periodontal ligament of the mouse mandibular molar. *Aust Orthod J* 10(1): 21-4.
- Sloan, P. (1982). Structural Organization of the Fibres of the Periodontal Ligament. *The Periodontal Ligament in Health and Disease*. B. Berkovitz, B. Moxham and H. Newman. Oxford, Pergamon Press.
- Sloan, P. and D. Carter (1995). Structural Organization of the Fibres of the Periodontal Ligament. *The Periodontal Ligament in Health and Disease*. B. Berkovitz, B. Moxham and H. Newman. Oxford, Pergamon Press.
- Takahashi, N., T. Kitagami and T. Komori (1979). Effects of Pin Hole Position on Stress Distributions and Interpulpal Temperatures in Horizontal Nonparallel Pin Restorations. *J Dent Res* 58: 2085-2090.
- Takahashi, N., T. Kitagami and T. Komori (1980). Behaviour of Teeth Under Various Loading Conditions with Finite Element Method. *J Oral Rehab* 7: 453-461.
- Tanne, K., H. A. Koenig and C. J. Burstone (1988). Moment to force ratios and the center of rotation. *Am J Orthod Dentofacial Orthop* 94: 426-31.
- Tanne, K., Y. Shibaguchi, Y. Terada, J. Kato and M. Sakuda (1992). Stress Levels in the PDL and Biological Tooth Movement. *The Biological Mechanisms of Tooth Movement and Craniofacial Adaptation*. Z. Davidovitch. Columbus, The Ohio State University College of Dentistry: 201-209.

- Tanne, K., S. Yoshida, T. Kawata, A. Sasaki, J. Knox and M. L. Jones (1998). An Evaluation of the Biomechanical Response of the Tooth and Periodontium to Orthodontic Forces in Adolescent and Adult Subjects. *British Journal of Orthodontics* 25: 109-115.
- Toms, S. R., G. J. Dakin, J. E. Lemons and A. W. Eberhardt (2002). Quasi-linear viscoelastic behavior of the human periodontal ligament. *Journal of Biomechanics* 35: 1411-1415.
- Toms, S. R., J. E. Lemons, A. A. Bartolucci and A. W. Eberhardt (2002). Nonlinear stress-strain behaviour of periodontal ligament under orthodontic loading. *Am J Orthod Dentofacial Orthop* 122: 174-179.
- van Driel, W. D., E.J. van Leeuwen, J.W Von den Hoff, J.C. Maltha, Kuijpers-Jagtman, A.M. (2000). Time-dependent mechanical behaviour of the periodontal ligament. *Proc Inst Mech Eng* 214(5): 497-504.
- van Rossen, I. P., L. H. Braak, C. Putter and K. de Groot (1990). Stress-Absorbing Elements in Dental Implants. *J Prosthet Dent* 64(2): 198-205.
- Weinstein, A. M., J. J. Klawitter and S. D. Cook (1979). Finite Element Analysis as an Aid to Implant Design. *Biomater Med Devices Artif Organs* 7(2): 169-175.
- Widera, G. E. O., J. A. Tesk and E. Privitzer (1976). Interaction Effects Among Cortical Bone, Cancellous Bone, and Periodontal Membrane of Natural Teeth and Implants. *J Biomed Mater Res* 7: 613-623.
- Williams, K. R. and J. T. Edmundson (1984). Orthodontic tooth movement analysed by the Finite Element Method. *Biomaterials* 5: 347-351.
- Wills, D. J., D. C. A. Picton and W. I. R. Davies (1972). An investigation of the viscoelastic properties of the periodontium. *J periodont Res* 7: 42-51.
- Wills, D. J., D. C. A. Picton and W. I. R. Davies (1976). A study of the fluid systems of the periodontium in macaque monkeys. *Archs oral Biol* 21: 175-185.
- Wilson, A. N., J. Middleton, M. L. Jones and N. J. McGuinness (1994). The finite element analysis of stress in the periodontal ligament when subject to vertical orthodontic forces. *Br J Orthod* 21: 161-7.
- Wilson, A. N., J. Middleton, N. J. McGuinness and M. Jones (1991). A Finite Element Study of Canine Retraction with a Palatal Spring. *Br J Orthod* 18(3): 211-218.
- Wineman, A. S. and K. R. Rajagopal (2000). Mechanical Response of Polymers: An Introduction. Cambridge, Cambridge University Press.
- Wright, K. W. J. and A. L. Yettram (1978). Finite Element Stress Analysis of a Class I Amalgam Restoration Subjected to Setting and Thermal Expansion. *J Dent Res* 57: 715-723.
- Yamane, A., S. Ohshima, K. Komatsu and M. Chiba (1990). Mechanical Properties of the Periodontal Ligament in Incisor Teeth of Rats from 6 to 24 Months of Age. *Gerodontology* 9(1): 17-23.
- Yettram, A. L., K. W. J. Wright and H. M. Pickard (1977). Centre of Rotation of a Maxillary Central Incisor Under Orthodontic Loading. *Br J Orthod* 4(1): 23-27.

- Yoshida, N., Y. Koga, C. L. Peng, E. Tanaka and K. Kobayashi (2001). In vivo measurement of the elastic modulus of the human periodontal ligament. *Med Eng Phys* 23(8): 567-72.
- Young, B. and J. W. Heath (2002). *Functional Histology: A Text and Colour Atlas*, Churchill Livingstone.
- Zhou, S.-M., H.-P. Hu and Y.-F. Wang (1989). Analysis of Stresses and Breaking Loads for Class I Cavity Preparations in Mandibular First Molars. *Quintess Int* 20(3): 205-210.

Machine Specifications

Instrumentation

Two types of machines were used to perform mechanical tests. The custom-made shear-testing machine and the commercial Instron MicroTester 5848. Specimens were observed using an SZX12 Olympus optical microscope, and images were captured using a Sony CCD video camera and an Olympus 3.3 megapixel digital camera.

The Shear Testing Machine

The custom-made shear testing machine is an electromechanical testing instrument that applies static or cyclic test forces in tension and/or compression. The machine is specially designed and dimensioned to accommodate transverse PDL specimens. The shear testing machine conducts tests a very low forces upto ± 200 N (limit of load cell).

The load frame structure is rigid and stable machined from aluminium. The frame support is micro-centered around three bars of hardened stainless steel.

To conduct a test, a specimen is placed into the SLS-made (selective laser sintering) fixtures between a movable actuator attached to a load cell, and the stationary base. The displacement sensor is incorporated in the actuator mechanisms to measure displacement as close to the axis of motion as possible (6,8 mm). The software to control the actuator was self-written using National Instruments LabVIEW.

The actuator assembly, located in the upper portion of the machine, is comprised of a 10 W DC Maxon Motor, coupling, micro-precision ball-bearing screw that transferred the rotary motion of the motor into a linear motion. When the ball-bearing screw turns, the attached piston advances in a linear manner, guided by a custom-made guiding system on three precision shafts. The linear travel path of the machine is limited to 5 mm.

Performance Specifications

Parameter	Specifications
Load Capacity	± 500 N (static)
Maximum Speed	180 mm/min
Minimum Speed	0.0000083 mm/min

Parameter	Specifications
Position Resolution	0.5 micron up to 90 mm/min 1 micron between 90 mm/min and 180 mm/min
Position Measurement Accuracy Under No Load	± 0.5 microns over 2 mm travel ± 1.0 microns under 5 mm travel
Actuator Speed Accuracy (Zero or Constant Load)	$\pm 0.1\%$ of set speed
Total Actuator Travel	5 mm
Total Vertical Space	200 mm Distance inferior support to actuator connection with the actuator fully retracted excluding load cell, grips and test fixtures.
Height	650 mm
Width	30 mm
Depth	30 mm
Width of Base	5 mm
Space Between Columns	15.5 mm
Weight - Load Frame	10 kg
Maximum Power Requirement	2.5 amps at 240 volts
Voltage	220 V AC
Frequency	47/63 Hz
Ball screws	Precision ground ball screw.
Guide columns	3 Hardened and ground columns
Drive system	Coupling connected to motor shaft
Motor	Maxon DC motor - Precious Metal Brushes, 10 W. Ball bearings, 2 shafts. Motor ID: 118746
Linear Encoder	MIP10 Maxon Motor Control Encoder with ASCII programming capabilities.
Hardware	Stainless steel screws. Parts machined on cylindrical design out of aluminium to ensure centering.
Load Cell	Transmetra Load Cell - Miniature AL311U.200 Load range: ± 200 N non linearity: $\pm 0.15\%$ operating temperature: $-55^{\circ}\text{C} - 120^{\circ}\text{C}$ temperature effect: $\pm 0.027\%/K$ Limit load: 150% Deflection: 50 microns Material: stainless steel 17-4PH
Load Cell Amplifier	Transmetra Sensor Interface Type SI-U Supply voltage: 16-32 V DC Output signal: $\pm 5\text{V}$, 0-20 mA

Parameter	Specifications
Digital Transistor Transistor Logic Incremental Displacement Sensor	Travel range: 0 - 5.2 mm Precision: ± 1 micron Maximum displacement speed: 1 m/sec Temperature range: 0°C - 50°C
Digital TTL Signal Converter for displacement sensor.	Power supply: 10,8 - 26,4 V DC Signal Input: 64 digital in signals Signal Output: 5 digits converted from binary input.

The Instron MicroTester 5848

The MicroTester is an electromechanical materials testing instrument that applies static or cyclic test forces in tension and/or compression to a wide range of specimens. The MicroTester is a versatile system that conducts tests at very low forces up to 2 kN, with extremely high displacement resolution.

The load frame structure is rigid and stable. It can be configured either horizontally or vertically. A load cell connected in series with the specimen, converts forces into an electrical signal for the control system to measure and display.

To conduct a test, a specimen is placed into the grips or fixtures between a movable actuator and the stationary load cell that is mounted to the base beam. A load cell can also be attached to the moving actuator.

A frame control panel, or handset, is attached to one of the load frame columns. The control panel, combined with 5800 Console software provides a flexible user interface to perform functions that are pre-set using the software. The type of software application, Console only, Merlin, Max or WaveMaker, determines which functions are available from the control panel.

Series 5800 Console software runs on the system computer. Console appears at the top of the computer screen as a series of icons that provide live displays and access to transducer setup, calibration, loop tuning and other features. Optional applications such as Merlin, Max or WaveMaker, provide functions for cyclic testing, and block/sequential programming.

The actuator assembly, located behind the actuator cover, is comprised of the motor, belt drive, ball screw, linear bearing, piston and travel limit assemblies. A brushless servomotor provides the main drive power to the ball screw through a belt drive system. When the ball screw turns, the ball nut and the attached piston advance in a linear manner, guided by the linear bearing. A pair of electrical limit switches detects the actuator piston travel and shuts down the motor if the actuator moves beyond its limits.

Performance Specifications

Parameter	Specifications
Load Capacity	± 2 kN (static)
Maximum Speed	1500 mm/min
Minimum Speed	0.000024 mm/min
Return Speed	100 mm in 10 seconds
Position Resolution	0.020 micron up to 200 mm/min 1 micron between 200 mm/min and 1500 mm/min
Position Measurement Accuracy Under No Load	± 0.5 microns over 250 microns travel ± 2.5 microns over 10 mm travel ± 6.0 microns over 100 mm travel
Actuator Speed Accuracy (Zero or Constant Load)	± 0.1% of set speed
System Stiffness	8.32 kN/mm
Total Actuator Travel	110 mm
Total Vertical Space	680 mm Distance from base plate to actuator connection with the actuator fully retracted and the crosshead at maximum distance from base, excluding load cell, grips and test fixtures.
Height	1500 mm
Width	452 mm
Depth	440 mm
Width of Base Tray	378 mm
Space Between Columns	190 mm
Weight - Load Frame	89 kg
Maximum Power Requirement	5 amps at 120 volts 2.5 amps at 240 volts
Operating Temperature	10°C to +38°C
Humidity	10% 90% (non-condensing)
Voltage	100/120/220/240 V AC
Frequency	47/63 Hz
Power Rating	435 VA
Ball screws	Precision ground ball screw: diameter 16,0 x 2,0 lead backlash free. Single nut using oversize ball.
Guide columns	Hardened and ground columns
Drive system	Timing belts & pulleys
Motor	High performance brushless DC servo motor. High torque to size and inertia ratios.
Rotary Encoder	1000 lines optical incremental rotary encoder attached to motor.

Parameter	Specifications
Linear encoder	Grating period: 8 mm Accuracy: ± 3 mm over 120 mm Used for control feedback.
Hardware	Zinc plated or stainless steel screws. Load cell and base adapter screws are Dacromet coated grade 12.9 strength.
Power Amplifier	DC Brushless PWM servo amplifier Power supply: +24 V to +90 V Current: 6 A (continuous) 20 A (peak) Power: 600 W

The Power Law: a nonlinear viscoelastic model for the PDL

Since the PDL clearly exhibits viscoelastic properties such as relaxation and creep, time-dependency must be taken into account. Investigated in the thesis work by Justiz [Justiz 2004], attempts to model the PDL under classical viscoelastic models, such as the 3-parameter standard model (figure 2.9), did not sufficiently describe the experimental data of this thesis. As a result, a more comprehensive theoretical model, the *Power Law* (PL), is proposed by Justiz to predict the mechanical behaviour of the PDL.

In general terms, the PL is a nonlinear version of the standard model. The standard model consists of two linear springs that are described by Hooke's law:

$$S^e = \varepsilon E \quad (\text{EQ 11.1})$$

where ε is the spring constant, and a linear viscous dashpot that is described by the relation:

$$S^v = \mu E \quad (\text{EQ 11.2})$$

where μ is viscosity. Solving these two equations yield a set of linear differential equations that, when solved, give the formulae of the constitutive equations for the standard model.

In the case of the PL in 1D, the elastic and viscous elements are not represented by linear relations such as equations 11.1 & 11.2, rather, they are represented by nonlinear relationships. For the linear elements:

$$S^e = \kappa(E) \cdot E \quad (\text{EQ 11.3})$$

such that $\kappa(E)$ is a nonlinear power function of E given by:

$$\kappa(E) = \kappa|E|^{n-1} \quad (\text{EQ 11.4})$$

where n represents the degree of nonlinearity, i.e. the linear law is obtained for $n=1$.

Likewise, the viscous element is represented by a nonlinear relationship given by:

$$S^v = \mu(\dot{E}) \cdot \dot{E} \quad (\text{EQ 11.5})$$

such that $\mu(\dot{E})$ is the nonlinear power function of the strain rate \dot{E} given by:

$$\mu(\dot{E}) = \mu|\dot{E}|^{m-1} \quad (\text{EQ 11.6})$$

where m represents the degree of nonlinearity, i.e. the linear law is obtained for $m=1$.

Solving equations 11.3 & 11.5 would give the constitutive equations that would describe a nonlinear case of the standard model in 1D. Solving these equations is beyond the scope of this thesis, however, excerpts from some simulations performed by Justiz with the PL have been included in this section.

Shear Simulation of PDL

The PL is fit to the experimental data obtained in shear experiments. This is shown graphically in figure 1. A FE mesh of the transverse portion of the ligament subjected to shear is presented in figure 3, and shows that the distribution of Von Mises stress is homogeneous throughout the ligament.

Uniaxial Simulation of PDL

The PL is fit to the experimental data obtained in uniaxial experiments. This is shown graphically in figure 2. A FE mesh of an entire uniaxial specimen at different strains give the stress distribution of the PDL in three different states; this is presented in figure 4. It appears, from this simulation that the deformation is somewhat homogeneous, however, this model does not yet take into account the anisotropies due to unknown role of the components that make up the structural configuration of the PDL. Nevertheless, the PL is the most sophisticated model that predicts PDL behaviour.

Poisson's Ratio

The 3-dimensional elastic power-model consists of 6 independent parameters, two powers n and m , and two elastic parameters κ and μ . In order to identify these parameters, the shear and traction experiments presented in this thesis were performed. Identification of these parameters involves assuming trace free strain, i.e. $\text{tr}\mathbf{E} = 0$. This assumption is exact for small strains only, however, it is a good approximation for finite strains. As a result, the shear test (refer to figure 3.14) enables the identification of the constants μ and n by fitting the resulting one dimensional law:

$$S_{HR} = 2\mu|E_{HR}|^{n-1}E_{HR} \quad (\text{EQ 11.7})$$

to the experimental data. Determining the constants k and m is not as straightforward because no closed expression for the traction stress, S_{RR} as a function of the traction strain E_{RR} (refer to figure 3.9) exists. Obtaining such an expression involves assuming that the two powers are equal, i.e. $n = m$. In doing so, a Poisson's ratio with an equivalent definition as in the linear case can be obtained as follows:

Assuming pure traction, we have

$$\mathbf{S} = \begin{bmatrix} S_{RR} & 0 & 0 \\ 0 & 0 & 0 \\ 0 & 0 & 0 \end{bmatrix} \quad \text{and} \quad \mathbf{E} = \begin{bmatrix} E_{RR} & 0 & 0 \\ 0 & E_{HH} & 0 \\ 0 & 0 & E_{BB} \end{bmatrix} \quad (\text{EQ 11.8})$$

The deviatoric strain is then given by

$$\begin{aligned} \mathbf{E}' &= \mathbf{E} - \frac{1}{3}\text{Tr}(\mathbf{E})\mathbf{I} \\ &= \frac{1}{3} \begin{bmatrix} 2(E_{RR} - E_{HH}) & 0 & 0 \\ 0 & E_{HH} - E_{RR} & 0 \\ 0 & 0 & E_{BB} - E_{RR} \end{bmatrix} \end{aligned} \quad (\text{EQ 11.9})$$

and the deviatoric stress by

$$\mathbf{S}' = \mathbf{S} - \frac{1}{3} \text{Tr}(\mathbf{S}) \mathbf{I}$$

$$= \frac{1}{3} \begin{bmatrix} 2S_{RR} & 0 & 0 \\ 0 & -S_{RR} & 0 \\ 0 & 0 & -S_{RR} \end{bmatrix} \quad (\text{EQ 11.10})$$

Defining the Poisson's ratio as the ratio of the perpendicular strain and the traction strain gives:

$$\nu = -\frac{E_{HH}}{E_{RR}} = -\frac{E_{BB}}{E_{RR}}$$

$$\nu = \frac{(2\mu)^{1/n} - 3(\kappa)^{1/n}}{(2\mu)^{1/n} + 3(2\kappa)^{1/n}} \quad (\text{EQ 11.11})$$

For full elaboration of formulae and a discussion of the limitations of the PL, the reader is asked to refer to Justiz [Justiz 2004].

Figure B.1 Experimental result from PDL shear specimen fit to the nonlinear power law

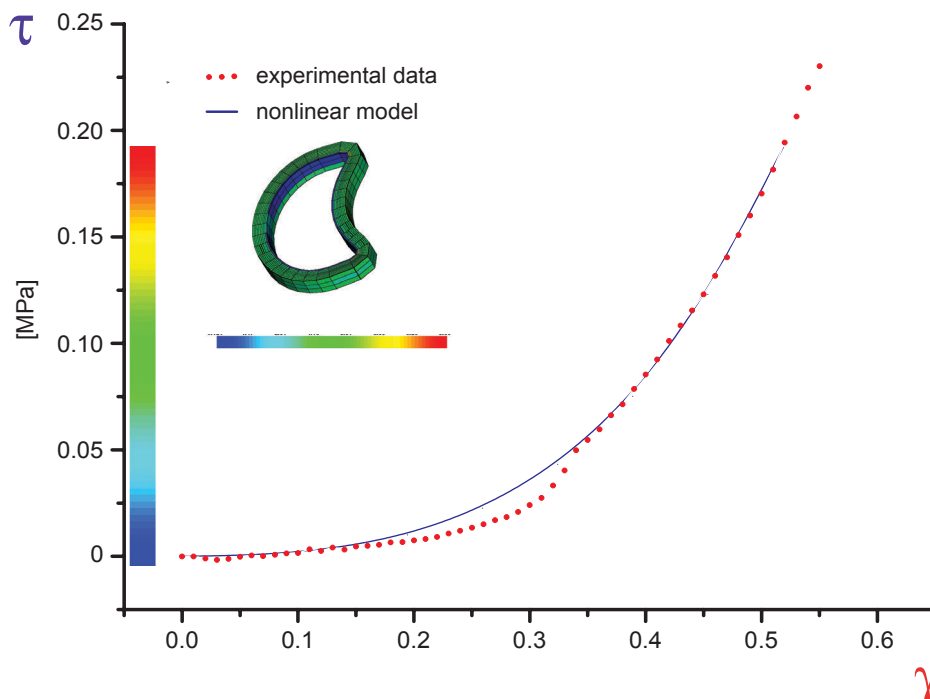


Figure B.2 Experimental result from PDL uniaxial specimen fit to the nonlinear power law showing (a) PDL is responsible for deformation and, (b) the stress field within the PDL.

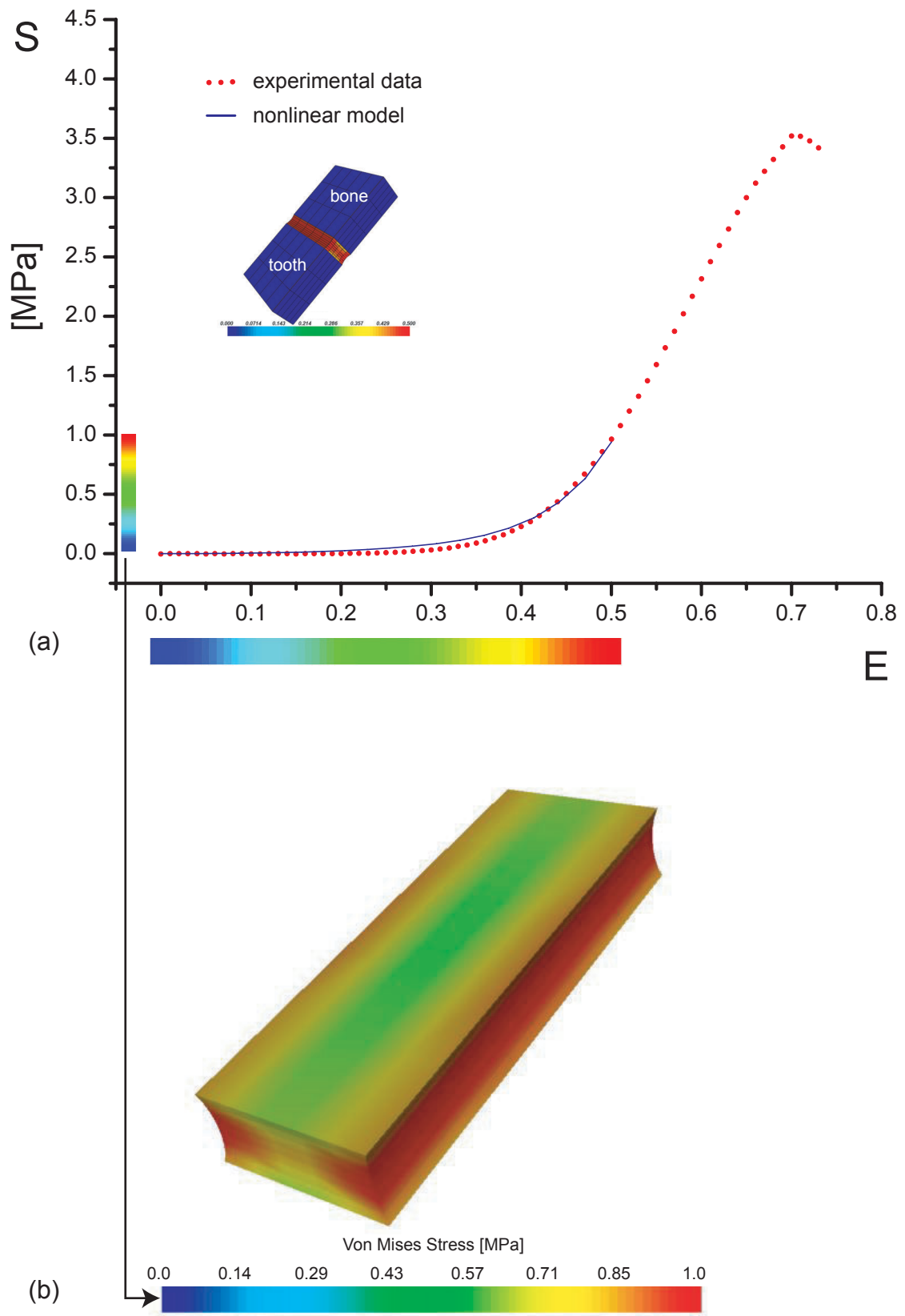


Figure B.3 Transverse section of PDL showing Von Mises stress distributions (a) from coronal-apical direction, and (b) from a perspective to show interior stress.

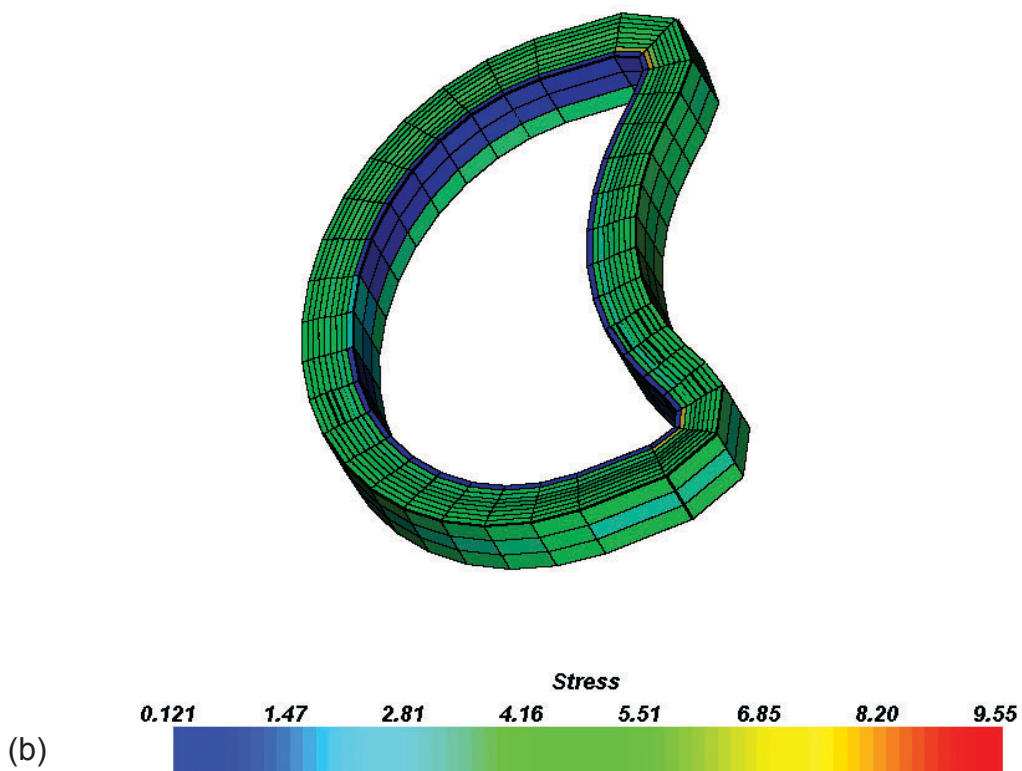
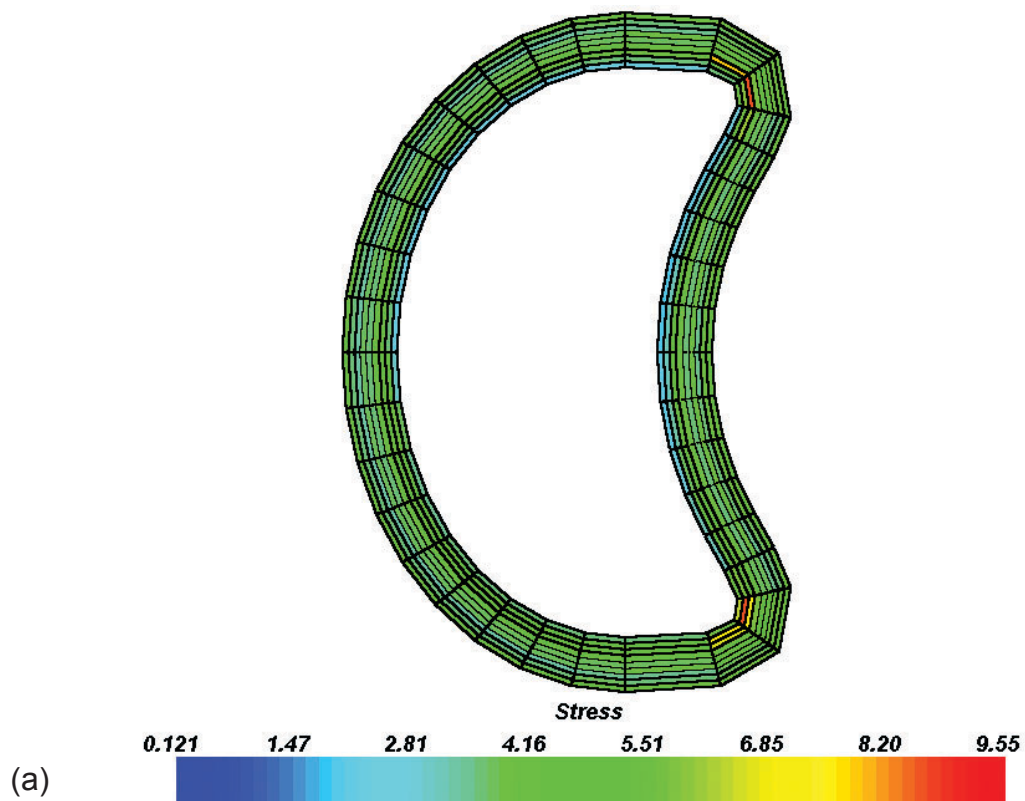
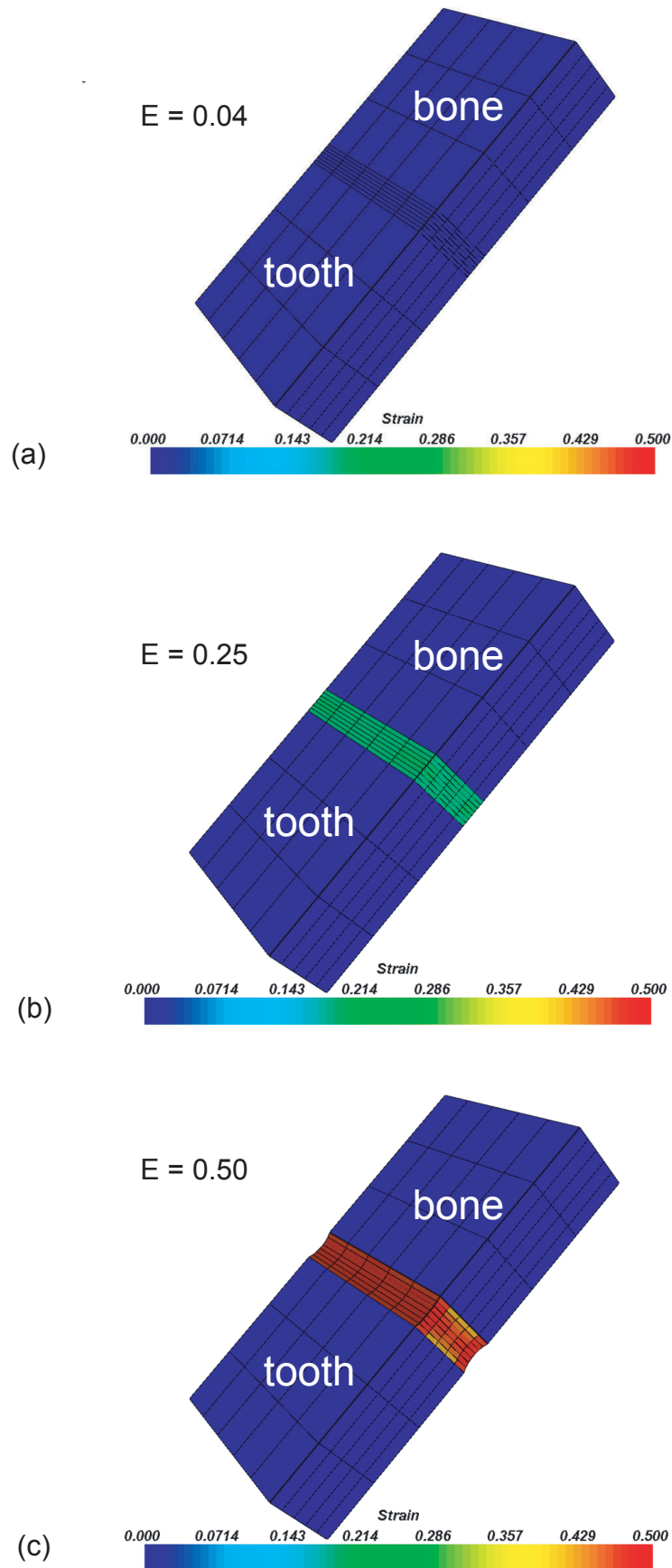


Figure B.4 PDL uniaxial specimen showing Von Mises stress distributions (a) from coronal-apical direction, and (b) from a perspective to show interior stress



CURRICULUM VITAE

SANCTUARY Colin

Date of Birth: 23 May 1974

WORK EXPERIENCE

Chalmers University of Technology Materials Engineering, Gothenburg, Sweden	Apr. 1999 – Nov. 1999
EMTS Consulting Materials Engineering, Aix-en-Provence, France	Sep 1998 – Mar. 1999
Teck Cominco Limited Student Work Internship, Vancouver, Canada	May 1995 – Jun. 1995
Mount Isa Mines Limited Student Work Internship, Brisbane, Australia	May 1994 – Aug. 1994

EDUCATION

Chalmers University of Technology, Sweden International Master's in Materials Engineering	Sep. 1999 – Nov. 1999
McGill University, Montreal, Canada Bachelors in Engineering, Metallurgical	Sep. 1993 – Dec. 1997

